

REPUBLIQUE DU CAMEROUN
PAIX-TRAVAIL-PATRIE

UNIVERSITE DE YAOUNDE I

CENTRE DE RECHERCHE ET DE
FORMATION DOCTORALE EN SCIENCES
TECHNOLOGIQUE ET GEOSCIENCE

UNITE DE RECHERCHE ET DE FORMATION
DOCTORALE PHYSIQUE ET APPLICATION

DEPARTEMENT DE PHYSIQUE
BP 812 Yaounde

Email : crfd_stg@uy1.uninet.cm



REPUBLIC OF CAMEROON
PAECE-WORK-FATHERLAND

UNIVERSITY OF YAOUNDE I

POSTGRADUATE SCHOOL OF SCIENCE,
TECHNOLOGY & GEOSCIENCE

RESEARCH AND POSTGRADUATE
TRAINING UNIT FOR PHYSICS AND
APPLICATIONS

DEPARTMENT OF PHYSICS
P.O. Box 812 Yaounde

Email: crfd_stg@uy1.uninet.cm

Dynamic and Decoherence of Polaron and Bipolaron in Transition Metal Dichalcogenides

Thesis

submitted and defended publicly in partial fulfillment of the requirements for the degree of

Doctor of Philosophy. in Physics

Speciality: **Mechanics, Materials and Structures**

Option: **Fundamental Mechanics and Complex Systems**

Written and presented by:

NGUEPNANG Jean Valère

Registration Number: 18W5514

M. Sc. in Physics

Under the supervision of:



KENFACK JIOTSA Aurélien

Professor
University of Yaoundé 1

KENFACK SADEM Christian

Associate Professor
University of Dschang

Jury

President: **ZEKENG Serge Sylvain**, Professor, University of Yaoundé I;

Supervisor: **-KENFACK JIOTSA Aurélien**, Professor, University of Yaoundé 1;
-Pr. KENFACK SADEM Christian, Associate Professor, University of Dschang;

Members: **-DJAKA Jean-Marie Bienvenu**, Professor, University of Yaoundé I;
-FEWO Serge Ibraïd, Associate Professor, University of Yaoundé I;
-NANA Bonaventure, Associate Professor, University of Bamenda.

Year 2024

DEDICATION

I dedicate this work to one of the Greatest Physicist, **GOD**, who called me to follow Him on the path of His work of creation, and of understanding the physical laws that govern the world. Without Him, I could not stride along with wisdom, courage, and faith, which together enabled me to finalize the present dissertation. May He bless my supervisors; my teachers, my family, my friends and all those who contributed from far and near to my training and the realization of this research.

To my mother:

Late **WANDJA Françoise**.

And to my brother:

Late **TCHOUENTE Armel Brice**

ACKNOWLEDGMENTS

In the writing of this thesis, I have benefitted from the continuous support and encouragement of many good supervisors, professors, lecturers, friends and family.

I am particularly grateful to my supervisors Pr. **KENFACK SADEM Christian**, and Pr. **KENFACK JIOTSA Aurelien** for the opportunity that they gave me to work on this very interesting subject. Their careful reading and comments on each new project have made this thesis much better and more enjoyable than it would otherwise have been. They were always ready to discuss and offer a critical look at the issues I had in mind. Thanks to their patience, and the fact that they never failed to help me.

I am grateful and thankful to the members of the jury for accepting to evaluate the work. I am sure I will learn a lot from their experience and contributions during the defense. I am indebted to them for that.

I would like to thank the Pre-defense and Audition jury's members for their contributions, their advices and their discussion which helped me to ameliorate the quality of this work.

My gratitude goes to members of the Academic staff of the Mechanic, Material and Structures laboratory, without forgetting the entire staff of the Physics Department of the University of Yaounde 1 led by Pr. **NDJAKA Jean Marie Bienvenu**, and the entire staff of the Physics Department of the University of Dschang for giving me a good academic foundation. I am very grateful for their administrative contribution and encouragement

I would like to acknowledge my lectures especially Pr. **FEWO Serge Ibraïd**, Pr. **FAI Cornelius**, Pr. **FOTUE Alain Jerve** for their encouragements during the writing of this thesis. Thank you for your advices.

I also thank the Abdous Salam International center for Theoretical Physics and Cameroon Physical Society for summer schools it allowed me to attend; it is from this framework that I learned several new approaches to common problems through discussion with experts.

I would like to thank Dr. **FOBASSO Florette** in particular, who, in having offered her assistance as a reader and discussion partner, deserves acknowledgment and credit for her positive influence on my work. I am indebted for a great generosity.

I express my recognition to all the members and students of the Mechanic and Complex System division of the university of yaounde 1, and the Condensed Matter and Nanomaterials research division of the University of Dschang for the discussion and their productive critics.

My deep gratitude goes to my entire family, especially Mr. **KOUTEU Pascal**, Mr. **TCHUENTE Jean**, Mr. **NGUEMDJOP Fidèle**, Mr. **DJIKI Michel**, Mrs. **NGNENZE Celine**, Mr. **TOUKAM Samuel**, Mr. **KETCHOUANG Bertrand**, Mr. **KETCHOUANG Carlos**, my brother Mr. **DJEMI Anelka**, my sisters Mrs. **TENKAP Christiane**, Mrs. **CHAIWO Maiva**, Mrs. **TCHEBON Laurette**, Mrs. **CHIMI Ornella** for their love and multiform supports. Thanks for their support and encouragement throughout my education and for the unfailed belief they have in me.

Special gratitude to my friends Dr. **HIKOUATCHA Princes**, Dr. **NGUENBU Telesphore**, Dr. **KOUFOUET Hervice**, Dr. **JEAZET Alain**, Dr. **NGOMADE Armel**, Mr. **NGOMADE Serges**, Mr. **KOUOMEGNE Pascal**, Mrs. **ANOUMEDEM Elalie**, Mr. **NGUEMASSON Charles**, Mr. **KITIO Arthur**, Dr. **DONFACK Bernard** and Dr. **NGANFO willy**, Mr. **MANFOUO Francis**, Dr. **MWEBI Clautaire**. In the same line, I express my gratitude to families **TADADJIO**, **KENTSA**, **TAGUELA**, **AKUM** and also to all members of the “**COMPAGNONS**” group for their love, fraternal and warm climate that they created around me

I am also thankful and grateful to everyone who contributed in any way for the success of this work; may the Almighty God who always guided me until nowadays, complete in me what he began.

CONTENTS

DEDICATION	1
ACKNOWLEDGMENTS	2
CONTENTS	4
LIST OF ABBREVIATIONS	8
LIST OF TABLES	9
LIST OF FIGURES	10
ABSTRACT	14
TITLE IN FRENCH	16
RESUME	17
GENERAL INTRODUCTION	19
CONTEXT	19
MOTIVATION	22
PROBLEMATIC	23
OBJECTIVES	24
OUTLINES	24
1) CHAPTER 1: LITERATURE REVIEW	26
INTRODUCTION	26
1.1 GENERALITIES ON TRANSITION METAL DICHALCOGENIDES	26
1.1.1 STRUCTURE OF TMDS	28
1.1.2 SYNTHESIS METHOD OF TRANSITION METAL DICHALCOGENIDES	28
1.1.3 PHYSICAL AND THERMODYNAMIC PROPERTIES	30
1.1.4 BAND STRUCTURE	31
1.1.5 APPLICATIONS OF TMDS	34
1.2 CONCEPT OF QUASI PARTICLES	35
1.2.1 CONCEPT OF PHONONS	35
1.2.1.1 DEFINITION OF PHONONS	35
1.2.1.2 TYPES OF PHONONS	36
1.2.1.3 PHONONS APPLICATIONS	38

1.2.2 CONCEPT OF POLARON	39
1.2.2.1 DEFINITION OF POLARON	39
1.2.2.2 CONCEPT AND REPRESENTATION.....	39
1.2.2.3 APPLICATIONS.....	41
1.2.3 CONCEPT OF BIPOLARON.....	42
1.2.3.1 PRESENTATION AND DEFINITION OF BIPOLARON	42
1.2.3.2 STABILITY OF BIPOLARON.....	43
1.2.3.3 APPLICATIONS.....	44
1.2.4 CONCEPT OF EXCITON-POLARON	45
1.2.4.1 CONCEPT OF EXCITON	45
1.2.4.2 FORMATION OF EXCITON POLARON.....	46
1.3 DECOHERENCE	46
1.3.1 DEFINITION.....	46
1.3.2 DECOHERENCE PARAMETERS.....	47
1.3.3 APPLICATION OF DECOHERENCE	48
CONCLUSION.....	49
CHAPTER 2: MATHEMATICAL TOOLS AND THEORITICAL MODELS	50
INTRODUCTION.....	50
2.1 VARIATIONALS METHODS.....	50
2.1.1 HAMILTONIAN	50
2.1.1.1 HAMILTONIAN OF AN ELECTRON	50
2.1.1.2 HAMILTONIAN OF PHONON	51
2.1.1.3 HAMILTONIAN OF ELECTRON-PHONON INTERACTION.....	52
2.1.2 LEE-LOW PINES VARIATIONAL METHOD	53
2.1.2.1 GROUND STATE ENERGY	55
2.1.2.2 EFFECTIVE MASS OF POLARON.....	60
2.1.3 HUYBRECHT VARIATIONAL METHOD	60
2.1.3.1 DETERMINATION OF THE GROUND STATE ENERGY	60
2.1.3.2 FIRST EXCITED STATE ENERGY	63
2.1.3.3 DIFFERENCE BETWEEN LLP AND HUYBRECHT METHODS	64
2.1.4 PEKAR VARIATIONAL METHOD	64
2.2 SOME PARAMETERS OF QUASIPARTICLES	66
2.2.1 POLARON LIFETIME IN WEAK COUPLING REGIME.....	66
2.2.2 EFFECTIVE MASS OF POLARON IN ALL COUPLING REGIME.....	67
2.2.3 MOBILITY OF POLARON.....	73

2.2.4 SHANNON ENTROPY.....	74
2.2.5 DECOHERENCE TIME.....	75
2.3 THEORITICAL MODELS.....	78
2.3.1 POLARON IN TRANSITION METAL DICHALCOGENIDES.....	78
2.3.1.1 POLARON UNDER ELECTRIC FIELD IN TRANSITION METAL DICHALCOGENIDES QUANTUM DOT.....	78
2.3.1.2 EFFECT OF MICROWAVES AND RADIO WAVES ON POLARON IN TRANSITION METAL DICHALCOGENIDES QUANTUM DOT.....	81
2.3.2 EXCITON-POLARON IN TRANSITION METAL DICHALCOGENIDES.....	87
2.3.2.1 MAGNETIC BARRIER EFFECT ON EXCITON-POLARON IN TRANSITION METAL DICHALCOENIDES.....	88
2.3.2.2 ELECTRON-PHONON COUPLING CONTRIBUTION ON EXCITON- POLARON IN TMDs quantum dot.....	97
2.3.3 BIPOLARON IN TRANSITION METAL DICHALCOGENIDES.....	104
2.3.3.1 BIPOLARON IN TMDs: ALL COUPLING APPROACH.....	104
2.3.3.2 BIPOLARON IN TMDs quantum PSEUDODOT.....	109
CONCLUSION.....	112
CHAPTER 3: NUMERICAL RESULTS AND DISCUSSIONS.....	113
INTRODUCTION.....	113
3.1 DYNAMIC OF POLARON, EXCITON-POLARON AND BIPOLARON IN TRANSITION METAL DICHALCOGENIDES.....	114
3.1.1 GROUND AND FIRST EXCITED STATES ENERGIES.....	114
3.1.1.1 ENERGIES OF POLARON.....	114
3.1.1.2 ENERGIES OF EXCITON-POLARON.....	121
3.1.2 MOBILITY.....	127
3.1.2.1 MOBILITY OF POLARON.....	127
3.1.2.2 MOBILITY OF EXCITON-POLARON.....	130
3.1.2.3 MOBILITY OF BIPOLARON.....	131
3.1.3 EFFECTIVE MASS OF EXCITON-POLARON.....	132
3.1.4 LIFETIME OF POLARON.....	134
3.2 STABILITY, OPTICAL ABSORPTION AND BANDGAP MODULATION.....	138
3.2.1 STABILITY OF BIPOLARON.....	138
3.2.2 MAGNITUDE OF BANDGAP MODULATION.....	139
3.2.2.1 CASE OF POLARON.....	139
3.2.2.2 CASE OF BIPOLARON.....	141
3.2.3 OPTICAL ABSORPTION COEFFICIENT.....	143

3.2.3.1 CASE OF EXCITON-POLARON	143
3.2.3.2 OPTICAL ABSORPTION OF BIPOLARON	147
3.3 DECOHERENCE OF POLARON, EXCITON-POLARON AND BIPOLARON	150
3.3.1 TRANSITION FREQUENCY	150
3.3.1.1 TRANSITION FREQUENCY OF POLARON	150
3.3.1.2 TRANSITION FREQUENCY OF EXCITON-POLARON	154
3.3.1.3 TRANSITION FREQUENCY OF BIPOLARON	155
3.3.2 DENSITY PROBABILITY	157
3.3.2.1 CASE POLARON	157
3.3.2.2 CASE OF EXCITON-POLARON	158
3.3.2.3 CASE OF BIPOLARON	159
3.3.3 SHANNON ENTROPY	161
3.3.3.1 SHANNON ENTROPY OF POLARON	161
3.3.3.2 SHANNON ENTROPY OF EXCITON-POLARON	163
3.3.3.3 SHANNON ENTROPY OF BIPOLARON	164
3.3.4 DECOHERENCE TIME	166
3.3.4.1 DECOHERENCE TIME OF EXCITON-POLARON	166
3.3.4.2 DECOHERENCE TIME OF BIPOLARON	167
CONCLUSION	170
GENERAL CONCLUSION AND PERSPECTIVES	171
REFERENCES	175
LIST OF PUBLICATIONS	187

LIST OF ABBREVIATIONS

0D: Zero Dimensional.

1D: One Dimensional.

2D: Two Dimensional.

3D: Three Dimensional.

AlN: Aluminium Nitride.

Al₂O₃: Aluminium Oxide.

BCS: Barden Cooper Schrieffer.

BE: Binding Energy.

h-BN: hexagonal Boron Nitride.

LLP: Lee-Low Pines.

LO: Longitudinal Optical.

MBM: Magnitude of Bandgap Modulation.

MoS₂: Molybdenum Disulfide.

MoSe₂: Molybdenum Diselenide.

MW: Microwave.

RW: Radiowave.

SiC: Silicon Carbide

SiO₂: Silicon Dioxide

SO: Surface Optical.

TMDS: Transition Metal Dichalcogenides.

WS₂: Tungsten Disulfide.

WSe₂: Tungsten Diselenide.

LIST OF TABLES

Table 1 : Electronic character of different layered TMDs [68].....	27
Table 2 : physical and thermodynamic characteristic of some TMDs [78]	31
Table 3 : Indirect and direct bandgap of some TMDs [93].....	33
Table 4 : Coupling range and corresponding mobility [157, 158]	97
Table 5 : Parameters of different polar substrates and surfaces optical phonon modes [164]	113
Table 6 : The magnitude of bandgap modulation for the different TMDs and the energies of LO phonons of different TMDs [168].....	113

LIST OF FIGURES

Figure 1 : possible layered structure TMDs materials consist of 16 transition metals and 3 chalcogen atoms [68].	27
Figure 2 : Representation of the steps of mechanical exfoliation technique on TMDs [89]....	29
Figure 3 : sulfurization of metal thin film (a) synthesis of MoS ₂ layer by MoO ₃ sulfurization; (b) MoS ₂ layer on a sapphire [90]	30
Figure 4 : sulfurization of metal thin film: synthesis procedure for the ADL-based WS ₂ [91]	30
Figure 5 : Crystal arrangement of compound MX ₂ (M=W; Mo, X=S; Se) consist of a stack monolayer coupled by weak bonds of Van der Waals [92]	31
Figure 6 : Band structure of MX ₂ ; a: MoS ₂ , b: WS ₂ , c: MoSe ₂ , d: WSe ₂ [94].....	33
Figure 7 : Band structure of MX ₂ in monolayer form; a: MoS ₂ , b: WS ₂ , c: WSe ₂ , d: MoSe ₂ [94]	34
Figure 8 : phonon dispersion curves of (b) monolayer and (c) bulk layer TMDs [107]	38
Figure 9 : Crystal lattice vibration [108]	39
Figure 10 : formation of the polaron due to deformation of the crystal [111].	42
Figure 11 : Cartoon illustrating bipolaron formation. a) Two separated polarons each in its own polarisation well. b) Bipolaron where two electrons are localized in the same potential well [115].	43
Figure 12 : Magnetic barrier using two long narrow magnetic stripes perpendicular to the monolayer TMD.	93
Figure 13 : sketch of the optical absorption of the bipolaron in the monolayer TMDs [162]	105
Figure 14 : Polaron energies as a function of effective confinement length for : (a) ground state energy (b) first excited.	114
Figure 15 : Polaron energies as a function wave vector : (a) ground state energy (b) first excited	115
Figure 16 : Polaron energies as a function of electric field: (a) ground state energy (b) first excited.	115
Figure 17 : Polaron energies as a function of electric field for: (a) ground state energy (b) first excited	116
Figure 18 : Ground-state energy of polaron with SO phonon mode as function of frequency of RW on different polar substrates.....	117
Figure 19: Ground-state energy of polaron with SO phonon mode as function of frequency of MW on different polar substrates.....	117
Figure 20 : Ground-state energy of polaron with SO phonon mode as function of amplitude of RW for different polar substrate.....	119
Figure 21 : Ground-state energy of polaron with SO phonon mode as function of amplitude of MW for different polar substrate.....	119
Figure 22 : Ground-state energy of polaron with LO phonon mode as function of frequency of RW for different TMD monolayers	120
Figure 23 : Ground-state energy of polaron with LO phonon mode as function of amplitude of MW for different TMD monolayers.....	120
Figure 24 : Ground state energy of exciton polaron versus length of magnetic barrier for different TMDs monolayers	121
Figure 25 : First excited state energy of Exciton-polaron versus the length of magnetic barrier for various TMDs monolayers in strong coupling regime	122

Figure 26 : Energy of exciton-polaron as a function of magnetic field for different TMDs monolayer in intermediate coupling regime.....	123
Figure 27 : Energy of exciton-polaron versus magnetic field for different TMDs monolayer in strong coupling regime.....	124
Figure 28 : Energy of exciton-polaron with LO phonon versus magnetic field for different TMDs monolayers in the intermediate coupling regime.....	125
Figure 29 : Variation of exciton-polaron energy versus internal distance z_0 between WS ₂ and polar substrates in weak coupling regime for various polar substrates.....	125
Figure 30 : Energy of exciton-polaron versus internal distance z_0 in intermediate coupling regime for various polar substrates	126
Figure 31 : Energy of exciton-polaron versus internal distance z_0 in strong coupling regime for various polar substrates	126
Figure 32 : Polaron mobility versus wavelength for different value of electric field	127
Figure 33 : Polaron mobility versus internal distance between TMDs monolayer and polar substrate.....	128
Figure 34 : Polaron mobility versus electric field for different TMDs monolayers	128
Figure 35 : Mobility of polaron with SO phonon mode as function of amplitude of RW (fig.35A) and amplitude of MW (fig.35B) for different TMDs monolayers	129
Figure 36 : Mobility of exciton-polaron versus the length of magnetic barrier for different TMDs monolayer	130
Figure 37 : Mobility of bipolaron versus the chemical potential for different values of zero	131
Figure 38 : Mobility of bipolaron versus zero point of the pseudo-harmonic potential for various TMDs monolayer	132
Figure 39 : variation of effective mass of exciton-polaron versus the length of magnetic barrier for various TMDs monolayer.....	133
Figure 40 : Effective mass of exciton-polaron coupling with SO phonon as function of the magnetic field in a strong coupling regime for various TMDs monolayer.....	134
Figure 41 : Effective mass of exciton-polaron coupling with SO phonon as a function of the magnetic field in intermediate coupling regime for various TMDs monolayer.....	134
Figure 42 : Lifetime of polaron versus wavelength for different TMDs monolayers for	135
Figure 43 : Lifetime of polaron versus internal distance between TMDs monolayer and polar substrate for different value of electric field	136
Figure 44 : Life time of polaron with LO phonon mode as function of amplitude of RW (fig.44A) and amplitude of MW (fig.44B) for different TMDs monolayer.....	137
Figure 45 : Life time of polaron with SO phonon mode as function of amplitude of RW (Fig.45A) and amplitude of MW (Fig.45B) for different TMDs monolayer.....	138
Figure 46 : Binding energy of the bipolaron versus magnetic field in MoS ₂ for different polar substrate (intermediate coupling regime)	139
Figure 47 : Binding energy of the bipolaron with parameter η_0 in weak coupling regime for different TMDs monolayer.....	139
Figure 48 : The MBM of polaron with SO phonon mode as function of frequency of RW for different polar substrates	140
Figure 49 : The MBM of polaron with SO phonon mode as function of internal distance for different polar substrates. (Fig.48A) without RW and MW, (Fig.48B) with RW and MW ..	140

Figure 50 : The MBM of polaron with LO phonon mode as function of amplitude of RW (Fig.50A) and amplitude of MW (Fig.50B) for different TMDs monolayer	141
Figure 51 : Magnitude of bandgap modulation different TMDs as function of :.....	142
Figure 52 : Absorption of exciton-polaron as function of photon energy in weak coupling regime for LO phonon for different TMDs monolayer.....	144
Figure 53 : Absorption of exciton-polaron as function of photon energy in intermediate coupling regime for LO phonon for different TMDs monolayer.....	144
Figure 54 : Absorption of exciton-polaron versus photon energy in weak coupling regime coupling for different polar substrate	145
Figure 55 : Absorption of exciton-polaron versus photon energy for intermediate coupling regime coupling with SO phonon for different TMDs monolayer.....	146
Figure 56 : Absorption of exciton-polaron as function magnetic field in intermediate coupling regime for different value of the internal distance between monolayer TMDs and polar substrates	146
Figure 57 : Absorption of exciton-polaron as function of photon energy for LO phonon for different electron phonon coupling in different TMDs Monolayer.....	147
Figure 58 : Optical absorption coefficient of bipolaron versus photon energy in LO phonon in different monolayer TMDs materials for bipolaron in weak coupling regime	148
Figure 59 : Optical absorption coefficient of bipolaron (case of SO phonon) versus magnetic field B in MoS ₂ intermediate coupling regime.....	149
Figure 60 : Optical absorption coefficient of bipolaron (case of SO phonon) versus magnetic field B in MoS ₂ intermediate coupling regime for different polar substrate.....	150
Figure 61 : Transition frequency of polaron qubit versus effective confinement length for different value of electric field	151
Figure 62 : Transition frequency of polaron versus electric field strength for different TMDs monolayer.....	152
Figure 63 : Transition frequency of polaron with SO phonon mode as function of amplitude of MW for different polar substrates	152
Figure 64 : variation of transition frequency of polaron for SO phonon mode as function of amplitude of the RW for different TMDs	153
Figure 65 : Transition frequency of polaron for SO phonon mode as function of frequency of RW and for different amplitude of MW.....	154
Figure 66 : Transition frequency of exciton-polaron as function of the length of magnetic barrier for different TMDs monolayer	155
Figure 67 : Transition frequency of bipolaron versus zero point of the pseudo-harmonic potential for various the chemical potential of the two-dimensional electron gas.....	156
Figure 68 : Transition frequency bipolaron versus the chemical potential of the two-dimensional electron gas for different TMDs monolayer	157
Figure 69 : Probability density of polaron versus time: (a) $F = 0.1mV / nm$, (b) $F = 0.5mV / nm$, (c) $F = 1mV / nm$, (d) $F = 1.5mV / nm$	158
Figure 70 : Probability density of polaron versus time: (a) MoSe ₂ , (b) MoS ₂ , (c) WSe ₂ , (d) WS ₂ ,	158
Figure 71 : variation of probability of excitonic-polaron density as function of the length of magnetic barrier for various TMDs monolayer.....	159
Figure 72 : Density probability of bipolaron as function of time for different values of the chemical potential of the two-dimensional electron gas for.....	160

Figure 73 : density probability of bipolaron versus the zero point of the pseudo-harmonic potential.....	161
Figure 74 : Shannon entropy of polaron versus time: (a) $F = 0.1mV / nm$, (b) $F = 0.5mV / nm$, (c) $F = 1mV / nm$, (d) $F = 1.5mV / nm$	162
Figure 75 : Shannon entropy of polaron versus electric field : (a) MoSe ₂ , (b) MoS ₂ , (c) WSe ₂ , (d) WS ₂ ,.....	162
Figure 76 : variation of the entropy of exciton-polaron versus time for various TMD	164
Figure 77 : variation of Shannon entropy of exciton-polaron with respect to the length of magnetic barrier for different TMDs monolayer.....	164
Figure 78 : Shannon entropy of bipolaron versus the chemical potential of the two-electron gas	165
Figure 79 : Shannon entropy of bipolaron versus zero point of the pseudo-harmonic potential	166
Figure 80 : Decoherence time of exciton-polaron versus the length of magnetic barrier for different TMDs monolayers.	167
Figure 81 : Decoherence time of bipolaron versus dispersion coefficient for different value of the chemical potential of the two-dimensional electron gas	168
Figure 82 : Decoherence time of bipolaron versus dispersion coefficient for different value of the zero point of the pseudo-harmonic potential	169
Figure 83 : Decoherence time of bipolaron as function of the chemical potential of the two-electron gas for different TMDs monolayer.....	170

ABSTRACT

Recent progress in atomically thin two-dimensional Transition Metal Dichalcogenides (TMDs) have led to the production of very small-scale semiconductor devices where a controllable number of polarons are confined into a small volume. Unlike conventional materials such as germanium and gallium arsenide, TMDs have interesting electronic and optical properties and above all, the flexibility of their gap makes them advanced materials for the new generation of electronic devices. Optimizing the performance of quasi-particles in these materials remains a key issue for the miniaturization of next-generation devices.

In this thesis, investigations on dynamic, decoherence and optical properties of polarons, exciton-polaron and bipolaron in TMDs (molybdenum disulfide (MoS_2), molybdenum diselenide (MoSe_2), tungsten disulfide (WS_2), and tungsten diselenide (WSe_2)) have been presented. In order to achieve our goals, we have used different variational methods of calculations such as Lee Low-Pines (LLP), Huybrecht and Pekar variational method. The ground state and first excited state of the eigen energies of optical polarons, exciton-polaron and bipolaron in different TMDs monolayers were calculated.

The study of polarons in TMDs reveals that external potential such as electric field, amplitude of radiowave (RW) or amplitude of microwave (MW) increase the polaron ground state energy, the first excited state energy, the mobility, the coherence of polaronic states, allow information transfer and can be helpful to control the state of the system. Also, we showed that electric field reduces polaron lifetime, while the amplitudes of RW or MW increase polaron lifetime and reduce the magnitude of bandgap modulation. We also found that the frequencies of RW or MW create fluctuation in the polaron state energies and in the magnitude of bandgap modulation. Among the chosen monolayers, polarons move more freely and live longer in WS_2 in the presence of electric field. Furthermore, study of exciton-polaron in TMDs showed that magnetic barrier or magnetic field, strongly affected the state energies, reduce the effective mass of exciton polarons and increase their mobility. We also observed that the magnetic barrier length allows the transition from the valence band to conduction band, increases the information transfer and can be used to adjust the decoherence of exciton-polaron state in TMDs. It is also found that the optical absorption coefficient of exciton-polarons have a threshold value in the presence of the magnetic field, it increases with the increasing of magnetic field and decreases with internal distance between TMDs and polar substrates, optical absorption strongly depends on the choice of the polar substrates, and on the electron-phonon coupling. Besides, results on

bipolaron in TMDs reveals that, the higher the coupling strength, the stronger is the magnetic field effect on bandgap modulation, the highest bandgap modulation is obtained with MoS₂ monolayer, we found that the bipolaron is stable in all chosen monolayer. Optical absorption of bipolaron in presence of magnetic field also present a threshold values with correspond to the energy of photon equal to the frequency of optical phonon and increase in the sequency of WSe₂, MoSe₂, WS₂ and MoS₂. We also demonstrated that in presence of pseudo harmonic potential, the chemical potential increases the mobility of bipolaron, the transition frequency and decreases the decoherence time whereas the zero point of pseudo harmonic potential decrease the mobility of bipolaron, transition frequency and increase decoherence time. Thus decreasing the zero point of pseudo harmonic potential resulting to large transition frequency which destroy the decoherence. We found that bipolaron moves more freely in WS₂ monolayer. We also found that pseudo harmonic potential is useful to information transfer; to destroy the decoherence of bipolaron state and permits to manage the state of a system.

The results obtained in this thesis are useful for society in general because they make it possible to improve the performance of electronic devices such as transistors, LEDs logic gates while reducing their size. also for the scientific community because the control of the polaronic states in TMDs systems open a path towards the improvement of quantum computing by proposing a new system for the design and construction of the quantum computer, for the transfer and storage of quantum information.

Keywords: polaron, exciton-polaron, bipolaron, dynamic, decoherence, TMDs.

TITLE IN FRENCH

**DYNAMIQUE ET DECOHERENCE DU POLARON ET
DU BIPOLARON DANS LES DICHALCOGENURES DE
METAUX DE TRANSITION**

RESUME

Les récents progrès dans le domaine des Dichalcogenures de Métaux de Transition (Transition Metal Dichalcogenides (TMDs) en anglais), matériaux bidimensionnels de taille atomique ont conduit à la fabrication des dispositifs semi-conducteurs de très petites tailles dans lesquelles un nombre de polaron est confiné dans un petit volume. Contrairement au matériaux classiques tels que l'arséniure de Gallium et le Germanium, les TMDs présentent des propriétés électroniques intéressantes. La flexibilité de leur gap fait d'eux des matériaux de pointes pour la nouvelle génération de composants électroniques. L'optimisation de la performance des quasi-particules dans ces matériaux reste un enjeu déterminant pour la miniaturisation des appareils de nouvelle génération.

Dans cette thèse, nous étudions la dynamique, la décohérence et les propriétés optiques du polaron, de l'exciton-polaron et du bipolaron dans les TMDs (disulfure de molybdène (MoS_2), diséléniure de molybdène (MoSe_2), disulfure de tungstène (WS_2), diséléniure de tungstène (WSe_2) via des méthodes variationnelles tel que la méthode de Lee-Löw Pines (LLP), la méthode de Huybrecht et la méthode de Pekar. Les énergies propres de l'état fondamental et du premier état excité du polaron, de l'exciton-polaron et du bipolaron dans les monocouches de TMDs ont été calculées.

L'étude du polaron dans les TMDs révèle que les potentiels externes tels que le champ électrique, l'amplitude de l'onde radio (RW) ou de la micro onde (MW) augmente l'énergie de l'état fondamental du polaron, l'énergie du premier état excité, la mobilité, la cohérence des états polaroniques, permettent le transfert de l'information quantique et peuvent être utilisés pour contrôler l'état d'un système. En outre, nous avons montré que le champ électrique réduit la durée de vie du polaron, par contre les amplitudes de la RW ou de la MW augmentent la durée de vie du polaron et réduisent l'amplitude de la bande interdite modulée. Nous avons également constaté que la fréquence de la RW ou de la MW crée des fluctuations dans les énergies des états du polaron et dans l'amplitude de la bande interdite modulée. Parmi les monocouches de TMDs choisies, le polaron se déplace plus librement et vit plus longtemps dans le WS_2 en présence du champ électrique. De plus, l'étude de l'exciton-polaron dans les TMDs montre que la barrière magnétique ou le champ magnétique affecte fortement les énergies des états, réduit la masse effective de l'exciton-polaron et augmente leur mobilité. Nous avons également observé que l'augmentation de la longueur de la barrière magnétique facilite la transition de la bande de valence vers la bande de conduction, augmente le transfert

de l'information ainsi, peut être utilisée pour ajuster la cohérence des états de l'exciton-polaron dans les TMDs. On n'a aussi observé que le coefficient d'absorption optique de l'exciton polaron admet une valeur seuil, augmente avec l'augmentation du champ magnétique mais diminue avec l'augmentation de la distance interne entre la TMD et le substrat polaire. L'absorption optique dépend fortement du choix du substrat polaire ainsi que du couplage électron phonon. En outre, les résultats sur le bipolaron dans les TMD montrent que plus le couplage électron-phonon est élevée, plus l'effet du champ magnétique sur la modulation de la bande interdite est fort, la modulation de la bande interdite la plus élevée est obtenue pour la monocouche de MoS₂, le bipolaron est stable dans toute les monocouches de TMD choisies. L'absorption optique présente également une valeur seuil qui correspondent à l'énergie du photon égale à l'énergie du phonon optique, il augmente à la séquence de WSe₂, MoSe₂, WS₂ et MoS₂. Nous avons également démontré qu'en présence d'un pseudo potentiel harmonique, le potentiel chimique augmente la mobilité du bipolaron, la fréquence de transition mais diminue le temps de décohérence tandis que le point zéro du pseudo potentiel diminue la mobilité du bipolaron, la fréquence de transition mais augmente le temps de décohérence. La diminution du point zéro du pseudo potentiel entraîne une fréquence de transition élevée qui détruit la décohérence des états bipolaroniques. Nous avons constaté que le pseudo potentiel harmonique est utile pour le transfert de l'information, la destruction de la décohérence et la gestion des états du système.

Les résultats obtenus dans ce travail sont utiles pour la société en générale car ils permettent d'améliorer les performances des composants électroniques tel que les portes logiques, les transistors et les LED tout en réduisant leurs de tailles. Également pour la communauté scientifique car Le control des états polaroniques des systèmes à TMDs ouvre une voie vers l'amélioration du calcul quantique en proposant un système nouveau pour la conception et la réalisation de l'ordinateur quantique, pour le transfert et le stockage de l'information quantique.

Mots clés : polaron, exciton-polaron, bipolaron, dynamique, décohérence, TMDs

GENERAL INTRODUCTION

CONTEXT

According to Christoph Tillman [1], advanced semiconductor expertise permits the fabrication semiconductor nanodevices with small size. In the past decade research focusses on many types of semiconductor nanodevices with dimensions of 10 nm or less. Even commercial mass production of nanodevices has grasped a length scale of few nanometers and the International Technology Roadmap for semiconductors predict a thinning of this scale below 10 nm over the next decade [1], but at these length scales, transport is conquered by quantum mechanics phenomena such as quantum confinement, decoherence and quantum consideration of some classical properties. Furthermore, the discovery of graphene has ignited intensive interest in a wide range of two-dimensional (2D) layer materials [2]. In general, there are a wide range of layer materials in which the atomic layers are weakly bonded together by van der Waals interactions and can be readily isolated into single or few-layer nanosheets through mechanical exfoliation or liquid exfoliation processes [2]. These atomically thin 2D nanosheets derived from the layer materials share many interesting characteristics of the well-known graphene, such as exceptional electronic properties, extraordinary mechanical flexibility. With the reduced dimensionality and/or quantum confinement effect, these 2D nanosheets can exhibit unique properties distinct from their 3D bulk counterpart. The Transition Metal Dichalcogenides (TMDs) are part of the large family of the 2D layer materials, it is call layer material to show their surprising narrowness. TMDs have properties that are different from those of the graphene, e.g. semiconducting TMDs monolayers have a direct bandgap and can be used in electronic as transistor, in optic as emitters and detectors [3, 4], the crystal structure has no inversion center, which allows to access a new degree of freedom of charge carriers, namely the k-valley index, and open a new field of physics: valleytronics [4- 6]. TMDs are often combined with other 2D materials like graphene and hexagonal boron nitride to make Van der Waals heterostructures. These heterostructures need to be optimized to be possible used as building blocks for many different devices such as transistors, solar cells, leds, photodetectors, fuel cell, photocatalytic and sensing devices. Some of these devices are already used in everyday life and can become smaller, cheaper and more efficient by using TMDs monolayers [7, 8]. Others are still being developed and promise a huge impact on our technology. A thorough understanding of electronic, optical and transport properties in nanoscale devices are required to build a theoretical model of carrier in such nanostructures. As

these devices are never free of deficiency, any charge carrier is defied with its environment as phonons. This is particularly true when the device is subjected to small temperatures which rise the phonon vibrations. Therefore, a truthful model for transport in semiconductor nanodevices must address carrier confinement, carrier dynamics, nanostructure properties and nanostructure environments [9].

Then, it is well known that a local change in the electronic state of a crystal leads to corresponding local changes in the interactions between the individual atoms of the crystal. And mutually, any local change in the state of the network ions changes the local electronic state. It is common in this situation to speak of electron-phonon interaction. Electron-phonon coupling arises when polarization of the lattice vibration is coupled to electron charge [10, 11]. This interaction even manifests itself at absolute zero temperature and results in a number of specific microscopic and macroscopic phenomena. In TMDs as in others polar materials, a particular coupling arises between electron and phonon, this phonon interacts with electron via polarization density to form an entity called polaron. Polaron is a quasiparticle having particular characteristics, such as effective mass, total momentum, energy [12]. And perhaps other quantum numbers describing the internal state of the quasiparticles in the presence of an external magnetic field or in case of very strong lattice polarization that causes the electron to locate itself in the polarization with the appearance of discrete energy levels. The formation of this polaron is a consequence of the dynamic of electron-lattice interaction that is also responsible for the diffusion of charge carriers, the renormalization of the frequency of phonons as well as the screening of the interaction between charge carriers in solid [13]. The concept of the polaron was first studied by Pekar [14], who investigated the most essential properties of the stationary polaron in the uncertain case of a very intense electron-phonon interaction, so that the polaron behavior can be examined in what is entitled adiabatic approximation.

A polaron is a quasiparticle used in condensed matter physic to explain the interaction between electrons and atoms in a solid material. For a local, 1D electron-phonon interaction, there is permanently a polaron. On the other hand, in 2D and more, the establishment of a polaron necessitate an adequately strong local coupling [15, 16]. In this case the polaron's are always very small, i. e. located on a single site. In the absence of Coulomb repulsion, two polarons form a bipolaron. Its consists of two electrons in a singlet state, located on the same site. If the repulsion between electrons becomes very strong, the bipolaron disappears to form two unbound polaron's. The exciton being a quasi-particle that can be seen as an electron-hole pair linked by coulomb forces. We have two types of excitons, the Mott-Vanier excitons and

the Frenkel excitons. Indeed, the combination of phonon and exciton gives rise to another quasi-particle name exciton-polaron. So exciton-polaron is formed when exciton interact with acoustic or optical phonons via coupling to the deformation potentials associated to the conduction and valence band. In other hand, the created bare exciton is further dressed with phonons. This leads to the formation of a quasi-composite particle which is the coherent mixture of the electron-hole and phonon pair that can be called exciton-polaron. So exciton-polaron can be seen as the mixture of two polarons, one polaron form with electron an another polaron form with hole.

Many researchers have devoted to the development of polaron theory [17-20]. But, even if the formulation of polaron is simple, the polaron problem has not yet been fully solved and continues to attract much attention especially in 2D materials. It plays an essential part in solid state physic, statistical mechanic and quantum field theory due to the fact that it can be consider as the simplest example of a non-relativistic quantum particle interacting with a quantum field. This is why many mathematical tools have been skilled for the first time using this problem as a model. One of the most important contributions to polaron theory is made by Bogolubov who used various schemes such as adiabatic perturbation theory, the formalism of functional integration, the T-product method [21-23] to solve polaron problem. As for polaronic theories, several bipolaronic theories taking into account quantum fluctuations in the network have been developed to try to explain superconductivity. With low electron-phonon coupling, the Barden Cooper Schrieffer theory has proven the existence of pairs of electrons (Cooper's pairs) formed in a self-consistent manner in a superconducting phase. These pairs remain spatially very large over a distance that is the length of coherence. For bipolaronic superconductivity, it is speculated that pairs of electrons (small bipolaron) pre-exist and behave like a boson liquid. These bipolarons would condense into a superfluid phase. However, this is not the case, a very strong argument disproves this hypothesis: when a bipolaron exists in 2D and 3D its effective mass is so high that it does not allow a condensation of Bose at a reasonable temperature. The bipolarons would then correspond to chemical bonds and condense into a spatially ordered or unordered phase. For a strong electron-phonon coupling, the bipolaronic system is modelled by a network of $1/2$ spins coupled with two types of interaction. The competition between electron phonon coupling and electron repulsion can generate a high mobility of bipolarons with a relatively strong binding energy.

Improvement of Coulomb interactions in 1D semiconductors leads to formation of closely related excitations when electron-hole pairs are excited as well as to the improvement

of the role of interactions involving several charge carriers. Excitons are electrically neutral particles and can move freely through a crystal [24]. Nowadays, realization of device components with impurities placed with atomic precision have been achieved [25], with these single dopants strongly tailoring the behaviour of low-dimensional systems [26, 27]. So, it is essential to understand the underlying mechanisms of donor impurities, both for transport and for qubit applications.

MOTIVATION

Lately, as an interdisciplinary field of information science and quantum mechanic, quantum computation and quantum communication have enlarged the research ranges of quantum mechanic and significantly improved the development of quantum theory [28-31]. Experimental and theoretical researchers are attracted by some effects appearing in crystal and in nanoscales systems such as the Jahn-Teller and polaronic effects [32-36]. So, we are more interested in the polaronic effect in novel material as TMDs because it can help to provide systems useful in quantum information science and also because of the importance of the interaction between electrons and the crystal lattice in nanoscale. In quantum information science, the construction and manipulation of a qubit in nanostructures are important subjects, so that exploring those topics is necessary and valuable not only to understand quantum mechanics but also to achieve extra information processing methods [37]. Quantum system should be isolated for any interaction with its environment to preserve the destruction of its states which lead to the loss of information, quantum systems are very frail and the interaction of a quantum memory with its environment destroys the quantum coherence of the stored information leading to the process named decoherence [38]. Therefore, quantum decoherence plays a very important role in the formalism of quantum computing. So a great deal of considerable efforts [39-42] have been made to investigate the quantum decoherence and how to prolong coherence time in semiconductors in past years. In addition, Electron-phonon interactions of polaron-type play a very important role in the properties of small-scale quantum systems [43-48]. Thus, the interest in the polaron problem is growing in TMDs materials because the electron-phonon interaction in TMDs monolayers systems is stronger than in others semiconductors. So the decoherence process and the dynamic of the quasiparticles in these materials need to be investigated.

In addition, in TMDs, Polaronic state can have long lifetimes and can be controlled and manipulated, making them potential candidates for qubit implementations in quantum

computers. However, there are some challenges associated with using of the polaronic state in TMDs for quantum computation such as: the polaronic state that can be sensitive to external environmental factors which can lead to decoherence and loss of quantum information, quantum gate operation on polaronic qubits can be challenging due to their interactions with the lattice vibrations and the polaronic qubit can be difficult to scale due to their interactions with the lattice vibrations. So, ongoing research aims to address these limitations and explore the potential of the polaronic state in TMDs for quantum computing

PROBLEMATIC

Supplementary properties of quantum confinement can be providing by the replacement of particles with nano-sized by the layers with nano-sized, this can also give rise to new components with new properties. Indeed, some nanoparticles factors such as its large surface/volume ratio, its shape, its arrangement in one medium or another, its compatibility with other components can modify the optical and electronic properties of materials containing them. For all these factors, research on nanoparticles has taken off significantly over the last two decades. A wide range of methods are required for quantum bit control. However, a strong confinement offers much more possibilities on the quantum control of these quantum bits. Modelling the behaviour of the quantum bit made up of polaron, exciton-polaron and bipolaron under the action of external potential in TMDs monolayers is one of our tasks. Although several works [49-52] have been done on the quasiparticles in TMDs, particularly on the bandgap modulation where the results show that the bandgap can be modulated by varying different polar substrates or internal distance between substrate and TMDs or by increasing electric field. Also, lot of theoretical physics research on electron-phonon interaction in TMDs [51-53] and bandgap engineering [54-56] has been done in order to build optoelectronic devices. Some important aspects of the problem have not yet been solved such as dynamic properties (mobility, lifetime...), decoherence properties (decoherence time, density probability...) or optical properties of quasiparticles in the monolayer TMDs knowing that their presence can affect the properties of materials. Thus, research on the effect of the polaron, exciton-polaron and bipolaron in TMDs has become an essential topic in small-scale physics because it can be easily integrated in the low dimensional systems. There is then a good reason to believe that quasiparticles such as polaron, exciton-polaron and bipolaron can exhibit other new characteristics in the presence of electric field, magnetic field, magnetic barrier, microwave, radiowave; as well as in the presence of confinement as pseudo-harmonic potential.

There are several attempts to solve the physical problems of the polaron, exciton-polaron and bipolaron in the presence of external effects using different models proposed in the literature. However, a complete description of the behaviour of these quasiparticles remains incomplete using traditional methods like, Huybrecht method, particularly in TMDs nanostructures. The dynamic, optical and decoherence properties of the polaron, exciton-polaron and bipolaron in TMDs should be adequately studied to evaluate the effect of electron-phonon coupling, electric field, magnetic field, magnetic barrier, pseudo-harmonic potential, microwave and radiowave on dynamic and decoherence of these quasiparticles in TMDs. Thus, what will be the effect of those external potential as same as the electron-phonon coupling on dynamic, optical and decoherence properties of the polaron, the exciton-polaron and bipolaron in TMDs? In addition, can electron-phonon coupling or magnetic field affect the optical absorption of exciton-polaron and bipolaron in TMDs system? These questions are studied in detail in this thesis, taking into account the imperfections observed in TMDs, while solving the problem of bipolaron stability.

OBJECTIVES

Presently, the study of correlated quantum systems in TMDs monolayers as in others semiconductors provides a new platform to explore new quantum properties. Our main objective is to explore the behavior of polaron, exciton-polaron and bipolaron confined in TMDs materials and explore their features, by examining new quantum phenomena with theoretical methods, thus we will study the dynamic, optical and decoherence properties of polaron, exciton-polaron and bipolaron in TMDs monolayers under various external potential. The specific objectives are to first of all model each of the system in order to theoretically investigate the associated quantum phenomena; we will also study the effect of electron-phonon coupling on dynamic and optical absorption of exciton-polaron and the optical signature of bipolaron in TMDs. For the purpose we will propose models that will characterize the qubit in TMDs with different quasi-particles under different external potential. Subsequently we will calculate some parameters like ground and first excited states energies, effective mass, absorption coefficient, stability, mobility, lifetime, magnitude of bandgap modulation, transition frequency, probability density, decoherence time and Shannon entropy.

OUTLINES

This thesis is structured as follows: chapter one provides generalities on the recent evolution on 2D TMDs; quasiparticles such as polaron, exciton-polaron, bipolaron and

decoherence effect. In chapter two, the variational methods as LLP, Huybrecht and Pekar type methods are presented in standard polaronic system. The LLP method describes the polaronic effect in a weak electron-phonon coupling limit. Huybrecht method allow to solve polaronic problems in all electron-phonon coupling and the Pekar variational method allow to solve polaronic problem in strong electron-phonon coupling regime. Also, some parameters of quasiparticles are presented, different systems that polaron, exciton-polaron and bipolaron can exist in TMDs materials are presented by a suitable Hamiltonian. Thus, the energies of the ground and the first excited states energies are obtained in the different electron-phonon coupling regime in TMDs. The effective mass and others dynamic properties of some quasiparticles are also investigated. Chapter three is devoted to the numerical results achieved. Here, expressions linking transition frequency to electric field, magnetic barrier, pseudo-harmonic potential, microwave and radiowave are presented. To study decoherence, probability density, Shannon entropy and decoherence time are also presented. The optical absorption, lifetime and the magnitude of bandgap are also displayed in TMDs. Finally, this thesis ends with general conclusion and perspectives are outlined for further researches.

CHAPTER 1: LITERATURE REVIEW

INTRODUCTION

Nowadays nanotechnology has attracted a lot of research works due to the wide range of domain in which it can be applied; in fact, nanotechnology has created opportunities for the fabrication of new nanoscale systems. The aim of this chapter is to give a general concept on nanostructures, polaronic quasiparticles that we have been working on throughout this thesis. Thus we will focus on TMDs nanomaterials, we will present generalities on polaron, exciton-polaron and bipolaron. At the end we will present decoherence concept.

1.1 GENERALITIES ON TRANSITION METAL DICHALCOGENIDES

The great success of graphene has been followed by an equally impressive surge for the development of the other 2D materials that can form atomic sheets with extraordinary properties. Interestingly, the 2D library grows every year and feature more than 150 exotic layer materials that can be easily split into a sub-nanometer thick material [59–61]. These include 2D TMDs (e.g. MoS₂, MoSe₂, WS₂ and WSe₂), h-BN, 2D boron, 2D silicon, 2D germanium, and MXenes. Depending on their chemical composition and structural configuration, atomically thin 2D materials can be categorized as metallic, semi-metallic semiconducting, insulating, or superconducting. The first graphene descendants that sparked intense research activity are TMDs, which are almost as thin, transparent and flexible as graphene [62-67]. TMDs belong to the family of lamellar materials of formula MX₂. M is a transition metal of group 4, 5, 6, 7, 9 or 10 of the periodic classification table and X is a chalcogen. Generally, TMDs materials containing group 4 to 7 transition elements have a layered structure, while those with group 9 to 10 transition metals have non-layered structures. Fig.1 shows the possible layered and non-layered structures of TMDs materials. Each layer has a thickness of 6 to 7 Angstrom, which consists of a hexagonally packed layer of metal atoms combined by weak Van der Waals forces [68]. Electronically, it covers a wide range of properties from insulator to metal trough semiconductor [69]. Table 1 summarize the electronic character of different layered TMDs.

MX_2 ----- **X = Chalcogen**

M = Transition Metal

H																	He
Li	Be											B	C	N	O	F	Ne
Na	Mg	3	4	5	6	7	8	9	10	11	12	Al	Si	P	S	Cl	Ar
K	Ca	Sc	Ti	V	Cr	Mn	Fe	Co	Ni	Cu	Zn	Ga	Ge	As	Se	Br	Kr
Rb	Sr	Y	Zr	Nb	Mo	Tc	Ru	Rh	Pd	Ag	Cd	In	Sn	Sb	Te	I	Xe
Cs	Ba	La-Lu	Hf	Ta	W	Re	Os	Ir	Pt	Au	Hg	Tl	Pb	Bi	Po	At	Rn
Fr	Ra	Ac-Lr	Rf	Db	Sg	Bh	Hs	Mt	Ds	Rg	Cn	Uut	Ff	Uup	Lv	Uus	Uuo

Figure 1 : possible layered structure TMDs materials consist of 16 transition metals and 3 chalcogen atoms [68].

Table 1 : Electronic character of different layered TMDs [68]

Group	M	X	Properties
4	Ti, Hf, Zr	S, Se, Te	Semiconducting ($(E_g = 0.2 \approx 2eV)$)
5	V, Nb, Ta	S, Se, Te	Narrow band metal or semimetals
6	Mo, W	S, Se, Te	Sulfides and selenides are semiconducting. Tellurides are semimetal
7	Tc, Re	S, Se, Te	Small gap semiconductors
10	Pd, Pt	S, Se, Te	Sulfides and selenides are semiconducting. Tellurides are metallic. PdTe ₂ is superconducting

2D TMDs is a new generation of thin atomic material with special physical properties.

Today, these materials are the focus of much scientific research. With the development of the field of nanotechnology in recent years, a great deal of attention has been paid to study TMDs from both theoretical and experimental aspects. 2D TMDs exhibit unique electrical and optical properties that involve from the quantum confinement and surface effects that arise during the transition of an indirect bandgap to a direct bandgap when bulk materials are scaled down to monolayers. This tunable bandgap in TMDs is accompanied by a strong photoluminescence and large exciton binding energy, making them promising candidate for a variety of opto-electronic devices, including solar cells, photo-detectors, light-emitting diode and photo-transistors [70–73]. Another aspect of the weakly bonded 2D TMDs atomic layers is that they

can be easily isolated and stacked with others TMDs to construct a wide range of van der Waals heterostructures without the limitation of lattice matching [74, 75].

1.1.1 STRUCTURE OF TMDS

TMDs are layered materials in which each unit is composed of a transition metal (M) layer sandwiched between two chalcogen (X) atomic layers. They are made of 2D sheets, stacked along the crystallographic axis (C). Depending on the arrangement of the atoms, the structures of 2D TMDs can be categorized as trigonal prismatic where the atom of metal is sandwiched between two planes of atoms of chalcogen. Metal is linked to six chalcogen by covalent bonds, the adjacent planes of two sheets contain only chalcogen, which leads to the formation of weak bonds known as the Van der Waals bond. The stacking of the sheets along the C axis give rise to numerous polytypes, the common one for the studied compound are 2H and the 3R polytypic. The 2H polytypic corresponds to a hexagonal stacking, it includes 2 layers per unit cell it belong to the D_{6h}^4 space group. The 3R polytypic corresponds to a rhombohedral stack, it includes three layers per unit cell and belongs to the C_{3v}^5 space group [76-78]. The planes perpendicular to the C axis are defined by the (002) planes and they are called basal planes. The basal surfaces are constituted by the external layer of chalcogen atom. The bonds of the chalcogen atom on the surface of the sheet being saturated, the basal surfaces are little chemically reactive. On the other hand, the dangling bonds at the edges of the sheets make the non-basal surfaces chemically active. It should be noted that molybdenum and tungsten disulfides exist in nature in the form of minerals called molybdenite and tungstenite, but the selenides of these transition metals are not found naturally on the surface of the earth [79].

1.1.2 SYNTHESIS METHOD OF TRANSITION METAL DICHALCOGENIDES

In 2004, Novoselov et al. successfully produced various single-layer 2D crystals from bulk materials, such as graphite, BN, NbSe₂ using mechanical exfoliation method [80]. This method is typically adopted to prepare single-layer TMDs samples. The single crystal TMDs prepared by this method are good quality, and can be used for studying their basic properties [81, 82]. Fig.2 presents different steps of this method use in transition metal dichalcogenides. However, the size of the TMDs materials prepared by the mechanical exfoliation method is quite small approximately on tens of microns' scale, posing a limitation to real devices applications. To obtain large quantities of TMDs nanosheets or few-layer TMDs nanosheets, a solution processing strategy would be more appropriate. Thus the first report on the liquid phase exfoliation of sheets of clay materials in the early 1960s [83] has inspired many studies into

methods of exfoliating nanosheets of TMDs [84-86]. Due to their layered structure, TMDs bulk materials can be intercalated by various kinds of intercalates such as organic molecules, transition metal halides and lithium ions [86]. The resulting intercalated compounds can be exfoliated in single and few layer 2D nanosheets by ultrasonication [87, 88]. However, this method is time-consuming and the degree of intercalates insertion is not controllable, which limit its feasibility. To apply TMDs materials to real devices, their large scale growth is essential. The chemical vapor deposition (CDV) method is the most effective way to achieve large area growth. This method can be divided into two types, the sulfurization of metal thin films and vapor phase reaction of metal oxides with chalcogen precursor. In this method, the size and thickness of the predeposited metal films determine the size and thickness of the TMDs thin film respectively. However, it is challenging to deposit a uniform metal film.

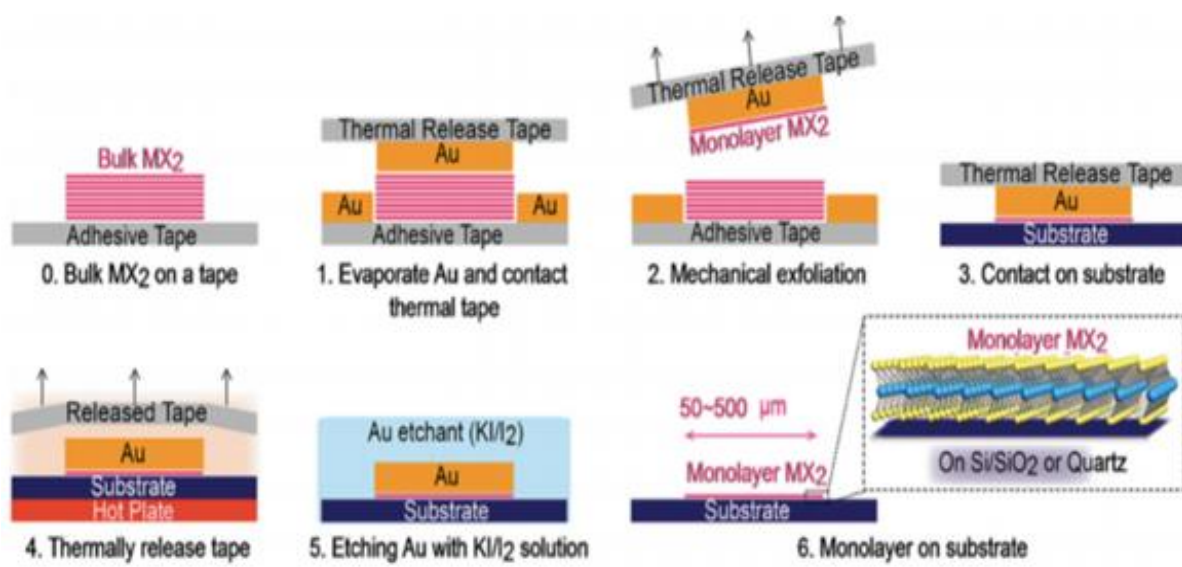


Figure 2 : Representation of the steps of mechanical exfoliation technique on TMDs [89]

Fig.3 is an illustration for the synthesis of the MoS_2 layers by MoO_3 sulfurization. A layer of MoO_3 was thermally evaporated on the sapphire substrate, the MoO_3 is converted to MoS_2 by a two step thermal process. Fig.4 present the synthesis procedure for the ALD-based WS_2 nanosheets. The synthesis of the TMDs by the direct sulfurization of a metal oxide thin film has several limitations, such as the difficulty to control the thickness of the predeposited metal oxide or metal thin film, which affects the wafer-scale uniformity. Thus to obtain high quality TMDs with the desired number of layers, the thickness of the metal oxide needs to be precisely controlled. Thus with the synthesis process by depositing metal oxide layers via atomic layer deposition (ADL), we obtained a thin TMDs nanosheets with systematic thickness controllability and wafer-scale uniformity.

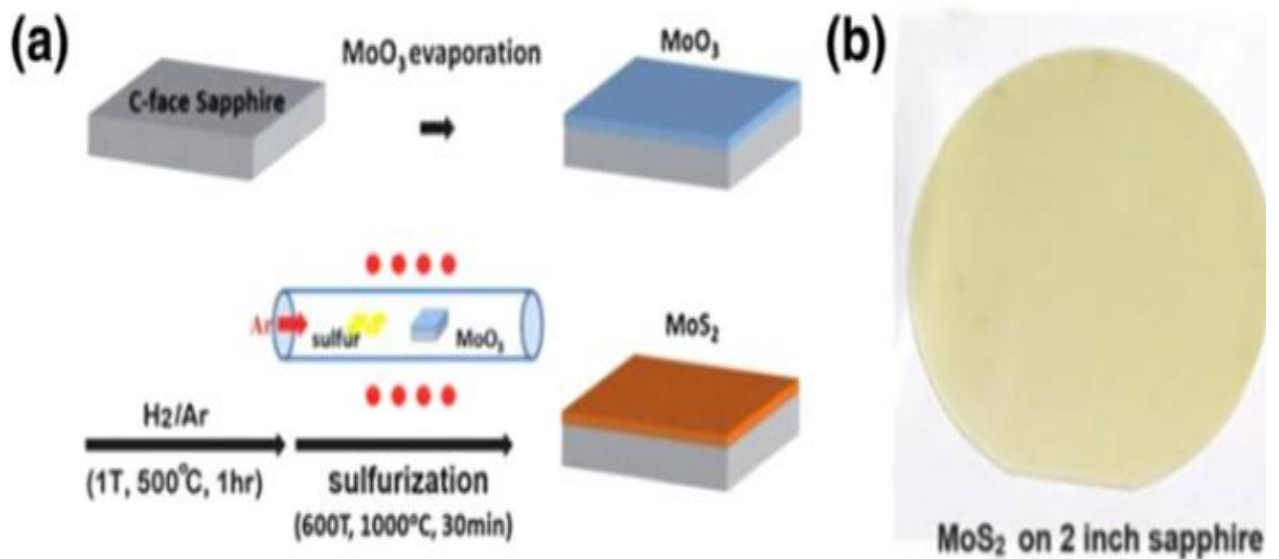


Figure 3 : sulfurization of metal thin film (a) synthesis of MoS₂ layer by MoO₃ sulfurization; (b) MoS₂ layer on a sapphire [90]

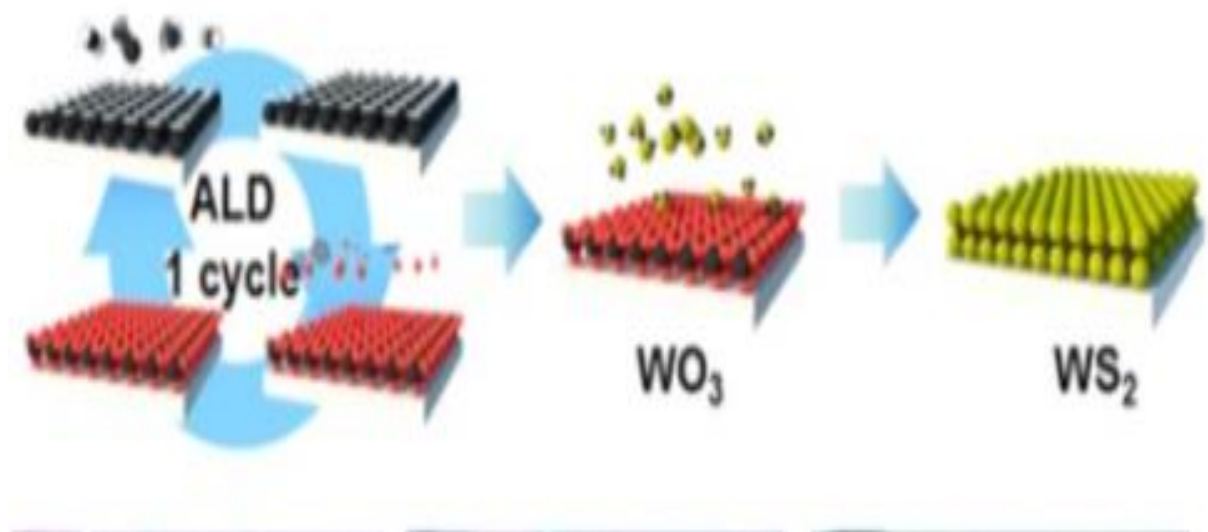


Figure 4 : sulfurization of metal thin film: synthesis procedure for the ADL-based WS₂ [91]

1.1.3 PHYSICAL AND THERMODYNAMIC PROPERTIES

The properties of the TMDs are often strongly linked to their lamellar structures. There are therefore very anisotropic like graphite. Table 2 shows some physical and thermodynamic characteristic of the four compounds. Fig.5 present the crystal arrangement of compound MX₂

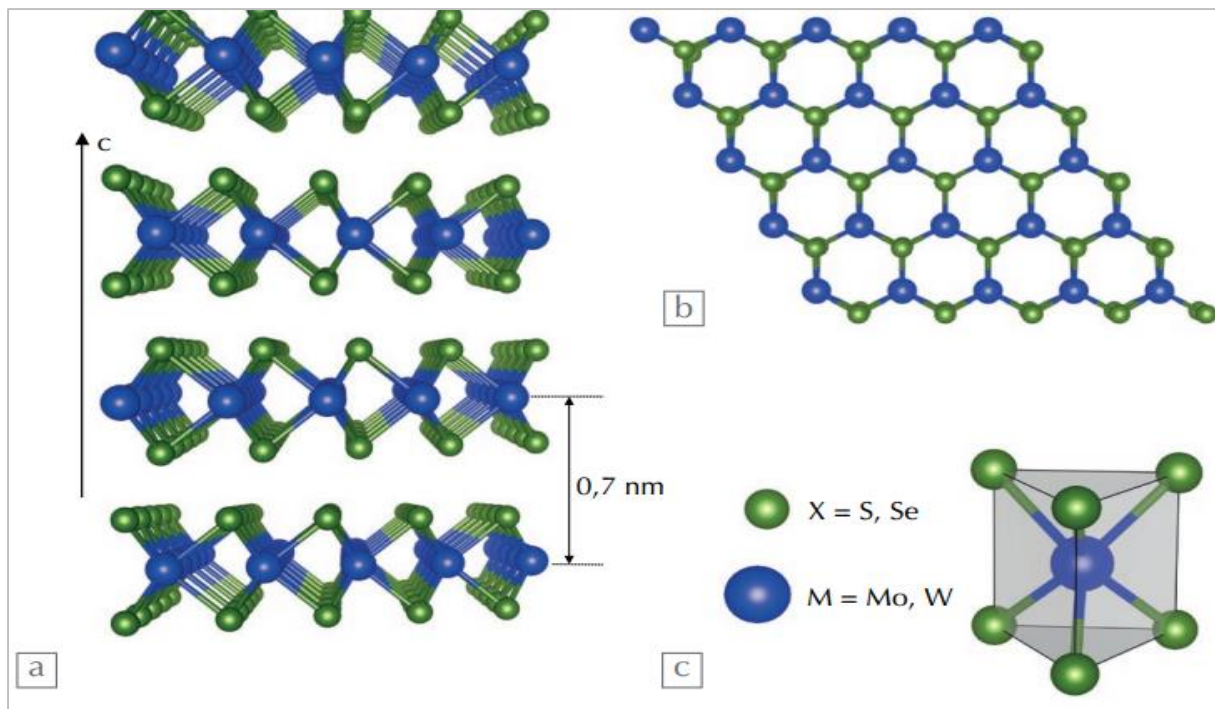


Figure 5 : Crystal arrangement of compound MX₂ (M=W; Mo, X=S; Se) consist of a stack monolayer coupled by weak bonds of Van der Waals [92]

- (a) Transverse view (the vertical arrow represents the crystallographic axis C)
- (b) Top view of the monolayer
- (c) Prismatic trigonal coordination of sulfur or selenide atoms around a metal atom

Table 2 : physical and thermodynamic characteristic of some TMDs [78]

compound	Molar mass(g/mol)	$\Delta H^\circ (K.J.mol^{-1})$	$\Delta S^\circ (J.K^{-1}.mol^{-1})$	Temperature(C)
MoS ₂	160.07	-275.04 ± 5.02	62.5	570
MoSe ₂	253.86	-196/05 ± 41.18	87.78 ± 8.36	> 340
WS ₂	247.98	-259.16 ± 6.72	64.76 ± 6.27	□ 400
WSe ₂	341.17	-188.1 ± 62.7	89.87 ± 12.57	480

1.1.4 BAND STRUCTURE

The notion of the gap or bandgap is related to the representation of the dispersion of a semiconductor, the behavior of semiconductors, such as metals and insulators, is described by the theory of bands. The energy band structure defines the possible energy state that an electron can take in a crystal as function of a wave vector. In the phase diagram, the energy is represented according to the direction with the highest symmetry, it is divided into valence band, conduction

band and band gap. The energy distance between the maximum of the valence band and the minimum of the conduction band is called bandgap. In the phase diagram, the maximum of the valence band and the minimum of the conduction band can correspond to the same value of the wave or to different values of it; in the first case we speak of direct bandgap while in the second case, we speak of indirect bandgap. Direct gap and indirect gap materials behave very differently from the optoelectronic point of view because the charge carriers of the direct gap materials can pass from one band to the other by simply exchanging a photon whose momentum is negligible at this level of energy. While the charge carriers of the indirect gap materials have to interact with both a photon and a phonon in order to modify their wave vectors which makes the transition much less likely.

The TMDs are semiconductors characterized by an indirect band gap between 0.788-0.917eV and direct transitions between 1.393-1.679eV [93]. The indirect band gap comes from the upper part of the valence band located at the Γ point down to the halfway of the conduction band between Γ and the K points, while the direct transition are located at the K point of the Brillouin zone. Fig.6 represent the band structure of different compounds in massif form where Table 3 summarizes their indirect and direct band gap value obtained by the density functional theory.

The structure of the energy bands of the TMDs in the form of the thin films show that all these materials have a direct energy gap at the K point of the Brillouin zone. Fig.7 presents the band structure of different compounds in the thin form. When the number of layer decrease, the fundamental indirect gap increase due to confinement effects. In the case of monolayer it becomes larger than the indirect bandgap located at K point. In the limit of a single layer, it become direct at K point. Thus, the TMDs change from indirect gap semiconductors in the bulk state to direct gap semiconductors in two dimensions.

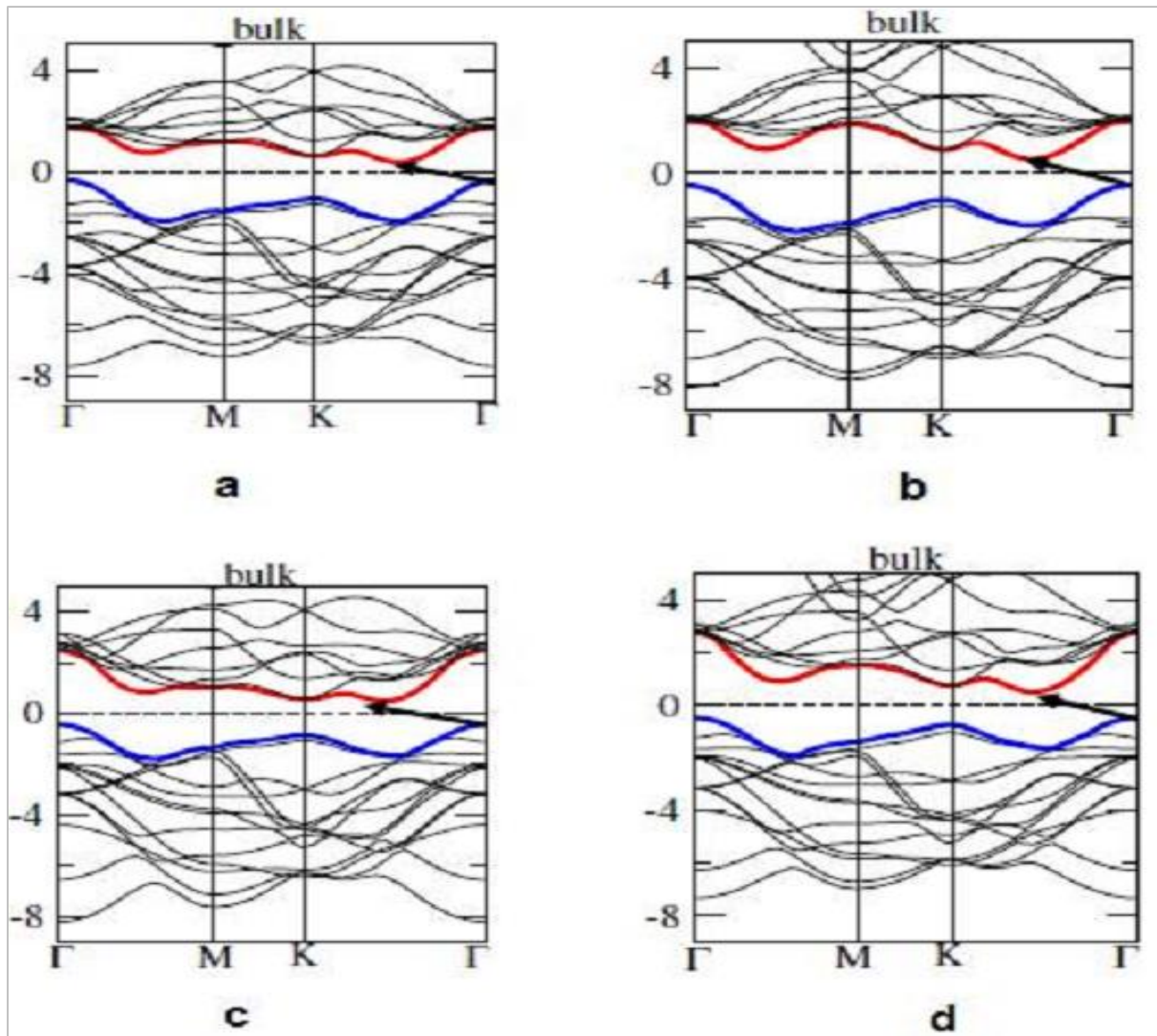


Figure 6 : Band structure of MX_2 ; a: MoS_2 , b: WS_2 , c: MoSe_2 , d: WSe_2 [94]

Table 3 : Indirect and direct bandgap of some TMDs [93]

Material (solid)	Indirect bandgap (Ev)	Direct bandgap (Ev)
MoS_2	0.788	1.679
WS_2	0.917	1.636
MoSe_2	0.852	1.393
WSe_2	0.910	1.407

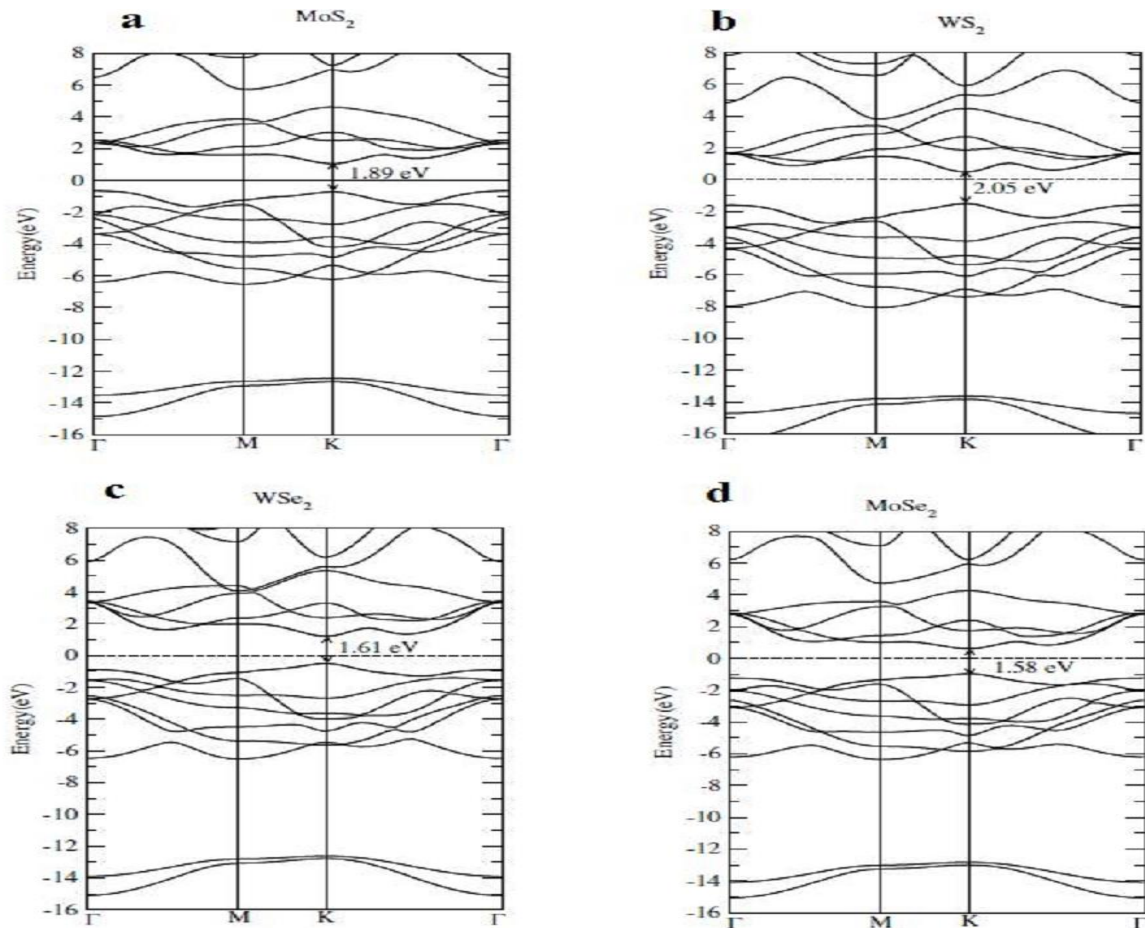


Figure 7 : Band structure of MX_2 in monolayer form; a: MoS_2 , b: WS_2 , c: WSe_2 , d: MoSe_2 [94]

1.1.5 APPLICATIONS OF TMDS

2D TMDs materials are considered attractive for diverse applications including electronics, photonics, sensing, and energy devices. These applications are inspired by the unique properties of layered materials such as thin atomic profile that represents the ideal conditions for maximum electrostatic efficiency, mechanical strength, tunable electronic structure, optical transparency, and sensor sensitivity [95]. Of particular interest for applications is flexible nanotechnology, which is considered for potentially ubiquitous electronics and energy devices that can benefit from the range of outstanding properties afforded by 2D materials. Flexible technology comprises a wide array of scalable large-area devices including thin film transistors, displays, sensors, transducers, solar cells and energy storage on mechanically compliant substrates. As TMDs might be applicable for future generation large-scale electronics [96], provided manufacturing and integration challenges can be resolved. 2D TMDs are gaining significant attention as electrode materials for energy storages, such as super-

capacitors and Li-ion batteries, due to their atomically layered structure, high surface area and excellent electrochemical properties. Such layered structures provide more sites for ions in energy storage while maintaining structure stability during charge and discharge cycles. The high surface area of 2D materials when combined with surface functionality and electrical conductivity, make them as an ideal electrode for energy storages [97–99]. Due to its excellent semiconducting properties with direct bandgap of 1.83eV, the single-layer MoS₂ nanosheets are seen as one of the most appropriate supplementing materials to graphene for the fabrication of the low power electronic devices. The performance limit of MoS₂ transistor with HfO₂ as dielectric has been theoretically studied [100] by Yoon et al., and showed that on/off current ratio exceeding 10¹⁰ can be achieved. It was observed that the field effect transistor based sensors fabricated using bilayer, trilayer and quadrilayer MoS₂ nanosheets exhibited high sensitivity with the detection limit of less than 1pm. The large-scale production of single and multi-layer MoS₂ nanosheets using exfoliation techniques can enable their wide spread applications for energy storage devices such as batteries. MoS₂ nanosheets prepared by chemical lithiation and exfoliation in stacking structure were fabricated for use as electrodes for lithium batteries and compared with the electrodes made from the bulk MoS₂, the stacked MoS₂ nanostructure showed much better cycling stability than the bulk MoS₂ retaining a high capacity even after 50 cycles [101]. The stability and Li-storage capacity of MoS₂ based energy storing devices can be improved to a greater extent by adding polymer molecules such as polyethylene oxide to the Li-intercalation solution [102], as the presence of the polyethylene oxide can increase in the interlayer spacing of the MoS₂ nanosheets. Much improved Li-storage capacity and cycling stability are observed in the case of electrodes made from the MoS₂-polyethylene oxide nanocomposites. This improvement in performance is attributed to the fact that large amounts of lithium ions can be accommodated over the polyethylene oxide. The MoS₂ can be used for the fabrication of supercapacitors or bi-layer capacitors, as they possess a large interlayer space, as well as a large specific surface area, that can be used for ion intercalation and exhibit several stable oxidation states [103] Moreover, in this timeframe, several articles have reviewed breakthroughs and perceived applications of 2D materials [104,105].

1.2 CONCEPT OF QUASI PARTICLES

1.2.1 CONCEPT OF PHONONS

1.2.1.1 DEFINITION OF PHONONS

Quasiparticles are a type of particles that emerge as a result of interactions between others particles in a material. There are not particles, but excitations that behave like particles and have certain properties. Quasiparticles can help us understand and predict the behavior of materials and their properties such as electronic, magnetic, and optical properties. There are various types of quasiparticles, but some of the most well known include: electron holes that can be seen as as lack of electron, and phonons, which are quasiparticles that arise due to the collective vibrations of atoms in a material. The vibrations of atoms will form a vector field called the displacement field, which can be quantized; the quanta of the displacement field are called phonons [106]. Phonons are considered as quasiparticles, which means that they have no physical existence as separate materials entities, but as a collective excitation in a crystalline solid. Phonons can be imagined as energy packets that propagate through the solid, carrying vibrational energy. A normal vibration mode is a mode in which all the element of a network vibrates at the same frequency. The mode of vibrations of atoms in a crystal lattice are essentially periodic oscillations of the positions of the atom around their equilibrium positions. The phonons can be dispersive, which means that their speed and frequency can vary depending on the direction of propagation and the properties of the material. Phonons are quasi-particles of spin 0. We have many types of phonons such as acoustic phonons and optical phonons, acoustic and optical Phonons exist only within a crystal lattice with a large number of particles, and the only known physical structures corresponding to this definition are crystal solids. In the following we will therefore only deal with phonons in this context and, for sake of clarity, we will call the particles constituting the network atoms, although they may be ions in an ionic solid.

The forces acting between the different atoms in the lattice lead to movement of one or more atoms around their equilibrium position that will cause the vibration and propagation of waves through the lattice. The Fig.9 below shows a vibration wave in a network. The amplitude of the wave is given by the amplitude of the displacement of the atoms around their equilibrium position. The wavelength corresponds to the smallest interval between two identical repetitions of the arrangement of atoms, it is noted λ on the figure.

1.2.1.2 TYPES OF PHONONS

In a real solid, there are two types of phonons: "Acoustic" and "Optical" phonons [106]. Acoustic phonons are compression and decompression waves that propagate through a solid. They are responsible for the propagation of the sound in materials. They are commonly found

in metals, ceramics, and semiconductors. Optical phonons are present in solids that have several atoms per mesh. They are called "optical" because in ionic crystals they are very easily excited by light waves. This is due to the fact that they correspond to vibration mode for which positive and negative ions located on adjacent sites of the network approach and move away from each other by creating an electric dipole moment oscillating with time. Optical phonons that interact in this way with light are called active in the infrared. Noticed that they are others types of phonons like amorphous phonons that propagate in amorphous materials such as glass. Unlike crystalline materials, amorphous materials do not possess a periodic structure, which gives rise to a broader and more complex phonon frequency distribution. The presence of different types of phonons depends on the materials. For example, some materials exhibit only acoustic phonons, while others may exhibit both acoustic and optical phonons. Also the nature of phonons can vary depending on temperature and other environmental conditions.

In TMDs the phonon dispersion of a monolayer has three acoustics and six optical branches inheriting from the nine vibrational modes at Γ point. The three acoustics branches include the in-plane longitudinal acoustic, the transverse acoustic and the out-of-plane acoustic. The in-plane branches have a linear dispersion and higher frequency than the out-of-plane. The six optical branches are two in-plane longitudinal optical branches, two in-plane transverse optical branches and two out-of-plane optical branches [107]. These six optical modes at Γ point correspond to the irreductible representation in Fig. 8. Since TMDs are slightly polar materials, certain R-active phonons modes displays optical splitting due to coupling of the lattice to the macroscopic electric field created by the relative displacement of M and X atoms in the long wavelength limit.

For two-layers and bulk TMDs, there are 18 phonons branches which are split from 9 phonons branches in monolayers TMDs. Owing to the weak van der waals interaction in two-layers and bulk TMDs, the frequency of the splitting corresponding for the two optical branches is very small, resulting in resemblance of optical phonon dispersion curves among mono, two layers and bulk TMDs. For example, the phonon dispersion of monolayer Fig. 8B and bulk Fig. 8C are much similar except three new branches due to interlayer vibration below 100cm^{-1} in bulk due to interlayer vibrations. The general features of theses TMDs are similar to each other. But, their phonon frequencies are more different. In comprarison to monolayer MoS_2 the phonon bands, of monolayer WS_2 are shifted down to lower frequencies, which mainly due to the larger mass of W atoms. Furthermore, the interlayer phonons in bulk are different from each

other, which is due to their intrinsic differences in both the whole mass of TMDs and interlayer coupling strengths.

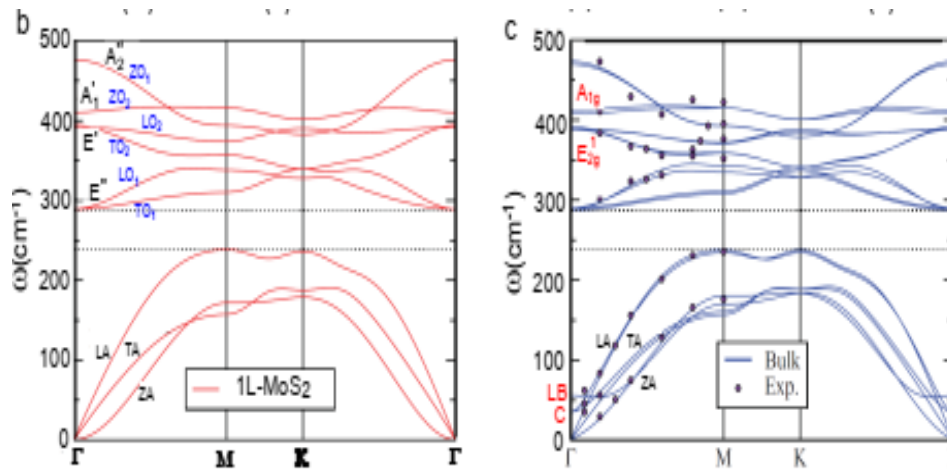


Figure 8 : phonon dispersion curves of (b) monolayer and (c) bulk layer TMDs [107]

1.2.1.3 PHONONS APPLICATIONS

The study of phonons continues to gain momentum because of its various domains of applications such as

- Optical phonons can be used to detect chemical bonds and determine the compositions of materials through a process called infrared spectroscopy. They can also be used in phonon-assisted thermoelectricity to convert heat or mechanical energy into electricity.
- Acoustic phonons are useful in thermal management, which consists of avoiding heating in electrical devices by removing heat from them. They are also used to set up materials that absorb sound waves, thus limiting the propagation of noise. In TMDs, acoustic phonon branches also contribute to the thermal conductivity.
- Phonons are used as phonon-based sensors in sensing to detect change in temperature, pressure, or other physical properties. They can also be used in high-temperature superconductivity. They are used instead of photons to produce coherent sound waves in a process called phonon laser.
- Amorphous phonons can be used in thermics, where phonons play an important role in the conduction of heat in materials. Understanding and controlling the properties of amorphous phonons can lead to the development of materials with high thermal efficiency, useful in the fields of electronics, energy, and heat management.

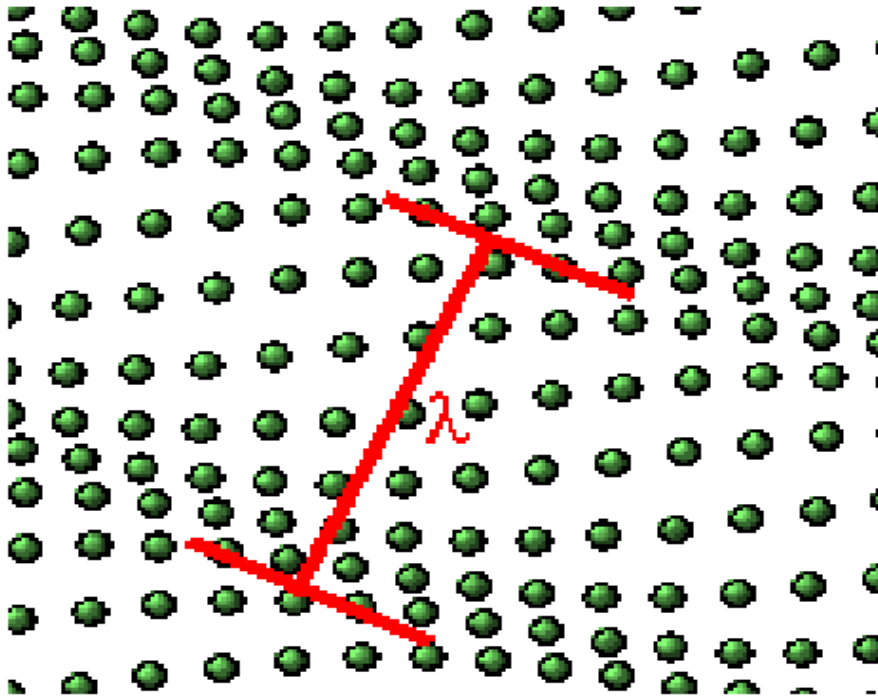


Figure 9 : Crystal lattice vibration [108]

1.2.2 CONCEPT OF POLARON

1.2.2.1 DEFINITION OF POLARON

To explain the concept of polaron, we begin first with the description of crystals. The structure of all crystals can be described in terms of a lattice (a lattice is a regular periodic array of point in space) with a group of atoms attached to every lattice point. The group of atoms is called basis, when repeated periodically in space it forms the crystal structure. At room temperature, the atoms are not fixed but vibrate around their equilibrium positions (the lattice points). Ionic polarization in the crystal occurs by the electric field of a conduction electron in which the electric field of the electron displaces the positive and negative ions with respect to one another (attracts the positive ions and repels the negative ions according to coulomb forces). This displacement can be described as cloud of phonons. A conduction electron or hole together with its self-induced polarization in a polar semiconductor or an ionic crystal forms a Polaron [109]. As a result of the formation of a polaron, the electron polarizes the lattice producing a potential well around itself in which it becomes trapped. The self-trapping is considered in ionic (polar) materials, so the notation "polaron" is due to this fact. This concept was first introduced by Landau [110].

1.2.2.2 CONCEPT AND REPRESENTATION

A charge placed in a polarizable medium is screened. Dielectric theory describes the Phenomenon by the induction of a polarization around the charge Carrier. The induced Polarization will follow the charge carrier when it is moving through the medium. The carrier together with its self-induced polarization is considered as one entity (Fig.10), named a polaron [111]. The physical properties of a polaron are different from those of a band-carrier. In particular, the polaron is characterized by its binding (or self-) energy, an effective mass and its characteristic response to external electric or magnetic fields (e.g. mobility and optical absorption coefficient). We have two types of polaron: the large or Fröhlich polaron (when the spatial extension of a polaron is large compared to the lattice parameter of the solid), and the small or Holstein polaron (when the self-induced polarization caused by an electron or a hole is of the order of the lattice parameter). The difference between the large polaron and small polaron is that small polaron are governed by short-range interactions. Historically, Fröhlich planned a Hamiltonian model to investigate a polaron in a continuum medium, he used the second quantization form of the electron lattice interaction (Eq.1a). Later, Landau and Pekar investigated the self-energy and the effective mass of the polaron, for what was shown by Fröhlich corresponding to the adiabatic or strong-coupling regime. This particular study made with free electron interacting with a dielectric polarizable continuum, described by the static dielectric constant ϵ_0 and the optical (or high frequency) dielectric constant ϵ_1 [110]. So we have three cases of the coupling regime: the weak coupling regime, strong coupling and intermediate coupling regime depending on the value of the coupling strength.

$$H = \frac{\hat{p}^2}{2m} + \sum_{\vec{k}} \hbar \omega_{\vec{k}} a_{\vec{k}}^+ a_{\vec{k}} + \sum_{\vec{k}} \left(V_{\vec{k}} a_{\vec{k}}^- e^{i\vec{k}\vec{r}} + V_{\vec{k}}^* a_{\vec{k}}^+ e^{-i\vec{k}\vec{r}} \right) \quad (1a),$$

$$V_{\vec{k}_j} = \frac{\hbar \omega_{LO}}{k_j} \left(\frac{4\pi\alpha}{V} \left(\frac{\hbar}{2m\omega_{LO}} \right)^{\frac{1}{2}} \right)^{\frac{1}{2}} \quad (1b),$$

$$\alpha = \frac{e^2}{2\hbar r_p \omega_{LO}} \left(\frac{1}{\epsilon_{\infty}} - \frac{1}{\epsilon_0} \right) \quad (1c),$$

r is the position coordinate operator of the electron with band mass m , P is its canonical conjugate momentum operator, k is the wave vector, $a_{\vec{k}}^+$ and $a_{\vec{k}}$ are the creation and annihilation operators for longitudinal optical phonons of wave-vector and phonon energy $\hbar\omega_{LO}$. With ω_{LO} the longitudinal optical frequency. The $V_{\vec{k}}$ are the Fourier components of the

electron phonon interaction (Eq. 1b). α is the dimensionless electron-LO phonon coupling strength (Eq. 1c). With $\varepsilon_\infty(\varepsilon_0)$, the high-frequency (static) dielectric constant of the medium

$r_p = \left(\frac{\hbar}{2m\omega_{LO}} \right)^{1/2}$ is the polaron radius.

1.2.2.3 APPLICATIONS

We have many extensions of the polaron concept such as acoustic polaron, piezoelectric polaron, electronic polaron, bound polaron, trapped polaron, spin polaron, molecular polaron, solvated polarons, polaronic exciton, Jahn-Teller polaron, small polaron, bipolarons and multi-polaron systems which are important [112]. These extensions of the concept are interested, for example, to study the properties of conjugated polymers, colossal magneto-resistive perovskites, high T superconductors, layered MgB₂ superconductors, fullerenes, quasi-1D conductors, semiconductor nanostructures. The physical properties of multi-polaron system has renewed interest due the fact that it is possible that polaron play a role in high-T superconductivity which could have important implications for energy generation and storage [113, 114]. Recents applications of polarons has been in the development of organic light emitting diodes, which are used in the displays of many modern electronic devices. By controlling the movement of polarons with the organic light emitting diodes, researchers have been able to improve their efficiency and brightness. Another application of polarons is in the development of quantum computing technologies by exploring the use of polarons as qubits due to their long coherence time and strong coupling to their environment. Polaron could also be used to transport information in electronic devices at a much higher speed than traditional electrons, this opens the door to significant advances in the field of telecommunications and computing. Due to its small size, polaron can be used to create nanoscale devices such as transistors, sensors optoelectronics components. These potential polaron applications could revolutionize the industry and open up new avenues for more advanced technologies. In addition, the polaron exhibits unique properties when it comes to electrical conductivity so, researchers are currently studying how to exploit these properties to improve the efficiency of solar cells for conversion devices. It can also be used in the field of medicine to selectively target and destroy certain cancer cells, providing new treatment approaches for cancer.

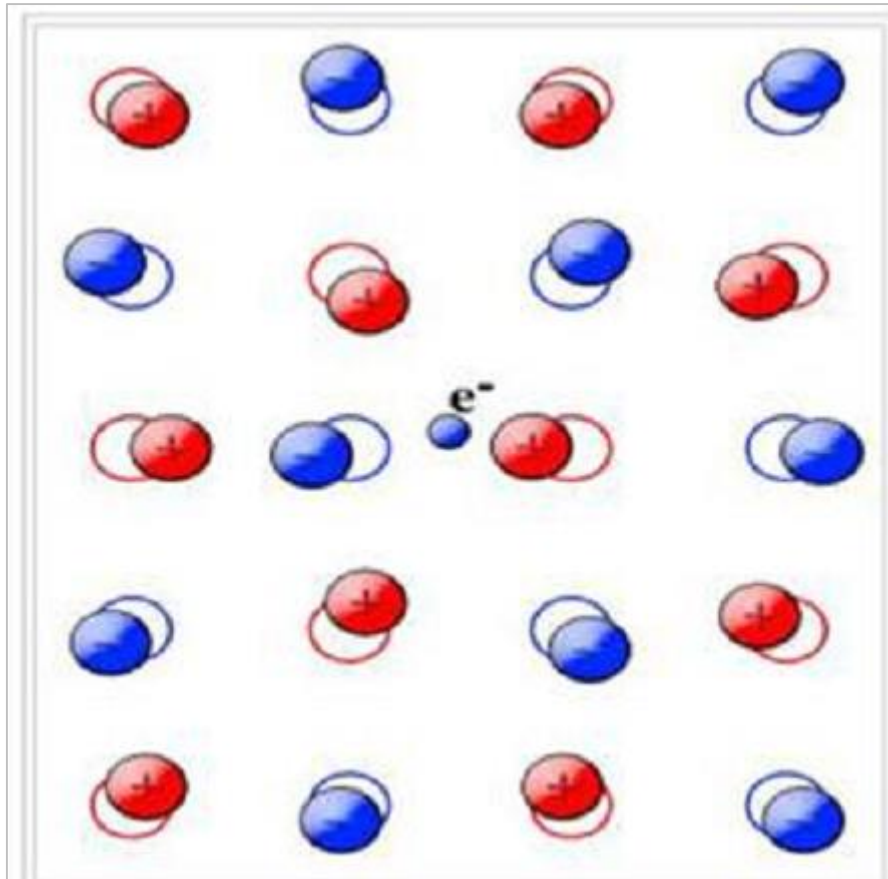


Figure 10 : formation of the polaron due to deformation of the crystal [111].

1.2.3 CONCEPT OF BIPOLARON

1.2.3.1 PRESENTATION AND DEFINITION OF BIPOLARON

For certain system parameters, two polarons with the same charge can become mutually coupled, forming a new type of a quasiparticle named bipolaron [115]. Therefore, the energy gains for creating a bipolaron from two separated polarons (Fig.11a) is the sum of the Coulomb repulsion which tends to separate polarons, and the lattice deformation energy gained by having two particles in the same potential well (Fig.11b). The bipolaron can also be form with two electrons or two holes localize at the same atomic site in the lattice. In this case, the bipolaron obtained is so-called one-center bipolaron [115]. Electron or hole bipolaron has an electric charge equal either to $2e^-$ or $2e^+$, respectively. The bipolarons obey to the Bose-Einstein stactistic because their spin is interger. Moreover, it is thought that at low temperatures they form a Bose condensate similarly to Cooper pairs in superconductors. Due to their unique properties bipolarons formation takes a special place in the polaron physics.

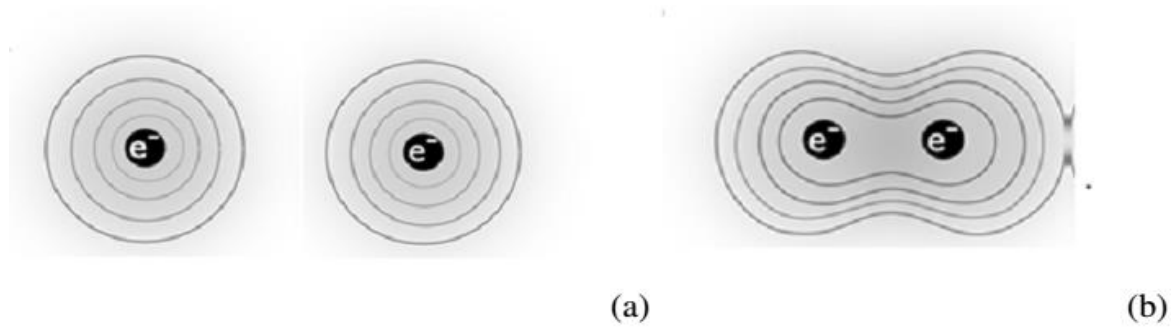


Figure 11 : Cartoon illustrating bipolaron formation. a) Two separated polarons each in its own polarisation well. b) Bipolaron where two electrons are localized in the same potential well [115].

A bipolaron is a bound pair of two electrons dressed with a cloud of virtual phonons [116]. Considering the electron-phonon coupling in bipolaron formation, the strong electron-phonon coupling receive intensive study in recent years due not only to general theoretical interest in the problem but also to its important applications. For a long time, calculation errors have been calling into the question of the possibility of bipolaron existence. So, the description of the bipolaron state start with the Hamiltonian proposed by Pekar and Frohlich made up of two electrons or holes interacting with a phonon cloud. After that, several researchers used used variational approach to describe the bipolaron with the wave function. Among those works, the energy of bound bipolaron was achieved in [117] with the use of wave function chosen in correlation with electron. Notice that there was no solutions in the case of weak and intermediate coupling constant α . So, the bound bipolaron state exist only for sufficiently large values of the coupling constanst ($\alpha = 5.2$) [118].

1.2.3.2 STABILITY OF BIPOLARON

In the Fröhlich approximation, a pair of electron or hole interacting with LO phonon in the continuum limit; is referred as Fröhlich bipolaron. The study is focused in optical phonon because in this context the polaronic effects are extremely important and should therefore be taken into consideration when making devices with them [116]. The stability of bipolaron in 2D and 3D in the Fröhlich approximation has been examined with the use of operator techniques where the center of mass of the bipolaron was approximately separated from the relative electron motion [119]. The result was similar to those obtained in [120, 121] using the Feynman path integral with bipolaron in 2D and 3D. Also, the stability of bipolaron was also investigated [122] in the path-integral representation; in this work the combined effect of optical phonons and acoustic phonons was analyzed. Early work on bipolarons had been based on

strong-coupling theory in which case the bipolaron stability was expressed with parameter $\eta = \epsilon_{\infty} / \epsilon_0$ and the confinement length of the quantum dot. Recently, investigation in graphene show that bipolaron stability depend on the strength of electron-phonon interactions. Thus, bipolarons are stable in graphene in presence of electric field lower than 3mV/A [123]. It turns out that the stability criteria of bipolaron depend of various parameters such as coupling constant α or others parameters of the system as confinement length, the electric field. The stability of bipolaron is influenced by the force of the interaction between the particles which compose it. A strong interaction favors the formation of a stable bipolaron, because it allows the particles to remain bound together despite possible external disturbances. The stability of bipolaron can also be affected by the environment it is in. temperature and density can play a crucial role in the formation and stability of bipolarons. For example, at low temperature, the interactions between the particles can be stronger and thus promote the formation of stable bipolarons. It is also important to note that the stability of the bipolaron can vary depending on the material in which it is formed. Some materials may promote the formation of stable bipolarons, while others may be less conducive to their existence.

1.2.3.3 APPLICATIONS

The bipolaron problem is interesting for both academic reasons and for its practical importance in polar semiconductors and semiconducting glass. However, above all, the discovery of the high temperature superconductivity in CuO₂ based layered ceramic materials and the subsequent proposal of the bipolaronic mechanism for pairing has made the bipolaron problem most fascinating and has brought it to the forefront of the current research [116]. In particular, the search for alternative microscopic mechanism for high T_C superconductivity has stimulated a renewed interest in the bipolaron problem. So, bipolaron is useful in high temperature superconductivity in the models with pierls-like coupling at low carrier density [124]. Bipolaron is also helpful in tunneling experiments or in transport through molecular dots, but also to its important applications, such as a treatment of high-temperature superconductivity.

If many bipolarons form but are not too close, they are likely to form a Bose-Einstein condensate. This led that bipolarons could be a mechanism for superconductivity at high temperature. This could, for example, lead to a very direct interpretation of the isotopic effect. The theory of bipolaron explains some thermodynamic properties of high-temperature superconductivity such as availability and value of the jump in the heat capacity which is

lacking in the theory of the condensation of an ideal gas. The theory explains the occurrence of a gap and a pseudogap in high-temperature superconductivity materials. Bipolaron is necessary to explain the experiments on high-temperature superconductors, the possible ways of raising the critical temperature of the high-temperature superconductors [125]. Bipolarons are responsible for electrical conduction in semiconductor polymers. The formation of bipolarons is characterized by the appearance of states located on the chains and is manifested by the appearance in the forbidden band of discrete states or even at higher concentrations of the polaronic bands. These polaronic bands should allow a metallic behaviour.

1.2.4 CONCEPT OF EXCITON-POLARON

1.2.4.1 CONCEPT OF EXCITON

Excitons are very interesting physical entities that, in polarizable media, are relevant for polarons: in polar systems, they can be apprehended as two polarons interacting with opposite charges. The energy excentric from the ground in a polar crystal was determined taking into account that the potential energy of the electron-hole interaction depending on the quantum state of the particles in question [126, 127]. Later, many books have been devoted to this problem. Similar considerations were applied [128] to explain the dependence of the binding energy of an excited-ionized donor complex on the electron-hole mass ratio in CdS and TiCl, and to show that ratio of the binding energy of D-centers to that of neutral donors in AgBr and AgCl is up to an order of magnitude larger than in the non-polar crystal [129]. An exciton is a coulombically bound electron-hole pair that is generated in a material either by light absorption or electrical charge injection. Excitonic materials can be very efficient absorbers of light, possess high light emission yields, and exhibit a variety of unique optical phenomena, such as up- and down- conversion, that can enable new technologies to move beyond the efficiency limits of the existing material.

For an excitonic system with elementary charge in a medium with dielectric constant and reduced mass, the ground state Bohr radius is given by:

$$a = \frac{\hbar^2 \epsilon}{\mu e^2} \quad (2).$$

There are two types of excitons which are characterized by the ratio between the excitonic Bohr radius and the lattice constant: Wannier-Mott Exciton and Frenkel Excitons. When the Bohr radius is larger than the lattice, we have the Wannier-Mott Exciton, it has a smaller binding

energy and is delocalized over a number of lattice sites. Both the electron and the hole are mobile. The underlying lattice of atoms is treated as a background field in which the electrons and the holes exist as free particles, and an exciton consists of an electron and a hole orbiting each other in this medium [130]. In contrast, if the Bohr radius is smaller than lattice, we have Frenkel exciton; such exciton is strongly bound and usually localized on one site. The electron and the hole do not move independently. The motion of Frenkel excitons is viewed as hopping of both the electron and the hole from one atom to another. If an electron is excited from a valence shell of an atom into an excited state of a nearby atom, the Coulomb repulsion of the electron on the valence electrons of the new atom will be tied to push one of them into the hole left in the valence shell of the original atom when the electron was excited.

1.2.4.2 FORMATION OF EXCITON POLARON

Exciton-polaron is a hypothetical many-body quasiparticle that involves an exciton dressed with a polarized electron-hole cloud. the exciton-polaron is formed when exciton interact with acoustic or optical phonons via coupling to the deformation potentials associated with the conduction and valence band. The exciton and its accompanying lattice distortion can be conceptualized as a dressed particle or excitonic-polaron, with a self-energy and a renormalized mass. The formation of a composite exciton-polaron has been examined in material systems of various configurations [131-133]. The theory of three-dimensional excitonic polarons (excitons interacting with phonons in bulk) has been well developed and have shown that the subsequent behaviour of an exciton gets modified depending on its strength of interaction with phonons. Exciton-phonon interactions, in particular, play an important role in the optical and intrinsic transport properties of material systems. The exciton effective mass and energy undergo shifts which are dependent on the strength of the exciton-phonon coupling.

1.3 DECOHERENCE

1.3.1 DEFINITION

When a system interacts with its environment, a decoherence process occurs. Decoherence is the process by which the quantum properties of a system interact with its environment, causing the quantum state to become mixed or entangled with the state of the environment. This process can cause the quantum state to collapse into a classical state and can make it difficult to observe and manipulate quantum system. Decoherence is a process that occurs in quantum systems whereby the coherence between different states become disrupted by the system's interaction with environment. Thus results in the loss of quantum information

and the emergence of classical behavior. Whereas the quantum coherence is a property of quantum systems that allows them to maintain a stable and coordinated state over time. It refers to the ability of quantum particles to maintain their relative phase relationship, even as they interact with their environment. In quantum mechanics, quantum decoherence is the loss of coherence or ordering of the phase angles between the components of a system in a quantum superposition. The study of decoherence, though based at the heart of quantum theory, is a relatively young subject. It was initiated in the 1970s and 1980 with the work of Zeh and Zurek on the emergence of the classicality in the quantum framework. It is a ubiquitous phenomenon in quantum systems, and it is often characterized by various parameters such as transition frequency, density probability, Shannon entropy, decoherence time, coherence time, environment coupling strength and decoherence rate.

1.3.2 DECOHERENCE PARAMETERS

Decoherence is characterized by various parameters: The transition frequency which refers to the rate at which the quasiparticles transit between two states. The transition frequency can be used to measure how quickly a quantum system loses coherence, and thus how quickly decoherence occurs. The Shannon entropy is the measure of the amount of uncertainty or information in a system. In the case of the quantum system, the Shannon entropy can be used to measure how much information is lost due to decoherence. The higher the entropy, the more information is lost and the greater the level of decoherence. Density probability is the probability of finding a particle at a particular location in space. Decoherence time and decoherence rate are terms used in quantum mechanics to describe the loss of coherence in a quantum system due to its interaction with environment. Decoherence time refers to the amount of time it takes for a quantum system to lose its coherence, while decoherence rate refers to the rate at which coherence is lost. The coherence time is a measure of how long the system can maintain its quantum state before it becomes too entangled with its environment, causing it to lose its coherence and become a classical system. An example of a quantum system where decoherence can occur via those parameters is the well-known quantum qubit which is formed by the superposition of two states in a quantum system. In order to restrain the decoherence processes, several authors achieved some useful results in investigating respectively the effects of pseudo-harmonic potential [134], of temperature and electric field [135], and a magnetic field [136] on the properties of quantum pseudodot qubit, and the properties of an unsymmetrical parabolic quantum dot qubit [137] and a Coulomb bound potential quantum rod qubit [138]. However, most research works are focused on the properties of the ground and the

first excited states, instead of the quantum transition of the electron in an anisotropic quantum dot. To further reveal the factors and conditions which affect the state properties of the electron, the influences of the transverse confinement length, the longitudinal confinement length, the electron-phonon coupling strength, the oscillation period, and the transition probability of the electron in anisotropic quantum dot are studied [139].

At the heart of quantum mechanical theory is the superposition principle. The power of quantum computers lies in the quantum bit (qubit), a superposition of the classical bit of 1 and 0. The two level system is employed as an elementary unit in storing information. The name qubit to two state memory cell formed from the superposition of states was first given by Schumacher. It is employed as the elementary unit of storing information.

$$|\psi\rangle = \alpha|0\rangle + \beta|1\rangle \quad (3),$$

here α and β are complex numbers with normalization condition $\alpha^2 + \beta^2 = 1$. The bra-ket notation is tailor-made for the description of closed mechanical system. When considering an open system, the ket notation becomes less suitable. The unlimited amount of states that a qubit can take at any time can be traditionally represented by the sphere where the north-pole is 1 and the south pole 0. Any amount of numbers can be between one and zero. A classical bit can have only two states; 1 or 0. It can be represented by a transistor switch set of on and off

1.3.3 APPLICATION OF DECOHERENCE

Decoherence has a variety of applications in science and technology including quantum teleportation, quantum information and computation, entangled states, and the quantum-classical interface. Decoherence represents a challenge for the practical realization of quantum computers since such machines are expected to rely heavily on the undisturbed evolution of quantum coherences. The development of quantum computers is still in its infancy, but experiments have been carried out in which quantum computational operations were executed on a very small number of quantum bits [140, 141]. For the implementation of a quantum computer, high quantum coherence semiconductors quantum dot is needed [142]. It is necessary to note that the environment coupling for the case of atoms can be strongly suppressed by ultrahigh vacuum and ultralow temperature. For the case of artificial atoms, the problem seems to be different due to the fact that the atoms are intimately incorporated in the surrounding solid-state environment and suffer from various decoherence channels. This happens even for optical excitation of electron-hole pairs in the states of lowest energy, for example, the exciton or

biexciton ground state, which causes the deformation of the surrounding lattice (i.e., formation of a polaron state) whereas relaxation is completely inhibited because of the atomic-like carrier density of states.

In coherent optical spectroscopy [143], which is sensitive to the optically induced coherence, this partial transfer of quantum coherence from the electron hole state to the lattice degrees of freedom (i.e. phonons), results in dephasing [142]. Since the electronic (or excitonic) states in a system of quantum dots are designed to play the role of qubits which must be manipulated with great precision, the exact knowledge of the energetic spectrum of a quantum dot is of major importance. Moreover, because of the necessary quantum coherence during quantum computing processes, the interaction between the localized electron and the surrounding medium must be well understood. Also decoherence is used to determine the system's ability to perform quantum computation, to ensure the security of communication channels by detecting and correcting errors caused by environmental noise in cryptography. Qubits find applications in many fields as seen in the following: Quantum dots (nanocrystal) are used in LEDs and Lasers [144] Quantum dots realized by epitaxy which are of interest in our studies are frequently used in optoelectronics.

Decoherence is a difficult problem to solve, but there are some things we can do to reduce their effects. For example, we can implement error correcting codes, which can be necessary to protect the system against quantum noise and mitigate the effects of the decoherence. We can also use technique such as dynamical decoupling or quantum error correction, which can help to suppress decoherence by actively working to reduce the interaction between the system and its environment. Another method is to try to improve the coherence time of the system by using high quality qubits or by optimizing the experimental setup.

CONCLUSION

In this chapter, we presented the generalities on nanostructures and quasiparticles, precisely polaron, bipolaron and exciton-polaron. We have presented some notion on decoherence. In the next chapter we will present an overview on mathematics tools, some quasiparticles parameters useful to describe the dynamic and decoherence of those quasiparticles. We will also model each of our system by an appropriate Hamiltonian, and by using the above mathematics tools, we will investigate the states energy for each system.

CHAPTER 2: MATHEMATICAL TOOLS AND THEORITICAL MODELS

INTRODUCTION

In the earlier chapter, we presented the overviews on Transition Metal Dichalcogenides, quasiparticles such as polaron, bipolaron and exciton polaron and decoherence parameters. This chapter is devoted firstly, to present an overview on variational method such as Lee Low Pine (LLP) method of a polaron in the weak coupling regime, the Huybrecht method well known as the modified Lee Low Pine method proposed by Huybrecht for all coupling regime and the Pekar variational method for strong coupling regime, secondly to present some parameters of quasiparticles and finally to model each of our system and investigate some parameters by using the above variational methods.

2.1 VARIATIONALS METHODS

The variational methods make it possible to determine the energies of the ground and first excited state using trial function which is a linear combination of basis function. These methods are often used for complex system where it is difficult to solve the Schrodinger equation exactly, so these methods find an approximate solution for the system using optimal trial function. The limit of those variational methods depends on the accuracy of the approximations used in the calculations, the complexity of the system being studied, and the computational resources available. Although more advanced methods such as the Monte Carlo method, the density functional theory method are more precise and efficient than variational methods in solving complex systems, they can be more expensive in terms of calculations time and computing resources. Thus, to use variational method, it would be wise to choose a good trial function for the system to be studied because this can have a significant impact on the precision of the results, also optimizing the parameters of the trial function makes it possible to improve the precision of the results using variational methods. So, the trial function is chosen so as to minimize the total energy of the system.

2.1.1 HAMILTONIAN

2.1.1.1 HAMILTONIAN OF AN ELECTRON

The Hamiltonian of a free electron or free hole in a medium is given as follow:

$$H_e = \frac{\hat{p}^2}{2m} \quad (4),$$

whith m being the mass of electron or hole and \hat{p} the kinetic momentum of the electron or the hole.

2.1.1.2 HAMILTONIAN OF PHONON

The energy of the phonon changes with the advancement of the lattice polarization vector is given as:

$$E_{ph} = \frac{M}{2} \int [\dot{\hat{p}}^2(r) + \omega^2 \hat{p}^2(r)] dr \quad (5),$$

$$\text{with } \begin{cases} \bar{P}(r) = \frac{1}{4\pi\epsilon} \bar{D} \\ \frac{1}{\epsilon} = \frac{1}{\epsilon_\infty} - \frac{1}{\epsilon_0} \end{cases} \quad (6),$$

\bar{D} is the electric induction, r is the position of the electron, ω is the frequency of the phonon, ϵ , ϵ_0 and ϵ_∞ are respectively the polarizability of the medium, the polarizability of the vacuum and the polarizability at infinity. The Hamiltonian of lattice vibration is equal to the phonon Hamiltonian and can be written as follow:

$$H_{ph} = \frac{M}{2} \int [\dot{\hat{p}}^2(r) + \omega^2 \hat{p}^2(r)] dr \quad (7).$$

$$\text{Let us consider } \begin{cases} \dot{y}(r) = \frac{\partial H_{ph}}{\partial \hat{p}(r)} = M\dot{\hat{p}}(r) \\ x(r) = \hat{p}(r) \end{cases} \quad (8),$$

thus, we can write the Hamiltonian of the phonon as follow:

$$H_{ph} = \frac{1}{2} \int \left[\frac{y^2(r)}{M} + M\omega^2 x^2(r) \right] dr \quad (9),$$

$$H_{ph} = \frac{1}{2} \sum_k \hbar\omega_k \left[\left(\sqrt{\frac{M\omega_k}{2\hbar}} x_k - i \sqrt{\frac{1}{M\hbar\omega_k}} y_k \right) \left(\sqrt{\frac{M\omega_k}{2\hbar}} x_k + i \sqrt{\frac{1}{M\hbar\omega_k}} y_k \right) \right] \quad (10),$$

k is the wave vector of phonon with frequency ω , x_k and y_k are canonical variables then the Hamiltonian of phonon takes the following form:

$$H_{ph} = \sum_k \hbar\omega_k a_k^+ a_k \quad (11),$$

with

$$\begin{aligned} a_k^+ &= \sqrt{\frac{M\omega_k}{2\hbar}} x_k - i \sqrt{\frac{1_k}{M\hbar\omega_k}} y_k \\ a_k &= \sqrt{\frac{M\omega_k}{2\hbar}} x_k + i \sqrt{\frac{1_k}{M\hbar\omega_k}} y_k \end{aligned} \quad (12).$$

2.1.1.3 HAMILTONIAN OF ELECTRON-PHONON INTERACTION

Let us consider a model where an electron interact with the dielectric polarization labelled by the polarizability of the vacuum \mathcal{E}_0 and the polarizability at infinity \mathcal{E}_∞ . If the carriers interact with optical phonons in the ionic crystal under the condition that the lattice constant is small compared to the size of the self-trapped state, so the lattice discreteness is unrelated. The ionic crystal can be considering as a polarizable dielectric continuum, notice that only ionic part contributes to the polaron state formation. During the relaxation time, the polaron can moves a distance less than the polaron radius, thus the polarization will follow the polaron motion and is defined by the following expression:

$$\rho(r) = \text{div} \vec{P}(r) \quad (13),$$

the Hamiltonian of interaction between the field and the charge is given as:

$$H_{\text{int}} = -eV(r), \quad e > 0 \quad (14),$$

where $V(r)$ is the electron potential in the crystal field given as follow:

$$\nabla^2 V(r) = -4\pi\rho = 4\pi \text{div} \vec{p}(r) \quad (15),$$

Or

$$\nabla V(r) = -4\pi\vec{p}(r) \quad (16).$$

Notice that in perfect crystal, due to translational symmetry, polaron can move, thus the dynamical deformation does not perfectly follow the polaron motion. The delay is responsible

for the polaron mass enhancement. Inside the continuum harmonic approximation, the energy of the phonon changes with the progression of the lattice polarization vector $\vec{p}(r)$:

$$H_{ph} = \frac{M}{2} \int \left[\dot{\vec{P}}^2(r) - \omega^2 \vec{P}^2(r) \right] dr \quad (17).$$

If we consider the ionic part of the total polarization we have a relation between $\vec{P}(r)$ and $\vec{D}(r)$ as given in Eq. (6), this relation permits to find the deformation potential energy of the ionic polarization of the crystal. By quantizing the phonon energy, we obtained the same expression as in Eq. (11). In the second quantization, the electron-phonon interaction Hamiltonian is given after using Fourier series for and is expressed through bosonic variables may now take the following form:

$$H_{int} = H_{e-ph} = \sum_{\vec{k}} V_{\vec{k}} a_{\vec{k}}^- e^{i\vec{k}r} + V_{\vec{k}}^* a_{\vec{k}}^+ e^{-i\vec{k}r} \quad (18).$$

2.1.2 LEE-LOW PINES VARIATIONAL METHOD

Let us consider a free electron in movement in a polar crystal. The Fröhlich Hamiltonian has three parts: The Hamiltonian of the electron; the Hamiltonian of the phonon and the Hamiltonian of interaction (electron-phonon). Thus the total Hamiltonian can be write using Eqs. (4), (11) and (18) as follow:

$$H = \frac{\hat{p}^2}{2m} + \sum_{\vec{k}} \hbar \omega a_{\vec{k}}^- a_{\vec{k}}^+ + \sum_{\vec{k}} \left(V_{\vec{k}} a_{\vec{k}}^- e^{i\vec{k}\vec{r}} + V_{\vec{k}}^* a_{\vec{k}}^+ e^{-i\vec{k}\vec{r}} \right) \quad (19),$$

where

$$V_{\vec{k}} = -i \frac{\hbar \omega}{k} \left(\frac{\hbar}{2m\omega} \right)^{\frac{1}{4}} \left(\frac{4\pi\alpha}{V} \right)^{\frac{1}{2}} \quad (20),$$

and

$$\alpha = \frac{e^2}{\hbar} \left(\frac{m}{\hbar\omega} \right)^{\frac{1}{2}} \left(\frac{1}{\epsilon_{\infty}} - \frac{1}{\epsilon_0} \right) \quad (21),$$

α is the coupling element for electron-phonon interaction, r is the position coordinate operator of the electron with mass m , \hat{p} is momentum operator, $a_{\vec{k}}^+$ and $a_{\vec{k}}$ are the creation and annihilation operators for phonons of wave-vector k and phonon energy $\hbar\omega$, with ω the

frequency. V_k are Fourier components of the electron phonon interaction, V is the volume of the crystal.

We apply the LLP method [145] to Hamiltonian given by Eq. (19). The total momentum operator is obtained as follows:

$$\vec{P} = \sum_{\vec{k}} \hbar \vec{k} a_{\vec{k}}^- a_{\vec{k}}^+ + \vec{p} \quad (22),$$

where the momentum of the electron is given by: $\vec{p} = -i\hbar \vec{\nabla}$. Then we apply the unitary transformation

$$\Phi = \vec{U}_1 \Psi \quad (23),$$

where the wave function Φ is obtained by solving the following Schrödinger equation

$$H\Phi = E\Phi \quad (24).$$

The first canonical transformation of LLP necessary to eliminate the electron coordinate from Eq. (19) is given as:

$$U_1 = \exp \left\{ \frac{i}{\hbar} \left(\vec{p} - \sum_{\vec{k}} \hbar \vec{k} a_{\vec{k}}^- a_{\vec{k}}^+ \right) \cdot \vec{r} \right\} \quad (25),$$

applying this first transformation on different operators we obtained:

The electron momentum operator is:

$$U_1^{-1} \vec{p} U_1 = \vec{p} - \sum_{\vec{k}} \hbar \vec{k} a_{\vec{k}}^- a_{\vec{k}}^+ \quad (26),$$

then we obtain:

$$U_1^{-1} \vec{p}^2 U_1 = \left(\vec{p} - \sum_{\vec{k}} \hbar \vec{k} a_{\vec{k}}^- a_{\vec{k}}^+ \right)^2 \quad (27),$$

the phonon operator is

$$U_1^{-1} a_{\vec{k}}^- U_1 = a_{\vec{k}}^- e^{-i\vec{k}\vec{r}} \quad (28),$$

$$U_1^{-1} a_{\vec{k}}^+ a_{\vec{k}}^- U_1 = U_1^{-1} a_{\vec{k}}^+ U_1 U_1^{-1} a_{\vec{k}}^- U_1 = a_{\vec{k}}^- e^{-i\vec{k}\vec{r}} a_{\vec{k}}^+ e^{i\vec{k}\vec{r}} = a_{\vec{k}}^+ a_{\vec{k}}^- \quad (29),$$

$$U_1^{-1} \left(V_{\vec{k}} a_{\vec{k}} e^{i\vec{k}\vec{r}} + V_{\vec{k}}^* a_{\vec{k}}^+ e^{-i\vec{k}\vec{r}} \right) U_1 = V_{\vec{k}} U_1^{-1} a_{\vec{k}} U_1 e^{i\vec{k}\vec{r}} + V_{\vec{k}}^* U_1^{-1} a_{\vec{k}}^+ U_1 e^{-i\vec{k}\vec{r}} = V_{\vec{k}} a_{\vec{k}} + V_{\vec{k}}^* a_{\vec{k}}^+ \quad (30),$$

Combining eqs. (26), (27), (28), (29) and (30), one gets

$$H_1 = U_1^{-1} H U_1 = \frac{\left(\hat{p} - \sum_{\vec{k}} \hbar \vec{k} a_{\vec{k}} a_{\vec{k}}^+ \right)^2}{2m} + \sum_{\vec{k}} \hbar \omega_{\vec{k}} a_{\vec{k}}^+ a_{\vec{k}} + \sum_{\vec{k}} \left(V_{\vec{k}} a_{\vec{k}} + V_{\vec{k}}^* a_{\vec{k}}^+ \right) \quad (31).$$

According to Fröhlich perturbation analysis, the number of virtual phonon is not negligible in the intermediate coupling regime then it is not possible to apply perturbation theory to the Hamiltonian given by Eq. (31). But it is possible to eliminate with the canonical transformation the main part of the interaction term of Hamiltonian. For the case LLP we use a variational method of calculation with a trial wave function chose as follow:

$$\Psi = U_2 |0\rangle \quad (32),$$

where $|0\rangle$ is the vacuum state of phonon satisfying the following condition:

$$a_{\vec{k}} |0\rangle = 0, \quad \langle 0|0\rangle = 1, \quad (33).$$

The second canonical transformation corresponding to this variational method is:

$$U_2 = \exp \left[\sum_{\vec{k}} \left(a_{\vec{k}}^+ f_{\vec{k}} + a_{\vec{k}} f_{\vec{k}}^* \right) \right] \quad (34),$$

where $f_{\vec{k}}$ is a variational function obtained by minimizing of the ground state energy. U_2 is use to displace the operator $a_{\vec{k}}$ and $a_{\vec{k}}^+$, thus we have:

$$\begin{cases} U_2^{-1} a_{\vec{k}} U_2 = a_{\vec{k}} + f_{\vec{k}} \\ U_2^{-1} a_{\vec{k}}^+ U_2 = a_{\vec{k}}^+ + f_{\vec{k}}^* \end{cases} \quad (35).$$

2.1.2.1 GROUND STATE ENERGY

The ground state energy is given as:

$$E = \langle \Psi | H | \Psi \rangle = \langle 0 | U_2^{-1} H U_2 | 0 \rangle \quad (36),$$

using Eq. (35), Eq. (31) is transformed as follow:

$$H_2 = U_2^{-1} H_1 U_2 = \frac{\left[\hat{p} - \sum_{\vec{k}} \hbar \vec{k} (a_{\vec{k}}^+ + f_{\vec{k}}^*) (a_{\vec{k}} + f_{\vec{k}}) \right]^2}{2m} + \sum_{\vec{k}} \hbar \omega (a_{\vec{k}}^+ + f_{\vec{k}}^*) (a_{\vec{k}} + f_{\vec{k}}) + \sum_{\vec{k}} \left[V_{\vec{k}} (a_{\vec{k}} + f_{\vec{k}}) + V_{\vec{k}}^* (a_{\vec{k}}^+ + f_{\vec{k}}^*) \right] \quad (37),$$

after development, we obtain:

$$H_2 = \frac{\left[\hat{p} - \sum_{\vec{k}} \hbar \vec{k} a_{\vec{k}}^+ a_{\vec{k}} - \sum_{\vec{k}} \hbar \vec{k} |f_{\vec{k}}|^2 - \sum_{\vec{k}} \hbar \vec{k} (a_{\vec{k}}^+ + f_{\vec{k}}^*) (a_{\vec{k}} + f_{\vec{k}}) \right]^2}{2m} + \sum_{\vec{k}} \hbar \omega (a_{\vec{k}}^+ a_{\vec{k}} + a_{\vec{k}}^+ f_{\vec{k}} + a_{\vec{k}} f_{\vec{k}}^* + f_{\vec{k}}^* f_{\vec{k}}) + \sum_{\vec{k}} \left[V_{\vec{k}} (a_{\vec{k}} + f_{\vec{k}}) + V_{\vec{k}}^* (a_{\vec{k}}^+ + f_{\vec{k}}^*) \right] \quad (38),$$

then the expression in Eq. (38) can be separate into two part: $H_2 = H' + H''$ where

$$H' = \frac{\left[\hat{p} - \sum_{\vec{k}} \hbar \vec{k} a_{\vec{k}}^+ a_{\vec{k}} \right]^2}{2m} + \frac{\left[\sum_{\vec{k}} \hbar \vec{k} |f_{\vec{k}}|^2 \right]^2}{2m} + \sum_{\vec{k}} (V_{\vec{k}} f_{\vec{k}} + V_{\vec{k}}^* f_{\vec{k}}^*) + \sum_{\vec{k}} |f_{\vec{k}}|^2 \left\{ \hbar \omega - \frac{\hbar \vec{k} \cdot \hat{p}}{m} + \frac{\hbar^2 k^2}{2m} \right\} + \frac{\hbar^2 k^2}{2m} \sum_{\vec{k}} \vec{k} a_{\vec{k}}^+ a_{\vec{k}} \cdot \sum_{\vec{k}'} \vec{k}' |f_{\vec{k}'}|^2 + \sum_{\vec{k}} a_{\vec{k}} \left[V_{\vec{k}} + f_{\vec{k}}^* \left\{ \hbar \omega - \frac{\hbar \vec{k} \cdot \hat{p}}{m} + \frac{\hbar^2 k^2}{2m} + \frac{\hbar^2 \vec{k}}{m} \cdot \sum_{\vec{k}'} \vec{k}' |f_{\vec{k}'}|^2 \right\} \right] + \sum_{\vec{k}} a_{\vec{k}}^+ \left[V_{\vec{k}}^* + f_{\vec{k}} \left\{ \hbar \omega - \frac{\hbar \vec{k} \cdot \hat{p}}{m} + \frac{\hbar^2 k^2}{2m} + \frac{\hbar^2 \vec{k}}{m} \cdot \sum_{\vec{k}'} \vec{k}' |f_{\vec{k}'}|^2 \right\} \right] + \sum_{\vec{k}} \hbar \omega a_{\vec{k}}^+ a_{\vec{k}} \quad (39),$$

and

$$H'' = \sum_{\vec{k}, \vec{k}'} \frac{\hbar^2 \vec{k} \cdot \vec{k}'}{2m} \left[a_{\vec{k}} a_{\vec{k}'} f_{\vec{k}}^* f_{\vec{k}'}^* + 2a_{\vec{k}}^+ a_{\vec{k}'} f_{\vec{k}}^* f_{\vec{k}'} + a_{\vec{k}}^+ a_{\vec{k}'}^+ f_{\vec{k}} f_{\vec{k}'} \right] + \sum_{\vec{k}, \vec{k}'} \frac{\hbar^2 \vec{k} \cdot \vec{k}'}{2m} \left[a_{\vec{k}}^+ a_{\vec{k}'} a_{\vec{k}'} f_{\vec{k}}^* + a_{\vec{k}}^+ a_{\vec{k}'}^+ a_{\vec{k}} f_{\vec{k}'} \right] \quad (40),$$

using Eq. (33), we obtain from Eq. (36) that

$$E = \frac{P^2 + \left[\sum_{\vec{k}} \hbar \vec{k} |f_{\vec{k}}|^2 \right]^2}{2m} + \sum_{\vec{k}} (V_{\vec{k}} f_{\vec{k}} + V_{\vec{k}}^* f_{\vec{k}}^*) + \sum_{\vec{k}} |f_{\vec{k}}|^2 \left\{ \hbar \omega - \frac{\hbar \vec{k} \cdot \hat{p}}{m} + \frac{\hbar^2 k^2}{2m} \right\} \quad (41),$$

Then minimize Eq. (41) and setting that

$$\frac{\partial E}{\partial f_{\vec{k}}} = \frac{\partial E}{\partial f_{\vec{k}}^*} = 0 \quad (42),$$

we have

$$V_{\vec{k}} + f_{\vec{k}}^* \left\{ \hbar\omega - \frac{\hbar\vec{k} \cdot \hat{p}}{m} + \frac{\hbar^2 k^2}{2m} + \frac{\hbar^2}{m} \left(\sum_{\vec{k}'} \vec{k}' |f_{\vec{k}'}|^2 \right) \cdot \vec{k} \right\} = 0 \quad (43)$$

then

$$f_{\vec{k}}^* = - \frac{V_{\vec{k}}}{\left\{ \hbar\omega - \frac{\hbar\vec{k} \cdot \hat{p}}{m} + \frac{\hbar^2 k^2}{2m} + \frac{\hbar^2}{m} \left(\sum_{\vec{k}'} \vec{k}' |f_{\vec{k}'}|^2 \right) \cdot \vec{k} \right\}}. \quad (44)$$

Let introduce a new parameter η associated to \hat{p} because the only preferred direction in this problem is \hat{p}

$$\eta \hat{p} = \sum_{\vec{k}} \hbar \vec{k} |f_{\vec{k}}|^2 \quad (45)$$

thus, Eq. (44) becomes

$$f_{\vec{k}}^* = - \frac{V_{\vec{k}}}{\left\{ \hbar\omega - \frac{\hbar\vec{k} \cdot \hat{p}}{m} (1-\eta) + \frac{\hbar^2 k^2}{2m} \right\}} \quad (46)$$

the ground state energy of the system which is given by Eq. (41) satisfying Eq. (46). Using Eq. (46), Eq. (41) can be rewritten as follows:

$$E = \frac{P^2 + (\eta \hat{p})^2}{2m} - 2 \sum_{\vec{k}} \frac{|v_{\vec{k}}|^2}{\hbar\omega - \frac{\hbar\vec{k} \cdot \hat{p}}{m} (1-\eta) + \frac{\hbar^2 k^2}{2m}} + \sum_{\vec{k}} \frac{|v_{\vec{k}}|^2}{\left(\hbar\omega - \frac{\hbar\vec{k} \cdot \hat{p}}{m} (1-\eta) + \frac{\hbar^2 k^2}{2m} \right)^2} \left\{ \hbar\omega - \frac{\hbar\vec{k} \cdot \hat{p}}{m} + \frac{\hbar^2 k^2}{2m} \right\} \quad (47)$$

then we have:

$$E = \frac{P^2 (1+\eta^2)}{2m} - 2 \sum_{\vec{k}} \frac{|v_{\vec{k}}|^2}{\hbar\omega - \frac{\hbar\vec{k} \cdot \hat{p}}{m} (1-\eta) + \frac{\hbar^2 k^2}{2m}} + \sum_{\vec{k}} \frac{|v_{\vec{k}}|^2}{\left(\hbar\omega - \frac{\hbar\vec{k} \cdot \hat{p}}{m} (1-\eta) + \frac{\hbar^2 k^2}{2m} \right)^2} \left\{ \hbar\omega - \frac{\hbar\vec{k} \cdot \hat{p}}{m} + \frac{\hbar^2 k^2}{2m} \right\} \quad (48)$$

introducing the parameter η in the Eq. (48) we obtain:

$$E = \frac{P^2 (1+\eta^2)}{2m} - 2 \sum_{\vec{k}} \frac{|v_{\vec{k}}|^2}{\hbar\omega - \frac{\hbar\vec{k} \cdot \hat{p}}{m} (1-\eta) + \frac{\hbar^2 k^2}{2m}} + \sum_{\vec{k}} \frac{|v_{\vec{k}}|^2 \left(\hbar\omega + \frac{\hbar^2 k^2}{2m} \right)}{\left(\hbar\omega - \frac{\hbar\vec{k} \cdot \hat{p}}{m} (1-\eta) + \frac{\hbar^2 k^2}{2m} \right)^2} - \frac{P^2}{m} \eta \quad (49)$$

then Eq. (48) can be rewritten as follow:

$$E = \frac{P^2(1-\eta^2)}{2m} - 2 \sum_{\vec{k}} \frac{|v_{\vec{k}}|^2}{\hbar\omega - \frac{\hbar\vec{k}\cdot\hat{p}}{m}(1-\eta) + \frac{\hbar^2k^2}{2m}} + \sum_{\vec{k}} \frac{|v_{\vec{k}}|^2 \left(\hbar\omega + \frac{\hbar^2k^2}{2m} \right)}{\left(\hbar\omega - \frac{\hbar\vec{k}\cdot\hat{p}}{m}(1-\eta) + \frac{\hbar^2k^2}{2m} \right)^2} \quad (50),$$

after a few calculations, we obtained:

$$E = \frac{P^2(1-\eta^2)}{2m} - 2 \sum_{\vec{k}} \frac{|v_{\vec{k}}|^2}{\hbar\omega - \frac{\hbar\vec{k}\cdot\hat{p}}{m}(1-\eta) + \frac{\hbar^2k^2}{2m}} + \sum_{\vec{k}} \frac{|v_{\vec{k}}|^2 \left(\hbar\omega + \frac{\hbar^2k^2}{2m} - \frac{\hbar\vec{k}\cdot\hat{p}}{m}(1-\eta) + \frac{\hbar\vec{k}\cdot\hat{p}}{m}(1-\eta) \right)}{\left(\hbar\omega - \frac{\hbar\vec{k}\cdot\hat{p}}{m}(1-\eta) + \frac{\hbar^2k^2}{2m} \right)^2} \quad (51),$$

Finally, we obtain the ground state energy given by:

$$E = \frac{P^2(1-\eta^2)}{2m} - 2 \sum_{\vec{k}} \frac{|v_{\vec{k}}|^2}{\hbar\omega - \frac{\hbar\vec{k}\cdot\hat{p}}{m}(1-\eta) + \frac{\hbar^2k^2}{2m}} + \frac{1-\eta}{m} \sum_{\vec{k}} \frac{|v_{\vec{k}}|^2 \hbar\vec{k}\cdot\hat{p}}{\left(\hbar\omega - \frac{\hbar\vec{k}\cdot\hat{p}}{m}(1-\eta) + \frac{\hbar^2k^2}{2m} \right)^2} \quad (52).$$

Let do the series expansion of Eq. (52) with respect to \hat{p} in second order

$$I = - \sum_{\vec{k}} \frac{|v_{\vec{k}}|^2}{\hbar\omega - \frac{\hbar\vec{k}\cdot\hat{p}}{m}(1-\eta) + \frac{\hbar^2k^2}{2m}} = - \frac{1}{\hbar} \sum_{\vec{k}} \frac{1}{\omega} \frac{|v_{\vec{k}}|^2}{\left(1 + \frac{\hbar k^2}{2m\omega} - \frac{\vec{k}\cdot\hat{p}}{m\omega}(1-\eta) \right)} \quad (53a),$$

then after some calculations we obtained

$$I = - \frac{1}{\hbar} \sum_{\vec{k}} \frac{1}{\omega} \frac{|v_{\vec{k}}|^2}{(1 + \beta_v^2 k^2)} \left[1 + \frac{2\beta_v^2 \vec{k}\cdot\hat{p}}{\hbar(1 + \beta_v^2 k^2)} + \frac{4\beta_v^4 \vec{k}\cdot\hat{p}(1-\eta)^2}{\hbar^2(1 + \beta_v^2 k^2)^2} + 0(P^4) \right] \quad (53b),$$

where $\beta_v = \sqrt{\frac{\hbar}{2m\omega}}$ then, $|v_{\vec{k}}|^2 = \frac{\hbar^2 \omega^2}{k^2} \left(\beta_v \frac{4\pi\alpha}{V} \right)^{1/2}$. The integral form of Eq. (53b) is:

$$I = \frac{V}{(2\pi)^3} \int \frac{4\pi\alpha\beta_v\hbar^2\omega^2}{\hbar\omega k^2 V(1 + \beta_v^2 k^2)} 2\pi \sin\theta k^2 dk \left[1 + \frac{2\beta_v^2 \vec{k}\cdot\hat{p}}{\hbar(1 + \beta_v^2 k^2)} + \frac{4\beta_v^4 \vec{k}\cdot\hat{p}(1-\eta)^2}{\hbar^2(1 + \beta_v^2 k^2)^2} + 0(P^4) \right] \quad (54),$$

then we obtain:

$$I = -\frac{\hbar\omega\alpha}{2} - \frac{P^2}{12m}\alpha(1-\eta) + 0(P^4) \quad (55).$$

From the expression of $|f_{\vec{k}}|$, we have:

$$\eta\vec{p} = \eta p^2 = \sum_{\vec{k}} \hbar\vec{k}\hat{p} |f_{\vec{k}}|^2 = \sum_{\vec{k}} \frac{|v_{\vec{k}}|^2 \hbar\vec{k}\hat{p}}{\hbar^2\omega^2(1+\beta_v^2k^2)} \left[1 + \frac{2\beta_v^2\vec{k}\cdot\hat{p}}{\hbar(1+\beta_v^2k^2)} + \frac{4\beta_v^4\vec{k}\cdot\hat{p}(1-\eta)^2}{\hbar^2(1+\beta_v^2k^2)^2} + 0(P^4) \right] \quad (56a),$$

therefore, by integrating,

$$\eta p^2 = \frac{V}{(2\pi)^2} \frac{\int 4\pi\alpha\beta_v\hbar^3\omega^2\vec{k}\cdot\hat{p}}{\hbar\omega k^2 V(1+\beta_v^2k^2)} 2\pi \sin\theta d\theta k^2 dk \left[1 + \frac{2\beta_v^2\vec{k}\cdot\hat{p}}{\hbar(1+\beta_v^2k^2)} + \frac{4\beta_v^4\vec{k}\cdot\hat{p}(1-\eta)^2}{\hbar^2(1+\beta_v^2k^2)^2} + 0(P^4) \right] \quad (56b),$$

finally, we have:

$$\eta p^2 = \frac{p^2}{6}\alpha(1-\eta) \quad (56c).$$

Then by simplification, we have:

$$\eta = \frac{1}{6}\alpha(1-\eta) \quad (57),$$

therefore, we obtained

$$\eta = \frac{\alpha/6}{1+\alpha/6} \quad (58).$$

So, Eq. (55) become

$$I = \frac{1-\eta}{m} \sum_{\vec{k}} \frac{|v_{\vec{k}}|^2 \hbar\vec{k}\hat{p}}{\left(\hbar\omega - \frac{\hbar\vec{k}\cdot\hat{p}}{m}(1-\eta) + \frac{\hbar^2k^2}{2m} \right)^2} = \frac{1-\eta}{m} \eta p^2 \quad (59).$$

Thus, the expression of the energy becomes:

$$E(p^2) = -\hbar\omega\alpha - \frac{p^2}{2m}(1-\eta)^2 + \frac{1-\eta}{m}\eta p^2 + \frac{p^2}{2m}(1-\eta)^2 + 0(p^4) \quad (60),$$

Then introducing Eq. (58) into Eq. (60), the expression of energy becomes

$$E(p^2) = -\hbar\omega\alpha - \frac{p^2}{2m(1 + \alpha/6)} + O(p^4) \quad (61),$$

then, the ground state energy is obtained as:

$$E_0 = -\hbar\omega\alpha \quad (62).$$

2.1.2.2 EFFECTIVE MASS OF POLARON

The effective mass of polaron can be derived in Eq. (61), it is given as:

$$m_{eff} = m(1 + \alpha/6) \quad (63).$$

2.1.3 HUYBRECHT VARIATIONAL METHOD

Other mathematic tools use for solving the problem of polaron in nanostructures is the Huybrecht method also known as Lee-Low-Pines-Huybrecht method introduced by Huybrecht [146]. It is an all coupling approach.

2.1.3.1 DETERMINATION OF THE GROUND STATE ENERGY

To determine the fundamental energy of the polaron, by the method of Huybrecht [146], one start from Hamiltonian given in Eq. (19). Let us transform this Hamiltonian by the following unitary operator:

$$U_1 = \exp\left(-ia\left[\bar{P} - \sum_k ka_k^+ a_k\right] \cdot \vec{r}\right) \quad (64),$$

with

$$\bar{P} = \vec{p} - a \sum_k ka_k^+ a_k. \quad (65).$$

The Hamiltonian in Eq. (19) can be rewritten as follow:

$$H = \frac{1}{2m} \left(\vec{p} - a \sum_k a_k^+ a_k \right)^2 + \sum_k \hbar\omega_k a_k^+ a_k + \sum_k \left(V_{\vec{k}} a_{\vec{k}} e^{i(1-a)\vec{k}\vec{r}} + V_{\vec{k}}^* a_{\vec{k}}^+ e^{-i(1-a)\vec{k}\vec{r}} \right) \quad (66),$$

a is the Huybrechts parameter. when $a = 0$, this approach is corresponding for strong coupling regime, when $a = 1$, this approach is reduces to the LLP which is treated in the previous part.

when $0 < a < 1$ one can have a consistent theory encompassing the entire parameter space. We introduce the creation and annihilation operators b_j^+ and b_j by

$$\begin{cases} P_j = (m\lambda\hbar)^{\frac{1}{2}} \sum_j (b_j^+ + b_j + \bar{p}_{0j}) \\ r_j = i \left(\frac{\hbar}{4m\lambda} \right)^{\frac{1}{2}} \sum_j (b_j - b_j^+) \end{cases} \quad (67),$$

j denotes the $\vec{x}, \vec{y}, \vec{z}$ directions and $\lambda; \bar{p}_{0j}$ are the variational parameter. Using Eq. (67), the Eq. (66) is transformed as:

$$\bar{H}' = \tilde{H}_1 + \tilde{H}_2 \quad (68),$$

with

$$\begin{aligned} \tilde{H}_1 = & \frac{\lambda\hbar}{2} \sum_j (b_j^+ b_j + \frac{3}{2}) + \sum_k \left(\hbar\omega + \frac{k^2 \hbar^2 a^2}{4m} \right) a_k^+ a_k + \frac{\lambda\hbar}{4} \sum_j (b_j^+ b_j^+ + b_j b_j) + \\ & + \sum_k \left(v_k^* a_k^+ \exp\left(-\frac{\hbar}{4m\lambda} (1-a)^2 k^2\right) \exp\left(-\left(\frac{\hbar}{2m\lambda}\right)^{\frac{1}{2}} (1-a) \sum_k k b_j^+\right) \exp\left(\left(\frac{\hbar}{2m\lambda}\right)^{\frac{1}{2}} (1-a) \sum_k k b_j\right) + h.c \right) \end{aligned} \quad (69),$$

and

$$\tilde{H}_2 = -a \left(\frac{\lambda\hbar}{2m} \right)^{\frac{1}{2}} \sum_{(\vec{k}, j) f_k} \hbar \vec{k}_j (b_j^+ + b_j) a_{\vec{k}}^+ a_{\vec{k}} + \frac{a^2}{2m} \sum_{\vec{k}, \vec{k}'} \hbar^2 \vec{k} \vec{k}' a_{\vec{k}}^+ a_{\vec{k}}^+ a_{\vec{k}'} a_{\vec{k}'}. \quad (70),$$

where

$$\vec{p}_{0j} = 0 \quad (71).$$

Performing the second Lee- Low- Pines canonical transformation

$$U_2 = \exp\left(a_{\vec{k}}^+ f_{\vec{k}}^- - a_{\vec{k}}^- f_{\vec{k}}^{*+}\right) \quad (72),$$

where $f_{\vec{k}}^+ (f_{\vec{k}}^-)$ are obtained by minimizing the energy. Applying all these operators on the Eq. (68) we obtain:

$$\begin{aligned} \bar{H}' &= \langle U_2^{-1} | \tilde{H}_1 + \tilde{H}_2 | U_2 \rangle \\ &= \frac{\lambda\hbar}{2} \sum_j b_j^\dagger b_j + \frac{3\lambda\hbar}{4} (1-a)^2 + \sum_{\bar{k}} \left(\hbar\omega + \frac{k^2\hbar^2 a^2}{4m} \right) (a_{\bar{k}}^+ + f_{\bar{k}}^*) (a_{\bar{k}} + f_{\bar{k}}) + \frac{\lambda\hbar}{4} \sum_j (b_j^\dagger b_j^\dagger + b_j b_j) + \\ &+ \sum_{\bar{k}} \left(v_{\bar{k}}^* (a_{\bar{k}}^+ + f_{\bar{k}}^*) \exp\left(-\frac{\hbar}{4m\lambda} (1-a)^2 k^2\right) \exp\left(-\left(\frac{\hbar}{2m\lambda}\right)^{\frac{1}{2}} (1-a) \sum_{\bar{k}} k b_j^+\right) \exp\left(\left(\frac{\hbar}{2m\lambda}\right)^{\frac{1}{2}} (1-a) \sum_{\bar{k}} k b_j\right) + h.c \right) + \bar{H} \end{aligned} \quad (73),$$

the part \tilde{H}_2 of Eq. (68) have some terms with no importance for supplementary calculations.

The phonon vacuum state $|0_{ph}\rangle$ is taken such as the below relations should be satisfies,

$$\begin{cases} b_j^+ |0_{ph}\rangle = a_{\bar{k}}^+ |0_{ph}\rangle = |1\rangle \\ b_j |0_{ph}\rangle = a_{\bar{k}} |0_{ph}\rangle = 0 \end{cases} \quad (74),$$

then the ground state energy is obtained as:

$$\begin{aligned} E_0 &= \langle 0_{ph} | \bar{H}' | 0_{ph} \rangle \\ &= \frac{3\lambda\hbar}{4} + \sum_{\bar{k}} \left(\hbar\omega + \frac{k^2\hbar^2 a^2}{2m} \right) |f_{\bar{k}}^-|^2 + \sum_{\bar{k}} \left(v_{\bar{k}}^* f_{\bar{k}}^* \exp\left(-\frac{\hbar}{4m\lambda} (1-a)^2 k^2\right) + h.c \right) \end{aligned} \quad (75),$$

the variationnal function $f_{\bar{k}}^+(f_{\bar{k}}^-)$ are obtained by minimizing the above ground state energy;

then after minimizing Eq. (75) we obtain

$$\begin{cases} f_{\bar{k}}^- = -\frac{v_{\bar{k}}^* \exp\left(-\frac{\hbar}{4m\lambda} (1-a)^2 k^2\right)}{\hbar\omega + \frac{k^2\hbar^2 a^2}{2m}} \\ f_{\bar{k}}^* = -\frac{v_{\bar{k}} \exp\left(-\frac{\hbar}{4m\lambda} (1-a)^2 k^2\right)}{\hbar\omega + \frac{k^2\hbar^2 a^2}{2m}} \end{cases} \quad (76).$$

Replacing Eq. (76) into Eq. (75), the ground state energy becomes

$$E_0 = \frac{3\lambda\hbar}{4} - \sum_{\bar{k}} \frac{|v_{\bar{k}}^-|^2}{\left(\hbar\omega + \frac{k^2\hbar^2 a^2}{2m}\right)} \exp\left(-\frac{\hbar}{2m\lambda} (1-a)^2 k^2\right) \quad (77),$$

transforming the summation into integration after replacing $v_{\bar{k}}^-$ by its expression given by Eq.

(20), we have

$$E_0 = \frac{3\lambda\hbar}{4} - \alpha \frac{\hbar\omega}{2\pi^2} \left(\frac{\hbar}{2m\omega} \right)^{\frac{1}{2}} \int_0^\infty \frac{dk}{k^2 \left(1 + \frac{k^2 \hbar^2 a^2}{2m\omega} \right)} \exp\left(-\frac{\hbar}{2m\lambda} (1-a)^2 k^2 \right) \quad (78).$$

2.1.3.2 FIRST EXCITED STATE ENERGY

In polar materials with intermediate coupling between electron and phonon, a strong correlation between phonon is induced, therefore there appears a potential well created by the virtual phonon field which implies that electron can be excited in a higher potential level. In our model we will calculate the energy in the first approximation of the first excited state by using the same parameters as those used for the calculation of the fundamental energy. To calculate the energy in the first approximation of the first excited state, we evaluate the following relation:

$$E_1 = \langle 1 | \bar{H} | 1 \rangle \quad (79),$$

where $|1\rangle = b_j^+ |0\rangle$.

By doing the same calculation as in the ground state, the approximation energy of the first excited state is obtained as follow:

$$E_1 = \frac{5\lambda\hbar}{8} + \sum_{\vec{k}} \left(\hbar\omega + \frac{k^2 \hbar^2 a^2}{2m} \right) |f_{\vec{k}}|^2 + \sum_{\vec{k}} \left(v_{\vec{k}}^* f_{\vec{k}}^* \left(1 - \frac{\hbar}{2m\lambda} (1-a)^2 \frac{k^2}{3} \right) \exp\left(-\frac{\hbar}{4m\lambda} (1-a)^2 k^2 \right) + h.c \right) \quad (80),$$

then the variational function $f_{\vec{k}}^{\pm}(f_{\vec{k}})$ are given by:

$$\left\{ \begin{array}{l} f_{\vec{k}} = -\frac{v_{\vec{k}}^* \exp\left(1 - \frac{\hbar}{2m\lambda} (1-a)^2 \frac{k^2}{3} \right) \exp\left(-\frac{\hbar}{4m\lambda} (1-a)^2 k^2 \right)}{\hbar\omega + \frac{k^2 \hbar^2 a^2}{2m}} \\ f_{\vec{k}}^* = -\frac{v_{\vec{k}} \exp\left(1 - \frac{\hbar}{2m\lambda} (1-a)^2 \frac{k^2}{3} \right) \exp\left(-\frac{\hbar}{4m\lambda} (1-a)^2 k^2 \right)}{\hbar\omega + \frac{k^2 \hbar^2 a^2}{2m}} \end{array} \right. \quad (81),$$

thus the first excited energy becomes

$$E_1 = \frac{5\lambda\hbar}{8} - \sum_{\vec{k}} |v_{\vec{k}}|^2 \frac{\left(1 - \frac{\hbar}{2m\lambda}(1-a)^2 \frac{k^2}{3}\right) \exp\left(-\frac{\hbar}{4m\lambda}(1-a)^2 k^2\right)}{\left(\hbar\omega + \frac{k^2\hbar^2 a^2}{2m}\right)}. \quad (82),$$

finally Replacing $v_{\vec{k}}$ by its expression and transforming summation into integration, we have:

$$E_1 = \frac{5\lambda\hbar}{8} - \alpha \frac{\hbar\omega}{2\pi^2} \left(\frac{1}{2m\omega}\right)^{\frac{1}{2}} \int_0^\infty \frac{\left(1 - \frac{\hbar}{6m\lambda}(1-a)^2\right) \exp\left(-\frac{\hbar}{4m\lambda}(1-a)^2 k^2\right) dk}{\left(1 + \frac{k^2\hbar^2 a^2}{2m\omega}\right)} \quad (83).$$

2.1.3.3 DIFFERENCE BETWEEN LLP AND HUYBRECHT METHODS

The difference between the LLP and Huybrecht methods is in the first unitary operators. This operator in the case of Huybrecht is given as follows:

$$U_1 = \exp\left(-ia\left[\vec{P} - \sum_k ka_k^+ a_k\right] \cdot \vec{r}\right) \quad (84),$$

a is the parameters calling Hubrecht parameter in the case of Huybrecht method, in the LLP method, this parameter takes the values 1. Thus one can observe that Huybrecht method is an all coupling method: strong coupling ($a=0$), intermediate coupling ($0 < a < 1$) and weak coupling regime ($a=1$) which the calculation is similar to LLP method which is also a weak coupling method. Another difference is that in the case of Huybrecht method, new operators of creation and annihilation related to position and momentum of electron are introduced.

2.1.4 PEKAR VARIATIONAL METHOD

We consider a polaron in presence of magnetic field and confining potential [147]. The electron under this consideration is in movement in an asymmetric quantum dot with three-dimensional Anisotropic harmonic potential, and interacting with bulk LO phonons, under the influence of a magnetic field along the z-direction with vector potential of $A = B(-y/2; x/2; 0)$.

The Hamiltonian of the polaron system can be written as :

$$H = \frac{1}{2m} \left(p_x - \frac{\beta^2}{4} y\right)^2 + \frac{1}{2m} \left(p_y + \frac{\beta^2}{4} x\right)^2 + \frac{p_z^2}{2m} + \sum_{\vec{q}} \hbar\omega_{LO} a_{\vec{q}}^+ a_{\vec{q}} + \frac{1}{2} m\omega_1^2 \rho^2 \quad (85),$$

$$+ \frac{1}{2} m\omega_2^2 z^2 + \sum_{\vec{q}} \{V_{\vec{q}} a_{\vec{q}} \exp(i\vec{q}\vec{r}) + hc\}$$

where $\beta^2 = (2e/c)$, m is the band mass, ω_1 and ω_2 are the magnitude of the transverse and longitudinal confinement strengths of the potentials in the $x-y$ plane and the z -direction, respectively. $a_{\bar{q}}^+(a_{\bar{q}})$ are the creation (annihilation) operator of the bulk phonon with wave vector q , $p = (p_x, p_y, p_z)$ and $r = (\rho, z)$ are the momentum and position vector of electron, $\rho = (x, y)$ is the position vector of the electron in the $x-y$ plane. This Hamiltonian will be used to explicit the Pekar variational method, thus following this method the appropriate wave function of strong coupling regime is divided into two parts one describing the electron and other for the phonon. This function is written as follows:

$$|\psi\rangle = |\phi\rangle U |0_{ph}\rangle \quad (86),$$

where $|\phi\rangle$ depends only on the electron coordinate and $|0_{ph}\rangle$ represents the phonon's vacuum state satisfying the following relation $a_q |0_{ph}\rangle = 0$, the coherent state of phonon is given by $U |0_{ph}\rangle$ with

$$U = \exp \left[\sum_{\bar{q}} (a_{\bar{q}}^+ f_{\bar{q}} + a_{\bar{q}} f_{\bar{q}}^*) \right] \quad (87),$$

$f_{\bar{q}}(f_{\bar{q}}^*)$ is the variational function. By solving the Schrodinger equation using Eq. (85), we obtained the following appropriate ground and first excited state wave functions of the electron

$$|\phi_0\rangle = \left(\frac{2\lambda_0}{\pi} \right)^{1/2} \left(\frac{\mu_0}{\pi} \right)^{1/4} \exp \left(-\frac{\lambda_0 \rho^2}{2} \right) \exp \left(-\frac{\mu_0 z^2}{2} \right) \quad (88),$$

$$|\phi_1\rangle = 2 \left(\frac{\lambda_1}{\pi} \right)^{1/2} \left(\frac{\mu_1^3}{\pi} \right)^{1/4} z \exp \left(-\frac{\lambda_1 \rho^2}{2} \right) \exp \left(-\frac{\mu_1 z^2}{2} \right) \quad (89),$$

where $\lambda_0, \mu_0, \lambda_1$ and μ_1 are the variational parameters. These wave functions of the electron satisfy the normalized relation given as:

$$\langle \phi_0 | \phi_0 \rangle = \langle \phi_1 | \phi_1 \rangle = 1 \text{ and } \langle \phi_0 | \phi_1 \rangle = 0 \quad (90).$$

The polaron ground state energy is obtained by minimizing the expectation value of the Hamiltonian, thus we have:

$$E_0 = \langle \phi_0 | H | \phi_0 \rangle \quad (91).$$

After some calculations, we obtain the ground state energy in the form

$$E_0 = \frac{\hbar^2 \lambda_0}{2m} + \frac{\hbar^2 \mu_0}{4m} + \frac{m\omega_1^2}{2\lambda_0} + \frac{m\omega_c^2}{8\lambda_0} + \frac{m\omega_2^2}{4\mu_0} - \left(\frac{\hbar}{2m\omega_{LO}} \right)^{\frac{1}{2}} 8\sqrt{\pi} \hbar \alpha \omega_{LO} \left(\frac{2\lambda_0}{\pi(1-\lambda_0/\mu_0)} \right)^{\frac{1}{2}} \arcsin(1-\lambda_0/\mu_0)^{\frac{1}{2}} \quad (92).$$

By the same sheme, the first excited state energy is given as:

$$E_1 = \lambda_1 + \frac{3\mu_1}{2} + \left(\frac{1}{\lambda_1 r_0^4 u_1^4} + \frac{3}{\mu_1 r_0^4 u_1^4} \right) \left[1 + \frac{\gamma^2}{16 \left(\frac{1}{\lambda_1 u_1^4} + \frac{3}{\mu_1 u_1^4} \right)} \right] - 8\alpha r_0 \sqrt{\pi} \left(\frac{2\lambda_1}{\pi(1-\lambda_1/\mu_1)} \right)^{\frac{1}{2}} \arcsin(1-\lambda_1/\mu_1)^{\frac{1}{2}} \quad (93).$$

2.2 SOME PARAMETERS OF QUASIPARTICLES

2.2.1 POLARON LIFETIME IN WEAK COUPLING REGIME

The effect of temperature and interaction between electron and phonon in a system give rise to quantum transition, provided that the energy exchanges correspond to the energies necessary for these transitions. The transition rate from fundamental to first excited state can be investigated by using the Fermi golden principle [139], it is expressed as follow:

$$\frac{\hbar}{\tau} = 2\pi \sum_{\vec{k}} \left| \langle \eta_{\vec{k}}' | \langle \Psi | H_{e-ph} | \Psi \rangle | \eta_{\vec{k}} \rangle \right|^2 \delta(\vec{E}_{\vec{k}}' - \vec{E}_{\vec{k}}) \quad (94),$$

H_{e-ph} is the Hamiltonian of electron-phonon coupling given by Eq.(18), Ψ is the electronic wave function in the ground state or excited state and \mathcal{D} is the kronecker, τ is the lifetime of the polaron in the ground or first excited states, E is the state energy as the polaron transite from ground state to first excited state. The following expression can be written due to fact that polaron absorbs phonon

$$\eta_{\vec{k}}' = \eta_{\vec{k}} - 1 \quad (95),$$

replacing Eqs. (18) and (95) into Eq. (94), we obtain:

$$\frac{\hbar}{\tau} = 2\pi \sum_{\bar{k}} \left| \langle \eta_{\bar{k}}' | \langle \Psi | H_{e-ph} | \Psi \rangle | \eta_{\bar{k}} \rangle \right|^2 = 2\pi \sum_{\bar{k}} \left| \langle \eta_{\bar{k}} - 1 | \langle \Psi | v_{\bar{k}} e^{i\bar{k}r} a_{\bar{k}} + v_{\bar{k}}^* e^{-i\bar{k}r} a_{\bar{k}}^+ | \Psi \rangle | \eta_{\bar{k}} \rangle \right|^2 \quad (96),$$

then after developing we have:

$$\frac{\hbar}{\tau} = 2\pi \left(\sum_{\bar{k}} \left| \langle \Psi | v_{\bar{k}} e^{i\bar{k}r} | \Psi \rangle \langle \eta_{\bar{k}} - 1 | a_{\bar{k}} | \eta_{\bar{k}} \rangle + \langle \Psi | v_{\bar{k}} e^{i\bar{k}r} | \Psi \rangle \langle \eta_{\bar{k}} - 1 | a_{\bar{k}}^+ | \eta_{\bar{k}} \rangle \right|^2 \right) \quad (97),$$

then using this assumption $a_{\bar{k}} | \eta_{\bar{k}} \rangle = \sqrt{\eta_{\bar{k}}} | \eta_{\bar{k}} - 1 \rangle$ and $a_{\bar{k}}^+ | \eta_{\bar{k}} \rangle = \sqrt{\eta_{\bar{k}} + 1} | \eta_{\bar{k}} + 1 \rangle$, we have:

$$\frac{\hbar}{\tau} = 2\pi \sum_{\bar{k}} \left| \langle \Psi | v_{\bar{k}} e^{i\bar{k}r} | \Psi \rangle \sqrt{\eta_{\bar{k}}} \langle \eta_{\bar{k}} - 1 | \langle \eta_{\bar{k}} \rangle \right|^2 = 8\pi^2 \alpha \eta_{\bar{k}} \frac{\hbar^2 \omega^2}{V} \beta_v \sum_{\bar{k}} \frac{1}{k} \langle \Psi | e^{i\bar{k}r} | \Psi \rangle \quad (98),$$

with $\beta_v = \sqrt{\frac{\hbar}{2m\omega}}$, after integrating we obtained:

$$\frac{\hbar}{\tau} = 8\pi^2 \alpha \eta_{\bar{k}} \frac{\hbar^2 \omega^2}{V} \beta_v \frac{V}{(2\pi)^3} \int \frac{dk^3}{k^2} = \eta_{\bar{k}} \beta_v \alpha \frac{\hbar^2 \omega^2}{\pi} \int \frac{dk^3}{k^2} \quad (99).$$

since $|e^{i\bar{k}r}|^2 = 1$,

$$\text{then we have:} \quad \frac{\hbar}{\tau} = \eta_{\bar{k}} \beta_v \alpha \frac{\hbar^2 \omega^2}{\pi} \int \frac{dk^3}{k^2} \quad (100),$$

and considering a quantum distribution of bosons, and the self coherence between $\hbar\omega$ and the difference of energy between of fundamental and first excited state, we have

$$n_{\bar{k}} = \left[\exp\left(\frac{\hbar\omega}{kT}\right) - 1 \right]^{-1} \quad (101).$$

2.2.2 EFFECTIVE MASS OF POLARON IN ALL COUPLING REGIME

In solid state physics, effective mass is a conceptual approach towards the investigation of the transport of electrons. Rather than describing electrons with a fixed mass moving at a given potential, they are described as free electrons whose effective mass varies. This effective mass can be positive or negative, greater or less than the actual mass of the electron. Let us use the

Hamiltonian described in Eq. (19) to present a method of calculation of the effective mass of polaron this calculation is based on [145]. This Hamiltonian can be separated into two parts:

$$\hat{H} = \hat{H}_{\downarrow} + \hat{H}_{\uparrow} \quad (102),$$

$$\text{where } \begin{cases} \hat{H}_{\downarrow} = \frac{p_z^2}{2m} \\ \hat{H}_{\uparrow} = \frac{p_{\uparrow}^2}{2m} + \sum_{\vec{k}} \hbar \omega_k a_{\vec{k}}^{-} a_{\vec{k}}^{+} + \sum_{\vec{k}} \left(V_{\vec{k}}^{-} a_{\vec{k}}^{-} e^{i\vec{k}\vec{r}} + V_{\vec{k}}^{*} a_{\vec{k}}^{+} e^{-i\vec{k}\vec{r}} \right) \end{cases} \quad (103).$$

To investigate the movement of the electron state in the plane xoy, we consider that the movement along the z-direction is slow so the quantity of momentum and position can be considering. As the movement is perpendicular to the xoy plane, we introduce the unitary transformation given by Eq. (67). Also, the linear combination of the creation b_j^{+} and annihilation operator b_j are introduced to signify the position and momentum operators of the electron and are satisfying the boson commutative relation $[b_j, b_j^{+}] = 1$. The subscript j stands for the x and y directions. Thus, the total momentum is given by:

$$\vec{P}_{\uparrow} = \vec{p}_{\uparrow} + \sum_{\vec{k}} \hbar \vec{k} a_{\vec{k}}^{-} a_{\vec{k}}^{+} \quad (104),$$

applying the unitary transformation given by Eqs. (64) and (34) and using the linear combination operator given by Eq. (104) we evaluate the momentum as follow:

$$\vec{P}_0 = \langle 0 | (U_2 U_1)^{-1} \vec{P}_{\uparrow} (U_1 U_2) | 0 \rangle \quad (105),$$

then we obtain:

$$\vec{P}_0 = \left(\frac{m \hbar \lambda}{2} \right)^{\frac{1}{2}} \vec{p}_{0j} + (1-a) \sum_{\vec{k}} \hbar \vec{k} |f_{\vec{k}}| \quad (106),$$

Let us choose an arbitrary multiplier \hat{U} called the Lagrange's multiplier which is used to optimize the problem. This lead to the new variational function as:

$$F(f_{ns}; f_{ns}^*; \vec{p}_{0j}; U; \lambda) = \tilde{H}_{\uparrow j} - U \vec{P}_0 \quad (107),$$

in the intermediate coupling regime ($0 < a < 1$),

$$F(f_{\eta S}; f_{\eta S}^*; \vec{p}_{0j}; U; \lambda) = \frac{\hbar\lambda}{4} + \frac{\hbar\lambda}{4} p_0^2 - \sum_{\vec{k}} \exp\left[-\frac{\hbar}{4m\lambda}(1-a)^2 k^2\right] (v_{\vec{k}}^- f_{\vec{k}}^- + v_{\vec{k}}^+ f_{\vec{k}}^{*+})$$

$$+ \sum_{\vec{k}} \left[\hbar\omega + \frac{a^2 \hbar^2 k^2}{2m} - \frac{a\hbar}{m} \left(\frac{\hbar\lambda}{2m}\right)^{\frac{1}{2}} \vec{k} \vec{p}_{0j} - \hbar(1-a)U\vec{k} \right] |f_{\vec{k}}^-|^2 - U \left(\frac{m\hbar\lambda}{2}\right)^{\frac{1}{2}} \vec{p}_{0j} \quad (108),$$

with

$$f_{\vec{k}}^* = \frac{\exp\left[-\frac{\hbar}{4m\lambda}(1-a)^2 k^2\right]}{\hbar\omega + \frac{a^2 \hbar^2 k^2}{2m} - \frac{a\hbar}{m} \left(\frac{\hbar\lambda}{2m}\right)^{\frac{1}{2}} \vec{k} \vec{p}_{0j} - \hbar(1-a)U\vec{k}} v_{\vec{k}} \quad (109),$$

Substituting these functions into Eq. (106) and using condition below,

$$\frac{\partial \tilde{F}(f_{\vec{Q}}; f_{\eta S}; \dots; \vec{p}_0; U; \lambda)}{\partial \vec{p}_0} = 0 \quad (110),$$

then expanding by \hat{p}_{0j} and \hat{U} up to the second-order, we have the relation with \hat{p}_{0j} and \hat{U} as,

$$\vec{p}_0 = \frac{\left(\frac{2m}{\hbar\lambda}\right)^{\frac{1}{2}} - \sum_{\vec{k}} \frac{2a\hbar^2(1-a)\left(\frac{2}{m\hbar\lambda}\right)^{\frac{1}{2}} k^2 \exp\left[-\frac{\hbar}{2m\lambda}(1-a)^2 k^2\right] \langle \varphi | v_{\vec{k}}^-|^2 | \varphi \rangle}{m \left(\hbar\omega + \frac{a^2 \hbar^2 k^2}{2m}\right)^3}}{1 - \left(\frac{2\hbar^2}{m^3}\right) \sum_{\vec{k}} \frac{a^2 k^2 \exp\left[-\frac{\hbar}{2m\lambda}(1-a)^2 k^2\right] \langle \varphi | v_{\vec{k}}^-|^2 | \varphi \rangle}{\left(\hbar\omega + \frac{a^2 \hbar^2 k^2}{2m}\right)^3}} U_{\uparrow}. \quad (111),$$

so, as the total momentum is perpendicular to x-y plane, we can obtain:

$$\vec{P}_0 = \langle \varphi | \langle 0 | (U_2 U_1)^{-1} \vec{P}_{\uparrow} (U_1 U_2) | 0 \rangle | \varphi \rangle = \left(\frac{m\hbar\lambda}{2}\right)^{\frac{1}{2}} \langle \varphi | \vec{p}_0 | \varphi \rangle + (1-a) \sum_{\vec{k}} \hbar \vec{k} \langle \varphi | |f_{\vec{k}}^-|^2 | \varphi \rangle. \quad (112),$$

by expanding the above expression in the second-order term of \hat{p}_{0j} and \hat{U} , we obtain:

$$\begin{aligned}
 |f_{\vec{k}}|^2 &= \frac{\exp\left[-\frac{\hbar}{2m\lambda}(1-a)^2k^2\right] \|v_{\vec{k}}\|^2}{\left(\hbar\omega + \frac{a^2\hbar^2k^2}{2m}\right)^2} + \frac{4\exp\left[-\frac{\hbar}{2m\lambda}(1-a)^2k^2\right] \|v_{\vec{k}}\|^2}{\left(\hbar\omega + \frac{a^2\hbar^2k^2}{2m}\right)^4} \times \\
 &\left[\frac{a^2\hbar^3\lambda}{2m^3} k^2 p_0^2 + \hbar^2(1-a)^2 k^2 U^2 + \frac{2a\hbar^2(1-a)\left(\frac{\hbar\lambda}{2m}\right)^{\frac{1}{2}} k^2 \vec{U} \vec{p}_{0j}}{m} \right] \quad (113),
 \end{aligned}$$

replacing Eq. (113) into Eq. (112) and assuming that the first order terms \vec{p}_{0j} and \vec{U} are zero we obtain:

$$\begin{aligned}
 \bar{p}_0 &= \frac{m - \sum_{\vec{k}} \frac{2a\hbar^2(1-a)}{m} \frac{k^2 \exp\left[-\frac{\hbar}{2m\lambda}(1-a)^2k^2\right] \langle\varphi \|v_{\vec{k}}\|^2 | \varphi\rangle}{\left(\hbar\omega + \frac{a^2\hbar^2k^2}{2m}\right)^3}}{1 - \left(\frac{2\hbar^2}{m^3}\right) \sum_{\vec{k}} \frac{a^2k^2 \exp\left[-\frac{\hbar}{2m\lambda}(1-a)^2k^2\right] \langle\varphi \|v_{\vec{k}}\|^2 | \varphi\rangle}{\left(\hbar\omega + \frac{a^2\hbar^2k^2}{2m}\right)^3}} U_{\uparrow}. \quad (114).
 \end{aligned}$$

In Eq. (114) \hat{U} has the sense of the velocity which can be considered as the average velocity of the polaron along the x-y plane. Then the effective mass is given by the term before \hat{U} . Transforming the summation into integration, the effective mass of polaron is given as:

$$\begin{aligned}
 m_{eff} &= \frac{m + \frac{4\pi\alpha}{(2\pi)^3} \int \frac{2a\hbar^2(1-a)}{m} \frac{\exp\left[-\frac{\hbar}{2m\lambda}(1-a)^2k^2\right] \langle\varphi | \hbar^2 \omega^2 \beta_v | \varphi\rangle}{\left(\hbar\omega + \frac{a^2\hbar^2k^2}{2m}\right)^3} d^3k}{1 - \frac{4\pi\alpha}{(2\pi)^3} \left(\frac{2\hbar^2}{m^3}\right) \int \frac{a^2 \exp\left[-\frac{\hbar}{2m\lambda}(1-a)^2k^2\right] \langle\varphi | \hbar^2 \omega^2 \beta_v | \varphi\rangle}{\left(\hbar\omega + \frac{a^2\hbar^2k^2}{2m}\right)^3} d^3k} \quad (115),
 \end{aligned}$$

by replacing wave functions into the Eq. (115), we obtain the effective mass of polaron as:

$$m_{\text{eff}} = \frac{m + \frac{4\pi\alpha\beta_v}{(2\pi)^3} \int \frac{2a\hbar^2(1-a)}{m} \frac{\exp\left[-\frac{\hbar}{2m\lambda}(1-a)^2 k^2\right] (\hbar\omega)^2}{\left(\hbar\omega + \frac{a^2\hbar^2 k^2}{2m}\right)^3} d^3k}{1 - \frac{4\pi\alpha\beta_v}{(2\pi)^3} \left(\frac{2\hbar^2}{m^3}\right) \int \frac{a^2 \exp\left[-\frac{\hbar}{2m\lambda}(1-a)^2 k^2\right] (\hbar\omega)^2}{\left(\hbar\omega + \frac{a^2\hbar^2 k^2}{2m}\right)^3} d^3k}. \quad (116),$$

by the same schemes, one can obtain the effective mass for the first-excited.

In the case of weak coupling regime ($a = 1$), we have :

$$F(f_{\vec{k}}; f_{\vec{k}}^*; \vec{p}_{0j}; U; \lambda) = \frac{\hbar\lambda}{4} + \frac{\hbar\lambda}{4} p_0^2 - U \left(\frac{m\hbar\lambda}{2} \right)^{\frac{1}{2}} \vec{p}_{0j} - \sum_{\vec{k}} (v_{\vec{k}}^- f_{\vec{k}} + v_{\vec{k}}^+ f_{\vec{k}}^*) + \sum_{\vec{k}} \left[\hbar\omega + \frac{\hbar^2 k^2}{2m} - \frac{\hbar}{m} \left(\frac{\hbar\lambda}{2m} \right)^{\frac{1}{2}} \vec{k} \vec{p}_{0j} \right] |f_{\vec{k}}^-|^2 \quad (117),$$

then the variational function stands as:

$$f_{\vec{k}}^* = \frac{v_{\vec{k}}^-}{\hbar\omega + \frac{\hbar^2 k^2}{2m} - \frac{\hbar}{m} \left(\frac{\hbar\lambda}{2m} \right)^{\frac{1}{2}} \vec{k} \vec{p}_{0j}} \quad (118),$$

replacing this function into Eq. (106) and expanding up to second order as in the case of intermediate limit, we obtain the new form of variational parameter. And using the condition given by Eq. (110), we obtain:

$$\vec{p}_0 = \frac{\left(\frac{2m}{\hbar\lambda} \right)^{\frac{1}{2}}}{1 - \left(\frac{2\hbar^2}{m^3} \right) \sum_{\vec{k}} \frac{k^2 \langle \varphi | v_{\vec{k}}^- |^2 | \varphi \rangle}{\left(\hbar\omega + \frac{\hbar^2 k^2}{2m} \right)^3}} U. \quad (119),$$

thus the total momentum is written as:

$$\vec{P}_0 = \langle \varphi | \langle 0 | (U_2 U_1)^{-1} \vec{P}_\uparrow (U_1 U_2) | 0 \rangle | \varphi \rangle = \left(\frac{m\hbar\lambda}{2} \right)^{\frac{1}{2}} \langle \varphi | \vec{p}_0 | \varphi \rangle \quad (120),$$

after calculations we have:

$$\bar{p}_0 = \frac{m}{1 - \left(\frac{2\hbar^2}{m^3}\right) \sum_{\vec{k}} \frac{k^2 \langle \varphi | v_{\vec{k}}^2 | \varphi \rangle}{\left(\hbar\omega + \frac{\hbar^2 k^2}{2m}\right)^3}} U \quad (121).$$

In the case of weak coupling regime, the effective mass of polaron in fundamental state is given as follows:

$$m_{\text{eff}} = \frac{m}{1 - \left(\frac{2\hbar^2}{m^3}\right) \sum_{\vec{k}} \frac{k^2 \langle \varphi | v_{\vec{k}}^2 | \varphi \rangle}{\left(\hbar\omega + \frac{\hbar^2 k^2}{2m}\right)^3}} U \quad (122),$$

using Eq. (102) and doing a little transformation, we obtain:

$$m_{\text{eff}} = \frac{m}{1 - \frac{4\pi\alpha\beta_v}{(2\pi)^3} \left(\frac{2\hbar^2}{m^3}\right) \int \frac{(\hbar\omega)^4}{k^2 \left(\hbar\omega + \frac{a^2 \hbar^2 k^2}{2m}\right)^3} d^3k} \quad (123).$$

For strong coupling regime ($a = 0$) the variation parameter is given as:

$$F(f_{\vec{k}}; f_{\vec{k}}^*; \bar{p}_{0j}; U; \lambda) = \frac{\hbar\lambda}{4} + \frac{\hbar\lambda}{4} p_0^2 - U \left(\frac{m\hbar\lambda}{2}\right)^{\frac{1}{2}} \bar{p}_{0j} - \sum_{\vec{k}} \exp\left[-\frac{\hbar}{4m\lambda} k^2\right] (v_{\vec{k}}^- f_{\vec{k}}^- + v_{\vec{k}}^+ f_{\vec{k}}^{*}) + \sum_{\vec{k}} [\hbar\omega - \hbar U \vec{k}] f_{\vec{k}}^- \quad (124),$$

then we have:

$$f_{\vec{k}}^* = \frac{\exp\left[-\frac{\hbar}{4m\lambda} k^2\right] v_{\vec{k}}^-}{\hbar\omega - \hbar U \vec{k}} \quad (125),$$

inserting into Eq. (106) the above expression and doing development up to second order term of \hat{U} and using condition given by Eq. (110), we obtain:

$$\bar{p}_0 = \sqrt{\frac{2m}{\hbar\lambda}} U \quad (126),$$

thus the total momentum is:

$$\vec{P}_0 = \langle \varphi | \langle 0 | (U_2 U_1)^{-1} \vec{P}_\uparrow (U_1 U_2) | 0 \rangle | \varphi \rangle = \left(\frac{m \hbar \lambda}{2} \right)^{1/2} \langle \varphi | \vec{p}_0 | \varphi \rangle + \sum_{\vec{k}} \hbar \vec{k} \langle \varphi | f_{\vec{k}}^2 | \varphi \rangle. \quad (127),$$

assuming that the first order term in \vec{U} is zero, then use the development of $|f_{\vec{k}}|^2$ we have:

$$\vec{p}_0 = m \left(1 + \sum_{\vec{k}} \hbar^2 k^2 \frac{\exp\left[-\frac{\hbar}{2m\lambda} k^2\right] \langle \varphi | v_{\vec{k}}^2 | \varphi \rangle}{(\hbar\omega)^4} \right) \vec{U}. \quad (128),$$

The effective mass of polaron is given by the following expression after some developments:

$$m_{eff} = m \left(1 + \frac{4\pi\alpha\hbar^2\beta_v}{(2\pi)^3} \int \frac{\exp\left(-\frac{\hbar}{2m\lambda} k^2\right)}{k^2} d^3k \right). \quad (129).$$

2.2.3 MOBILITY OF POLARON

Charge carrier mobility is a concept used in physic to characterize environment that conduct electric current. It shows the link between the average velocity of an electric charge carrier of the medium (electron, hole, ion, etc.) to the average velocity of the medium. The Mobility is used to describe the movement of the quasi-particles in nanomaterials. In the case of polaronic quasiparticles the mobility can be investigated by formula below

$$\mu = \frac{e}{2m\alpha\omega} \left(\frac{m_{eff}}{m} \right)^3 f(\alpha) \exp\left(\frac{\hbar\omega}{k_B T}\right) \quad (130).$$

This expression of the mobility was presented by Devreese [148]. It appears of this espression of mobility that mobility strongly depends on the coupling constant, effective mass of the quasi-particle and temperature. It also shows that the mobility varies with the frequency of the quasi-particle characterizing the amount of energy in the system. For low temperature, this mean weak electon-phonon coupling $f(\alpha)=1, \alpha < 3$. For intermediate electron-phonon coupling regime $f(\alpha) = 5/4, 3 < \alpha < 6$

The mobility can also be invstigated by using quantum statistic theory. So the average number of phonons is given by [149]:

$$\bar{N} = \frac{\left[\exp\left(\frac{E_0}{k_B T}\right) - 1 \right]^{-1} + \left[\exp\left(\frac{E_1}{k_B T}\right) - 1 \right]^{-1}}{2} \quad (131),$$

Where k_B and T are the Boltzmann constant and the temperature of the system, respectively. On the other hand, E_0 and E_1 are respectively the ground state and first-excited state energy. The mobility and the number of phonons are related by the following formula:

$$\mu \approx \frac{1}{\bar{N}} = \frac{2}{\left[\exp\left(\frac{E_0}{k_B T}\right) - 1 \right]^{-1} + \left[\exp\left(\frac{E_1}{k_B T}\right) - 1 \right]^{-1}} \quad (132).$$

2.2.4 SHANNON ENTROPY

Entropy, is a measurement of the number in which a thermodynamic system can be arranged, generally understood like disorder measures. According to the second law of thermodynamic the entropy of a closed system never decreases; such system will proceed spontaneously towards thermodynamic balance, the configuration with the maximum entropy. In this work, we deal with the Shannon entropy as in [150]. The entropy of Shannon, due to Claude Shannon, is a mathematical function which, intuitively, corresponds to the quantity of information contained or delivered by a source of information. This source can be an electric signal or an unspecified computer file. The entropy indicates then the quantity of information necessary so that the receiver can determine without ambiguity what the source transmitted. To evaluate Shannon entropy, when the electron is in the superposition of ground and first excited states, and its wave function is given by:

$$|\psi_{01}\rangle = \frac{1}{\sqrt{2}} (|\phi_0\rangle + |\phi_1\rangle) \quad (133),$$

with $|\phi_0\rangle$ is the electron ground state wave function and $|\phi_1\rangle$ the electron first excited state wave function. Then the time evolution law of these wave function can be written as:

$$\psi_{01}(t, x, y, z) = \frac{1}{\sqrt{2}} \phi_0 \exp\left(-\frac{iE_0 t}{\hbar}\right) + \frac{1}{\sqrt{2}} \phi_1 \exp\left(-\frac{iE_1 t}{\hbar}\right). \quad (134),$$

so, the Shannon entropy of the system can be investigated as [150]:

$$s(t) = \int dx dy dz |\psi_{01}(t, x, y, z)|^2 \ln |\psi_{01}(t, x, y, z)|^2 \quad (135),$$

where $|\psi_{01}(t, x, y, z)|^2$ is the density probability and is given by the following expression:

$$|\psi_{01}(t, x, y, z)|^2 = \frac{1}{2} \left[|\phi_0|^2 + |\phi_1|^2 + \phi_0^* \phi_1 \exp(-i\omega_{01}t) + \phi_0 \phi_1^* \exp(i\omega_{01}t) \right] \quad (136),$$

and ω_{01} is the transition frequency given by:

$$\omega_{01} = \frac{E_1 - E_0}{\hbar} \quad (137).$$

2.2.5 DECOHERENCE TIME

The decoherence time is an essential parameter that enable us to know the period during which our system is able to react in a favorable way or not; in the case of the polaron it will enable us to know the time during which the system can enable us to make interesting studies. In order to investigate de decoherence time, we will first evaluate the spontaneous emission rate. So, we consider a system made of a two level atom in the free electromagnetic field, the Hamiltonian of this system can be written as follow:

$$H = H_{at} + H_f + H_{at-f}. \quad (138a),$$

The Hamiltonian of the atom is given as: $H_{at} = E_a |a\rangle\langle a| + E_b |b\rangle\langle b|$, a and b are respectively the ground and first excited states of the atom. The free electromagnetic field is given by, $H_f = \sum_{k,s} \hbar \omega_{k,s} (a_{k,s}^+ a_{k,s} + 1/2)$ where $\omega_k = c|K| = ck$ is the frequency of

electromagnetic field. The interaction between the atom and the electromagnetic dipole is given by $H_{at-f} = -qr.E(r)$, where r is the position operator of the electron orbiting around the atom, $q = -e$ is the electron's charge, and $E(r)$ is the electric field operator given by:

$$E(r) = i \sum_{k,s} \sqrt{\frac{\hbar \omega_k}{2\epsilon_0 V}} (a_{k,s} e_{k,s} e^{ik \cdot r} - a_{k,s}^+ e_{k,s}^* e^{-ik \cdot r}), \text{ and } e_{k,s} \text{ the unit polarization vectors}$$

corresponding to each mode.

For allowed transitions, the transition rate is mostly coming from the leading order of

this interaction, which is $H_{at-f} \approx -qr.E(0)$ with $E(0) = i \sum_{k,s} \sqrt{\frac{\hbar \omega_k}{2\epsilon_0 V}} (a_{k,s} e_{k,s} - a_{k,s}^+ e_{k,s}^*)$. As we

will use the Fermi's golden rule, we choose the initial and final states describing the

phenomena we intend to explain, namely spontaneous emission. Using the notation,

$|\psi\rangle = |\psi_{at}\rangle \otimes |\psi_f\rangle$, the initial and possible final states are $|i\rangle = |b\rangle \otimes |0\rangle$ and $|f_{k,s}\rangle = |a\rangle \otimes |1_{k,s}\rangle$

where $|0\rangle$ is the vacuum state of the electromagnetic field, and $|1_{k,s}\rangle = a_{k,s}^+|0\rangle$ is the state,

where a single photon occupies mode k, s . The energies of these states are $E_i = E_b + E_0$ and

$E_{f,k} + \hbar\omega_k + E_0$ where $E_0 = \langle 0|H_f|0\rangle$ is the (infinite) energy of electromagnetic vacuum. To

calculate the spontaneous decay rate of the atom we replace all information above in Fermi's

golden rule. Thus, the transition rate for $|i\rangle \rightarrow |f_{k,s}\rangle$ is $A_{k,s} = \frac{2\pi}{\hbar^2} |\langle f_{k,s}|H_{at-f}|i\rangle|^2 \delta\left(\frac{E_i - E_{f,k}}{\hbar}\right)$,

which has to be summed over the different final states to get the total decay rate out of the

initial state $|i\rangle$, or in other words the transition rate from $|b\rangle \rightarrow |a\rangle$ is given by

$$\Gamma = \sum_{k,s} A_{k,s} = \sum_{k,s} \frac{2\pi}{\hbar^2} |\langle f_{k,s}|H_{at-f}|i\rangle|^2 \delta\left(\frac{E_i - E_{f,k}}{\hbar}\right). \quad (138b)$$

The most difficult part of evaluating this expression is the matrix element, so we have

$$\begin{aligned} \langle f_{k,s}|H_{at-f}|i\rangle &= \langle a|\otimes\langle 1_{k,s}|(-qrE(0))(|b\rangle\otimes|0\rangle) \\ &= \langle a|\otimes\langle 1_{k,s}| \left(-qr.i \sum_{k',s'} \sqrt{\frac{\hbar\omega_{k'}}{2\varepsilon_0 V}} (a_{k',s'} e_{k',s'} - a_{k',s'}^+ e_{k',s'}^*) \right) (|b\rangle\otimes|0\rangle). \end{aligned} \quad (138c)$$

here we are going to use the following rule of evaluating matrix elements between tensor

product states: $(|\psi\rangle\otimes|\alpha\rangle)(H_1\otimes H_2)(|\phi\rangle|\beta\rangle) = \langle\psi|H_1|\phi\rangle\langle\alpha|H_2|\beta\rangle$. Since r acts on the atomic

wave function and $a_{k,s}$ and $a_{k,s}^+$ act on the field wave function, the matrix element can be

written in the following form:

$$\begin{aligned} \langle f_{k,s}|H_{at-f}|i\rangle &= (-iq)(\langle a|r|b\rangle) \sum_{k',s'} \sqrt{\frac{\hbar\omega_{k'}}{2\varepsilon_0 V}} (\langle 1_{k,s}|a_{k',s'}|0\rangle e_{k',s'} - \langle 1_{k,s}|a_{k',s'}^+|0\rangle e_{k',s'}^*) \\ &= iq(\langle a|r|b\rangle) \sum_{k',s'} \sqrt{\frac{\hbar\omega_{k'}}{2\varepsilon_0 V}} \delta_{k,k'} \delta_{s,s'} e_{k',s'}^* = iq(\langle a|r|b\rangle) \sum_{k',s'} \sqrt{\frac{\hbar\omega_{k'}}{2\varepsilon_0 V}} e_{k',s'}^* \end{aligned} \quad (138d)$$

where we used the followings, $a_{k',s'}|0\rangle = 0$, $a_{k',s'}^+|0\rangle = |1_{k',s'}\rangle$, $\langle 1_{k',s'}||1_{k',s'}\rangle = \delta_{k,k'}\delta_{s,s'}$ and

$\sum_{\alpha} F(\alpha)\delta_{\alpha,\beta} = F(\beta)$. Defining $p = \langle a|r|b\rangle$ and plugging this expression for the matrix element back

to Fermi's golden rule, we get $\Gamma = \frac{2\pi}{\hbar^2} \sum_{k,s} \frac{\hbar\omega_k}{2\varepsilon_0 V} |pe_{k,s}^*|^2 \delta(\omega_0 - ck)$, where we introduced

$$\omega_0 = \frac{E_b - E_a}{\hbar} \text{ and used that } E_i - E_{f,k} = E_b - E_a - \hbar\omega_k = \hbar(\omega_0 - ck).$$

The next step is the evaluation of the sum over different k, s modes. The free electromagnetic field modes in a box with volume $V = L \times L \times L$ with periodic boundary conditions are

$$\text{Modes} = \left\{ (k, s) : k \in \left\{ \frac{2\pi}{L} (l_x; l_y; l_z) : l_i \in \mathbb{Z} \right\}, s \in (1, 2) \right\}. \text{ Thus there's a volume of}$$

$$\left(\frac{2\pi}{L} \right)^3 = \frac{(2\pi)^3}{V}, \text{ corresponding to each mode. In a real situation, } L \text{ is much larger than any}$$

relevant (atomic, or optical) size, thus the modes form a practically continuous set in k -space, $k \in \mathfrak{R}^3$. This allows us to turn the sum over the modes into an integral over k . The only thing which has to be taken into account is above calculated volume per mode. So

$$\sum_k \dots = \frac{V}{(2\pi)^3} \int d^3k \dots = \frac{V}{(2\pi)^3} \int_0^\infty k^2 dk \int_0^\pi \sin\theta d\theta \int_0^{2\pi} d\varphi \dots \text{ replacing these expressions of the}$$

summation and Eq. (138c) in the Eq. (138b), we gets

$$\begin{aligned} \Gamma &= \frac{2\pi}{\hbar^2} \frac{V}{(2\pi)^3} \int_0^\infty \frac{\hbar\omega_k}{2\varepsilon_0 V} \delta(\omega_0 - ck) k^2 dk \int_0^\pi \sin\theta d\theta \int_0^{2\pi} d\varphi \sum_s |pe_{k,s}^*|^2 \\ &= \frac{1}{8\pi^2 \varepsilon_0 c^3} \left[\int_0^\infty (ck)^3 d(ck) \delta(ck - \omega_0) \right] \left[\int_0^\pi \sin\theta d\theta \int_0^{2\pi} d\varphi \sum_s |pe_{k,s}^*|^2 \right] \\ &= \frac{\omega_0^3}{8\pi^2 \varepsilon_0 c^3} \int_0^\pi \sin\theta d\theta \int_0^{2\pi} d\varphi \sum_s |pe_{k,s}^*|^2 \end{aligned} \quad (138e).$$

The other thing we should deal with is the polarization sum. In order to make it controllable

we use the following construction for polarization vectors: $e_{k,1} = \frac{1}{|\hat{K} \times \hat{z}|} \hat{K} \times \hat{z}$ and

$$e_{k,2} = \hat{K} \times e_{k,1} = \frac{1}{|\hat{K} \times \hat{z}|} \hat{K} \times (\hat{K} \times \hat{z}) \text{ where } \hat{K} \text{ and } \hat{z} \text{ are two unit vectors pointing to the}$$

direction of z -axis and k vector, respectively. By definition of the cross product, this

construction ensures all properties of e , namely $e_{k,i}^* \bullet e_{k,j} = \delta_{ij}$ and $e_{k,i} \bullet K = 0$. Because we

expressed K as $K = k(\sin\theta \cos\phi, \sin\phi \sin\theta, \cos\theta)$, the polarization vectors have the following

components: $e_{k,1} = (\sin\theta \cos\phi, -\sin\phi \sin\theta, 0)$ and $e_{k,2} = (\cos\theta \cos\phi, -\sin\phi \cos\theta, -\sin\theta)$.

Now, consider a Cartesian coordinate system, where z-axis points to the direction of P , ($P = (0,0, p)$). The dot products give the following results for the two polarizations:

$$P \cdot e_{K,1}^* = \begin{pmatrix} 0 \\ 0 \\ p \end{pmatrix} \cdot \begin{pmatrix} \sin \theta \sin \phi \\ -\sin \theta \cos \phi \\ 0 \end{pmatrix} = 0 \text{ and } P \cdot e_{K,2}^* = \begin{pmatrix} 0 \\ 0 \\ p \end{pmatrix} \cdot \begin{pmatrix} \cos \theta \sin \phi \\ -\cos \theta \sin \phi \\ -\sin \theta \end{pmatrix} = -p \sin \theta, \text{ thus the}$$

polarization sum yields $\sum_{s=1,2} |p \cdot e_{k,s}^*|^2 = |0|^2 + |-p \sin \theta|^2 = p^2 \sin^2 \theta$. Replacing this back to the

last expression of the Femi's golden rules gives

$$\Gamma = \frac{\omega_0^3}{8\pi^2 \epsilon_0 c^3} \int_0^\pi \sin \theta d\theta \int_0^{2\pi} d\phi p^2 \sin^2 \theta = \frac{2\pi p^2 \omega_0^3}{8\pi^2 \epsilon_0 c^3} \int_0^\pi \sin^3 \theta d\theta = \frac{p^2 \omega_0^3}{4\pi \epsilon_0 c^3} \frac{4}{3} = \frac{p^2 \omega_0^3}{3\pi \epsilon_0 c^3}$$

so the spontaneous emission rate can be given by

$$\Gamma_{b \rightarrow a} = \frac{|p|^2 \omega_0^3}{3\pi \epsilon_0 c^3}. \quad (138f),$$

where $p = q \langle a | r | b \rangle$, and $\omega_0 = \frac{E_b - E_a}{\hbar}$ and $\Gamma_{b \rightarrow a}^{-1}$ is the decoherence time which is similar to that obtained [151]

2.3 THEORITICAL MODELS

2.3.1 POLARON IN TRANSITION METAL DICHALCOGENIDES

2.3.1.1 POLARON UNDER ELECTRIC FIELD IN TRANSITION METAL DICHALCOGENIDES QUANTUM DOT

In order to investigate the states energies, the mobility, the lifetime, the decoherence time, the density probability and the Shannon entropy of the polaron in presence of electric field, we consider a single free electron moving in a monolayer of TMDs quantum dot sandwiched between polar substrate and air, this cause an interaction between free electron and optical phonon situated on the surface of TMDs layer. The Hamiltonian of the system in the presence of an external electric field can be written as:

$$H = -\frac{\hbar}{2m} \nabla_r^2 + \frac{1}{2} m \sum_i \omega_{p,i}^2 x_i^2 + \hbar \omega_{SO} \sum_k a_k^+ a_k + \sum_{k,v} (T_{k,v} e^{ik \cdot r} a_k + hc) + eF \sum_{i=1} x_i \quad (139),$$

where $r'(x_1', x_2', x_3')$ refers to the position vector of the electron, m is the electron mass, $\omega_{p,i}$ is the frequency of the confining parabolic potential corresponding to the direction i , ω_{SO} is the surface-optical (SO) phonon frequency which is assumed to be dispersionless, a_k^+ (a_k) is the creation (annihilation) operator for an SO phonon with wave vector k , $T_{k,v}$ is the coupling parameter between electron and SO phonon and F is the strength of electric field. It is convenient to use the dimensionless units in which the energy is scaled by ω_{SO} and the lengths are scaled by r_0 . This scale is equivalent to put $\hbar = 1$. Thus Hamiltonian in Eq. (139) becomes:

$$H = -\frac{1}{2m}\nabla_r^2 + \frac{1}{2}m\sum_i\omega_i^2x_i^2 + \omega_{SO}\sum_k a_k^+ a_k + \sum_{k,v}(T_{k,v}e^{ikr}a_k + hc) + eF\sum_i x_i \quad (140).$$

In Eq. (140) everything is dimensionless, the dimensionless electron position vector $r(x_1, x_2, x_3)$ and the phonon wave vector k are respectively given by $r = \frac{r'}{r_0}$ and $k = \frac{k'}{k_0}$ with

$$r_0 = \left(\frac{\hbar}{\omega_{SO}}\right)^{1/2} \text{ and } k_0 = \left(\frac{\omega_{SO}}{\hbar}\right)^{1/2} \text{ the dimensionless frequency } \omega_i \text{ of the confining potential is}$$

given by $\omega_i = \frac{\omega_{p,i}}{\omega_{SO}}$ if we consider a symmetric quantum dot, in dimensionless units, we have

$\omega_1 = \omega_2 = \omega_3 = \omega$, thus the Hamiltonian in Eq. (140) becomes :

$$H = -\frac{1}{2}\nabla_r^2 + \frac{1}{2}\omega^2 r^2 + \omega_{SO}\sum_k a_k^+ a_k + \sum_{k,v}(T_{k,v}e^{ikr}a_k + hc) + eFr \quad (141).$$

The energies of polaron is evaluated by using the Lee-Low pines method. In order to achieve our goal, a specific wave function of weak electron-phonon coupling regime is choosing which can be separated into two parts describing individually electron and phonon. Thus the energy is obtained as:

$$E = \langle \psi | \langle \varphi | U_1^{-1} H U_1 | \varphi \rangle | \psi \rangle \quad (142),$$

$\psi(r)$ is a trial electronic wave function, $|\varphi\rangle$ is the phonon state given as:

$$|\varphi\rangle = \exp\left[\sum_k (f_k a_k^+ + f_k^* a_k)\right] |0_{ph}\rangle \quad (143),$$

U_1 is the first unitary transformation of LLP given by Eq. (25). the trial electronic wave functions in the ground and first excited states can be chosen as:

$$\begin{cases} \psi_0(r) = \left(\frac{\mu_0}{\sqrt{\pi}}\right)^{3/2} e^{-1/2\mu_0^2 r^2} \\ \psi_1(r) = \left(\frac{2\mu_1^5}{\pi^{3/2}}\right)^{1/2} z e^{-1/2\mu_1^2 r^2} \end{cases} \quad (144),$$

where μ_0 and μ_1 are the variational parameters to be evaluated by minimizing energies with respect to them. Eq. (144) satisfies the following normalized relations:

$$\begin{cases} \langle \psi_0 | \psi_0 \rangle = \langle \psi_1 | \psi_1 \rangle = 1 \\ \langle \psi_0 | \psi_1 \rangle = 0 \end{cases} \quad (145),$$

by minimizing the expectation value of the Hamiltonian of Eq. (141), that is

$$\begin{cases} E_0 = \langle \psi_0(r) | \langle \phi | U_1^{-1} H U_1 | \phi \rangle | \psi_0(r) \rangle \\ E_1 = \langle \psi_1(r) | \langle \phi | U_1^{-1} H U_1 | \phi \rangle | \psi_1(r) \rangle \end{cases} \quad (146),$$

we obtain the ground and first excited state energies of polaron under electric field in the following form:

$$E_0 = \frac{3\mu_0^2}{4m} + \frac{3m}{4l^4\mu_0^2} + \frac{2eF}{\mu_0\sqrt{\pi}} - \frac{e^2\eta\hbar\omega_{SO}}{4\pi\epsilon_0} I_0 \quad (147),$$

$$E_1 = \frac{7\mu_1^2}{12m} + \frac{5m}{4\mu_1^2 l^4} + \frac{8eF}{3\mu_1\sqrt{\pi}} - \frac{e^2\eta\hbar\omega_{SO}}{4\pi\epsilon_0} I_0 \quad (148),$$

$$\text{With } I_0 = -\frac{1}{2z_0} [\exp(-2k_c z_0) - 1] + \frac{1}{2m} \left[\exp(-2k_c z_0) \left(-\frac{k_c^2}{2z_0} - \frac{k_c}{2z_0^2} - \frac{1}{4z_0^3} \right) + \frac{1}{4z_0^3} \right] \quad (149).$$

l is the effective confinement length of the quantum dot, k_c is the cut-off wave vector, z_0 the internal distance between TMDs monolayer and substrate, ϵ_0 is the permittivity of the vacuum and η is the polarizability of the substrate. On can remarked that the energies of the polaron is proportional to the electric field and depends on others parameters as the internal distance between TMDs and polar substrate, the cut-off wave vector and the confinement leghth of the quantum dot. So, those parameters can be necessary to modulate the states energies.

• **Lifetime of polaron under electric field**

The transition rate from fundamental to first excited state is given by the Eq. (94), after few developments we obtain:

$$\frac{\hbar}{\tau} = \frac{\mu_0^5 e^2 \eta \hbar \omega_{SO}}{4\sqrt{2} \varepsilon_0 z_0 \pi^{5/2}} \left[\exp\left(\frac{E_0}{k_B T}\right) - 1 \right]^{-1} \quad (150),$$

where τ is the lifetime of polaron. The lifetime of polaron is a function of the parameters of the system such as electric field, internal distance between monolayer and polar substrate and wavelength of the phonon. Thus, those parameters are useful to control lifetime of polaron in TMDs. And can also influenced others parameters such as decoherence time, Shannon entropy, density probability, transition frequency and mobility which are linked to states energies of polaron.

2.3.1.2 EFFECT OF MICROWAVES AND RADIOWAVES ON POLARON IN TRANSITION METAL DICHALCOGENIDES QUANTUM DOT

Let us consider a polaron in TMDs under the cumulative radiation of a microwave and a radiowave and theoretically investigated the mobility, the Shannon entropy density probability and the transition frequency. The Hamiltonian of the system can be written as follow:

$$H = H_e + H_{ph} + H_{e-ph} + H_R + H_M \quad (151a),$$

$$\text{with : } H_{ph} = \sum_{k,v} \hbar \omega_v a_k^+ a_k \quad (151b),$$

$$H_e = V_F \gamma \frac{P_x^2}{2m} \sigma_x + V_F \gamma \frac{P_y^2}{2m} \sigma_y + V_F \gamma \frac{m g^2 x^2}{2} \sigma_x + V_F \gamma \frac{m g^2 y^2}{2} \sigma_y + V_F \gamma G \sigma_z + \gamma \frac{P_z^2}{2m} \quad (151c),$$

$$H_{e-ph} = \sum_{k,v} \left(T_{k,v} a_k e^{i\vec{k}\vec{r}} + T_{k,v}^* a_k^+ e^{-i\vec{k}\vec{r}} \right) \quad (151d),$$

$$H_M = A_2 \cos(\beta t + \phi) \sigma_y \quad (151e),$$

$$H_R = A_1 \cos \theta \sigma_x \quad (151f).$$

In Eq.(151a), the first term describes the free electron (hole) momentum energy (H_e) in a parabolic quantum dot, where V_F is the fermi velocity, ($\gamma = \pm 1$) stand for the electron and

hole respectively in the conduction and in the valence band, σ_i are Pauli matrices, P_i is the momentum of the carriers with $i = x, y, z$, m is the mass of the electron (hole), $2G$ is the bandgap of the TMD [51] and \mathcal{G} is the confinement strength of the parabolic quantum dot; the second and third terms stands for phonon energy (H_{ph}) and coupling between carriers and phonon (H_{e-ph}) respectively, with a_k^+ (a_k) the creation and annihilation operators of the phonon including LO and SO modes with frequency ω_ν and wavelength k , $T_{k,\nu}$ the amplitude of the interaction of charges with phonons [51], and r_i is the position of the carriers; the fourth and fifth terms stands respectively for radiowave energy (H_R) and microwave energy (H_M) taken in the cosine form, with θ the frequency of the radiowave, β the frequency of the microwave and ϕ is his phase. In the radiowaves and microwaves, both the electric and magnetic fields oscillate perpendicular to the direction of propagation, they are both present and necessary for the wave to propagate through space. So A_1 and A_2 are the amplitudes of the electric field and magnetic field of respectively the radiowave and microwave. The Hamiltonian in Eq. (151a) is transformed as follow:

$$H = V_F \gamma \left[\left(a_k^+ a_k + \frac{1}{2} \right) \hbar \mathcal{G} (\sigma_x + \sigma_y) + \sigma_z G \right] + \gamma \hbar \mathcal{G} l_z + A_2 \cos(\beta t + \phi) \sigma_y \quad (152),$$

$$+ A_1 \cos \theta t \sigma_x + \sum_{k,\nu} \hbar \omega_\nu a_k^+ a_k + \sum_{k,\nu} \left(T_{k,\nu} a_k e^{i\vec{k}\vec{r}} + T_{k,\nu}^* a_k^+ e^{-i\vec{k}\vec{r}} \right)$$

where l_z is the azimuthal quantum number. If we consider the case that $\gamma = 1$ and applying the second LLP unitary transformation given by Eq. (34) on the Eq. (152) as follow $H_1 = U_2^{-1} H U_2$ we obtain:

$$H_1 = V_F \left[\left((a_k^+ + f_k^+) (a_k + f_k) + \frac{1}{2} \right) \hbar \mathcal{G} (\sigma_x + \sigma_y) + \sigma_z G \right] + \hbar \mathcal{G} l_z + A_2 \cos(\beta t + \phi) \sigma_y \quad (153),$$

$$+ A_1 \cos \theta t \sigma_x + \sum_{k,\nu} \hbar \omega_\nu (a_k^+ + f_k^+) (a_k + f_k) + \sum_{k,\nu} \left(T_{k,\nu} (a_k + f_k) e^{i\vec{k}\vec{r}} + T_{k,\nu}^* (a_k^+ + f_k^+) e^{-i\vec{k}\vec{r}} \right)$$

by minimizing the Hamiltonian of Eq. (153), that is:

$$\begin{cases} E_{0+} = \langle \varphi_0 | \langle 0 | H_2 | 0 \rangle | \varphi_0 \rangle \\ E_{1+} = \langle \varphi_1 | \langle 1 | H_2 | 1 \rangle | \varphi_1 \rangle \end{cases} \quad (154),$$

$$\text{where } \begin{cases} \varphi_0 = \left(\frac{\zeta}{\pi}\right)^{1/2} \left(\frac{\xi}{\pi}\right)^{1/4} \exp\left(-\frac{\zeta}{2}\rho^2\right) \exp\left(-\frac{\xi}{\pi}z^2\right) \\ \varphi_1 = \sqrt{2}\left(\frac{\zeta}{\pi}\right)^{1/2} \left(\frac{\xi^2}{\pi}\right)^{1/4} \exp\left(-\frac{\zeta}{2}\rho^2\right) z \exp\left(-\frac{\xi}{\pi}z^2\right) \end{cases} \quad (155).$$

Notice that φ_0 and φ_1 satisfying the same normalisation condition as given by Eq. (145). After some calculations, the expression of ground and first excited states energies are obtained as follow:

$$E_{0+} = \frac{1}{2}V_F\hbar\mathcal{G}(\sigma_x + \sigma_y) + \hbar\mathcal{G}V_F \sum_{k,v} \frac{T_{k,v}^* T_{k,v} \exp\left(-\frac{k^2\chi^2}{\zeta} - \frac{k^2\chi^2}{2\xi}\right)}{(\hbar\omega_v + \sqrt{2}\hbar\mathcal{G}V_F)^2} (\sigma_x + \sigma_y) + \hbar\mathcal{G}l_z + A_2 \cos(\beta t + \phi)\sigma_y$$

$$+ A_1 \cos\theta\sigma_x + \sigma_z G + \sum_{k,v} \hbar\omega_{k,v} \frac{T_{k,v}^* T_{k,v} \exp\left(-\frac{k^2\chi^2}{\zeta} - \frac{k^2\chi^2}{2\xi}\right)}{(\hbar\omega_v + \sqrt{2}\hbar\mathcal{G}V_F)^2} - 2 \sum_{k,v} \frac{T_{k,v} T_{k,v}^* \exp\left(-\frac{k^2\chi^2}{2\zeta} - \frac{k^2\chi^2}{4\xi}\right)}{(\hbar\omega_v + \sqrt{2}\hbar\mathcal{G}V_F)} \quad (156),$$

$$E_{1+} = \frac{3}{2}V_F\hbar\mathcal{G}(\sigma_x + \sigma_y) + \hbar\mathcal{G}V_F \sum_{k,v} \frac{T_{k,v}^* T_{k,v} \exp\left(-\frac{k^2\chi^2}{\zeta} - \frac{k^2\chi^2}{2\xi}\right) \left(1 - \frac{k^2\chi^2}{2\xi}\right)}{(\hbar\omega_v + \sqrt{2}\hbar\mathcal{G}V_F)^2} (\sigma_x + \sigma_y) + \hbar\mathcal{G}l_z + A_2 \cos(\beta t + \phi)\sigma_y + \sigma_z G$$

$$+ A_1 \cos\theta\sigma_x + \sum_{k,v} \hbar\omega_{k,v} + \sum_v \hbar\omega_v \frac{T_{k,v}^* T_{k,v} \exp\left(-\frac{k^2\chi^2}{\zeta} - \frac{k^2\chi^2}{2\xi}\right) \left(1 - \frac{k^2\chi^2}{2\xi}\right)}{(\hbar\omega_v + \sqrt{2}\hbar\mathcal{G}V_F)^2} - 2 \sum_{k,v} \frac{T_{k,v} T_{k,v}^* \exp\left(-\frac{k^2\chi^2}{\zeta} - \frac{k^2\chi^2}{2\xi}\right) \left(1 - \frac{k^2\chi^2}{2\xi}\right)}{(\hbar\omega_v + \sqrt{2}\hbar\mathcal{G}V_F)} \quad (157).$$

Similarly if we consider the case that $\gamma = -1$, we obtained the following expression for the ground and first excited energies :

$$E_{0-} = -\frac{1}{2}V_F\hbar\mathcal{G}(\sigma_x + \sigma_y) - \hbar\mathcal{G}V_F \sum_{k,v} \frac{T_{k,v}^* T_{k,v} \exp\left(-\frac{k^2\chi^2}{\zeta} - \frac{k^2\chi^2}{2\xi}\right)}{(\hbar\omega_v + \sqrt{2}\hbar\mathcal{G}V_F)^2} (\sigma_x + \sigma_y) - \hbar\mathcal{G}l_z - A_2 \cos(\beta t + \phi)\sigma_y$$

$$- A_1 \cos\theta\sigma_x - \sigma_z G - \sum_{k,v} \hbar\omega_v \frac{T_{k,v}^* T_{k,v} \exp\left(-\frac{k^2\chi^2}{\zeta} - \frac{k^2\chi^2}{2\xi}\right)}{(\hbar\omega_v + \sqrt{2}\hbar\mathcal{G}V_F)^2} + 2 \sum_{k,v} \frac{T_{k,v} T_{k,v}^* \exp\left(-\frac{k^2\chi^2}{2\zeta} - \frac{k^2\chi^2}{4\xi}\right)}{(\hbar\omega_v + \sqrt{2}\hbar\mathcal{G}V_F)} \quad (158),$$

$$\begin{aligned}
 E_{1-} = & -\frac{3}{2}V_F\hbar g(\sigma_x + \sigma_y) - \hbar g V_F \sum_{k,\nu} \frac{T_{k,\nu}^* T_{k,\nu} \exp\left(-\frac{k^2\chi^2}{\zeta} - \frac{k^2\chi^2}{2\xi}\right) \left(1 - \frac{k^2\chi^2}{2\xi}\right)^2}{(\hbar\omega_\nu + \sqrt{2}\hbar g V_F)^2} (\sigma_x + \sigma_y) - \hbar g l_z - 2 \cos(\beta t + \phi) \sigma_y - \sigma_z G \\
 & - A_1 \cos \theta \sigma_x - \sum_{k,\nu} \hbar\omega_\nu - \sum_{k,\nu} \hbar\omega_\nu \frac{T_{k,\nu}^* T_{k,\nu} \exp\left(-\frac{k^2\chi^2}{\zeta} - \frac{k^2\chi^2}{2\xi}\right) \left(1 - \frac{k^2\chi^2}{2\xi}\right)^2}{(\hbar\omega_\nu + \sqrt{2}\hbar g V_F)^2} + 2 \sum_{k,\nu} \frac{T_{k,\nu} T_{k,\nu}^* \exp\left(-\frac{k^2\chi^2}{\zeta} - \frac{k^2\chi^2}{2\xi}\right) \left(1 - \frac{k^2\chi^2}{2\xi}\right)^2}{(\hbar\omega_\nu + \sqrt{2}\hbar g V_F)^2}
 \end{aligned} \quad (159).$$

Thus the Eigen values of those energies are given as follow:

$$\begin{aligned}
 E_{0\pm} = & \pm \left[+ 2(\hbar g)^2 \left(\sum_{k,\nu} \frac{|T_{k,\nu}|^2 \exp\left(-\frac{k^2\chi^2}{\zeta} - \frac{k^2\chi^2}{2\xi}\right)}{(\hbar\omega_\nu + \sqrt{2}\hbar g V_F)^2} \right)^2 + \frac{1}{2} (V_F \hbar g)^2 + V_F \hbar g (A_1 \cos \theta + A_2 \cos(\beta t + \phi)) + A_1^2 \cos^2 \theta \right. \\
 & \left. + A_2^2 \cos^2(\beta t + \phi) + G^2 + 2\hbar g (V_F \hbar g + A_1 \cos \theta + A_2 \cos(\beta t + \phi)) \sum_{k,\nu} \frac{|T_{k,\nu}|^2 \exp\left(-\frac{k^2\chi^2}{\zeta} - \frac{k^2\chi^2}{2\xi}\right)}{(\hbar\omega_\nu + \sqrt{2}\hbar g V_F)^2} \right]^{\frac{1}{2}} \\
 & \pm \hbar g l_z \pm \sum_{k,\nu} \hbar\omega_\nu \frac{|T_{k,\nu}|^2 \exp\left(-\frac{k^2\chi^2}{\zeta} - \frac{k^2\chi^2}{2\xi}\right)}{(\hbar\omega_\nu + \sqrt{2}\hbar g V_F)^2} \mp 2 \sum_{k,\nu} \frac{|T_{k,\nu}|^2 \exp\left(-\frac{k^2\chi^2}{\zeta} - \frac{k^2\chi^2}{2\xi}\right)}{(\hbar\omega_\nu + \sqrt{2}\hbar g V_F)^2}
 \end{aligned} \quad (160),$$

$$\begin{aligned}
 E_{1\pm} = & \pm \left[2\hbar g (3V_F \hbar g + A_1 \cos \theta + A_2 \cos(\beta t + \phi)) \sum_{k,\nu} \frac{|T_{k,\nu}|^2 \exp\left(-\frac{k^2\chi^2}{\zeta} - \frac{k^2\chi^2}{2\xi}\right) \left(1 - \frac{k^2\chi^2}{2\xi}\right)^2}{(\hbar\omega_\nu + \sqrt{2}\hbar g V_F)^2} + 3V_F \hbar g (A_1 \cos \theta + A_2 \cos(\beta t + \phi)) \right. \\
 & \left. + 2(\hbar g)^2 \left(\sum_{k,\nu} \frac{|T_{k,\nu}|^2 \exp\left(-\frac{k^2\chi^2}{\zeta} - \frac{k^2\chi^2}{2\xi}\right) \left(1 - \frac{k^2\chi^2}{2\xi}\right)^2}{(\hbar\omega_\nu + \sqrt{2}\hbar g V_F)^2} \right)^2 + \frac{1}{2} (3V_F \hbar g)^2 + A_1^2 \cos^2 \theta + A_2^2 \cos^2(\beta t + \phi) + G^2 \right]^{\frac{1}{2}} \\
 & \pm \hbar g l_z \pm \sum_{k,\nu} \hbar\omega_\nu \pm \sum_{k,\nu} \hbar\omega_\nu \frac{|T_{k,\nu}|^2 \exp\left(-\frac{k^2\chi^2}{\zeta} - \frac{k^2\chi^2}{2\xi}\right) \left(1 - \frac{k^2\chi^2}{2\xi}\right)^2}{(\hbar\omega_\nu + \sqrt{2}\hbar g V_F)^2} \mp 2 \sum_{k,\nu} \frac{|T_{k,\nu}|^2 \exp\left(-\frac{k^2\chi^2}{\zeta} - \frac{k^2\chi^2}{2\xi}\right) \left(1 - \frac{k^2\chi^2}{2\xi}\right)^2}{(\hbar\omega_\nu + \sqrt{2}\hbar g V_F)^2}
 \end{aligned}$$

(161).

For the SO phonon the coupling element is given as in [51] by:

$$T_{k,SO} = \sqrt{\frac{e^2 \eta \hbar \omega_{SO,\nu}}{2A \epsilon_0 k}} \exp(-kz_0) \quad (162),$$

where $\omega_{SO,\nu}$ is the frequency of SO phonon with two branches $\nu = 1, 2$. η is the polarizability of substrate. A is the surface area of TMD, ϵ_0 is the permittivity of vacuum and z_0 is the internal

distance between the monolayer TMD and polar substrate. Thus the Eigen values of ground and first excited states energies are:

$$(E_{0\pm})_{SO} = \pm \left[2 \left(\frac{e^2 \eta \hbar \mathcal{Q}_{0,SO}(k, \chi, z_0)}{4\pi\epsilon_0} \right)^2 \left(\sum_{v=1}^2 \frac{\hbar\omega_{SO,v}}{(\hbar\omega_{SO,v} + \sqrt{2}\hbar\mathcal{V}_F)^2} \right)^2 + \frac{1}{2} (V_F \hbar \mathcal{G})^2 \right. \\ \left. + V_F \hbar \mathcal{G} (A_1 \cos \theta + A_2 \cos(\beta t + \phi)) + A_1^2 \cos^2 \theta + A_2^2 \cos^2(\beta t + \phi) + G^2 \right. \\ \left. + (V_F \hbar \mathcal{G} + A_1 \cos \theta + A_2 \cos(\beta t + \phi)) \times \left(\frac{e^2 \eta \hbar \mathcal{Q}_{0,SO}(k, \chi, z_0)}{2\pi\epsilon_0} \right) \left(\sum_{v=1}^2 \frac{\hbar\omega_{SO,v}}{(\hbar\omega_{SO,v} + \sqrt{2}\hbar\mathcal{V}_F)^2} \right) \right]^{\frac{1}{2}} \quad (163),$$

$$\pm \hbar \mathcal{G}_z \pm \frac{e^2 \eta \mathcal{Q}_{0,SO}(k, \chi, z_0)}{4\pi\epsilon_0} \sum_{v=1}^2 \left(\frac{\hbar\omega_{SO,v}}{\hbar\omega_{SO,v} + \sqrt{2}\hbar\mathcal{V}_F} \right)^2 \mp \frac{e^2 \eta \mathcal{Q}_{0,SO}(k, \chi, z_0)}{2\pi\epsilon_0} \sum_{v=1}^2 \left(\frac{\hbar\omega_{SO,v}}{\hbar\omega_{SO,v} + \sqrt{2}\hbar\mathcal{V}_F} \right)$$

with

$$\mathcal{Q}_{0,SO}(k, \chi, z_0) = \int_0^{k_c} \exp\left(-\frac{k^2 \chi^2}{\zeta} - \frac{k^2 \chi^2}{2\xi} - 2kz_0\right) dk \quad (164),$$

and

$$(E_{1\pm})_{SO} = \pm \left[2 \left(\frac{e^2 \eta \hbar \mathcal{Q}_{1,SO}(k, \chi, z_0)}{4\pi\epsilon_0} \right)^2 \left(\sum_{v=1}^2 \frac{\hbar\omega_{SO,v}}{(\hbar\omega_{SO,v} + \sqrt{2}\hbar\mathcal{V}_F)^2} \right)^2 + G^2 + \frac{1}{2} (3V_F \hbar \mathcal{G})^2 \right. \\ \left. + 3V_F \hbar \mathcal{G} (A_1 \cos \theta + A_2 \cos(\beta t + \phi)) + A_1^2 \cos^2 \theta + A_2^2 \cos^2(\beta t + \phi) \right. \\ \left. + (3V_F \hbar \mathcal{G} + A_1 \cos \theta + A_2 \cos(\beta t + \phi)) \frac{e^2 \eta \hbar \mathcal{Q}_{1,SO}(k, \chi, z_0)}{2\pi\epsilon_0} \sum_{v=1}^2 \frac{\hbar\omega_{SO,v}}{(\hbar\omega_{SO,v} + \sqrt{2}\hbar\mathcal{V}_F)^2} \right]^{\frac{1}{2}} \quad (165),$$

$$\pm \hbar \mathcal{G}_z \pm \frac{e^2 \eta \mathcal{Q}_{1,SO}(k, \chi, z_0)}{4\pi\epsilon_0} \sum_{v=1}^2 \left(\frac{\hbar\omega_{SO,v}}{\hbar\omega_{SO,v} + \sqrt{2}\hbar\mathcal{V}_F} \right)^2 \mp 2 \frac{e^2 \eta \mathcal{Q}_{1,SO}(k, \chi, z_0)}{2\pi\epsilon_0} \sum_{v=1}^2 \frac{\hbar\omega_{SO,v}}{\hbar\omega_{SO,v} + \sqrt{2}\hbar\mathcal{V}_F} \pm \sum_{v=1}^2 \hbar\omega_{SO,v}$$

with

$$\mathcal{Q}_{1,SO}(k, \chi, z_0) = \int_0^{k_c} \exp\left(-\frac{k^2 \chi^2}{\zeta} - \frac{k^2 \chi^2}{2\xi} - 2kz_0\right) \left(1 - \frac{k^2 \chi^2}{2\xi}\right) dk \quad (166).$$

For the LO phonon the coupling elements is taken as in [51]:

$$T_{k,LO} = \sqrt{\frac{e^2 \eta_0 L_m \hbar \omega_{LO}}{2A\epsilon_0}} \operatorname{erfc}\left(\frac{k\nu}{2}\right) \quad (167),$$

where ω_{LO} is the frequency of LO phonon. η_0 is the dielectric constant of the TMDs monolayer and is also use to describe the intrinsic polarizability of monolayer TMDs. L_m is the atomic thickness of the monolayer erfc is the complementary error function, in which \mathcal{V} denotes the confinement effect between LO phonons and carriers in 2D materials. Thus the Eigen values of ground and first excited states energies are:

$$(E_{0\pm})_{LO} = \pm \left[\begin{aligned} & 2 \left(\frac{e^2 \eta_0 L_m \hbar \mathcal{G} \hbar \omega_{LO}}{4\pi\epsilon_0 (\hbar\omega_{LO} + \sqrt{2}\hbar\mathcal{G}V_F)^2} Q_{0,LO}(k, \chi, \nu) \right)^2 + \frac{1}{2} (V_F \hbar \mathcal{G})^2 \\ & + V_F \hbar \mathcal{G} (A_1 \cos \theta + A_2 \cos(\beta t + \phi)) + A_1^2 \cos^2 \theta + A_2^2 \cos^2(\beta t + \phi) + G^2 \\ & + (V_F \hbar \mathcal{G} + A_1 \cos \theta + A_2 \cos(\beta t + \phi)) \left(\frac{e^2 \eta_0 L_m \hbar \mathcal{G} \hbar \omega_{LO}}{2\pi\epsilon_0 (\hbar\omega_{LO} + \sqrt{2}\hbar\mathcal{G}V_F)^2} Q_{0,LO}(k, \chi, \nu) \right) \end{aligned} \right]^{\frac{1}{2}} \quad (168),$$

$$\pm \hbar \mathcal{G}_z \pm \frac{e^2 \eta_0 L_m (\hbar\omega_{LO})^2}{4\pi\epsilon_0 (\hbar\omega_{LO} + \sqrt{2}\hbar\mathcal{G}V_F)^2} Q_{0,LO}(k, \chi, \nu) \mp \frac{e^2 \eta_0 L_m \hbar \omega_{LO}}{2\pi\epsilon_0 (\hbar\omega_{LO} + \sqrt{2}\hbar\mathcal{G}V_F)} Q_{0,LO}(k, \chi, \nu)$$

where $Q_{0,LO}(k, \chi, \nu) = \int_0^{k_c} k \exp\left(-\frac{k^2 \chi^2}{\zeta} - \frac{k^2 \chi^2}{2\xi}\right) \left[\text{erfc}\left(\frac{k\nu}{2}\right) \right]^2 dk$ (169),

and

$$(E_{1\pm})_{LO} = \pm \left[\begin{aligned} & 2 \left(\frac{e^2 \eta_0 L_m \hbar \mathcal{G} \hbar \omega_{LO} Q_{1,LO}(k, \chi, \nu)}{4\pi\epsilon_0 (\hbar\omega_{LO} + \sqrt{2}\hbar\mathcal{G}V_F)^2} \right)^2 + \frac{1}{2} (3V_F \hbar \mathcal{G})^2 \\ & + 3V_F \hbar \mathcal{G} (A_1 \cos \theta + A_2 \cos(\beta t + \phi)) + A_1^2 \cos^2 \theta + A_2^2 \cos^2(\beta t + \phi) + G^2 \\ & + (3V_F \hbar \mathcal{G} + A_1 \cos \theta + A_2 \cos(\beta t + \phi)) \left(\frac{e^2 \eta_0 L_m \hbar \mathcal{G} \hbar \omega_{LO} Q_{1,LO}(k, \chi, \nu)}{2\pi\epsilon_0 (\hbar\omega_{LO} + \sqrt{2}\hbar\mathcal{G}V_F)^2} \right) \end{aligned} \right]^{\frac{1}{2}} \quad (170),$$

$$\pm \hbar \mathcal{G}_z \pm \frac{e^2 \eta_0 L_m (\hbar\omega_{LO})^2}{4\pi\epsilon_0 (\hbar\omega_{LO} + \sqrt{2}\hbar\mathcal{G}V_F)^2} Q_{1,LO}(k, \chi, \nu) \pm \hbar \omega_{LO} \mp \frac{e^2 \eta_0 L_m \hbar \omega_{LO} Q_{1,LO}(k, \chi, \nu)}{2\pi\epsilon_0 (\hbar\omega_{LO} + \sqrt{2}\hbar\mathcal{G}V_F)}$$

where $Q_{1,LO}(k, \chi, \nu) = \int_0^{k_c} k \exp\left(-\frac{k^2 \chi^2}{\zeta} - \frac{k^2 \chi^2}{2\xi}\right) \left[\text{erfc}\left(\frac{k\nu}{2}\right) \right]^2 \left(1 - \frac{k^2 \chi^2}{2\xi}\right) dk$ (171).

- **Magnitude of Bandgap Modulation**

The Magnitude of the Bandgap Modulation (MBM) is evaluated as follow [51]:

$$2\Delta G = 2G - (E_{\gamma+} - E_{\gamma-}) \quad (172),$$

Where $E_\gamma (\gamma = 0,1)$ stand for ground or first excited states energies of polaron including LO or SO phonons modes.

- **Lifetime of polaron under microwave and radiowave**

The effect of temperature and interaction between carriers and phonon in a system give rise to quantum transition. The transition rate from fundamental to first excited state can be calculated based on the Fermi golden rule. Thus, the lifetime of polaron is given by Eq. (94), then after little developments we obtain:

Then for SO phonon we obtained:

$$\frac{\hbar}{\tau} = \frac{e^2 \eta}{2\epsilon_0} \left[-\frac{1}{\left(\frac{\chi^2}{\zeta} + \frac{\chi^2}{2\xi}\right)k_c + 2z_0} \exp\left(-\left(\frac{1}{\zeta} + \frac{1}{2\xi}\right)k_c^2 \chi^2 - 2k_c z_0\right) + \frac{1}{2z_0} \sum_{v=1}^2 n_k \hbar \omega_{SO,v} \right] \quad (173),$$

with

$$n_k = \left[\exp\left(\frac{(E_{0+})_{SO}}{k_B T}\right) - 1 \right]^{-1} \quad (174),$$

and for LO phonon

$$\frac{\hbar}{\tau} = \frac{e^2 \eta_0 L_m \hbar \omega_{LO} n_k}{2\epsilon_0} \int_0^{k_c} \exp\left(-\frac{k^2 \chi^2}{\zeta} - \frac{k^2 \chi^2}{2\xi}\right) \left[\operatorname{erfc}\left(\frac{kV}{2}\right) \right]^2 dk \quad (175),$$

with

$$n_k = \left[\exp\left(\frac{(E_{0+})_{LO}}{k_B T}\right) - 1 \right]^{-1} \quad (176).$$

The lifetime of polaron in ground state obtained here are all influenced by the amplitudes and the frequencies of both microwave and radiowave and also by the parameters of the monolayers. This result is quiet similar to that obtained in [151]. So one can suggest that radiowave and microwave can be use to control the lifetime, the motion of polaron and the decoherence parameters of polaron in TMDs. The lifetime of polaron also depends on the type of electron-phonon coupling.

2.3.2 EXCITON-POLARON IN TRANSITION METAL DICHALCOGENIDES

2.3.2.1 MAGNETIC BARRIER EFFECT ON EXCITON-POLARON IN TRANSITION METAL DICHALCOENIDES

The overall Hamiltonian of the exciton, phonon and exciton-phonon interacting energy operators is displayed in a non-diagonal manner and needs suitable diagonalization techniques to obtain precise eigenvalues and eigenfunctions of the exciton-phonon composite system. In this part, we considered an individual exciton that moves in panel depicting the monolayer, and interacting with 2D phonons and calculate the ground state and first excited state energies, the mobility and the effective mass of exciton-polaron. Thus the full Hamiltonian of the combined exciton and LO-phonon composite scheme appears to be expressed as:

$$\hat{H} = \hat{H}_{exc} + \hat{H}_{ph} + \hat{H}_{exc-ph} \quad (177),$$

where \hat{H}_{exc} denotes the quasi-two-dimensional Hamiltonian of exciton written as

$$\hat{H}_{exc} = \sum_k E^{exc}(k) B_k^+ B_k + \hat{H}_Z \quad (178),$$

where B_k^+ (B_k) denotes the creation (annihilation) operators for the 2D exciton wave vector k in which occurring in the monolayer that represents the transition metal and the atomic planes of the chalcogen. Note that the former term of Eq. (178) is arranged diagonally in the exciton operators because the exciton spreads unobstructed in the monolayer plane. The exciton's energy is given by:

$$E^{exc}(k) = E_g + \frac{\hbar^2 k^2}{2M} - E_b(\rho_{||}) + \zeta^2 \quad (179),$$

where E_g stands for the bandgap of the monolayer along the direction $\Sigma - k$; ζ is a constant

define as follow $\zeta = \frac{\hbar}{l_B} \left(\frac{1}{2M} + \frac{1}{2\chi} \right)^{1/2}$, χ is the reduce mass given as: $\chi = \frac{m_e \times m_h}{m_e + m_h}$, M is the

mass of exciton, \hbar is the reduced Planck constant, e and h stand respectively for electron and hole, $E_b(\rho_{||})$ represents the binding energy of exciton owing to the coulomb action that takes place between the electron and the hole in the surface plane of the monolayer. \hat{H}_Z displays the Hamiltonian of exciton polaron in Z direction defined as:

$$\hat{H}_Z = \frac{P_{e,z}^2}{2m_e} + \frac{P_{h,z}^2}{2m_h} + V_e(z_e) + V_h(z_h) - E_b(z) \quad (180),$$

where $P_{e,z}$ and $P_{h,z}$ denote the momentum related to electrons and holes respectively, $V_e(z_e)$ and $V_h(z_h)$ stand for the trap of the electron and holes between inter-layers of the TMD materials.

These trapping potentials appear as:

$$\begin{cases} V_e(z_e) = \frac{1}{2} m_e \Omega^2 z_e^2 \\ V_h(z_h) = \frac{1}{2} m_h \Omega^2 z_h^2 \end{cases} \quad (181),$$

with Ω the confinement strength of the trap $E_b(z)$ represents the exciton binding energy in z -direction. Hence we assume that the binding energy depends on $r = z_e - z_h$ where $z_e(z_h)$ represents the distance coordinate for electron (hole). We note m_e and m_h the respective electron hole carrier mass supposing that we have anisotropic features, and \hat{H}_{ph} represents the phonon energy defined as:

$$\hat{H}_{ph} = \sum_q \hbar \omega_q b_q^\dagger b_q \quad (182),$$

with $b_q^\dagger (b_q)$ being the phonon creation (annihilation) operators and \hat{H}_{exc-ph} gives the quasi-2D exciton- phonon interaction expressed as:

$$\hat{H}_{exc-ph} = \sum_{k, q_{//}, q_z} E(q_{//}, q_z) B_{k+q_{//}}^\dagger B_k (b_{q_{//}, q_z} + b_{-q_{//}, q_z}^\dagger) \quad (183),$$

with $q_{//} (q_z)$ represents the component of the wave vector in x, y plane (and z direction), $E(q_{//}, q_z)$ denotes the exciton-phonon coupling function shown in Ref. [152]. Next, we apply an accurate 2D form of the coupling function in which the z component of the phonon wave vector q_z is removed from the coupling function. The latter is expressed as in Refs. [153]:

$$E^i(q_{//}) = \sqrt{\frac{\hbar q_{//}}{2A\rho u}} \left[\frac{D_c^i}{(1-b_e^2)^{\frac{3}{2}}} - \frac{D_v^i}{(1-b_h^2)^{\frac{3}{2}}} \right] \quad (184),$$

where A denotes the area of the layer plane, u denotes the velocity of the sound, ρ is the mass density of the phonon, $i = ac, op$ stands for the acoustic or optic phonons. $D_c (D_v)$ is the constant of the deformation trap for electron and optical (acoustic) phonon in the conduction band (for hole in the valence band) respectively in the critical point (K, K') . We also have

$$\begin{cases} b_e = \frac{2a_{ex}m_e}{(m_e + m_h)} q_{//} \\ b_h = \frac{2a_{ex}m_h}{(m_e + m_h)} q_{//} \end{cases} \quad (185),$$

with a_{ex} being the effective exciton bohr radius.

In order to obtain eigenvalues and eigenfunctions of the exciton-phonon composite system, we need a suitable diagonalization technique to transform the Hamiltonian. Thus diagonalization technique consist to transform the operator \hat{H}_{ex-ph} in Eq. (177) having a non-diagonal form. Therefore, we apply the unitary transformations as in Ref. [154], $U_{ex} = e^{iS}$ where S appears as:

$$S = \sum_{q_{//}, q_z} B_{k+q_{//}}^+ B_k [f_{ex}^*(k, q_{//}) b_{-q_{//}}^+ + f_{ex}(k, q_{//}) b_{q_{//}}] \quad (186).$$

notice that $S = S^* = S^{-1}$, then the function $f_{ex}(k, q_{//})$ can be determined by minimizing the energy $U_{ex}^{-1} \hat{H} U_{ex}$. Let us note by \hat{H}' the new Hamiltonian. It is given by:

$$\hat{H}' = e^{-iS} \hat{H} e^{iS} = e^{-iS} (\hat{H}_{exc} + \hat{H}_{ph} + \hat{H}_{exc-ph}) e^{iS} \quad (187),$$

$$\hat{H}' = \hat{H}_0 + (i[\hat{H}_0, S] + \hat{H}_{exc-ph}) + i\left[\frac{i}{2}[\hat{H}_0, S] + \hat{H}_{exc-ph}, S\right] + \dots \quad (188),$$

$$\text{with} \quad \hat{H}_0 = \hat{H}_{ex} + \hat{H}_{ph} + \hat{H}_z. \quad (189),$$

to have a rough term of the transformed Hamiltonian, we will use only the first three term of the series in Eq. (188). Using the expression of exciton-phonon interaction operator \hat{H}_{exc-ph} , phonon operator \hat{H}_{ph} and exciton phonon \hat{H}_{ex} , we obtained the following expression of the function $f_{ex}(k, q_{//})$ given by:

$$\begin{cases} f_{ex}(k, q_{//}) = \frac{E^{ex}(q_{//})}{E^{ex}(k + q_{//}) - E^{ex}(k) - \hbar\omega} \\ f_{ex}^*(k, q_{//}) = \frac{E^{ex}(q_{//})}{E^{ex}(k + q_{//}) - E^{ex}(k) + \hbar\omega} \end{cases} \quad (190),$$

for small values of $f_{ex}(k, q_{//})$ the series in Eq. (189) is convergent, see Ref. [58]. The transformed Hamiltonian $\hat{H}' = U_{ex}^{-1} \hat{H} U_{ex}$ is then evaluated as:

$$\hat{H}' = U_{ex}^{-1} \hat{H} U_{ex} \approx \hat{H}_{ex} + \hat{H}_{ph} + \hat{H}_z + \hat{H}_{ex-ph}^T \quad (191),$$

where the term \hat{H}_{ex-ph}^T is given by

$$H_{ex-ph}^T = \sum_{k,q_z,q_{||}} \left(E^i(q_{||})\right)^2 \left[\frac{1}{E^{ex}(k_{||} + q_{||}) - E^{ex}(k_{||}) - \hbar\omega} - \frac{1}{E^{ex}(k_{||} + q_{||}) - E^{ex}(k_{||}) + \hbar\omega} \right] B_{k_{||}}^+ B_{k_{||}+q_{||}} B_{k_{||}+q_{||}}^+ B_{k_{||}} \quad (192).$$

In order to follow our calculations, we are going to make some approximations. For this purpose, the Hamiltonian converted into Eq. (191) is not entirely biased; this procedure is therefore taken as an estimate but offers a quantifiably computed solution for evaluating the energy of the exciton polaron (see Ref. [58]).

The fundamental state energy of an exciton-polaron is calculated through the state vector $|k, n(q)\rangle = B_k^+ |0\rangle |n(q)\rangle$ with $|0; n(q_{||})\rangle = |0\rangle |n(q_{||})\rangle$ where $|0\rangle$ denotes the vacuum state vector of the exciton and $|n(q_{||})\rangle = |n_{q_{||1}}, n_{q_{||2}}, \dots\rangle$ represents the 2D acoustic or optical phonon state vector with $n_{q_{||}}$ being the occupation number of phonon with wave vector $q_{||}$. The ground state energy of exciton polaron is obtained at low thermalized phonon occupation, and it is expressed as:

$$E_{ex-pol}(0) = \langle n(q), k | \hat{H}^i | k, n(q) \rangle \quad (193),$$

after some calculations the expression of the ground state energy is obtained as follows:

$$E_{ex-pol}(0) = E_g + E_z - E_b + \frac{\hbar^2 k^2}{2M} + \zeta^2 - T_{ex}(k) \quad (194),$$

where E_z gives the energy obtained by transforming the Hamiltonian \hat{H}_z using Huybrecht method and $T_{ex}(k)$ is given by:

$$T_{ex}(k) = \sum_{q_{||}} \left(E^i(q_{||})\right)^2 \left[\frac{1}{E^{ex}(k + q_{||}) - E^{ex}(k) - \hbar\omega} - \frac{1}{E^{ex}(k + q_{||}) - E^{ex}(k) + \hbar\omega} \right] \quad (195).$$

Transforming the summation over $q_{||}$ into integration we have:

$$T_{ex}(k) = \frac{S}{(2\pi)^2} \int_0^{q_{||}^m} q_{||} dq_{||} \int_0^{2\pi} d\theta E(q_{||}, q_z)^2 \left[\frac{1}{E^{ex}(k + q_{||}) - E^{ex}(k) - \hbar\omega} - \frac{1}{E^{ex}(k + q_{||}) - E^{ex}(k) + \hbar\omega} \right] \quad (196),$$

after calculations one gets

$$T_{ex}(k) = \frac{\hbar(D_c^i - D_v^i)^2}{4\pi\rho\chi} \int_0^{q_{||}^m} q_{||}^2 dq_{||} \left[\frac{1}{\frac{\hbar^2 q_{||}^2}{2M} + \frac{\hbar^2 k q_{||}}{M} - \hbar\omega} - \frac{1}{\frac{\hbar^2 q_{||}^2}{2M} + \frac{\hbar^2 k q_{||}}{M} + \hbar\omega} \right] \quad (197),$$

the above expression can be now transformed as follows:

$$T_{ex}(k) = \frac{\hbar(D_c^i - D_v^i)^2}{4\pi\rho\chi} \int_0^{q_{//}} q_{//}^2 dq_{//} \left[\frac{\sqrt{T_1}}{\frac{\hbar^2 q_{//}}{M} \left(\frac{q_{//}}{2} - k\right) - \hbar\omega} - \left(\frac{\hbar^2 q_{//}}{M} \left(\frac{q_{//}}{2} + k\right) + \hbar\omega\right)^{-1} \left(1 - \frac{M}{T_2}\right)^{-\frac{1}{2}} \right]$$

(198),

$$\text{where } T_1 = \frac{\frac{\hbar^2 q_{//}^2}{2M} - \frac{\hbar^2 k q_{//}}{M} - \hbar\omega}{\frac{\hbar^2 q_{//}^2}{2M} + \frac{\hbar^2 k q_{//}}{M} - \hbar\omega} \quad T_2 = \left(\frac{\hbar^2 q_{//}}{M} \left(\frac{q_{//}}{2} + k\right) + \hbar\omega \right) \quad (199),$$

In TMDs, $b_e(b_h) < 1$. Considering this assumption, and at small wave vectors we can write

$$T_{ex} = T_{ex1} + T_{ex2} \quad (200),$$

$$\begin{cases} T_{ex1} = \frac{\pi\sqrt{\hbar\omega}(D_c^{op} - D_v^{op})^2}{\sqrt{2\hbar^2\rho\chi}} (m_e + m_h)^{\frac{3}{2}} \\ T_{ex2} = \frac{3\pi(D_c^{op} - D_v^{op})^2 (m_e + m_h)^{\frac{3}{2}}}{4\rho\chi\sqrt{\hbar\omega}\sqrt{2}} \left(\frac{\hbar^2 k^2}{2M} \right) \end{cases} \quad (201).$$

Now, we evaluate the contribution of the energy in z-direction E_z . We consider the Hamiltonian \hat{H}_z under the presence of the magnetic field barrier. The core structure of the magnetic barrier is composed of the magnetic field strength B_z along the Z direction describes as a delta-like function [155]. This barrier can be constructed as in ref [41], thus Fig.12 illustrates the present case. Here, two long narrow magnetic stripes are placed perpendicular to the TMD layer

$$B_z(x) = Bl_B[\delta(x) - \delta(x-L)] \quad (202),$$

where L is the width of the barrier, l_B is a length scale of the barrier. For $m_e = m_h = 1$ we have

$$\hat{H}_z = \frac{P_{e,z}^2}{2} + \frac{P_{h,z}^2}{2} + \frac{1}{2}\Omega^2(z_e^2 + z_h^2) \quad (203),$$

If we consider that $P = p_e + p_h$; $p = \frac{p_e - p_h}{2}$ then we have: $p_e^2 + p_h^2 = \frac{P^2 + 4p^2}{2}$ and

$$R = \frac{z_e + z_h}{2}, \quad r = z_e - z_h \quad \text{then we have } z_e^2 + z_h^2 = \frac{4R^2 + r^2}{2},$$

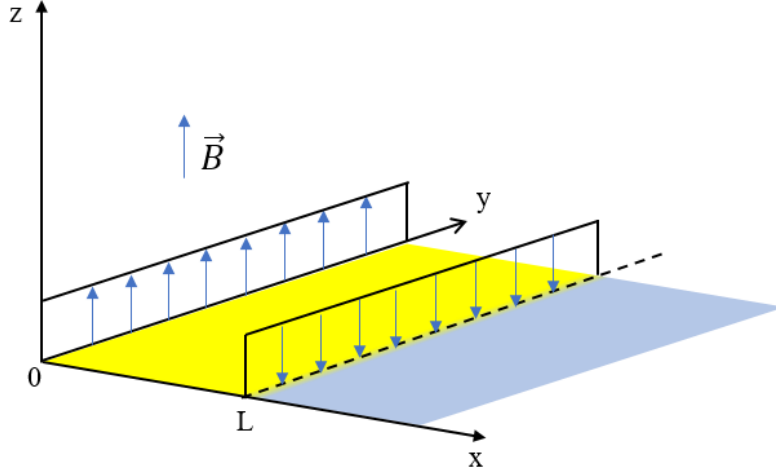


Figure 12 : Magnetic barrier using two long narrow magnetic stripes perpendicular to the monolayer TMD

Then we have

$$\hat{H}_z = \frac{P^2}{4} + \Omega^2 R^2 + E_r \quad (204),$$

with

$$E_r = \left\langle p^2 + \frac{1}{4} \Omega^2 r^2 \right\rangle \quad (205).$$

We minimize the Eq. (204) by the first unitary transformation of Huybrechts given by Eq. (64), and introducing operators of creation and annihilation given by Eq. (67), we have:

$$H'_z = \frac{1}{4} \left[\left(\frac{\hbar\lambda}{2} \right)^2 (b_j^+ + b_j) - a \sum_q \hbar q a_q^+ a_q \right]^2 - \Omega^2 \frac{\hbar}{2\lambda} (b_j^+ - b_j)(b_j^+ - b_j) + E_r \quad (206),$$

developing the above equation w obtain:

$$H'_z = \frac{\lambda\hbar}{8} \sum_j (b_j^+ b_j^+ + b_j^+ b_j + b_j b_j^+ + b_j b_j) + \hbar a \left(\frac{\lambda\hbar}{2} \right)^{1/2} \sum_{k,j} k (b_j^+ + b_j) a_k^+ a_k + \frac{\hbar^2 a^2}{8} \sum_{k,k'} k k' a_k^+ a_k^+ a_k a_k' - \Omega^2 \left(\frac{\hbar}{2\lambda} \right) \sum_j (b_j^+ b_j^+ - b_j^+ b_j - b_j b_j^+ + b_j b_j) + E_r \quad (207),$$

with $\lambda = \frac{eBl_B}{2}$, then averaging in the vacuum state as $E_z = \langle 0 | H'_z | 0 \rangle$, We obtain :

$$E_z = \frac{\lambda\hbar}{8} + -\Omega^2 \left(\frac{\hbar}{2\lambda} \right) + E_r \quad (208).$$

In Eq. (205) $\langle \dots \rangle$ denote an averaging over the fundamental state wave function, thus chosing the ground state oscillator wave function

$$\rho_0 = \left(\frac{b}{2\pi}\right)^{1/4} \exp\left(\frac{br^2}{4}\right) \quad (209),$$

where b is a variational parameter, we finally we obtain :

$$E_z = \frac{\hbar\lambda}{8} + \hbar \frac{\Omega^2}{2\lambda} + \frac{\Omega^2}{4b} \quad (210),$$

thus, the fundamental state energy of the exciton-polaron is given as follows:

$$E_{ex-pol}(0) = E_g + \frac{\hbar\lambda}{8} + \zeta^2 + \hbar \frac{\Omega^2}{2\lambda} + \frac{\Omega^2}{4b} - E_b + \frac{\hbar^2 k^2}{4} - T_{ex1} - T_{ex2} \quad (211).$$

By the same schemes as in the ground state, we derive the first excited state energy of exciton-polaron. The state vector used to derive the first excited state energy of exciton polaron is $|k, n(q)\rangle = B_k^+ |1\rangle |n(q)\rangle$ with $|1; n(q_{//})\rangle = |1\rangle |n(q_{//})\rangle$ where $|1\rangle$ represents the first state vector of exciton and $|n(q_{//})\rangle = |n_{q_{//1}}, n_{q_{//2}}, \dots\rangle$ previously defined. The exciton-polaron's energy in the first excited state can be evaluated at lower thermalization of the phonon state

$$E_{ex-pol}(1) = \langle n(q), k | \hat{H} | k, n(q) \rangle \quad (212),$$

after some calculation we obtain:

$$E_{ex-pol}(1) = \frac{3\hbar\lambda}{8} + 4\zeta^2 + 3\hbar \frac{\Omega^2}{2\lambda} + \frac{3\Omega^2}{4b} - T'_{ex1} - T'_{ex2} + 4E_g + \frac{4\hbar^2 k^2}{4} + \frac{\hbar^2 k^2 a^2}{4} - 4E_b + 2\hbar\omega \quad (213),$$

$$\text{with} \quad T'_{ex1} = 8T_{ex1} ; \quad T'_{ex2} = 8T_{ex2} \quad (214),$$

where T_{ex1} and T_{ex2} are given in Eq. (201). The ground and first excited states energies are independent of the width of the magnetic barrier; this is due to the fact that it is in the kronecker delta function which usually takes either 0 or 1.

- **Effective mass of exciton-polaron under magnetic barrier**

In order to investigate the effective mass of exciton-polaron, let's consider the Hamiltonian of the exciton-polaron given by Eq. (177), for the movement of exciton-polaron parallel to Z - axis, we introduce the unitary transformation and the linear combination of creation and annihilation operator $b_j^+(b_j)$ given by the following expression [156]

$$p_i = \left(\frac{\hbar\lambda}{2}\right)^{1/2} (b_j^+ + b_j + p_{0j}) \quad (215),$$

where P_{0j} is the variational parameter and the index j refers to the three directions. Let us put:

$$O = -2gk \left(\frac{\hbar\lambda}{2} \right)^{\frac{1}{2}} (b_j^+ + b_j + p_{oj}), \quad \text{where } g \text{ is a variational parameter. Then using}$$

diagonalization technique to evaluate the Hamiltonian via state vector as:

$|k, n(q)\rangle = B_k^+ |0, n(q)\rangle$, we have:

$$\hat{H}_1 = \sum_{k, q_{||}} E(q_{||})^2 \left[\frac{1}{E^{ex}(k + q_{||}) - E^{ex}(k) + (\hbar\omega - \hbar\theta)} - \frac{1}{E^{ex}(k + q_{||}) - E^{ex}(k) - (\hbar\omega - \hbar\theta)} \right] \quad (216)$$

$$+ \frac{\hbar\lambda}{8} + \zeta^2 + \hbar \frac{\Omega^2}{2\lambda} + \frac{\Omega^2}{4b} + \frac{\hbar\lambda}{8} p_{0j}^2 + E_g + \frac{\hbar^2 k^2}{4} - E_b(\rho_{||})$$

with $\theta = \langle 0 | O | 0 \rangle = -2gk \left(\frac{\hbar\lambda}{2} \right)^{\frac{1}{2}} (\langle 0 | b_j^+ | 0 \rangle + \langle 0 | b_j | 0 \rangle + \langle 0 | p_{oj} | 0 \rangle)$ thus $\theta = -2gk \left(\frac{\hbar\lambda}{2} \right)^{\frac{1}{2}} p_{oj}$

the minimization problem is now achieved by using Lagrange multipliers. With the choice of

an arbitrary constant multiplier ζ , we get: $G(k, q_{||}, q_z, p_0, \zeta, \lambda) = \hat{H}_1 - u\hat{P}_0$

where $G(k, q_{||}, q_z, p_0, \zeta, \lambda)$ represents a variational function and $\hat{P}_0 = \langle 0 | U_{ex}^{-1} U_1^{-1} \hat{P}_z U_1 U_{ex} | 0 \rangle$

where \hat{P}_z gives the total momentum of the exciton polaron then we have $\hat{P}_0 = \left(\frac{\hbar\lambda}{2} \right)^{\frac{1}{2}} p_0$ and

$$G(k, q_{||}, q_z, p_0, \zeta, \lambda) = \sum_{k, q_{||}} E(q_{||})^2 \left[\frac{1}{E^{ex}(k + q_{||}) - E^{ex}(k) - (\hbar\omega - \hbar\theta)} - \frac{1}{E^{ex}(k + q_{||}) - E^{ex}(k) + (\hbar\omega - \hbar\theta)} \right] \quad (217),$$

$$+ \frac{\hbar\lambda}{8} + \zeta^2 + \hbar \frac{\Omega^2}{2\lambda} + \frac{\Omega^2}{4b} + \frac{\hbar\lambda}{8} p_0^2 + E_g + \frac{\hbar^2 k^2}{4} - E_b(\rho_{||}) - \left(\frac{\hbar\lambda}{2} \right)^{\frac{1}{2}} \mathcal{P} p_0$$

we can now do this approximation

$$\frac{(E(q_{||}))^2}{E^{ex}(k + q_{||}) - E^{ex}(k) - \hbar\omega + \hbar\eta \left(\frac{\hbar\lambda}{2} \right)^{\frac{1}{2}} p_0} = \frac{(E(q_{||}))^2}{\frac{\hbar^2 q_{||}^2}{4} - \hbar\omega + \frac{\hbar^2 k q_{||}}{2}} \left(1 - \frac{\hbar\eta \left(\frac{\hbar\lambda}{2} \right)^{\frac{1}{2}} p_0}{\frac{\hbar^2 q_{||}^2}{4} - \hbar\omega + \frac{\hbar^2 k q_{||}}{2}} - \frac{\hbar^2 \eta^2 \left(\frac{\hbar\lambda}{2} \right)^2 p_0^2}{\left(\frac{\hbar^2 q_{||}^2}{4} - \hbar\omega + \frac{\hbar^2 k q_{||}}{2} \right)^2} + \dots \right) \quad (218)$$

with $\eta = 2gk$

then the expression of $G(k, q_{||}, q_z, p_0, \zeta, \lambda)$ take this form:

$$\begin{aligned}
 G(k, q_{\parallel}, q_z, p_0, \zeta, \lambda) = & \sum_{k, q_{\parallel}} \frac{(E(q_{\parallel}))^2}{\frac{\hbar^2 q_{\parallel}^2}{4} + \hbar\omega + \frac{\hbar^2 k q_{\parallel}}{2}} \left(1 + \frac{\hbar\eta \left(\frac{\hbar\lambda}{2}\right)^{\frac{1}{2}} p_0}{\frac{\hbar^2 q_{\parallel}^2}{4} + \hbar\omega + \frac{\hbar^2 k q_{\parallel}}{2}} + \frac{\hbar^2 \eta^2 \left(\frac{\hbar\lambda}{2}\right) p_0^2}{\left(\frac{\hbar^2 q_{\parallel}^2}{4} + \hbar\omega + \frac{\hbar^2 k q_{\parallel}}{2}\right)^2} + \dots \right) \\
 & + \frac{\hbar\lambda}{8} + \zeta^2 + \hbar \frac{\Omega^2}{2\lambda} + \frac{\Omega^2}{4b} + \frac{\hbar\lambda}{8} p_0^2 + E_g + \frac{\hbar^2 k^2}{4} - E_b(\rho_{\parallel}) - \left(\frac{\hbar\lambda}{2}\right)^{\frac{1}{2}} u p_0 \\
 & - \sum_{k, q_{\parallel}} \frac{(E(q_{\parallel}))^2}{\frac{\hbar^2 q_{\parallel}^2}{4} - \hbar\omega + \frac{\hbar^2 k q_{\parallel}}{2}} \left(1 - \frac{\hbar\eta \left(\frac{\hbar\lambda}{2}\right)^{\frac{1}{2}} p_0}{\frac{\hbar^2 q_{\parallel}^2}{4} - \hbar\omega + \frac{\hbar^2 k q_{\parallel}}{2}} - \frac{\hbar^2 \eta^2 \left(\frac{\hbar\lambda}{2}\right) p_0^2}{\left(\frac{\hbar^2 q_{\parallel}^2}{4} - \hbar\omega + \frac{\hbar^2 k q_{\parallel}}{2}\right)^2} + \dots \right)
 \end{aligned} \tag{219}.$$

Deriving Eq. (219) with respect to p_0 and setting it equal to zero we obtain the below expression for p_0 :

$$p_0 = \frac{\left(\frac{\hbar\lambda}{4}\right)^{\frac{1}{2}}}{\frac{\hbar\lambda}{4} + 2 \sum_{k, q_{\parallel}} \frac{(E(q_{\parallel}))^2 \hbar^2 \eta^2 \left(\frac{\hbar\lambda}{2}\right)}{\left(\frac{\hbar^2 q_{\parallel}^2}{4} + \hbar\omega + \frac{\hbar^2 k q_{\parallel}}{2}\right)^3} - 2 \sum_{k, q_{\parallel}} \frac{(E(q_{\parallel}))^2 \hbar^2 \eta^2 \left(\frac{\hbar\lambda}{2}\right)}{\left(\frac{\hbar^2 q_{\parallel}^2}{4} - \hbar\omega + \frac{\hbar^2 k q_{\parallel}}{2}\right)^3}} u \tag{220}.$$

The term u denotes the average velocity of the exciton-polaron in the z direction as the second term is neglected. Then the mass of exciton polaron can be approximated as:

$$m^* = \frac{1}{\left(\frac{\hbar\lambda}{2}\right)^{\frac{1}{2}} + s_1 + s_2} \tag{221},$$

$$\text{with } \begin{cases} s_1 = 2 \sum_{k, q_{\parallel}} \frac{(E(q_{\parallel}))^2 \hbar^2 \eta^2 \left(\frac{\hbar\lambda}{2}\right)^{\frac{1}{2}}}{\left(\frac{\hbar^2 q_{\parallel}^2}{2M^*} + \hbar\omega + \frac{\hbar^2 k q_{\parallel}}{M^*}\right)^3} \\ s_2 = -2 \sum_{k, q_{\parallel}} \frac{(E(q_{\parallel}))^2 \hbar^2 \eta^2 \left(\frac{\hbar\lambda}{2}\right)^{\frac{1}{2}}}{\left(\frac{\hbar^2 q_{\parallel}^2}{2M^*} - \hbar\omega + \frac{\hbar^2 k q_{\parallel}}{M^*}\right)^3} \end{cases} \tag{222}.$$

- **Mobility of exciton polaron under magnetic barrier effect**

According to the Eq. (130), the mobility of exciton-polaron is given in table 4 for all coupling range. These expressions of mobility are quiet similar for the case of polaron in weak and intermediate coupling regime, where mobility depends on the coupling constant, the effective mass of exciton-polaron, the energy of exciton-polaron and the temperature.

Table 4 : Coupling range and corresponding mobility [157, 158]

Coupling range	Expression of the mobility
for weak coupling ($\alpha < 3$) and $f(\alpha) = 1$	$\mu = \frac{e}{2\alpha m^* E_{ex-pol}(0)} \exp\left(\frac{E_{ex-pol}(0)}{k_B T}\right) \left(\frac{1}{1 + \frac{\alpha}{6}}\right)^3$
for intermediate coupling ($3 < \alpha < 6$) and $f(\alpha) = \frac{5}{4}$	$\mu = \frac{5e}{8\alpha m^* E_{ex-pol}(0)} \exp\left(\frac{E_{ex-pol}(0)}{k_B T}\right) \left(\frac{1}{1 + \frac{\alpha}{6}}\right)^3$
for strong coupling ($\alpha > 6$)	$\mu = \exp\left(\frac{E_{ex-pol}(0)}{k_B T}\right)$

The states energies of exciton-polaron are influenced by the length of magnetic barrier, the potentiel of deformation of electron in valence and conduction bands and others parameters of the system. Also, the mobility, the Shannon entropy, de probability density and the transition frequency which are related to the states energies are influenced by those parameters.

2.3.2.2 ELECTRON-PHONON COUPLING CONTRIBUTION ON EXCITON- POLARON IN TMDs QUANTUM DOT

We consider the system constituted by an exciton-polaron in TMDs monolayer (the exciton is formed by the interaction between an electron in the conduction band and a hole in the valence; the exciton interacting with a cloud of phonon via electron form the exciton-polaron) situated on polar substrate in a quantum dot under a uniform magnetic field, and investigate the ground state energy for all coupling range for both LO and SO phonons modes, the effective mass and the optical obsorption for weak and intermediate coupling regime. The total Hamiltonian can be written as:

$$H = H_{exc} + H_{ph} + H_{e-ph} + u(r) + U(|r_e - r_h|) \quad (223),$$

H_{exc} describes the Hamiltonian of the exciton define as:

$$H_{exc} = \gamma V_F \sum_{i=e,h} \left(\sigma_1 \left(\frac{p_{ix}}{m_i} - 2eA_x \right) + \sigma_2 \left(\frac{p_{iy}}{m_i} - 2eA_y \right) + \sigma_3 \left(\frac{p_{iz}}{m_i} - 2eA_z \right) + \sigma_3 G \right) \quad (224),$$

$\sigma_1, \sigma_2, \sigma_3$ are the Pauli matrices, V_F is the Fermi velocity, ($\gamma = \pm 1$) stand for the electron and hole respectively in the conduction and in the valence band, $2G$ is the magnitude of the bandgap and A is the potential vector. It is convenient to use the dimensionless units in $m_e = m_h = 1$.

The second term H_{ph} is the Hamiltonian of the phonon including SO and LO phonons modes define as:

$$H_{ph} = \sum_{k,\nu} \hbar \omega_\nu a_k^+ a_k \quad (225),$$

a_k^+, a_k are respectively creation and annihilation operators for phonon with wave vector k , ω_ν is the phonons frequency. The third term H_{e-ph} is the Hamiltonian of interaction between electron and phonon, $M_{k,\nu}$ is the coupling element of Fröhlich [51], and ν stand for LO or SO phonons modes

$$H_{e-ph} = \sum_{k,\nu} T_{k,\nu} (a_{-k}^+ + a_k) \exp(ikr) \quad (226).$$

The term $u(r)$ is the potential of confinement [159] in the quantum dot, whereas R , V and L are respectively the length, the depth and the smoothness of the quantum dot. C is a constant.

$$u(r) = \begin{cases} 0 & r < R - \frac{l}{2} \\ \frac{V}{2} \left(\frac{\tanh c \left(\frac{r-R}{L/2} \right)}{\tanh c} + 1 \right) & R - \frac{L}{2} \leq r \leq R + \frac{L}{2} \\ V & r > R + \frac{L}{2} \end{cases} \quad (227).$$

The last term $U(r) = \frac{U}{r_{eh}}$ is the coulomb potential between the electron and hole. Since exciton-polaron is a composite particle, it is convenient to introduce the notion of the center of mass and the relative coordinate and momentum, $P_x = p_{ex} + p_{hx}$, $P_y = p_{ey} + p_{hy}$, $P_z = p_{ez} + p_{hz}$,

$r_{eh} = r_e - r_h$, $R_1 = \frac{r_e + r_h}{2}$. r_{eh} is the distance between the electron and hole, r_h and r_e are respectively the hole position and the electron position. The distance between electron and hole can be defined as follow $r_{eh} = \sqrt{r^2 + D^2}$ with D the projection of the electron position in the band valence band (where the hole is) and r is the distance between the position of the hole and the projection of the electron position. Using relative coordinate relative to center of mass and the momentum, the Eq. (223) can be rewritten as:

$$H = V_F \sum_{i=e,h} (\sigma_1 \pi_{ix} + \sigma_2 \pi_{iy} + \sigma_3 \pi_{iz} + \sigma_3 G) + \sum_{k,v} B_{k,v} (a_{-k}^+ + a_k) \exp(ikR_1) + \sum_{k,v} \hbar \omega_v a_k^+ a_k + E_r + u(r) \quad (228),$$

with $B_{k,v} = 2M_{kv} \left\langle \cos\left(\frac{kr_{eh}}{2}\right) \right\rangle$; $E_r = \left\langle \frac{U}{r_{eh}} \right\rangle$ whit symbol $\langle \dots \rangle$ denoting an averaging over the

wave function thus using oscillator wave vector given by Eq. (209). Then we obtain:

$$B_{k,v} = \frac{(2b)^{1/2} T_{kv} \cos\left(\frac{kD^2}{2} - \frac{1}{2} \arctan \frac{k}{2b}\right)}{\left(\frac{b^2}{4} + \frac{k^2}{16}\right)^{1/4}} \quad \text{and} \quad E_r = \left(2\left(\frac{2\pi}{b}\right)^{3/2} + 8\pi^2 D^2\right) \frac{e^2}{\epsilon_\infty} \quad (229),$$

performing the first Huybrecht and second LLP unitary operators given respectively by Eq. (70) and Eq. (34) to the exciton-polaron Hamiltonian as $H' = U_2^{-1} U_1^{-1} H U_1 U_2$, the transformer Hamiltonian is given by :

$$H' = V_F \left[\sigma_i \pi_i - \sum_{k,i=e,h} \hbar \alpha \sigma_i k_i (a_k^+ + f_k^*) (a_k + f_k) + \sigma_3 G \right] + E_r + u(r) \quad (230),$$

$$+ \sum_{k,v} \hbar \omega_v (a_k^+ + f_k^*) (a_k + f_k) + \sum_{k,v} B_{k,v} (a_k^+ + f_k^*) (a_k + f_k) \exp[ikR_1(1-\alpha)]$$

The ground state energy is obtain by replacing into Eq. (230) p_i and r_i by the expression

given by Eq. (67), Then minimizing by the zero phonon $|\psi_0\rangle_e |0\rangle_{ph} = \begin{pmatrix} 0 \\ |0\rangle_e \end{pmatrix} |0\rangle_{ph}$ we obtain:

$$E = V_F \left[\sigma_3 G - \sum_{k,i} \hbar \alpha k_i \sigma_i f_k^* f_k \right] + \sum_{k,v} \hbar \omega_v f_k^* f_k + \sum_{k,v} B_{k,v} (f_k^* + f_k) \exp\left[-(1-\alpha)^2 \frac{\hbar}{2\lambda} k^2\right] + U + E_r \quad (231),$$

where $\lambda = \sqrt{eB/2\hbar}$ is the magnetic confinement length [51] and

$$f_k = - \frac{(2b)^{1/2} T_{k,\nu} \exp\left[-(1-\alpha)^2 \frac{\hbar}{2\lambda} k^2\right] \cos\left(\frac{kD^2}{2} - \frac{1}{2} \arctan \frac{k}{2b}\right)}{(V_F \alpha \hbar k + \hbar \omega_\nu) \left(\frac{b^2}{4} + \frac{k^2}{16}\right)^{1/4}} \quad (232),$$

$$U = \begin{cases} 0 & r < R - \frac{l}{2} \\ \frac{V}{2} \left(\frac{\tanh c \left(\frac{-2R}{L}\right)}{\tanh c} + 1 \right) & R - \frac{L}{2} \leq r \leq R + \frac{L}{2} \\ V & r > R + \frac{L}{2} \end{cases} \quad (233),$$

by replacing Eq. (232) into Eq. (231), the eigenvalues of the energies in the Landau level can now be obtained as:

$$E = \sqrt{(V_F G)^2 + \left(2b \hbar V_F \alpha \sum_{k;\nu} k \frac{T_{k,\nu}^2 \exp\left[-(1-\alpha)^2 \frac{\hbar}{\lambda} k^2\right] \cos^2\left(\frac{kD^2}{2} - \frac{1}{2} \arctan \frac{k}{2b}\right)}{(V_F \alpha \hbar k + \hbar \omega_\nu)^2 \left(\frac{b^2}{4} + \frac{k^2}{16}\right)^{1/2}} \right)^2} \\ + 2b \sum_{k,\nu} \hbar \omega_\nu \frac{T_{k,\nu}^2 \exp\left[-(1-\alpha)^2 \frac{\hbar}{\lambda} k^2\right] \cos^2\left(\frac{kD^2}{2} - \frac{1}{2} \arctan \frac{k}{2b}\right)}{(V_F \alpha \hbar k + \hbar \omega_\nu)^2 \left(\frac{b^2}{4} + \frac{k^2}{16}\right)^{1/2}} + U + \left(2 \left(\frac{2\pi}{b}\right)^{3/2} + 8\pi^2 D^2 \right) \frac{e^2}{\epsilon_\infty} \quad (234). \\ - 4b \sum_{k,\nu} \frac{T_{k,\nu}^2 \exp\left[-(1-\alpha)^2 \frac{\hbar}{2\lambda} k^2\right] \cos^2\left(\frac{kD^2}{2} - \frac{1}{2} \arctan \frac{k}{2b}\right)}{(V_F \alpha \hbar k + \hbar \omega_\nu) \left(\frac{b^2}{4} + \frac{k^2}{16}\right)^{1/4}}$$

The third term in Eq. (223) represented respectively the interaction between carriers and optical phonon, we obtain the following results for different coupling regime and for SO and LO phonons:

The energies of SO and LO in the weak coupling ($\alpha = 1$) are respectively:

$$\begin{aligned}
 E_{SO} = & \sqrt{(V_F G)^2 + \left(\frac{b\hbar V_F e^2 \eta}{2\pi\epsilon_0} \sum_{\nu=1,2} \hbar\omega_{SO} \int_0^{K_c} k dk \frac{\exp(-2kz_0) \cos^2\left(\frac{kD^2}{2} - \frac{1}{2} \arctan \frac{k}{2b}\right)}{(V_F \hbar k + \hbar\omega_{SO\nu})^2 \left(\frac{b^2}{4} + \frac{k^2}{16}\right)^{1/2}} \right)^2} \\
 & + \frac{be^2 \eta}{2\pi\epsilon_0} \sum_{\nu=1,2} (\hbar\omega_{SO})^2 \int_0^{K_c} dk \frac{\exp(-2kz_0) \cos^2\left(\frac{kD^2}{2} - \frac{1}{2} \arctan \frac{k}{2b}\right)}{(V_F \hbar k + \hbar\omega_{SO\nu})^2 \left(\frac{b^2}{4} + \frac{k^2}{16}\right)^{1/2}} + U + \left(2\left(\frac{2\pi}{b}\right)^{3/2} + 8\pi^2 D^2\right) \frac{e^2}{\epsilon_\infty} \\
 & - \frac{be^2 \eta}{\pi\epsilon_0} \sum_{\nu=1,2} \hbar\omega_{SO} \int_0^{K_c} dk \frac{\exp(-2kz_0) \cos^2\left(\frac{kD^2}{2} - \frac{1}{2} \arctan \frac{k}{2b}\right)}{(V_F \hbar k + \hbar\omega_{SO\nu}) \left(\frac{b^2}{4} + \frac{k^2}{16}\right)^{1/4}}
 \end{aligned} \tag{235a}$$

and

$$\begin{aligned}
 E_{LO} = & \sqrt{(V_F G)^2 + \left(\frac{\hbar b V_F e^2 \eta_0 L_m \hbar\omega_{LO}}{2\pi\epsilon_0} \int_0^{K_c} k^2 dk \frac{\left(\operatorname{erfc}\left[\frac{k\sigma}{2}\right]\right)^2 \cos^2\left(\frac{kD^2}{2} - \frac{1}{2} \arctan \frac{k}{2b}\right)}{(V_F \hbar k + \hbar\omega_{LO})^2 \left(\frac{b^2}{4} + \frac{k^2}{16}\right)^{1/2}} \right)^2} \\
 & + \frac{e^2 b \eta_0 L_m (\hbar\omega_{LO})^2}{2\pi\epsilon_0} \int_0^{K_c} k dk \frac{\left(\operatorname{erfc}\left[\frac{k\sigma}{2}\right]\right)^2 \cos^2\left(\frac{kD^2}{2} - \frac{1}{2} \arctan \frac{k}{2b}\right)}{(V_F \hbar k + \hbar\omega_{LO})^2 \left(\frac{b^2}{4} + \frac{k^2}{16}\right)^{1/2}} + U + \left(2\left(\frac{2\pi}{b}\right)^{3/2} + 8\pi^2 D^2\right) \frac{e^2}{\epsilon_\infty} \\
 & - \frac{e^2 b \eta_0 L_m \hbar\omega_{LO}}{\pi\epsilon_0} \int_0^{K_c} k dk \frac{\left(\operatorname{erfc}\left[\frac{k\sigma}{2}\right]\right)^2 \cos^2\left(\frac{kD^2}{2} - \frac{1}{2} \arctan \frac{k}{2b}\right)}{(V_F \hbar k + \hbar\omega_{LO}) \left(\frac{b^2}{4} + \frac{k^2}{16}\right)^{1/2}}
 \end{aligned} \tag{235b}$$

The energies of SO and LO exciton-polaron in the intermediate coupling ($0 < \alpha < 1$) are respectively:

$$\begin{aligned}
 E_{SO} = & \sqrt{(V_F G)^2 + \left(\frac{\hbar b V_F e^2 \alpha \eta}{2\pi\epsilon_0} \sum_{\nu=1,2} \hbar\omega_{SO,\nu} \int_0^{K_c} k dk \frac{\exp(-2kz_0) \exp\left[-(1-\alpha)^2 \frac{\hbar}{\lambda} k^2\right] \cos^2\left(\frac{kD^2}{2} - \frac{1}{2} \arctan \frac{k}{2b}\right)}{(V_F \hbar \alpha k + \hbar\omega_{SO,\nu})^2 \left(\frac{b^2}{4} + \frac{k^2}{16}\right)^{1/2}} \right)^2} \\
 & + U + \left(2 \left(\frac{2\pi}{b} \right)^{3/2} + 8\pi^2 D^2 \right) \frac{e^2}{\epsilon_\infty} + \frac{be^2 \eta}{2\pi\epsilon_0} \sum_{\nu=1,2} (\hbar\omega_{SO,\nu})^2 \int_0^{K_c} dk \frac{\exp(-2kz_0) \exp\left[-(1-\alpha)^2 \frac{\hbar}{\lambda} k^2\right] \cos^2\left(\frac{kD^2}{2} - \frac{1}{2} \arctan \frac{k}{2b}\right)}{(V_F \alpha \hbar k + \hbar\omega_{SO,\nu})^2 \left(\frac{b^2}{4} + \frac{k^2}{16}\right)^{1/2}} \quad (236a), \\
 & - \frac{be^2 \eta}{\pi\epsilon_0} \sum_{\nu=1,2} \hbar\omega_{SO,\nu} \int_0^{K_c} dk \frac{\exp(-2kz_0) \exp\left[-(1-\alpha)^2 \frac{\hbar}{2\lambda} k^2\right] \cos^2\left(\frac{kD^2}{2} - \frac{1}{2} \arctan \frac{k}{2b}\right)}{(V_F \hbar \alpha k + \hbar\omega_{SO,\nu})^2 \left(\frac{b^2}{4} + \frac{k^2}{16}\right)^{1/4}}
 \end{aligned}$$

and

$$\begin{aligned}
 E_{LO} = & \sqrt{(V_F G)^2 + \left(\frac{\hbar b \alpha V_F e^2 \eta_0 L_m \hbar\omega_{LO}}{2\pi\epsilon_0} \int_0^{K_c} k^2 dk \frac{\left(\operatorname{erfc}\left[\frac{k\sigma}{2}\right]\right)^2 \exp\left[-(1-\alpha)^2 \frac{\hbar}{\lambda} k^2\right] \cos^2\left(\frac{kD^2}{2} - \frac{1}{2} \arctan \frac{k}{2b}\right)}{(V_F \hbar \alpha k + \hbar\omega_{LO})^2 \left(\frac{b^2}{4} + \frac{k^2}{16}\right)^{1/2}} \right)^2} \\
 & + \frac{be^2 \eta_0 L_m (\hbar\omega_{LO})^2}{2\pi\epsilon_0} \int_0^{K_c} k dk \frac{\left(\operatorname{erfc}\left[\frac{k\sigma}{2}\right]\right)^2 \exp\left[-(1-\alpha)^2 \frac{\hbar}{\lambda} k^2\right] \cos^2\left(\frac{kD^2}{2} - \frac{1}{2} \arctan \frac{k}{2b}\right)}{(V_F \hbar \alpha k + \hbar\omega_{LO})^2 \left(\frac{b^2}{4} + \frac{k^2}{16}\right)^{1/2}} + U + \left(2 \left(\frac{2\pi}{b} \right)^{3/2} + 8\pi^2 D^2 \right) \frac{e^2}{\epsilon_\infty} \\
 & - \frac{be^2 \eta_0 L_m \hbar\omega_{LO}}{\pi\epsilon_0} \int_0^{K_c} k dk \frac{\left(\operatorname{erfc}\left[\frac{k\sigma}{2}\right]\right)^2 \exp\left[-(1-\alpha)^2 \frac{\hbar}{2\lambda} k^2\right] \cos^2\left(\frac{kD^2}{2} - \frac{1}{2} \arctan \frac{k}{2b}\right)}{(V_F \hbar \alpha k + \hbar\omega_{LO}) \left(\frac{b^2}{4} + \frac{k^2}{16}\right)^{1/4}}
 \end{aligned}$$

(236b).

The energies of SO and LO exciton-polaron in the strong coupling ($\alpha = 0$) are respectively:

$$\begin{aligned}
 E_{SO} = & V_F G + \frac{e^2 \eta}{2\pi\epsilon_0} \int_0^{K_c} \frac{\exp(-2kz_0) \exp\left[-\frac{\hbar}{\lambda} k^2\right] \cos^2\left(\frac{kD^2}{2} - \frac{1}{2} \arctan \frac{k}{2b}\right)}{\left(\frac{b^2}{4} + \frac{k^2}{16}\right)^{1/2}} dk + U \\
 & - \frac{e^2 \eta}{\pi\epsilon_0} \int_0^{K_c} \frac{\exp(-2kz_0) \exp\left[-\frac{\hbar}{2\lambda} k^2\right] \cos^2\left(\frac{kD^2}{2} - \frac{1}{2} \arctan \frac{k}{2b}\right)}{\left(\frac{b^2}{4} + \frac{k^2}{16}\right)^{1/4}} dk + \left(2 \left(\frac{2\pi}{b} \right)^{3/2} + 8\pi^2 D^2 \right) \frac{e^2}{\epsilon_\infty} \quad (237a),
 \end{aligned}$$

and

$$E_{LO} = V_F G + \frac{e^2 \eta_0 L_m}{2\pi \epsilon_0} \int_0^{K_c} \frac{k \left(\operatorname{erfc} \left[\frac{k\sigma}{2} \right] \right)^2 \exp \left[-\frac{\hbar}{\lambda} k^2 \right] \cos^2 \left(\frac{kD^2}{2} - \frac{1}{2} \arctan \frac{k}{2b} \right)}{\left(\frac{b^2}{4} + \frac{k^2}{16} \right)^{1/2}} dk + U \quad (237b).$$

$$- \frac{e^2 \eta_0 L_m}{\pi \epsilon_0} \int_0^{K_c} \frac{k \left(\operatorname{erfc} \left[\frac{k\sigma}{2} \right] \right)^2 \exp \left[-\frac{\hbar}{2\lambda} k^2 \right] \cos^2 \left(\frac{kD^2}{2} - \frac{1}{2} \arctan \frac{k}{2b} \right)}{\left(\frac{b^2}{4} + \frac{k^2}{16} \right)^{1/4}} dk + \left(2 \left(\frac{2\pi}{b} \right)^{3/2} + 8\pi^2 D^2 \right) \frac{e^2}{\epsilon_\infty}$$

- **Effect of electron-phonon coupling on effective mass of exciton polaron**

Many authors in literature have proposed various methods to evaluate the effective mass of quasiparticles. The effective mass can also be obtained by using the second derivative of energy of the state system. it is given as in [151]:

$$\frac{1}{m^*} = \frac{\partial^2 E_v}{\partial k^2} \quad (238),$$

thus, we have used Eq. (238) to investigate the exciton-polaron effective mass in whic E_v is the energy exciton-polaron with LO or SO Phonons

- **Optical absorption of exciton-polaron**

The absorption coefficient $\Gamma(\hbar\Omega)$ of the incident light with the energy $\hbar\Omega$ of a free quasiparticles, according to Fermi's golden rule, is [160, 161]

$$\Gamma(\hbar\Omega) = \frac{\pi}{\hbar c n \epsilon F^2} \sum_f |\langle \psi_0 | V | \psi_f \rangle|^2 \delta(E_0 + \hbar\Omega - E_f) \quad (239).$$

For more details, based on the formula given by Eq. (239), readers should refer to [162]. The calculation of the absorption coefficient is very difficult because the excited final state comprises all excited states of the quasiparticles, which is not well known. Thus, to prevent complicated summation on the final states, Devreese and his collaborators [160] have developed a simple model in which the wave functions ψ_f of the excited states have been suppressed by the Lee Löw Pines unit transformations. It was noted that Eq. (239) concerns the weak and intermediate coupling regime. Considering the system of exciton-polaron describe by the Hamiltonian of Eq. (223) and using the same formula established in the case of polaron to

evaluated the optical absorption in the case of exciton-polaron for SO and LO phonon mode, we obtain, in the weak coupling, the absorption coefficient for SO and LO exciton-polaron

$$\Gamma(\hbar\Omega) = \begin{cases} \frac{V_F b e^4 \eta}{2c n \epsilon \epsilon_0 m^2 (\hbar\Omega)^3} \sum_{v=1,2} \hbar \omega_{SO,v} \Theta_1^2 \frac{\exp[-2z_0 \Theta_1]}{\left(\frac{b^2}{4} + \left(\frac{\Theta_1}{4}\right)^2\right)^{1/2}} \cos^2\left(\frac{\Theta_1 D^2}{2} - \frac{1}{2} \arctan \frac{\Theta_1}{2b}\right) \\ \frac{V_F b e^4 \eta_0 L_m \hbar \omega_{LO} \Theta_2^2}{2\hbar c n \epsilon \epsilon_0 m^2 (\hbar\Omega)^3} \frac{\left[\operatorname{erfc}\left(\frac{\Theta_2 \sigma}{2}\right)\right]^2}{\left(\frac{b^2}{4} + \left(\frac{\Theta_2}{4}\right)^2\right)^{1/2}} \cos^2\left(\frac{\Theta_2 D^2}{2} - \frac{1}{2} \arctan \frac{\Theta_2}{2b}\right) \end{cases} \quad (240),$$

finally, the absorption coefficient of SO and LO exciton-polaron in the intermediate coupling gives:

$$\Gamma(\hbar\Omega) = \begin{cases} \frac{V_F b e^4 \eta}{2\alpha c n \epsilon \epsilon_0 (\hbar\Omega)^3} \sum_{v=1,2} \hbar \omega_{SO,v} \Theta_1^2 \frac{\exp\left[-\frac{2z_0 \Theta_1}{\alpha}\right]}{\left(\frac{b^2}{4} + \left(\frac{\Theta_1}{4\alpha}\right)^2\right)^{1/2}} \cos^2\left(\frac{\Theta_1 D^2}{2\alpha} - \frac{1}{2} \arctan \frac{\Theta_1}{2b\alpha}\right) \exp\left[-\left(\frac{1-\alpha}{\alpha}\right)^2 \frac{\hbar}{\lambda} \Theta_1^2\right] \\ \frac{V_F b e^4 \eta_0 L_m \hbar \omega_{LO} \Theta_2^2}{2\hbar \alpha c n \epsilon \epsilon_0 (\hbar\Omega)^3} \frac{\left[\operatorname{erfc}\left(\frac{\Theta_2 \sigma}{2\alpha}\right)\right]^2}{\left(\frac{b^2}{4} + \left(\frac{\Theta_2}{4\alpha}\right)^2\right)^{1/2}} \cos^2\left(\frac{\Theta_2 D^2}{2\alpha} - \frac{1}{2} \arctan \frac{\Theta_2}{2b\alpha}\right) \exp\left[-\left(\frac{1-\alpha}{\alpha}\right)^2 \frac{\hbar}{\lambda} \Theta_2^2\right] \end{cases} \quad (241),$$

with $\Theta_1 = \frac{\hbar\Omega - \hbar\omega_{SO,v}}{\hbar V_F}$ $\Theta_2 = \frac{\hbar\Omega - \hbar\omega_{LO}}{V_F \hbar}$.

We observe that energies in weak coupling regime as same as optical absorption are independant of the magnetic field which is differents from other coupling regime (intermediate and strong coupling regime). So, the optical absorption and ground state energy in weak coupling regime can not be altered by an external magnetic field. Both magnetic field and electron-phonon coupling can be used to tuned state energy and optical absorption.

2.3.3 BIPOLARON IN TRANSITION METAL DICHALCOGENIDES

2.3.3.1 BIPOLARON IN TMDs: ALL COUPLING APPROACH

Let us consider a bipolaron ungergoing the effect of an incident photon in monolayer of TMDs situates on a polar substrate in presence of uniform magnetic field applied on the third directions in a quantum dot illustrates by Fig.13. In this part we investigated the ground state energie for all coupling range, and the optical absorption for weak and intermediate coupling of the bipolaron. The total Hamiltonian of bipolaron can be written in this form

$$H_{bp} = H_e + H_{ph} + H_{e-ph} + u(|r_1 - r_2|) + U(|r_1 - r_2|) \quad (242),$$

where H_e is given as in Eq. (224) where the hole is replaced by another electron as bipolaron is form by two electron interacting via coulomb repulsion H_{ph} , H_{e-ph} and $u(r_1 - r_2)$ are respectively given by Eqs. (225), (226) and (227). The last term of Eq. (242) is the coulomb interaction potential between the two electrons. Using the same schemes as in the case of electron-phonon coupling contribution on the optical absorption and the dynamic of exciton-polaron in monolayer TMDs to obtain the ground state energy, we obtain:

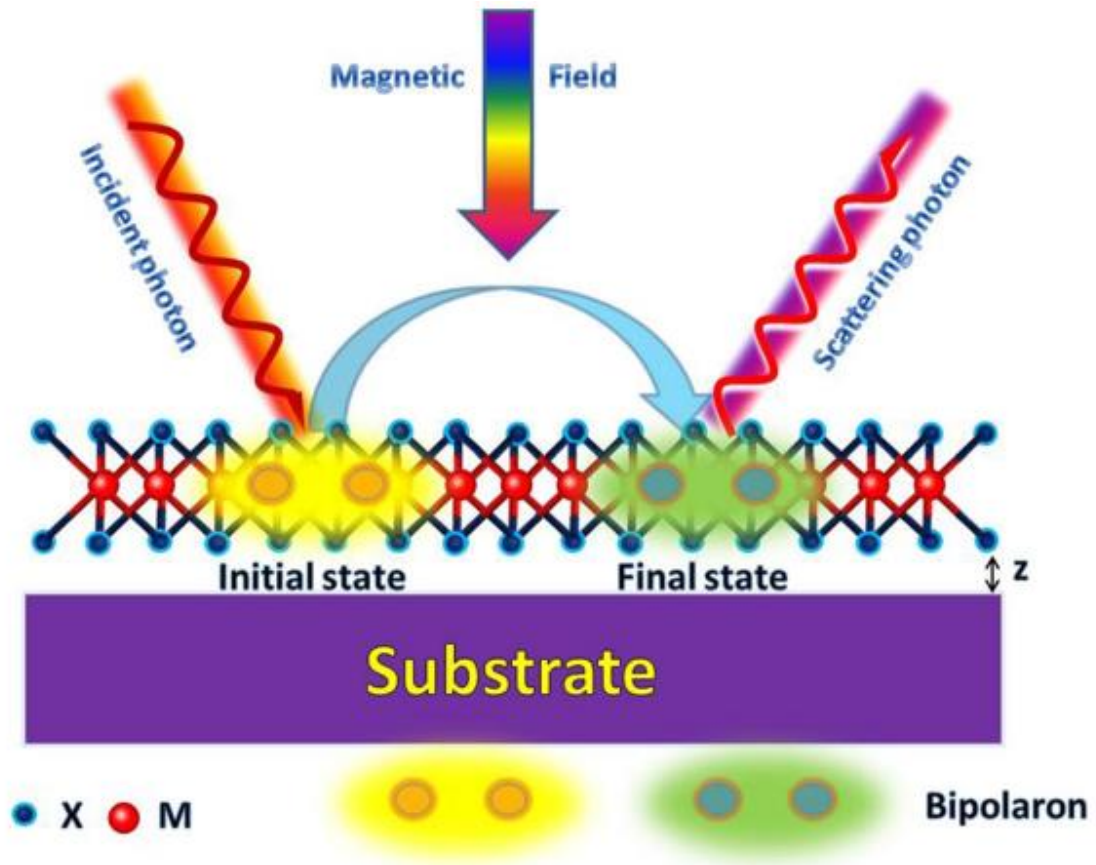


Figure 13 : sketch of the optical absorption of the bipolaron in the monolayer TMDs [162]

Then we obtain the bipolaron energy:

$$\begin{aligned}
 E_{bp0+} = & -\sum_{k,v} 4\alpha\sigma_1 \hbar V_F k_x \frac{T_{k,v} T_{k,v}^* \exp\left[-(1-\alpha)^2 \frac{\hbar}{m\lambda} k^2\right] \exp\left(-\frac{k^2}{b}\right)}{(V_F \alpha \hbar k + \hbar \omega_v)^2} - \sum_{k,v} 4\alpha\sigma_2 \hbar V_F k_y \frac{T_{k,v} T_{k,v}^* \exp\left[-(1-\alpha)^2 \frac{\hbar}{m\lambda} k^2\right] \exp\left(-\frac{k^2}{b}\right)}{(V_F \alpha \hbar k + \hbar \omega_v)^2} \\
 & - \sum_{k,v} 4\alpha\sigma_3 \hbar V_F k_z \frac{T_{k,v} T_{k,v}^* \exp\left[-(1-\alpha)^2 \frac{\hbar}{m\lambda} k^2\right] \exp\left(-\frac{k^2}{b}\right)}{(V_F \alpha \hbar k + \hbar \omega_v)^2} + \sum_{k,v} 4\hbar \omega_v \frac{T_{k,v} T_{k,v}^* \exp\left[-(1-\alpha)^2 \frac{\hbar}{m\lambda} k^2\right] \exp\left(-\frac{k^2}{b}\right)}{(V_F \alpha \hbar k + \hbar \omega_v)^2} + U \\
 & + 4\pi^2 \left(\frac{b}{2\pi}\right)^{1/2} \frac{e^2}{\epsilon_\infty b} + \sum_{k,v} 8 \frac{T_{k,v} T_{k,v}^* \exp\left[-(1-\alpha)^2 \frac{\hbar}{2m\lambda} k^2\right] \exp\left(-\frac{k^2}{2b}\right)}{(V_F \alpha \hbar k + \hbar \omega_v)} + \sigma_3 V_F G
 \end{aligned}$$

(244).

Finally, the eigenvalues of the energies in the zero Landau Levels can be written as:

$$\begin{aligned}
 E_{bp0\pm} = & \pm \sqrt{(V_F G)^2 + \left(4\hbar V_F \alpha \sum_{k,v} k \frac{T_{k,v}^2 \exp\left[-(1-\alpha)^2 \frac{\hbar}{m\lambda} k^2\right] \exp\left(-\frac{k^2}{b}\right)}{(V_F \alpha \hbar k + \hbar \omega_v)^2}\right)^2} \pm U \pm 4\pi^2 \left(\frac{b}{2\pi}\right)^{1/2} \frac{e^2}{\epsilon_\infty b} \\
 & \pm 4 \sum_{k,v} \hbar \omega_v \frac{T_{k,v}^2 \exp\left[-(1-\alpha)^2 \frac{\hbar}{m\lambda} k^2\right] \exp\left(-\frac{k^2}{b}\right)}{(V_F \alpha \hbar k + \hbar \omega_v)^2} \mp 8 \sum_{k,v} \frac{T_{k,v}^2 \exp\left[-(1-\alpha)^2 \frac{\hbar}{2m\lambda} k^2\right] \exp\left(-\frac{k^2}{2b}\right)}{(V_F \alpha \hbar k + \hbar \omega_v)}
 \end{aligned}$$

(245).

Replacing the coupling element for SO phonon and for LO phonon mode, we obtain the following results for different coupling regime and for SO and LO phonons:

The energies of SO and LO in the weak coupling ($\alpha = 1$) are respectively :

$$\begin{aligned}
 (E_{bp0\pm})_{SO} = & \pm \sqrt{(V_F G)^2 + \left(\frac{\hbar V_F e^2 \eta}{\pi \epsilon_0} \sum_{\nu=1,2} \hbar \omega_{SO,\nu} \int_0^{K_\nu} k dk \frac{\exp(-2kz_0) \exp\left(-\frac{k^2}{b}\right)}{(V_F \hbar k + \hbar \omega_{SO,\nu})^2}\right)^2} \pm U \pm 4\pi^2 \left(\frac{b}{2\pi}\right)^{1/2} \frac{e^2}{\epsilon_\infty b} \\
 & \pm \frac{e^2 \eta}{\pi \epsilon_0} \sum_{\nu=1,2} (\hbar \omega_{SO,\nu})^2 \int_0^{K_\nu} dk \frac{\exp(-2kz_0) \exp\left(-\frac{k^2}{b}\right)}{(V_F \hbar k + \hbar \omega_{SO,\nu})^2} \mp 2 \frac{e^2 \eta}{\pi \epsilon_0} \sum_{\nu=1,2} \hbar \omega_{SO,\nu} \int_0^{K_\nu} dk \frac{\exp(-2kz_0) \exp\left(-\frac{k^2}{2b}\right)}{(V_F \hbar k + \hbar \omega_{SO,\nu})^2}
 \end{aligned}$$

(246a),

and

$$(E_{bp0\pm})_{LO} = \pm \sqrt{(V_F G)^2 + \left(\frac{\hbar V_F e^2 \eta_0 L_m \hbar \omega_{LO}}{\pi \varepsilon_0} \int_0^{K_c} k^2 dk \frac{\left(\operatorname{erfc} \left[\frac{k\sigma}{2} \right] \right)^2 \exp\left(-\frac{k^2}{b}\right)}{(V_F \hbar k + \hbar \omega_{LO})^2} \right)^2} \pm U \pm 4\pi^2 \left(\frac{b}{2\pi} \right)^{1/2} \frac{e^2}{\varepsilon_\infty b}$$

$$\pm \frac{e^2 \eta_0 L_m (\hbar \omega_{LO})^2}{\pi \varepsilon_0} \int_0^{K_c} k dk \frac{\left(\operatorname{erfc} \left[\frac{k\sigma}{2} \right] \right)^2 \exp\left(-\frac{k^2}{b}\right)}{(V_F \hbar k + \hbar \omega_{LO})^2} \mp 2 \frac{e^2 \eta_0 L_m \hbar \omega_{LO}}{\pi \varepsilon_0} \int_0^{K_c} k dk \frac{\left(\operatorname{erfc} \left[\frac{k\sigma}{2} \right] \right)^2 \exp\left(-\frac{k^2}{2b}\right)}{(V_F \hbar k + \hbar \omega_{LO})}$$

(246b).

The energies of SO and LO bipolaron in the intermediate coupling ($0 < \alpha < 1$) are respectively:

$$(E_{bp0\pm})_{SO} = \pm \sqrt{(V_F G)^2 + \left(\frac{\hbar V_F e^2 \alpha \eta}{\pi \varepsilon_0} \sum_{\nu=1,2} \hbar \omega_{SO,\nu} \int_0^{K_c} k dk \frac{\exp(-2kz_0) \exp\left[-(1-\alpha)^2 \frac{\hbar}{m\lambda} k^2\right] \exp\left(-\frac{k^2}{b}\right)}{(V_F \hbar \alpha k + \hbar \omega_{SO,\nu})^2} \right)^2}$$

$$\pm U \pm 4\pi^2 \left(\frac{b}{2\pi} \right)^{1/2} \frac{e^2}{\varepsilon_\infty b} \pm \frac{e^2 \eta}{\pi \varepsilon_0} \sum_{\nu=1,2} (\hbar \omega_{SO,\nu})^2 \int_0^{K_c} dk \frac{\exp(-2kz_0) \exp\left[-(1-\alpha)^2 \frac{\hbar}{m\lambda} k^2\right] \exp\left(-\frac{k^2}{b}\right)}{(V_F \hbar \alpha k + \hbar \omega_{SO,\nu})^2} \mp$$

$$2 \frac{e^2 \eta}{\pi \varepsilon_0} \sum_{\nu=1,2} \hbar \omega_{SO,\nu} \int_0^{K_c} dk \frac{\exp(-2kz_0) \exp\left[-(1-\alpha)^2 \frac{\hbar}{2m\lambda} k^2\right] \exp\left(-\frac{k^2}{2b}\right)}{(V_F \hbar \alpha k + \hbar \omega_{SO,\nu})^2}$$

(247a),

and

$$(E_{bp0\pm})_{LO} = \pm \sqrt{(V_F G)^2 + \left(\frac{\hbar \alpha V_F e^2 \eta_0 L_m \hbar \omega_{LO}}{\pi \varepsilon_0} \int_0^{K_c} k^2 dk \frac{\left(\operatorname{erfc} \left[\frac{k\sigma}{2} \right] \right)^2 \exp\left[-(1-\alpha)^2 \frac{\hbar}{m\lambda} k^2\right] \exp\left(-\frac{k^2}{b}\right)}{(V_F \hbar \alpha k + \hbar \omega_{LO})^2} \right)^2} \pm U \pm 4\pi^2 \left(\frac{b}{2\pi} \right)^{1/2} \frac{e^2}{\varepsilon_\infty b}$$

$$\pm \frac{e^2 \eta_0 L_m (\hbar \omega_{LO})^2}{\pi \varepsilon_0} \int_0^{K_c} k dk \frac{\left(\operatorname{erfc} \left[\frac{k\sigma}{2} \right] \right)^2 \exp\left[-(1-\alpha)^2 \frac{\hbar}{m\lambda} k^2\right] \exp\left(-\frac{k^2}{b}\right)}{(V_F \hbar \alpha k + \hbar \omega_{LO})^2} \mp 2 \frac{e^2 \eta_0 L_m \hbar \omega_{LO}}{\pi \varepsilon_0} \int_0^{K_c} k dk \frac{\left(\operatorname{erfc} \left[\frac{k\sigma}{2} \right] \right)^2 \exp\left[-(1-\alpha)^2 \frac{\hbar}{2m\lambda} k^2\right] \exp\left(-\frac{k^2}{2b}\right)}{(V_F \hbar \alpha k + \hbar \omega_{LO})}$$

(247b).

The energies of SO and LO bipolaron in the strong coupling ($\alpha = 0$) are respectively :

$$(E_{bp0\pm})_{SO} = \pm V_F G \pm \frac{e^2 \eta}{\pi \varepsilon_0} \int_0^{K_c} \exp(-2kz_0) \exp\left[-\frac{\hbar}{m\lambda} k^2\right] \exp\left(-\frac{k^2}{b}\right) dk$$

$$\mp 2 \frac{e^2 \eta}{\pi \varepsilon_0} \int_0^{K_c} \exp(-2kz_0) \exp\left[-\frac{\hbar}{2m\lambda} k^2\right] \exp\left(-\frac{k^2}{2b}\right) dk \pm U \pm 4\pi^2 \left(\frac{b}{2\pi} \right)^{1/2} \frac{e^2}{\varepsilon_\infty b}$$

(248a),

and

$$\begin{aligned} (E_{bp0\pm})_{LO} = & \pm V_F G \pm \frac{e^2 \eta_0 L_m}{\pi \epsilon_0} \int_0^{K_f} k \left(\operatorname{erfc} \left[\frac{k\sigma}{2} \right] \right)^2 \exp \left[-\frac{\hbar}{m\lambda} k^2 \right] \exp \left(-\frac{k^2}{b} \right) dk \\ & \mp 2 \frac{e^2 \eta_0 L_m}{\pi \epsilon_0} \int_0^{K_f} k \left(\operatorname{erfc} \left[\frac{k\sigma}{2} \right] \right)^2 \exp \left[-\frac{\hbar}{2m\lambda} k^2 \right] \exp \left(-\frac{k^2}{2b} \right) dk \pm U \pm 4\pi^2 \left(\frac{b}{2\pi} \right)^{1/2} \frac{e^2}{\epsilon_\infty b} \end{aligned} \quad (248b).$$

- **Binding energy of bipolaron**

The binding energy (BE) is evaluate using the following formula given as [163]:

$$BE = 2E_p - E_{bp} \quad (249),$$

it characterises the stability criteria. Here, E_p is the single polaron ground state energy in the same approximation. In this, case the BE is given by:

$$BE = 2E_{p0} - E_{bp0} \quad (250).$$

From Eq. (246), we observe that E_{bp0+} and E_{bp0-} are independant of the magnetic field which is differents from other Landau levels energies in others coupling (Eqs. (247) and (248)). So the magnitude of bandgap modulation in weak coupling regime can not be altered by an external magnetic field. This result is similar to the case of polaron [51, 164]. In others coupling regime (intermediate and strong), the magnitude of the bandgap is a function of magnetic field.

- **Optical absorption of bipolaron**

The absorption coefficient $\Gamma(\hbar\Omega)$ of the incident light with the energy $\hbar\Omega$ of a free polaron, according to Fermi's golden rule, is given as in Eq. (239). Follow the same rule as in the case of exciton- polaron in TMDs we obtain the absorption coefficient for the weak and intermediate coupling regime. Thus, in the weak coupling regime, we obtain the absorption coefficient for SO and LO bipolaron as

$$\Gamma_{w-bp}(\hbar\Omega) = \begin{cases} \frac{e^4 \eta}{\hbar^2 V_F c n \epsilon \epsilon_0 m^2 (\hbar\Omega)^3} \sum_{v=1,2} \hbar\omega_{SO,v} (\hbar\Omega - \hbar\omega_{SO,v})^2 \exp \left[\frac{2z_0 (\hbar\Omega - \hbar\omega_{SO,v})}{\hbar V_F} \right] \exp \left[-\frac{(\hbar\Omega - \hbar\omega_{SO,v})}{b V_F \hbar} \right] \\ \frac{e^4 \eta_0 L_m \hbar\omega_{LO} (\hbar\Omega - \hbar\omega_{LO})^2}{\hbar^3 V_F c n \epsilon \epsilon_0 m^2 (\hbar\Omega)^3} \left[\operatorname{erfc} \left(\frac{(\hbar\Omega - \hbar\omega_{LO})\sigma}{2\hbar V_F} \right) \right]^2 \exp \left[-\frac{(\hbar\Omega - \hbar\omega_{LO})}{b V_F \hbar} \right] \end{cases} \quad (251),$$

in the intermediate coupling, the absorption coefficient of SO and LO bipolaron is given by:

$$\Gamma_{\text{int-bp}}(\hbar\Omega) = \begin{cases} \frac{e^4 \eta}{\hbar^2 V_F c n \epsilon \epsilon_0 m^2 (\hbar\Omega)^3} \sum_{\nu=1,2} \hbar \omega_{SO,\nu} (\hbar\Omega - \hbar \omega_{SO,\nu})^2 \exp\left[\frac{2z_0(\hbar\Omega - \hbar \omega_{SO,\nu})}{\hbar \alpha V_F}\right] \exp\left[-\frac{(\hbar\Omega - \hbar \omega_{SO,\nu})}{b \alpha V_F \hbar}\right] \exp\left[-\left(\frac{1-\alpha}{V_F \alpha \hbar}\right)^2 \frac{\hbar}{m\lambda} (\hbar\Omega - \hbar \omega_{SO,\nu})^2\right] \\ \frac{e^4 \eta_0 L_m \hbar \omega_{LO} (\hbar\Omega - \hbar \omega_{LO})^2}{\hbar^3 V_F c n \epsilon \epsilon_0 m^2 (\hbar\Omega)^3} \left[\operatorname{erfc}\left(\frac{(\hbar\Omega - \hbar \omega_{LO}) \sigma}{2 \hbar \alpha V_F}\right) \right]^2 \exp\left[-\frac{(\hbar\Omega - \hbar \omega_{LO})}{b \alpha V_F \hbar}\right] \exp\left[-\left(\frac{1-\alpha}{V_F \alpha \hbar}\right)^2 \frac{\hbar}{m\lambda} (\hbar\Omega - \hbar \omega_{LO})^2\right] \end{cases}$$

(252).

The ground state energy of bipolaron is not influenced by the magnetic field in the weak coupling regime, this remark is also true for the optical absorption and the magnitude of bandgap modulation. So, the ground state energy, the optical absorption and the magnitude of bandgap modulation are affected by magnetic field, electron-phonon coupling and others parameters such as distance between TMDs monolayer and polar substrates.

2.3.3.2 BIPOLARON IN TMDs QUANTUM PSEUDODOT

The system considered here is constituted of two electrons confined in 2D-TMDs quantum pseudodot interacting with SO-phonon, thus a quasiparticle called Fröhlich bipolaron can be formed. So, we evaluate ground and first excited state energies. The Hamiltonian is written as follow:

$$H = \sum_{\nu=1,2} \left[\frac{p_\nu^2}{2m} + \sum_k (T_k a_k e^{ikr_\nu} + T_k^* a_k^+ e^{-ikr_\nu}) + v(r_\nu) \right] + \sum_k \hbar \omega_{SO} a_k^+ a_k + u(|r_1 - r_2|) \quad (253),$$

$$\text{where } v(r_\nu) = V_O \left(\frac{r_\nu - r_O}{r_O} \right)^2 \quad (254).$$

In the Eq. (253), $p_\nu(r_\nu)$ are the operator's momentum (position) of the ν th electron ($\nu = 1, 2$), m is the effective band mass of the electrons, a_k^+ (a_k) stand respectively operators of creation (annihilation) of SO-phonons with the wave vector \vec{k} . $v(r_\nu)$ represent the pseudo-harmonic potential with both antidot potential and harmonic quantum dot potential, V_O represent the chemical potential of the two-dimensional electron gas and r_O is the zero point of the pseudo-harmonic potential. $u(r) = U/r$ is Coulomb interaction potential between the two electrons, with $U = e^2/\epsilon_\infty$, where ϵ_∞ represent the high-frequency dielectric constant of the substrate. Considering bipolaron as composite quasiparticle, the expression in Eq. (253) can be transformed by introducing the center of the mass coordinate as follows: $P = p_1 + p_2$,

$R = (r_1 + r_2)/2$ and relative coordinate $r = r_1 - r_2$ $p = (p_1 - p_2)/2$ for the two electron, thus we can rewrite Eq. (253) as:

$$H = \frac{P^2}{4m} + \sum_k (B_k a_k e^{ikR} + B_k^* a_k^+ e^{-ikR}) + \sum_k \hbar \omega_{SO} a_k^+ a_k + \frac{2V_o}{r_o^2} R^2 - 4V_o + E_r + 8V_o r_o^2 \frac{(4R^2 + r^2)}{(4R^2 - r^2)^2} \quad (255),$$

where, $B_k = 2T_k \left\langle \cos\left(\frac{kr}{2}\right) \right\rangle$ and $E_r = \left\langle \frac{p^2}{m} + \frac{U}{r} + \frac{V_o}{2r_o^2} r^2 \right\rangle$ with $\langle \dots \rangle$ denoting an averaging over the fundamental or first excited states wave functions.

The first unitary transformation proposed by Huybrecht given above is used to diagonalize Eq. (255) and the new creation b_j^+ and annihilation b_j operator's relative to mass center coordinate and momentum given by Eq. (67) are introduced, thus Eq. (255) can be rewritten as :

$$H' = H'_1 + H'_2 \quad (256),$$

with

$$\begin{aligned} H'_1 = & \frac{\lambda \hbar}{4m} \sum_j (b_j^+ b_j^+ + b_j b_j) + \frac{\lambda \hbar}{4m} \sum_j (2b_j^+ b_j + 3) + \sum_k \left(\hbar \omega_{SO} + \frac{k^2 \hbar^2 a^2}{4m} \right) a_k^+ a_k \\ & + \sum_{k,v} \left(B_k a_k e^{-(1-a)^2 \left(\frac{\hbar}{4m\lambda}\right) k^2} e^{- (1-a) \left(\frac{\hbar}{4m\lambda}\right)^{1/2} \sum_k k b_j} e^{(1-a) \left(\frac{\hbar}{4m\lambda}\right)^{1/2} \sum_k k b_j^+} + B_k^* a_k^+ e^{(1-a) \left(\frac{\hbar}{4m\lambda}\right) k^2} e^{(1-a)^2 \left(\frac{\hbar}{4m\lambda}\right)^{1/2} \sum_k k b_j} e^{- (1-a) \left(\frac{\hbar}{4m\lambda}\right)^{1/2} \sum_k k b_j^+} \right) \\ & - \frac{2V_o}{r_o^2} \left(\frac{\hbar}{4m\lambda} \right) \sum_j (b_j^+ b_j^+ + b_j b_j) + \frac{2V_o}{r_o^2} \left(\frac{\hbar}{4m\lambda} \right) \sum_j (2b_j^+ b_j + 3) - 4V_o + E_r \end{aligned} \quad (257),$$

$$H'_2 = \frac{\hbar a (m \lambda \hbar)^{1/2}}{2m} \sum_{k,j} k (b_j^+ + b_j) a_k^+ a_k + \frac{\hbar^2 a^2}{4m} \sum_{k,k'} k k' a_k^+ a_k^+ a_k a_{k'} + 8V_o r_o^2 \frac{(4R^2 + r^2)}{(4R^2 - r^2)^2} \quad (258).$$

Then using the second LLP unitary transformation, we obtained:

$$\begin{aligned}
 H'' = & \frac{\lambda\hbar}{4m} \sum_j (b_j^+ b_j^+ + b_j b_j) + \frac{\lambda\hbar}{4m} \sum_j (2b_j^+ b_j + 3) + \sum_k \left(\hbar\omega_{SO} + \frac{k^2 \hbar^2 a^2}{4m} \right) (a_k^+ + f_k^+) (a_k + f_k) \\
 & + \sum_{k,v} \left(B_k (a_k + f_k) e^{-(1-a)^2 \left(\frac{\hbar}{4m\lambda}\right) k^2} e^{-(1-a) \left(\frac{\hbar}{4m\lambda}\right)^{1/2} \sum_k k b_j} e^{(1-a) \left(\frac{\hbar}{4m\lambda}\right)^{1/2} \sum_k k b_j^+} + B_k^* (a_k^+ + f_k^+) e^{-(1-a)^2 \left(\frac{\hbar}{4m\lambda}\right) k^2} e^{(1-a) \left(\frac{\hbar}{4m\lambda}\right)^{1/2} \sum_k k b_j} e^{-(1-a) \left(\frac{\hbar}{4m\lambda}\right)^{1/2} \sum_k k b_j^+} \right) \\
 & - \frac{2V_o}{r_o^2} \left(\frac{\hbar}{4m\lambda} \right) \sum_j (b_j^+ b_j^+ + b_j b_j) + \frac{2V_o}{r_o^2} \left(\frac{\hbar}{4m\lambda} \right) \sum_j (2b_j^+ b_j + 3) + 2V_o i \left(\frac{\hbar}{4m\lambda} \right)^{1/2} \sum_j (b_j - b_j^+) - 4V_o + E_r
 \end{aligned}$$

(259).

The terms obtained with H_2' can be neglected, this because if we first perform the angular integration they will vanish. Then to obtain the ground and first excited states energies, the wave function is chosen as in [163]

$$\beta_n = |\psi_n(r)\rangle |n\rangle_a |n\rangle_{b_j} \tag{260},$$

ψ_n is oscillator wave function of an electron's. For the ground state and first excited state, we have the following wave function:

$$\begin{cases}
 \beta_0 = \left(\frac{\mu}{2\pi} \right)^{3/4} \exp\left(-\frac{\mu}{4} r^2 \right) |0\rangle_a |0\rangle_{b_j} \\
 \beta_1 = \sqrt{\frac{2}{3}} \left(\frac{\mu}{2} \right)^{5/4} \left(\frac{1}{\pi} \right)^{3/4} \exp\left(-\frac{\mu}{4} r^2 \right) |1\rangle_a |1\rangle_{b_j}
 \end{cases} \tag{261},$$

where μ is a variational parameter which can be obtained by minimizing the state energies. This waves function satisfying the normalization condition as given in Eq. (145). Performing in the Hamiltonian given by Eq. (259) the above wave function for fundamental and first excited states, we obtained the following expression of energies:

$$E_0 = \frac{3\hbar\lambda}{4} - 4V_o + \frac{3\hbar V_o}{2r_o^2 m\lambda} + \frac{3\mu\hbar^2}{4m} + \frac{3V_o}{2r_o^2 \mu} + \left(\frac{2\mu}{\pi} \right)^{1/2} \frac{e^2}{\epsilon_\infty} - \frac{e^2 \eta \hbar \omega_{SO}}{4\pi\epsilon_0} \int_0^{k_c} \frac{\exp\left(-(1-a)^2 \left(\frac{\hbar}{2m\lambda} \right) k^2 - \frac{k^2}{4\mu} - 2ky_0 \right) \left(4 - \frac{2k^2}{\mu} + \frac{k^4}{4\mu^2} \right)}{\left(\hbar\omega_{SO} + \frac{k^2 \hbar^2 a^2}{4m} \right)} dk$$

(262),

$$E_1 = \frac{5\hbar\lambda}{4} - 4V_o + \frac{5\hbar V_o}{2r_o^2 m\lambda} + \frac{7\mu\hbar^2}{12m} + \frac{5V_o}{2r_o^2 \mu} + \left(\frac{8\mu}{\pi}\right)^{\frac{1}{2}} \frac{e^2}{3\epsilon_\infty} - \frac{e^2 \eta \hbar \omega_{so,v}}{4\pi\epsilon_0} \int_0^{k_c} \frac{\exp\left[-(1-a)^2 \left(\frac{\hbar}{2m\lambda}\right) k^2 - \frac{k^2}{4\mu} - 2ky_0\right] \left(2 - \frac{k^2}{\mu} + \frac{k^4}{24\mu^2}\right)}{\left(\hbar\omega_{so} + \frac{k^2 \hbar^2 a^2}{4m}\right)} dk$$

(263).

The ground and first excited state energies are proportional of V_o and inversely proportional to r_o . These energies are also influenced by the coupling parameters a and the mass of the electron in monolayers. Thus, others parameters related to states energies also affected by V_o and r_o .

CONCLUSION

In this chapter, an overview on mathematics tools is are presented, some dynamic and decoherence parameters which characterises the quasiparticle are also presented. Therefore, we model each of our system by appropriate Hamiltonian and using the variational methods presented, we investigated the ground and first excited states energies of diffeents system in TMDs under various external field, also others parameters of quasiparticles such as lifetime, effective mass, optical absorption, bindng energy are also investigated. Decoherence proprieties which is link to states energies such as transition frequency, density probability, Shannon entropy and decoherence time can also be evaluated. Futhermore, we will later use these analyticals results in the following chapter to obtain some numericals results on ground and first excited states energies, lifetime, binding energy, effective mass optical absorption, transition frequency, density probability, Shannon entropy and decoherence time that can help to explain physics at the nanoscale level.

CHAPTER 3: NUMERICAL RESULTS AND DISCUSSIONS

INTRODUCTION

In the previous chapter, it was question for us to present different configurations where polaron, exciton-polaron and bipolaron can exist in TMDs materials and study their new properties in those systems. In this chapter, it is now question to present numerical results and discussions of the above calculations. We will focus on four different monolayers (MoS₂, MoSe₂, WS₂ and WSe₂) because their propreties have been studied and are well known in the literature. Several properties characterizing these quasi-particles will be numerically presented.

Numerical results are presented for fundamental, first excited states energies, mobility, effective mass, lifetime, transition frequency, probability density, Shannon entropy as well as optical absorption, bindind energy and the magnitude of bandgap modulation. The parameters using here have been taken in [58, 51, 164, 165, 166]. Others constants used in this section are outlined in Table 5 and Table 6. The Fermi velocity is assumed to be equal for all TMDs since it varies slightly for different TMDs [164], the value of internal distance adopted is equal to $z_0 = 0.5 \text{ nm}$. The fixed values of $L_m = 0.5 \text{ nm}$, $\sigma = 0.6 \text{ nm}$ are taken in all TMDs monolayer [167].

Table 5 : Parameters of different polar substrates and surfaces optical phonon modes [164]

Quantity (unit)	<i>h-BN</i>	<i>SiC</i>	<i>AiN</i>	<i>SiO₂</i>	<i>HfO₂</i>	<i>ZrO₂</i>	<i>Al₂O₃</i>
$k_0(\epsilon_0)$	5.1	9.7	9.1	3.9	22.0	24.0	12.5
$k_\infty(\epsilon_\infty)$	4.1	6.5	4.8	2.5	5.0	4.0	3.2
$\hbar\omega_{SO,1}(\text{meV})$	167	146	84	25	101	94	53
$\hbar\omega_{SO,2}(\text{meV})$	116	60	105	71	196	55	19
η	0.032	0.040	0.074	0.082	0.122	0.160	0.164

Table 6 : The magnitude of bandgap modulation for the different TMDs and the energies of LO phonons of different TMDs [168]

Quantity (unit)	MoS ₂	MoSe ₂	WS ₂	WSe ₂
$\hbar\omega_{LO}(\text{meV})$	48	34	43	30
$2G(\text{meV})$	1870	1560	2100	1650

3.1 DYNAMIC OF POLARON, EXCITON-POLARON AND BIPOLARON IN TRANSITION METAL DICHALCOGENIDES

3.1.1 GROUND AND FIRST EXCITED STATES ENERGIES

3.1.1.1 ENERGIES OF POLARON

- **Polaron under electric field: The numerical results presented here are obtained from Eqs. (147) and (148).**

In Figs.14-17, we have presented the plot of ground and first excited states energies of polaron as a function of effective confinement length for different values of electric field (Fig.14), wave vector for different values of electric field (Fig.15), electric field for different values of internal distance (Fig.16), and electric field for different TMDs monolayer (Fig.17). From Fig.14, one can observe that ground and first excited state energies are increasing function of the effective confinement length, in this same figure we can remark that ground and first excited state energies are increasing function of electric field strength. In Fig.15, one can observe that the energies are the decreasing function of the wave vector in the case of ground state energy, this behavior of energy is in accordance with [51].

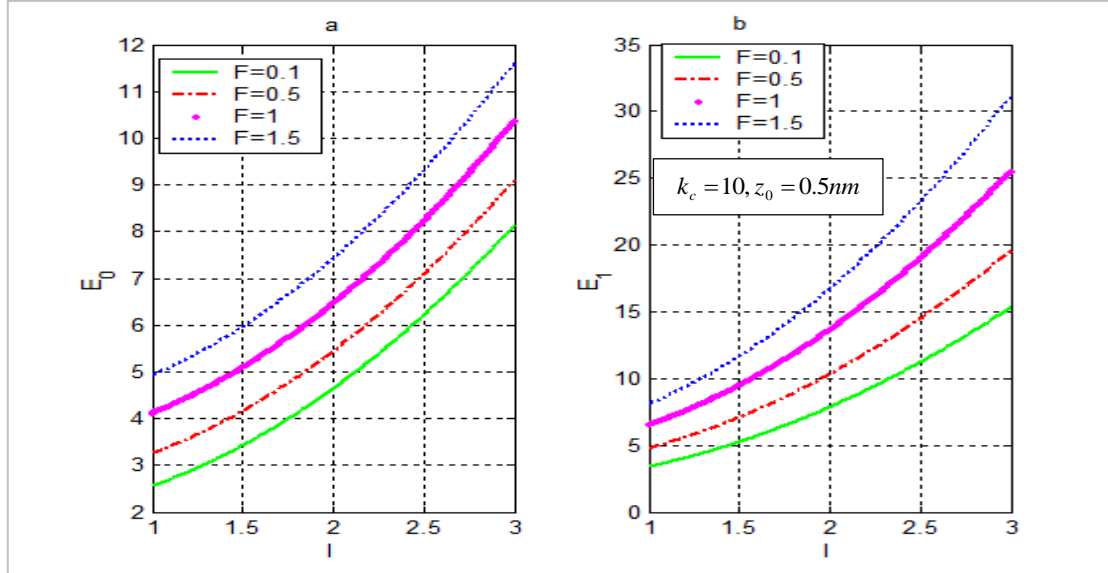


Figure 14 : Polaron energies as a function of effective confinement length for : (a) ground state energy (b) first excited.

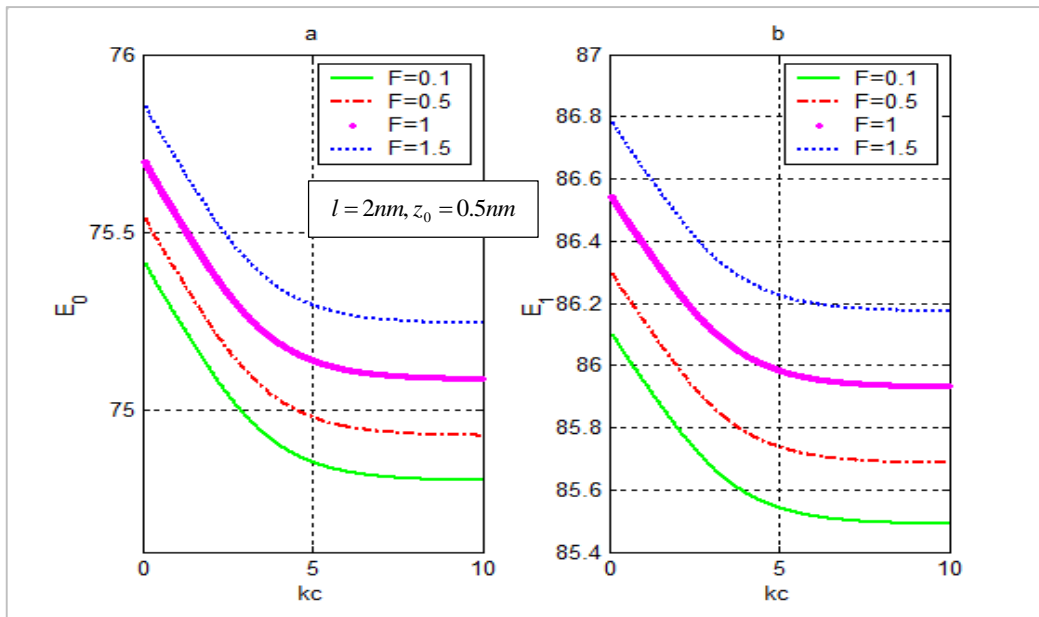


Figure 15 : Polaron energies as a function wave vector : (a) ground state energy (b) first excited

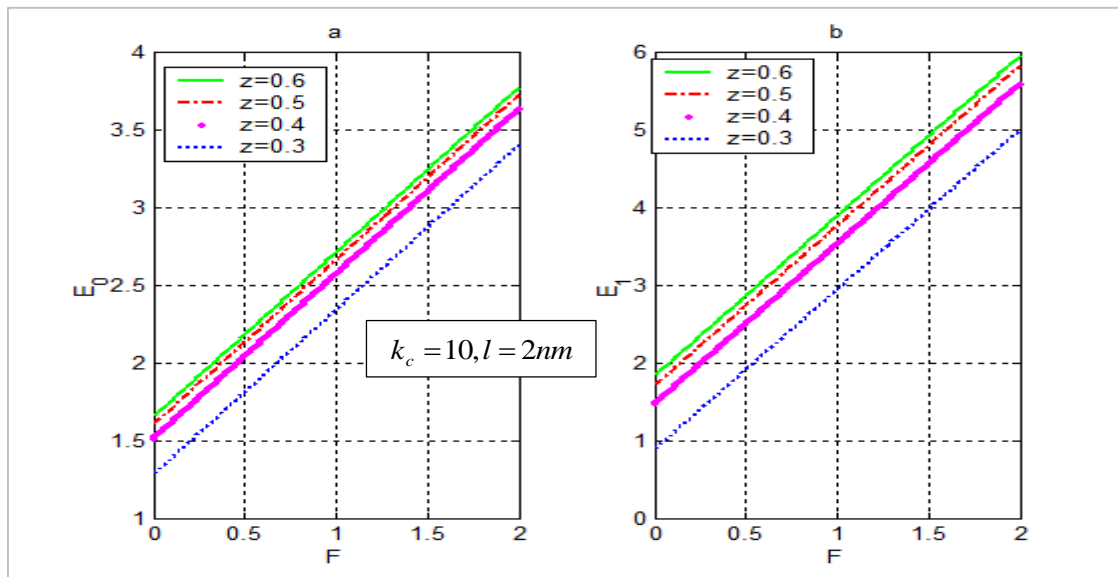


Figure 16 : Polaron energies as a function of electric field: (a) ground state energy (b) first excited.

Also, in this Fig.15, the energies are increasing function of electric field. In Fig.16, the ground and first excited state energies increase with increasing the electric field, this result confirms those obtained in Figs.14, 15. One can also observe in this plot (Fig.16) that the energies are an increasing function of the internal distance between polar substrate and TMDs monolayer z_0 , then as z_0 increases, the energies become less sensible to internal distance showing the fact that the further the TMDs is from polar substrate, less its effect is felt on the state energies of the polaron in TMDs. In Fig.17, the behavior of energies is the same as in Fig.16. One can also

observe that energies varying with different TMDs monolayer which can be attributed to the effective mass of electron in different monolayer, thus less the mass of electron in monolayer is less the energies is. This result is similar to [58]. From these figures we can conclude that increasing electric field allows us to increase the energies of polaron in different TMDs monolayer and the better contribution of electric field to the energies is obtained with WS₂ monolayer. The more electron is confined in presence of electric field, the higher are their energies Other parameters allowing us to control the energies states of polaron in TMDs are effective confinement length, the internal distance between polar substrate and monolayer and the effective mass of electron in different monolayer. This result of modulating the state by tuning its energies has a practical use in quantum information process.

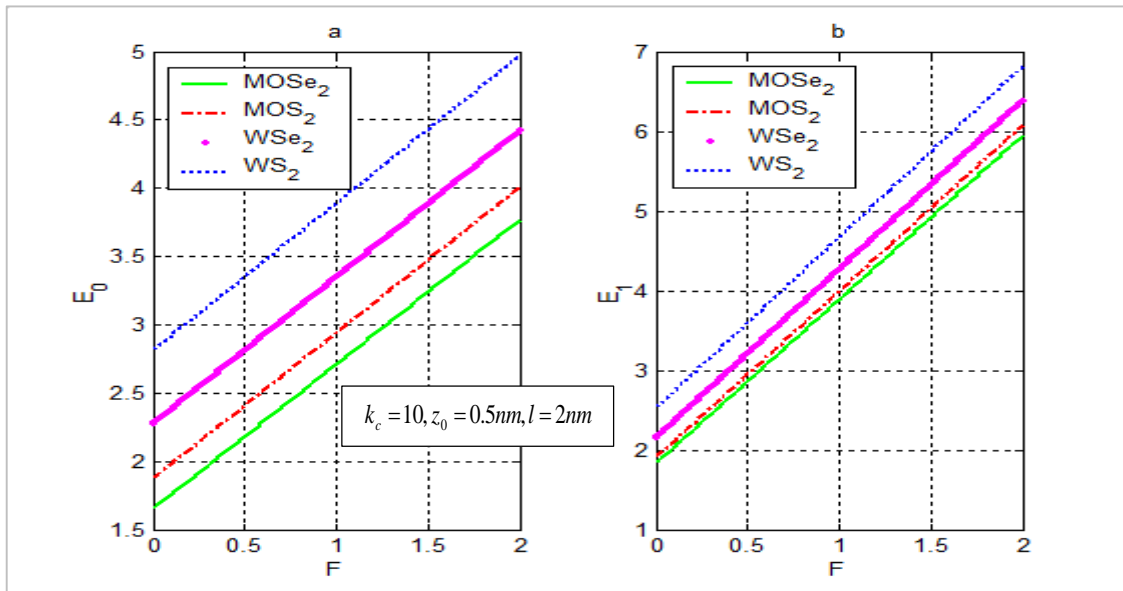


Figure 17 : Polaron energies as a function of electric field for: (a) ground state energy (b) first excited

- **Polaron under radiowave and microwave:** here, we presented numerical results from Eqs. (163), (165), (168) and (170).

Figs.18, 19 show the variations of E_{0+} and E_{0-} on the frequency of the RW and MW respectively in MoS₂ monolayer on different polar substrates. It is observed that E_{0+} and E_{0-} oscillate with the increasing of frequency. In Fig.18 we have a smooth periodical oscillation having the same amplitude whereas in Fig.19 we have a smooth periodical oscillation in which the amplitude decrease with the increasing of the amplitude of the MW. In the both case, RW and MW create the fluctuation in the ground state energy of polaron in MoS₂ monolayer, thus the modulated band gap also fluctuates. The ground state energy of polaron is

then affected by the presence of the RW and MW field. In this system, we can trap quasiparticles involves in the system. We achieve a way to better confine the quasiparticles in the system by tuning the frequencies of RW and MW. As the band gap characterizes the conductivity of a material, the RW and MW can be use to control the conductivity of TMDs.

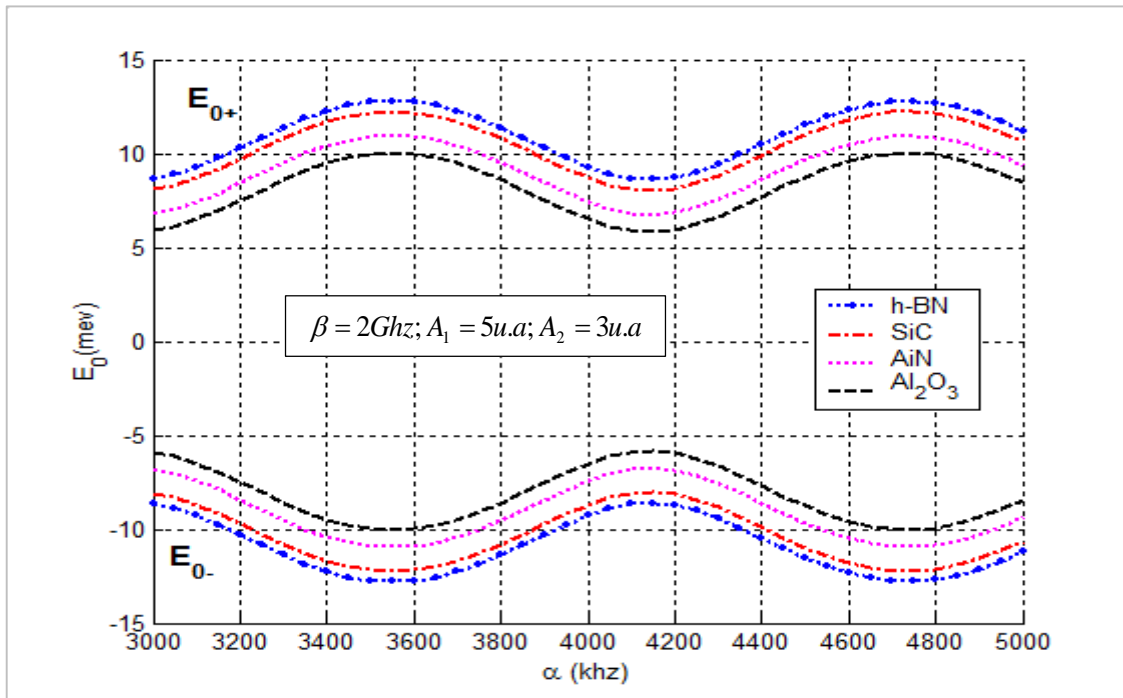


Figure 18 : Ground-state energy of polaron with SO phonon mode as function of frequency of RW on different polar substrates

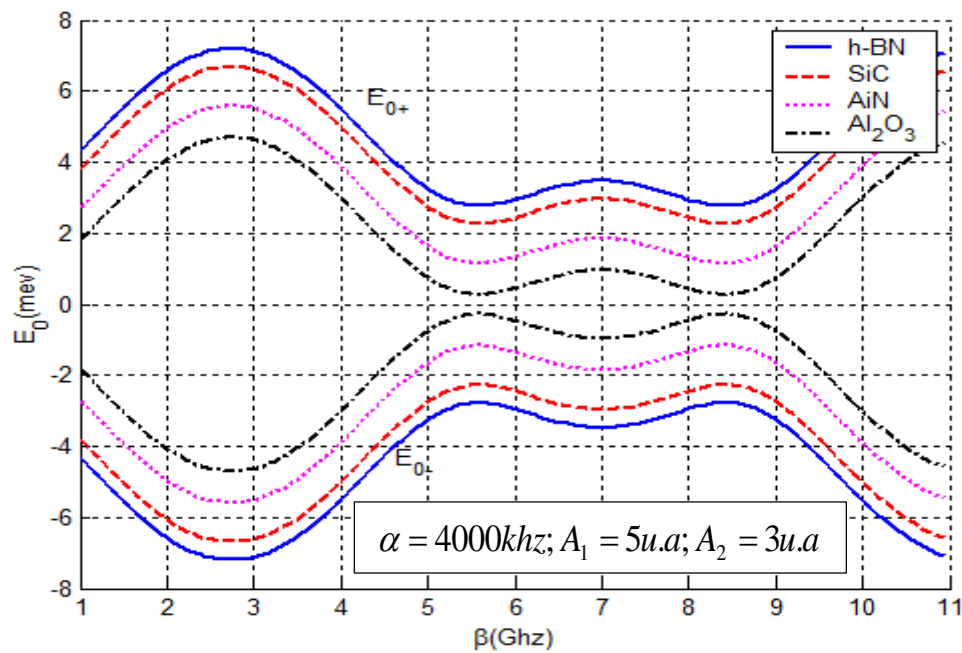


Figure 19: Ground-state energy of polaron with SO phonon mode as function of frequency of MW on different polar substrates

Also in these figures, the influence of different polar substrates is shown and it can be seen that the ground state energy in both case decrease in the following order h-BN, SiC, AiN and Al₂O₃ which can be attributed to the polarizability parameter increasing from h-BN to Al₂O₃. This result is in agreement with those obtained in ref [51]. Thus the TMDs is more conductive with Al₂O₃ polar substrate. our result suggests that the conductivity of TMDs monolayer can be modulated by tuning the frequencies of the RW or MW but also by changing different polar substrates. This result on conductivity can be use in high performance field effect transistors to allow charge carriers to move easily throught material which is important for the efficient switvhing of signals and amplifications of electrical signals. It can also be use in energy storage applications because concructivity of TMDs allow rapid charge and discharge rate

Figs.20, 21 presents the dependence of energies E_{0+} and E_{0-} as function of the amplitudes of the RW and the MW respectively. One can see that the ground state energy increase sharply with the increasing of the amplitude the RW and linearly with the amplitude of the MW. This behavior of fundamental energy state is similar to those obtained in [169]. Thus as the RW and the MW can be considering as a potential of confinement, their amplitude increases the ground state energy of polaron in MoS₂ monolayer, thus increasing the modulated bandgap. Comparing the modulated bandgap of the MoS₂ monolayer under the RW and those under MW, one can observe that the radiowave modulated better than radiowave.

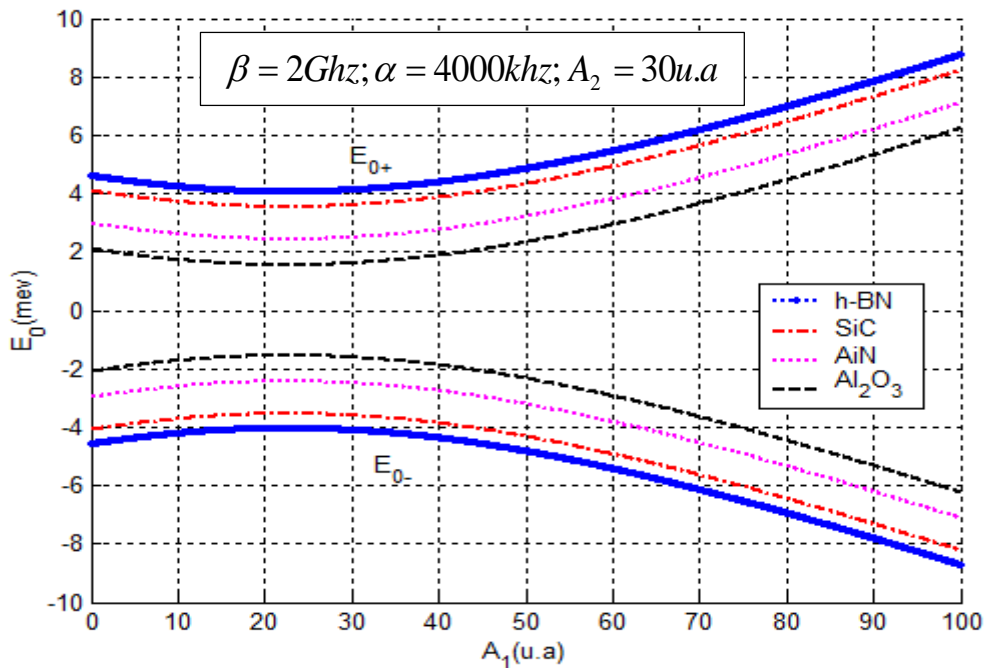


Figure 20 : Ground-state energy of polaron with SO phonon mode as function of amplitude of RW for different polar substrate

In these figures are also presented the variation of the ground state energy as function of different polar substrates. One can see that the polarizability of different polar substrate influences the modulated bandgap of MoS₂ monolayer which are in accordance with the previous result obtained in Figs.18 and 19.

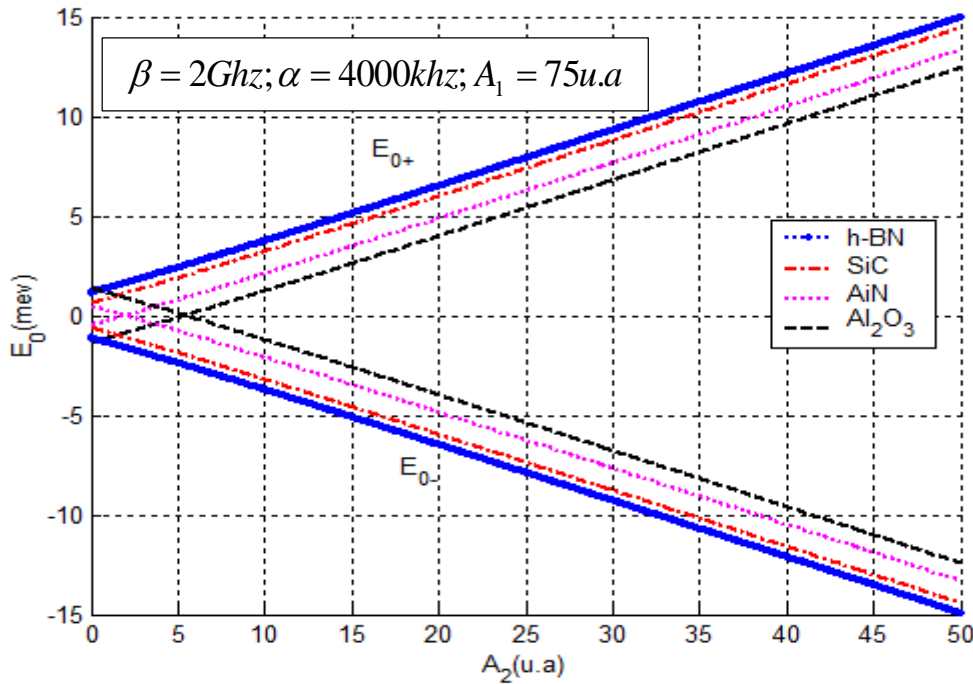


Figure 21 : Ground-state energy of polaron with SO phonon mode as function of amplitude of MW for different polar substrate

The largest modulated bandgap is obtained with h-BN polar substrates which have the smallest polarizability and the smallest bandgap modulation is obtained with Al_2O_3 polar substrate which have the largest polarizability parameter. As the polarizability parameter of polar substrate increase the modulated bandgap decrease the TMDs monolayer become more conductive. Thus the amplitude of both the microwave and the radiowave is viable tools necessary to increase the energies of polaron thus, useful to control the bandgap modulation and conductivity of the TMDs monolayer on different polar substrates.

In Figs.22, 23, we presented the dependence of energies E_{0+} and E_{0-} as function of the frequency of the RW and the amplitude of MW respectively for LO phonon mode. In Fig.22,

on can observed that as in Fig.18, the energies oscillate periodically with the increasing of the frequency of RW in all TMDs monolayer, thus the modulated bandgap fluctuates in all chosen monolayer. In Fig.23, the energies increase with the increasing of the amplitude of the microwave as in fig.20. In these figures the dependence of energies for different monolayer are presented and it observed that the energies increase in the sequence of MoSe₂, WSe₂, MoS₂ and WS₂ which can be attributed to the intrinsic band gap of these monolayer.

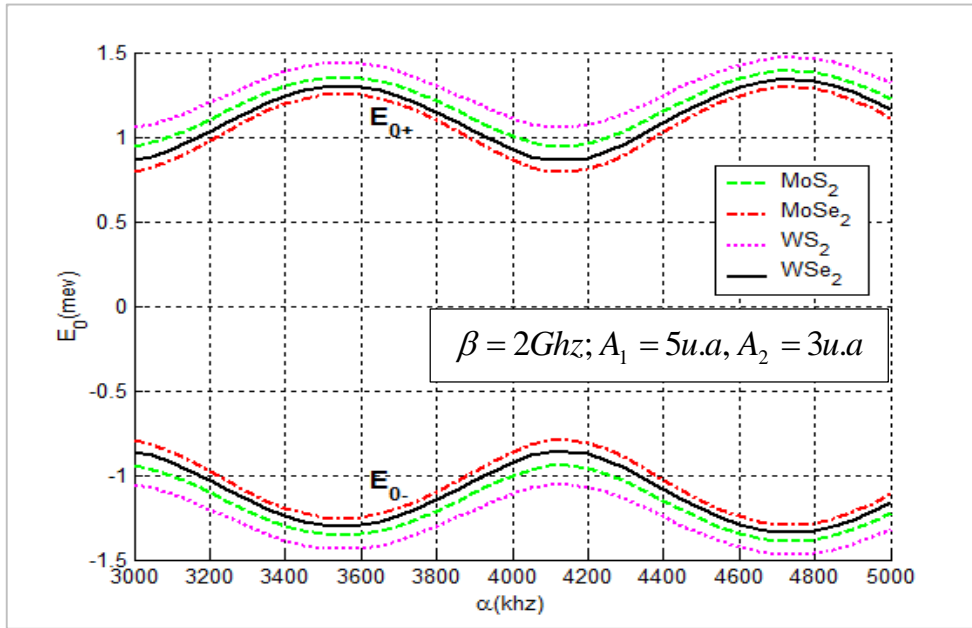


Figure 22 : Ground-state energy of polaron with LO phonon mode as function of frequency of RW for different TMDs monolayers

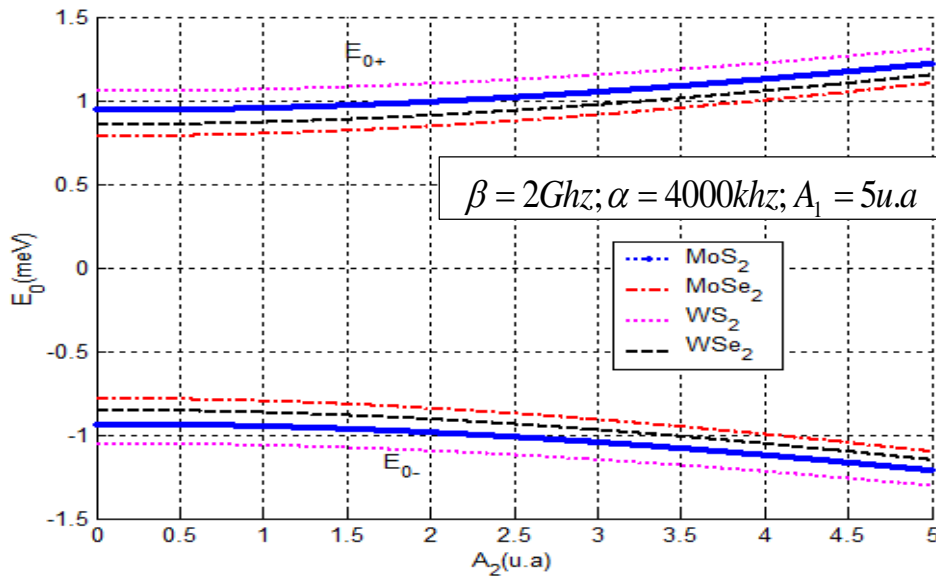


Figure 23 : Ground-state energy of polaron with LO phonon mode as function of amplitude of MW for different TMDs monolayers

The largest modulated bandgap is obtained with WS_2 monolayer where the lowest is obtained with $MoSe_2$. Comparing the ground state energy in the case of LO phonon with the case of SO phonon it can be seen that the energy is more enhanced with SO phonon than in case of LO phonon, the same is true for the modulated band gap. Thus in TMDs monolayer, the type of phonons mode is important to the modulation of band gap as far as polar substrate, amplitude and frequency of the RW and MW.

3.1.1.2 ENERGIES OF EXCITON-POLARON

- **Magnetic barrier effect on exciton-polaron: The numerical results presented here are obtained from Eqs. (211) and (213).**

Fig.24 presents the variation of the ground state energy of Exciton-polaron versus magnetic barrier length for different TMDs monolayers. Fig.25 displays the first excited state energy as function of magnetic barrier length for various TMDs. From those figures, one can observe that both state energies enhance with increase in magnetic barrier length for various TMDs. This behavior is similar to that obtained in [58]. Since the exciton-polaron energy is very large, exciton-polaron are said to be stable quasiparticles. This stability is increased with the presence of magnetic barrier. For instance, the connection with exciton-polaron energy level through a magnetic field of a given length is easily identified.

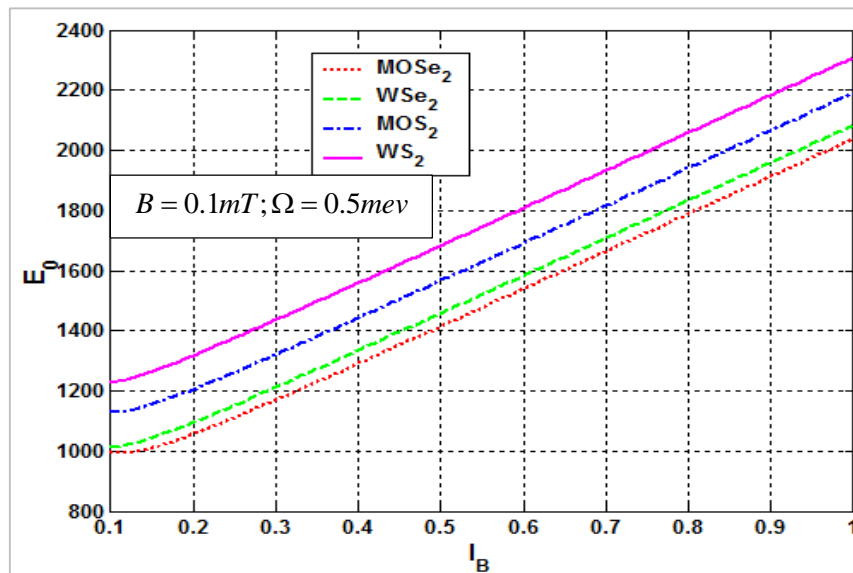


Figure 24 : Ground state energy of exciton polaron versus length of magnetic barrier for different TMDs monolayers

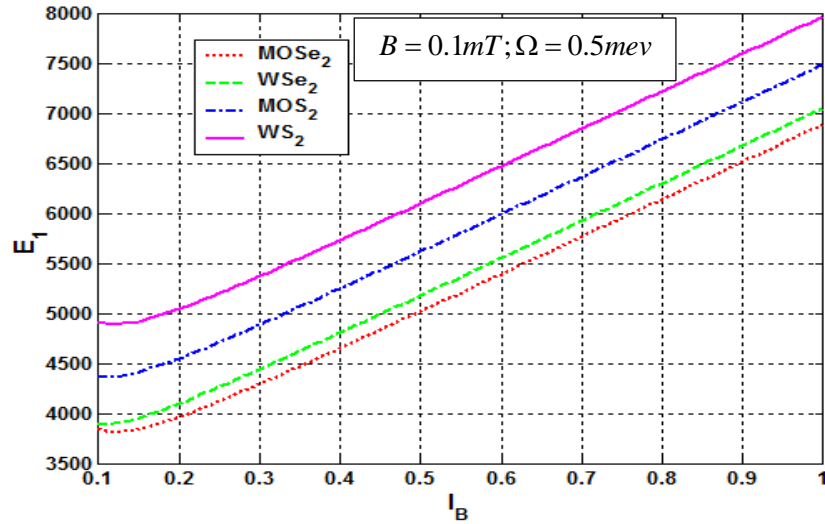


Figure 25 : First excited state energy of Exciton-polaron versus the length of magnetic barrier for various TMDs monolayers in strong coupling regime

These findings also present some situations in which carriers are not strictly confined in two-dimensional planes but rather trapped inside a narrow well. The highest ground state energy of exciton-polaron is obtained with WS₂ and the lowest is obtained with MoSe₂. Thus the exciton-polaron ground state energy should vary according to the magnitude of the deformation potentials of the different TMDs. We also observed in this figure that the monolayer with sulfur displays higher ground state energy than selenide. Because the existence of a magnetic potential equals an additional confinement potential, leading to a greater electron entanglement, the exciton-polaron interaction is reinforced and the ground state energy becomes more obvious. This result is in accordance with the analytically results obtained in the ground state, thus we can conclude that with diagonalization technics and that from our analysis the electron phonon coupling is a prominent parameter to enhance energy of exciton-polaron.

- **Electron-phonon coupling contribution on exciton-polaron: the results presented here come from Eqs. (235), (236) and (237).**

Fig.26 shows the energy variation with the magnetic field of exciton-polaron coupling with SO phonon in different TMDs monolayer deposited on SiO₂ polar substrate in intermediate coupling regime. One can see that the energy decrease sharply in small magnetic field range, then vary smoothly with increasing of magnetic field in all monolayer. This means that the magnetic field behaves as a trapping potential. Thus with small range of magnetic field, we have a better contribution to the correction of ground state energy of the Landau level. Furthermore, we can also observe in this figure that the energy decrease in the sequence WS₂, MoS₂, WSe₂, MoSe₂ which can be attributed to the width of the band gap of those monolayers,

where their values are respectively 1050mev, 935mev, 825mev and 725mev. Thus the smaller of the band gap width of monolayer is, smaller the contribution of correction of the ground state energy of Landau level is.

The dependences of energy on magnetic field of exciton-polaron coupling with SO phonon in various TMDs monolayer on SiO₂ polar substrate in strong coupling regime are shown in Fig.27. One can observe that the behavior of the energy is similar as in the intermediate coupling regime (Fig.26). Comparing to this later regime, the magnitude of the energy is greater in the case of strong coupling. This shows how the electron-phonon coupling affects the correction of the ground state energy in the Landau levels. This result on the energies of exciton-polaron is applicable is quantum information storage because lower ground state energy can potentially lead to more stable electronic states.

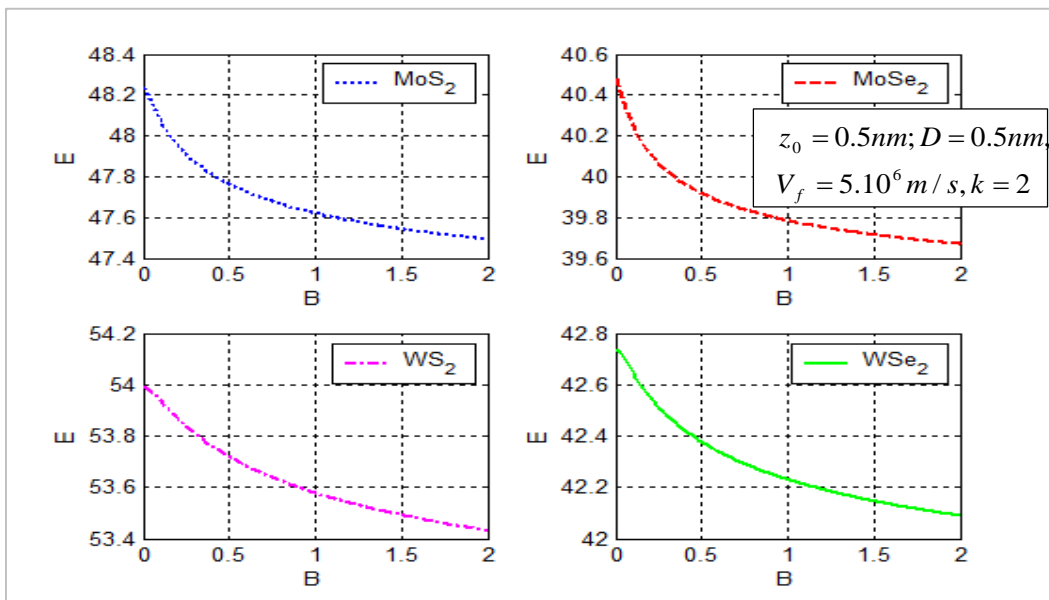


Figure 26 : Energy of exciton-polaron as a function of magnetic field for different TMDs monolayer in intermediate coupling regime

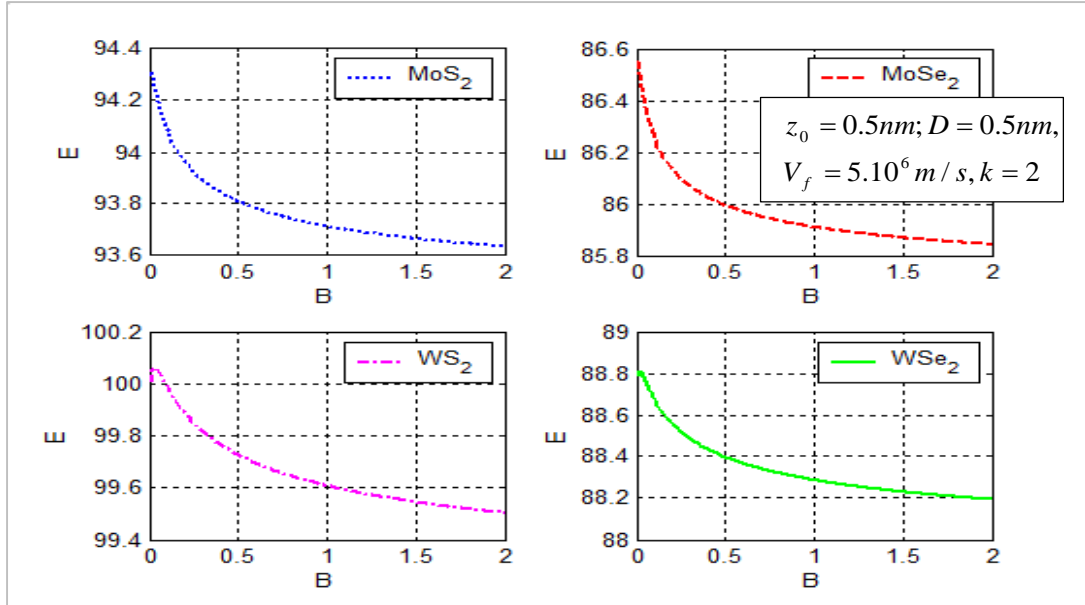


Figure 27 : Energy of exciton-polaron versus magnetic field for different TMDs monolayer in strong coupling regime

In Fig.28, we presented the variation of energy on magnetic field in intermediate coupling regime for LO phonon. The behavior of the energy is similar as in the case of SO phonon presented in figure 26. Moreover, the LO phonon displays enough energy than SO phonon, which means that the type of phonon coupling with electron affects the correction of zero Landau level energy of exciton-polaron in TMDs monolayers. Thus the polaron with LO phonon mode more impact the exciton than polaron with SO phonon mode, justified by the fact that exciton polaron with LO phonon mode displays enough energy than exciton with SO phonon. This result is in agreement with those of refs [170-172]. In weak coupling regime, the ground state energy is independent of magnetic field, this result is in accordance with [51]. Thus, in Figs.29-31 we plot the variation of energy on internal distance z_0 between polar substrates and WS₂ for weak coupling regime (Fig.29) intermediate coupling regime (Fig.30) and strong coupling regime (Fig.31). One can observe that in weak and intermediate coupling regime, for $z_0 < 1.5$, the energy decreases sharply and for $z_0 > 1.5$, the energy varies smoothly with increasing of internal distance between TMDs and polar substrates.

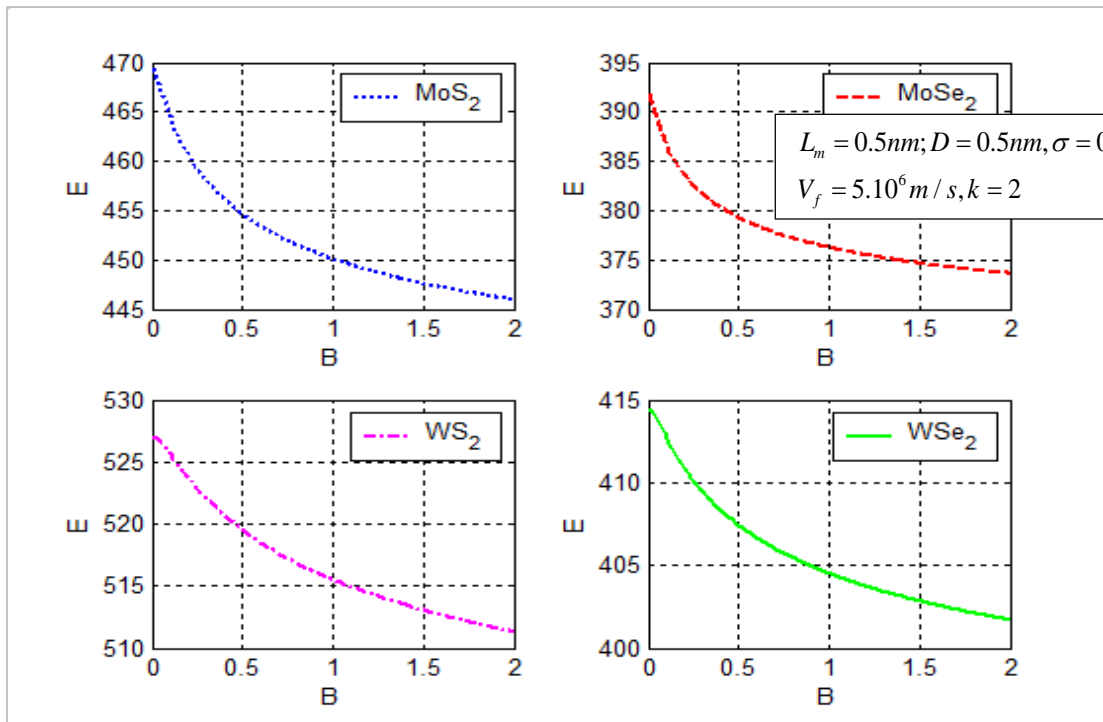


Figure 28 : Energy of exciton-polaron with LO phonon versus magnetic field for different TMDs monolayers in the intermediate coupling regime

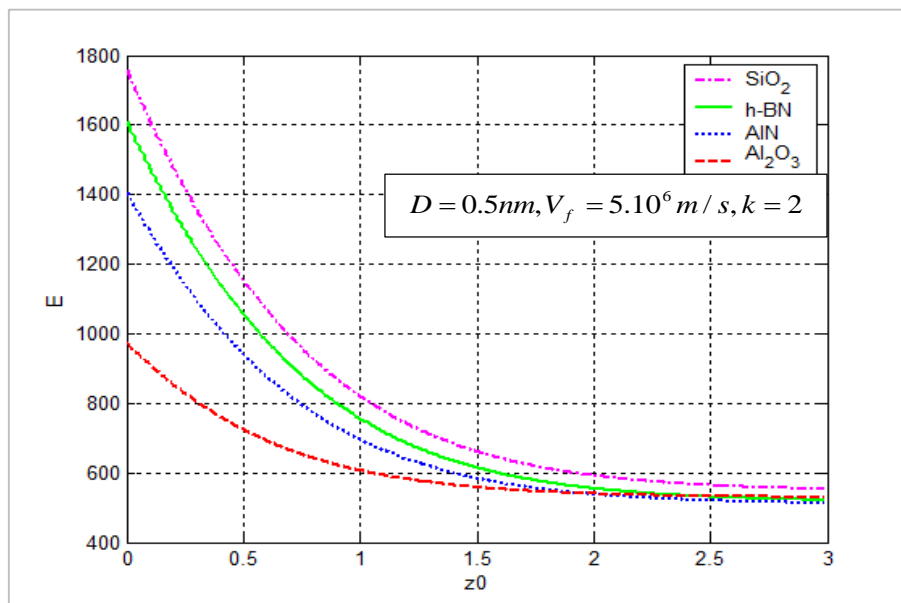


Figure 29 : Variation of exciton-polaron energy versus internal distance z_0 between WS₂ and polar substrates in weak coupling regime for various polar substrates

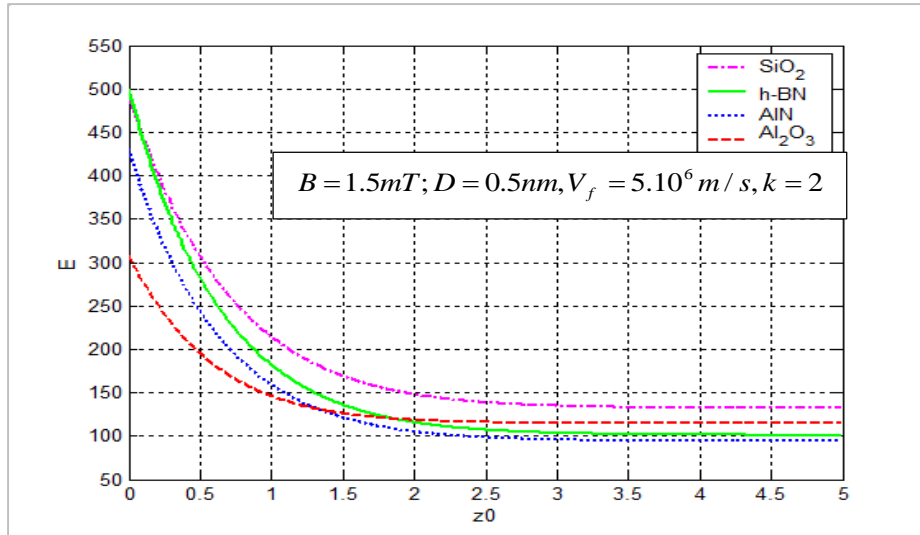


Figure 30 : Energy of exciton-polaron versus internal distance z_0 in intermediate coupling regime for various polar substrates

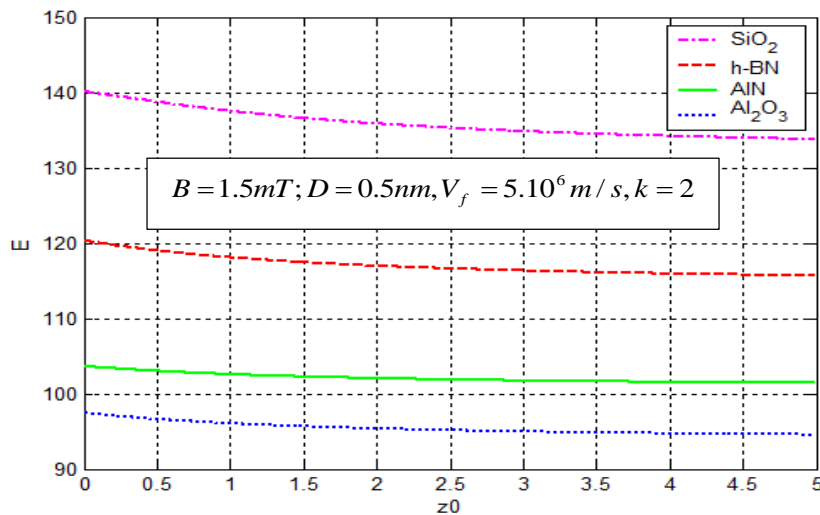


Figure 31 : Energy of exciton-polaron versus internal distance z_0 in strong coupling regime for various polar substrates

Thus for small range of internal distance between monolayer and polar substrates, we have a dominate contribution to the correction of the ground state energy of exciton-polaron. In strong coupling regime, energy varies smoothly with increasing of z_0 . For all this plot, as the internal distance increase the energies become less sensible for this internal distance. Comparing the three plots, the energies are more enhance in the case of a weak coupling regime showing how the electron-phonon coupling affects the ground states energies of exciton-polaron in TMDs monolayer

3.1.2 MOBILITY

3.1.2.1 MOBILITY OF POLARON

- **Polaron under electric field: the results presented here are obtained from Eq. (132) where the expressions of energies are from Eqs. (147) and (148).**

Fig.32 is the 3D plot of the mobility of polaron as a function of wave vector and electric field. It is observed that the mobility of polaron decreases with increasing of wave vector. Fig.33 displays the mobility of polaron as a function of internal distance between TMDs monolayer and polar substrate z_0 and electric field.

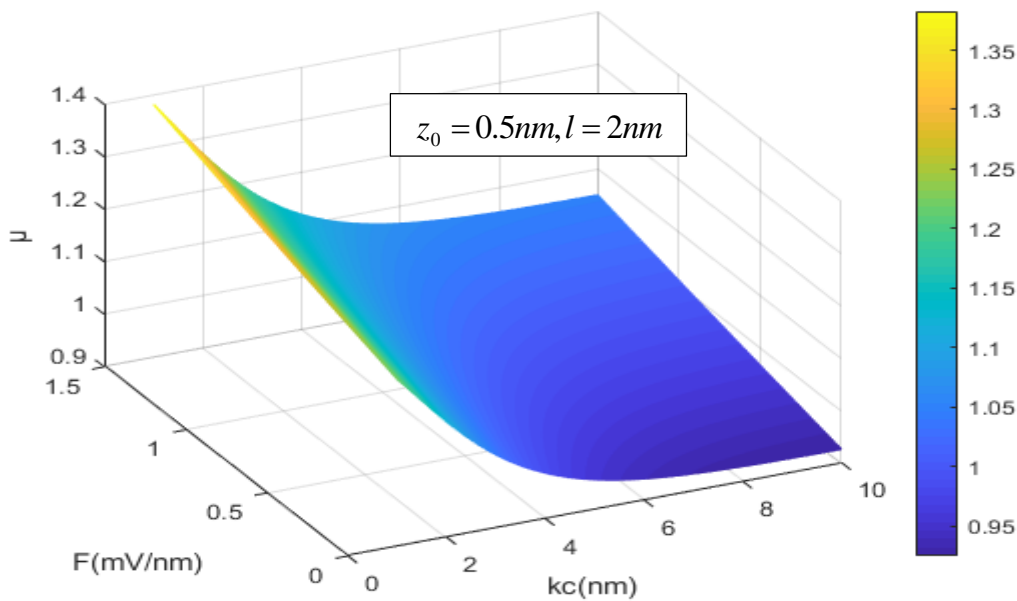


Figure 32 : Polaron mobility versus wavelength vector and electric field

One can observed that for small value of z_0 , mobility decreases sharply and then becomes linear with the increasing of z_0 . This behavior of mobility is in accordance with those obtained in graphene nanoribbon under laser control [151]. From these Figs.32 and 33, one can also observe that the mobility increases smoothly with increasing of electric field. In Fig.34, we plot the variation of mobility as a function of electric field for different TMDs monolayer. It is observed that the mobility increases with the increasing of the electric field. This result is in accordance with Fig.32 and 33. Also in Fig.34, one can remark that the mobility varying with different TMDs monolayer, the polaron moves more freely in WS_2 monolayer. This result was predictable in Fig.17 because it is in the same monolayer that we had the greatest energies. From these figures, our result suggest that electric field can be useful to increase the movement

of electron in different TMDs monolayer. But in order to minimize the displacement of electron in a system of TMDs monolayer under electric field, we can either increase internal distance between monolayer and polar substrate or increase the value of wave vector.

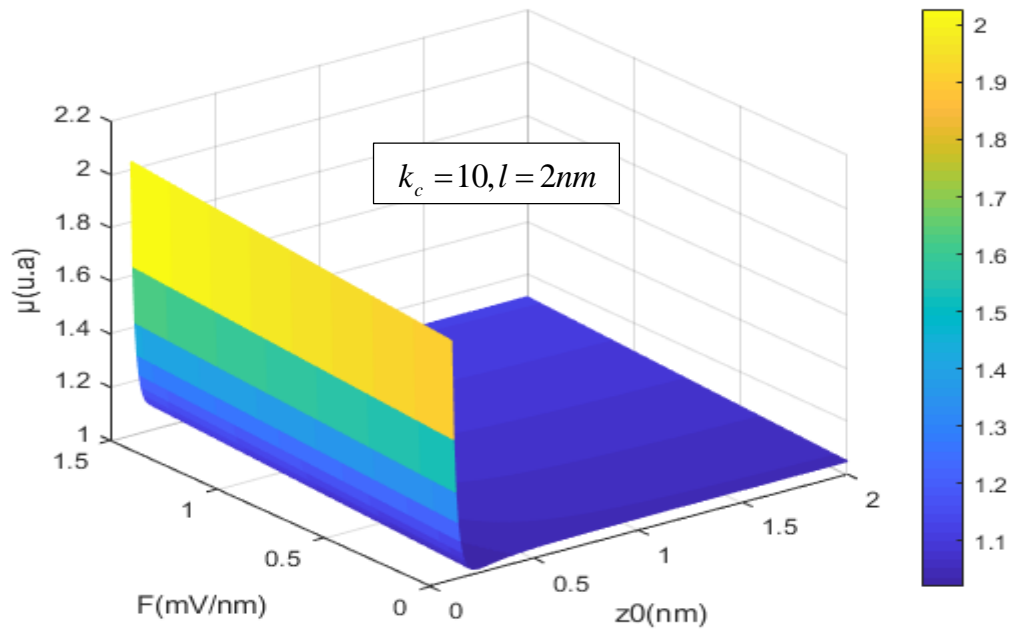


Figure 33 : Polaron mobility versus electric field and internal distance between TMDs monolayer and polar substrate

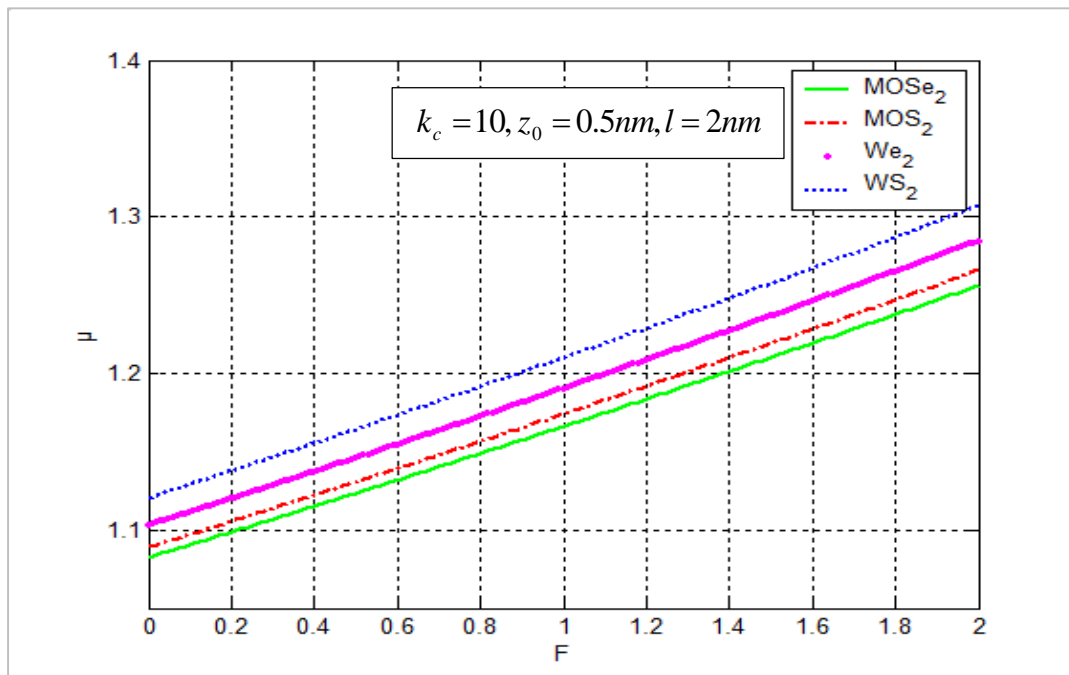


Figure 34 : Polaron mobility versus electric field for different TMDs monolayers

- **Polaron under microwave and radiowave: the results presented from Eq. (132) where the expressions of energies are from Eqs. (163) and (165).**

Fig.35 presents the mobility of polaron for SO phonon as function of amplitude of RW and MW for different TMDs monolayer. It is observed that the mobility increase with the increasing of the amplitude. This means that the more amplitudes are greater, the polaron moves faster in each TMDs monolayers. This shows that RW or MW field can be used to enhance the motion of particles in confining TMDs. But small amplitudes of these field will favor less mobility. So to reduce fast motion of quasi-particles in TMDs; it will be interesting to choose RW or MW with low amplitudes. So the greater the amplitude of the RW or the MW, the faster the mobility of the polaron, thus more the RW or the MW impact the system, big the polaron behavior is captured. In the same plot is presented the mobility as function of different TMDs and one can observed that polaron moves more freely in WS₂. This result reflects the fact that the polaron interacts effectively with other quasiparticles, thus promoting faster energy transfer and hence good electrical conductivity. This result can be used in electrical components where the electrical transition is desired such as electrical wires and electronic devices.

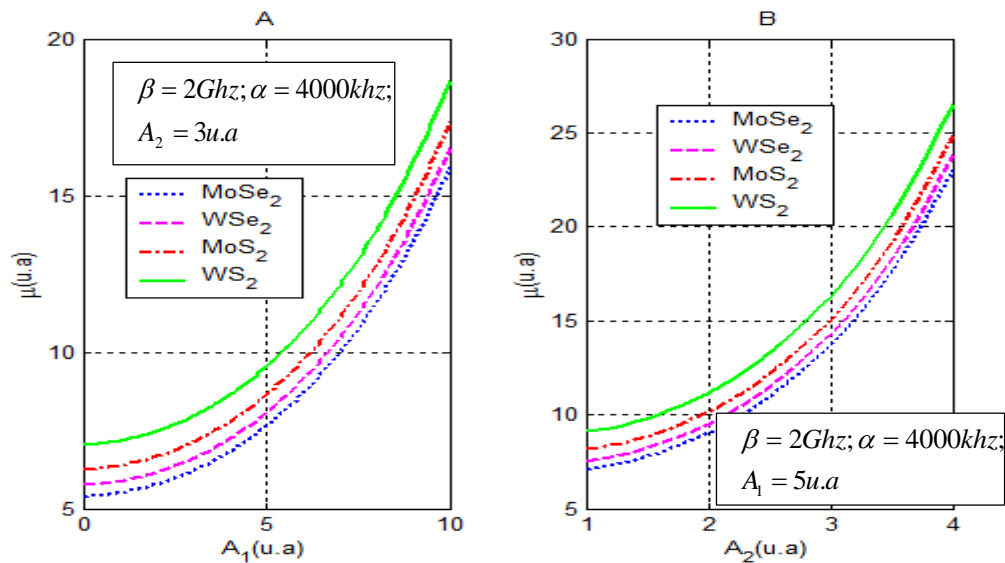


Figure 35 : Mobility of polaron with SO phonon mode as function of amplitude of RW (fig.35A) and amplitude of MW (fig.35B) for different TMDs monolayers

This result was predictable because it is in the same monolayer that we had the greatest energies. This result shows that the amplitude of the MW or the RW is helpful to varying the mobility of the carriers in TMDs monolayer.

3.1.2.2 MOBILITY OF EXCITON-POLARON

- **Magnetic barrier effect on exciton-polaron:** here, we presented the numerical result from Eq. (130) with the energies given by Eqs. (211) and (213).

The variation of the mobility of exciton-polaron versus magnetic barrier length is presented in Fig.36. One can observe that the mobility increases in all TMDs monolayer with increase in magnetic barrier length. We observe that the greater the magnetic barrier length, the faster the motion of the polaron. This result has been obtained also by Djomou et al [171]. To characterize environments that conduct electric current, we need to apply magnetic field in an exciton-polaron system. By increasing the magnetic barrier length, the mobility of exciton-polaron in TMDs monolayer become high in theory which is in accordance with [173]. Up to now, within all TMDs, experimental mobility is much lower due to the combined influence of external impurities becoming a major limitation in their applications.

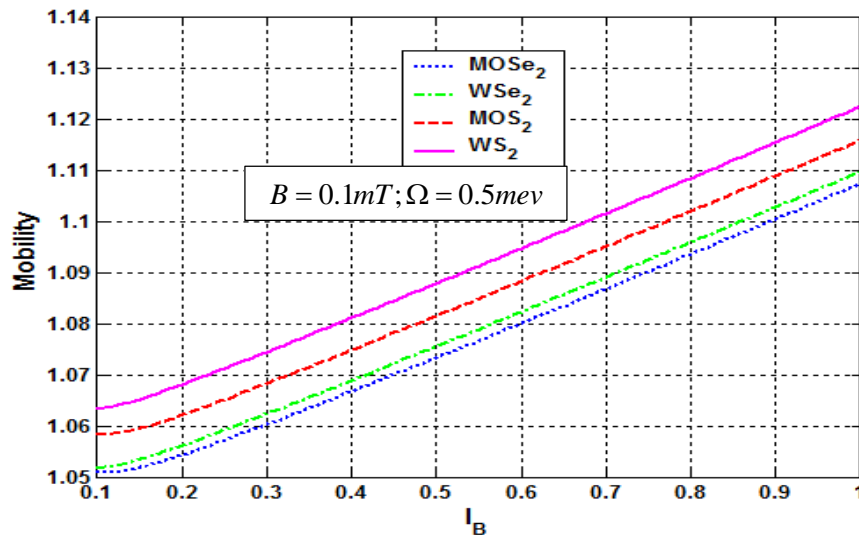


Figure 36 : Mobility of exciton-polaron versus the length of magnetic barrier for different TMDs monolayer

Here, we propose in order to increase the mobility in TMDs, to add magnetic field in the system and taking into account the phonons that affect the system considerably. Taking WS₂ for instance, this work examines the main reasons for the high mobility of TMDs, including the vibration network, charge doping, magnetic disturbances and potential traps. The available mobility results are good because we are capable of achieving trap and impurity densities for a broad variety of transistor devices. It is clear from our investigation that the transport of charge carriers in TMDs systems appears to be a quite sophisticated issue that needs to be handled with attention.

3.1.2.3 MOBILITY OF BIPOLARON

- **Bipolaron in quantum pseudodot:** here, we presented the numerical result from Eq. (132) with the energies given by Eqs. (262) and (233).

Fig.37 is the plot of the mobility of bipolaron as a function of the chemical potential for different values of zero point of the pseudo-harmonic potential. It is observed that the mobility is an increasing function of the chemical potential, this means that the more chemical potential is greater, the bipolaron moves faster in TMDs. This shows that pseudo harmonic potential can be used to enhance the movement of particles in TMDs monolayer by tuning the chemical potential. But low chemical potential values will favor less mobility. So to minimize the motion of quasi particles in the system; it will be necessary to choose pseudo harmonic potential with small chemical potential. In this same plot one can observe that mobility decrease with increasing of the zero point of the pseudo-harmonic potential. Fig.38 displays the mobility of bipolaron as a function of the zero point of the pseudo-harmonic potential for different TMDs monolayers. One can observe that mobility decreases with the increasing of the zero point of the pseudo-harmonic potential. This result is in accordance with Fig.37. This behavior of mobility is in accordance with those obtained in graphene nanoribbon under laser control [174].

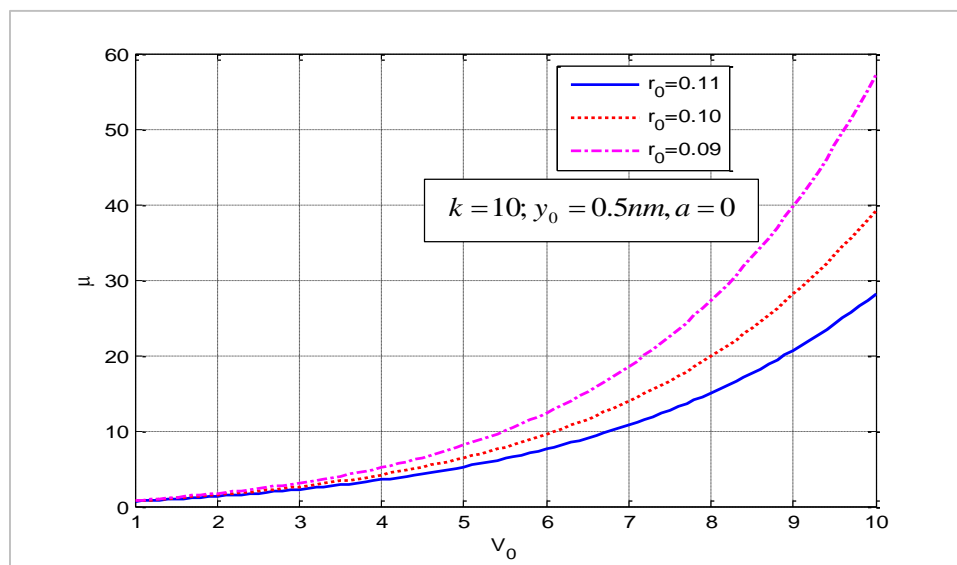


Figure 37 : Mobility of bipolaron versus the chemical potential for different values of zero point of the pseudo-harmonic potential

From Fig.38, one can also remark that the mobility varying with different TMDs monolayer, the bipolaron moves more freely in WS₂ monolayer. Our result suggests that both chemical potential and the zero point of the pseudo-harmonic potential can be useful to increase

the movement of electron in different TMDs monolayer. But in order to minimize the displacement of electron in a system of TMDs monolayer in pseudodot, we can either increase the zero point of the pseudo-harmonic potential or decrease the value chemical potential. Thus the system consisting of the bipolaron in TMDs constitutes a stable and therefore durable system and can be used for the storage of quantum information.

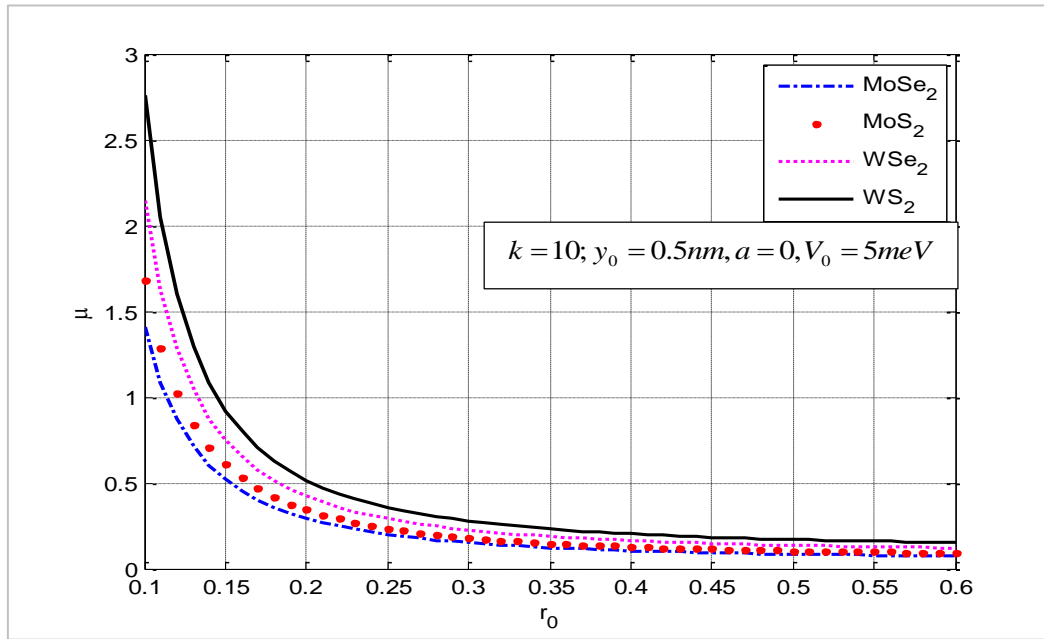


Figure 38 : Mobility of bipolaron versus zero point of the pseudo-harmonic potential for various TMDs monolayer

3.1.3 EFFECTIVE MASS OF EXCITON-POLARON

- **Magnetic barrier effect on exciton-polaron: the numerical result is obtained from Eq. (221).**

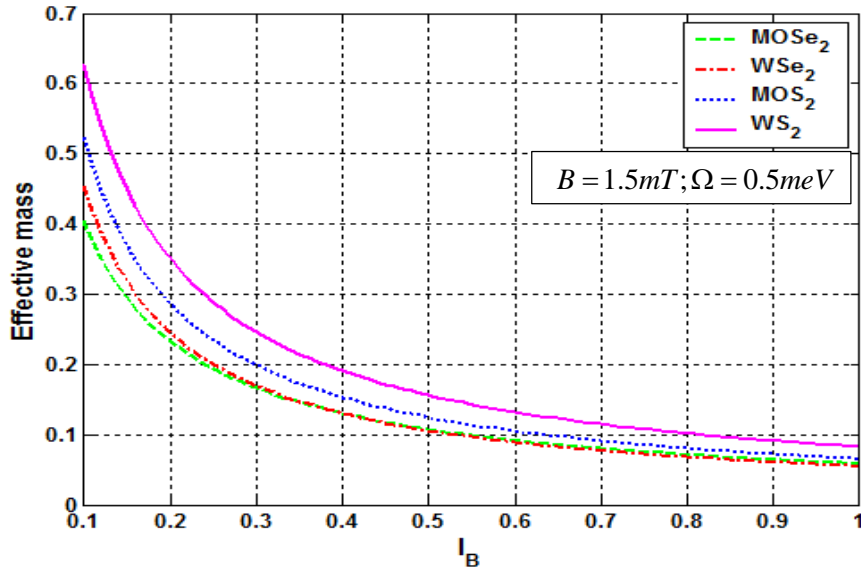


Figure 39 : variation of effective mass of exciton-polaron versus the length of magnetic barrier for various TMDs monolayer

Fig.39 presents the effective mass of the exciton-polaron versus magnetic barrier length. One can observe that the effective mass reduces with the increase of the magnetic barrier length. For high values of the magnetic barrier length, the mass variation of the exciton-polaron is higher, owing to the interplay of phonon and the electron (hole). This behavior is in accordance with [171, 175]. This result suggests that the length scale of the magnetic barrier can be necessary to tune the effective mass of exciton polaron in TMDs monolayer. Often, research experiments use a series of external conditions like the magnetic field to explore exciton dynamics in physical structures. As the present work is focused on the exciton-phonon interaction due to high deformation trap related to phonon, the magnetic barrier can contribute to the diffusion of charge carriers in monolayers. This result proves that the transport properties of an exciton-polaron are robust. Since the deformation trap characterizes the monolayers, we highlight differences that occur from monolayer TMDs when evaluating the polaronic effect due to magnetic barrier. In MoSe₂, the transport properties can be more interesting than the one of WS₂.

- **Electron-phonon coupling effect on exciton-polaron: the numerical results are obtained from Eq. (238).**

In Figs.40 and 41, we present the variations of the effective mass of the exciton-polaron coupling with SO phonon as a function of the magnetic field in a strong coupling regime (Fig.40) and intermediate coupling regime (Fig.41) for different TMDs monolayer. One can

observe that the effective mass decrease sharply with increasing of the magnetic field in all TMDs monolayers. This suggest that the effective mass of exciton-polaron in TMDs monolayer is greater than the mass of a free charged carriers. This is in accordance with [176]. Our result reveals that in all TMDs monolayer, the exciton-polaron participates in transport, also that the magnetic field can be used to control the motion of the exciton-polaron in TMDs monolayer for both intermediate and strong coupling regimes. The results obtained here can be useful in spintronic for the control and manipulation of the spin of charge carriers for the storage of quantum information

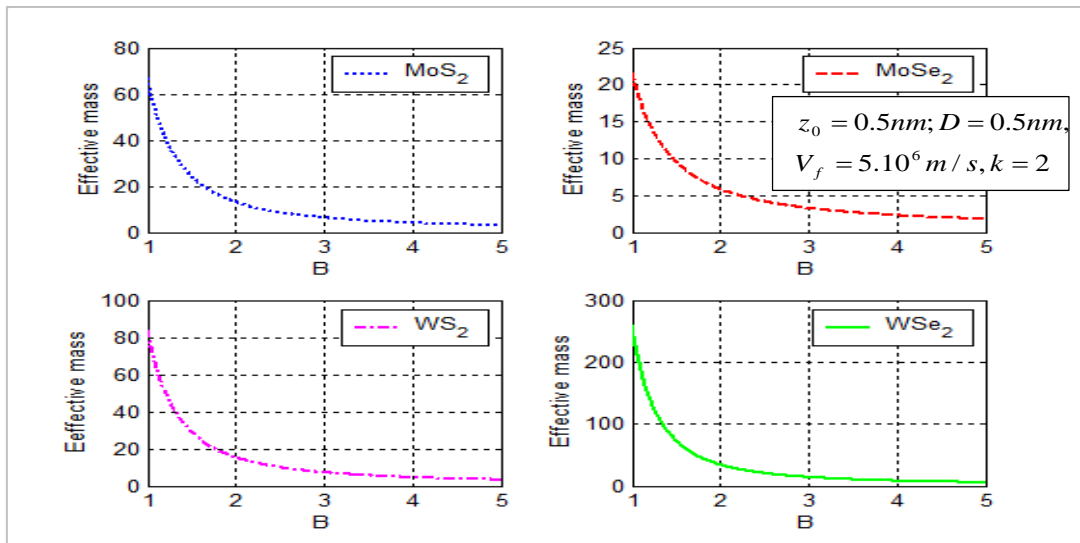


Figure 40 : Effective mass of exciton-polaron coupling with SO phonon as function of the magnetic field in a strong coupling regime for various TMDs monolayer

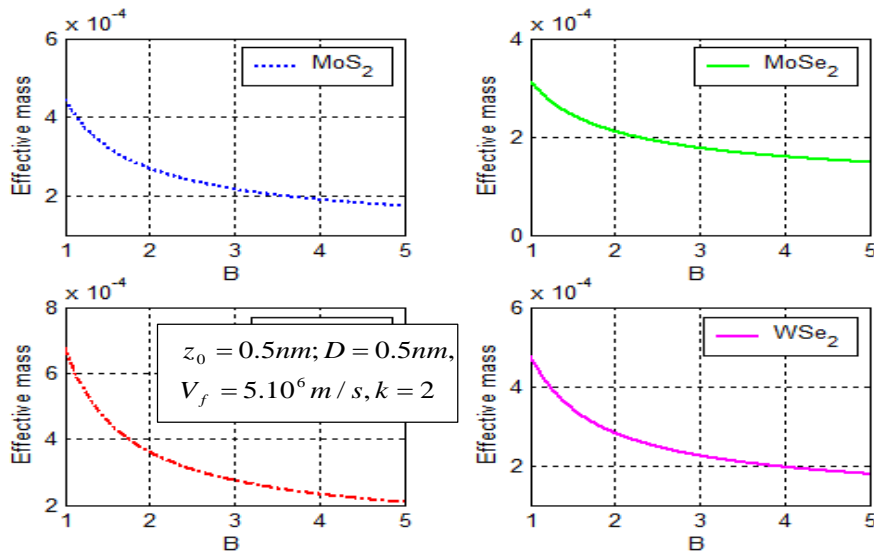


Figure 41 : Effective mass of exciton-polaron coupling with SO phonon as a function of the magnetic field in intermediate coupling regime for various TMDs monolayer

3.1.4 LIFETIME OF POLARON

- **Polaron under electric field: the numerical results presented are obtained from Eq. (150)**

Fig.42 displays the lifetime of polaron in the ground state as a function of wave vector for different TMDs monolayer. It is observed that the lifetime of polaron increases sharply with the increasing of wave vector up to $k_c < 2$. Then for $k_c > 2$ the variation of lifetime becomes horizontal with the increasing of wave vector. Hence, the wave vector no longer influences the lifetime of polaron in ground state. In this figure, the variation of the lifetime of polaron for different monolayer are also presented and one can observe that polaron lives long in WS₂ monolayer.

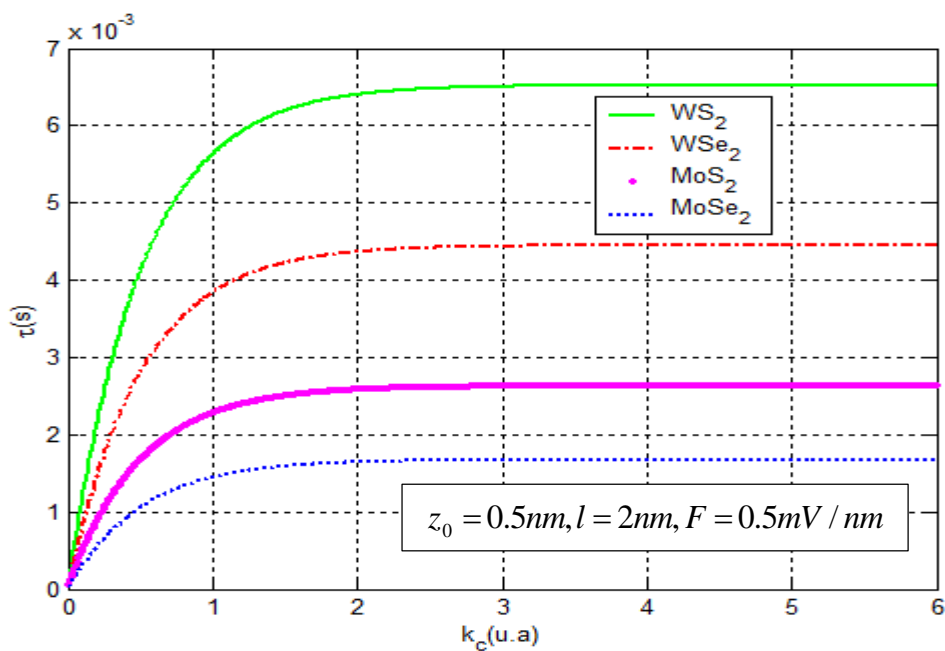


Figure 42 : Lifetime of polaron versus wavelength for different TMDs monolayers for

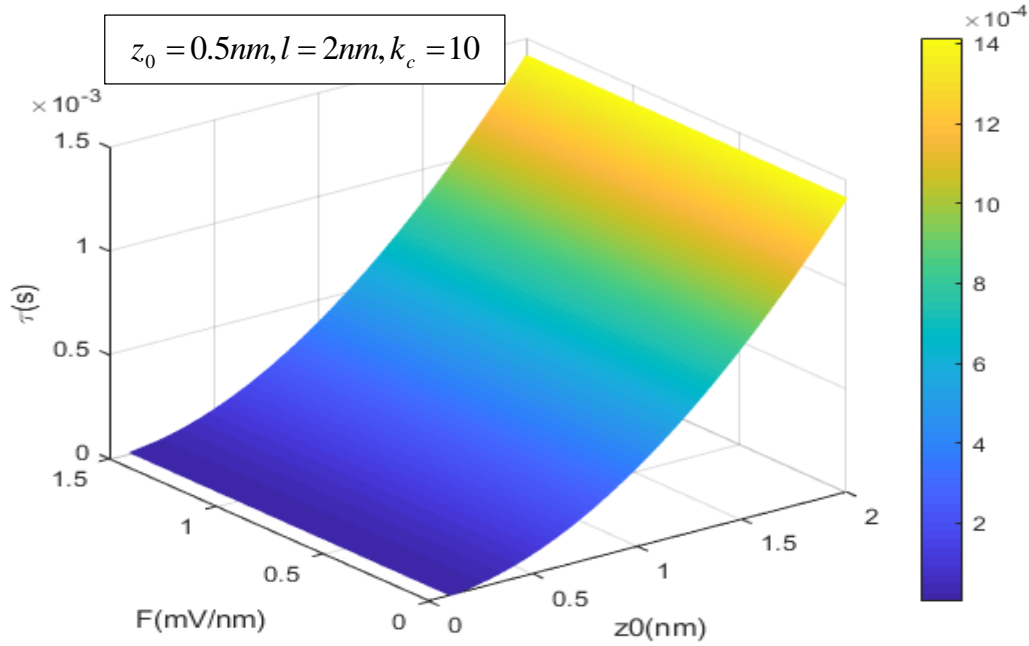


Figure 43 : Lifetime of polaron versus electric field and internal distance between TMDs monolayer and polar substrate

Fig.43 displays the lifetime of polaron in ground state as function of electric field and internal distance between TMDs monolayer and polar substrate z_0 . One can see that the lifetime increases with the increasing of z_0 . In this figure, it is observed that the lifetime decreases smoothly with the increasing of electric field strength and increase linearly with the increasing of z_0 . Our results suggest that electric field reduces the lifetime of polaron in TMDs, which can be due to the fact that electric field is a confinement potential in on hand, and the internal distance between TMDs and polar substrates enhances the life time in order hand. These results show that the lifetime of polaron in TMDs monolayer can be controlled by electric field, internal distance z_0 and wave vector. The lifetime of the polaron is in the order of milliseconds

- **Polaron under microwave and radiowave: the numerical results presented are obtained from Eq. (173) and (175)**

Figs.44, 45 displays respectively the polaron lifetime in ground state as function of amplitude for RW and MW for different TMDs for LO phonon mode and SO phonon mode. One can observe that in both case RW (Fig.44A) and MW (Fig.44B), the lifetime increases with the increasing of the amplitude. In case of SO phonon mode polaron lifetime increase with the increasing of the amplitude of the RW (Fig.45A). In Fig.45B the variation of the polaron lifetime has a parabolic behavior, it firstly decreases with increasing of the amplitude of the

MW and secondly increase with the amplitude. This result is similar to that obtained in [151]. Thus in TMDs monolayer, due to presence of MW and RW polaron live for a long period due to the fact that the lattice thermal motion becomes slow with the increasing of amplitude, so the higher the amplitude, the longer the polaron live.

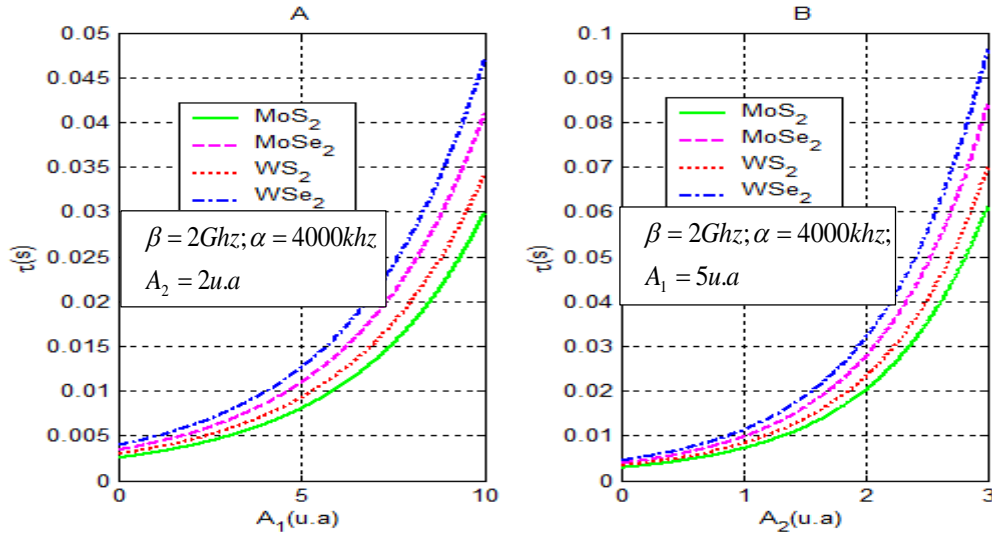


Figure 44 : Life time of polaron with LO phonon mode as function of amplitude of RW (fig.44A) and amplitude of MW (fig.44B) for different TMDs monolayer

This has the significance that the RW and the MW presence increase the lifetime of polaron in ground state. Other reason of the increase in polaron lifetime with amplitude can be explained by the fact that electron motion is increased due to the existence of the RW or the MW as confinement potential. In these same figures the dependence of the polaron lifetime for different TMDs are presented and it can be remarked that for SO phonon mode, polaron lives longer in TMDs with disulphide than with diselenide whereas for LO phonon mode polaron lives longer in TMDs with diselenide than with disulphide, which means that the type of electron-phonon coupling also affects polaron lifetime in TMDs monolayers. These results on the lifetime show that the system consisting of polaron in TMDs present a good stability due to interaction between electron and phonon but also to the confinement. These results can be used to the fabrication of electronic devices such transistors and LEDs

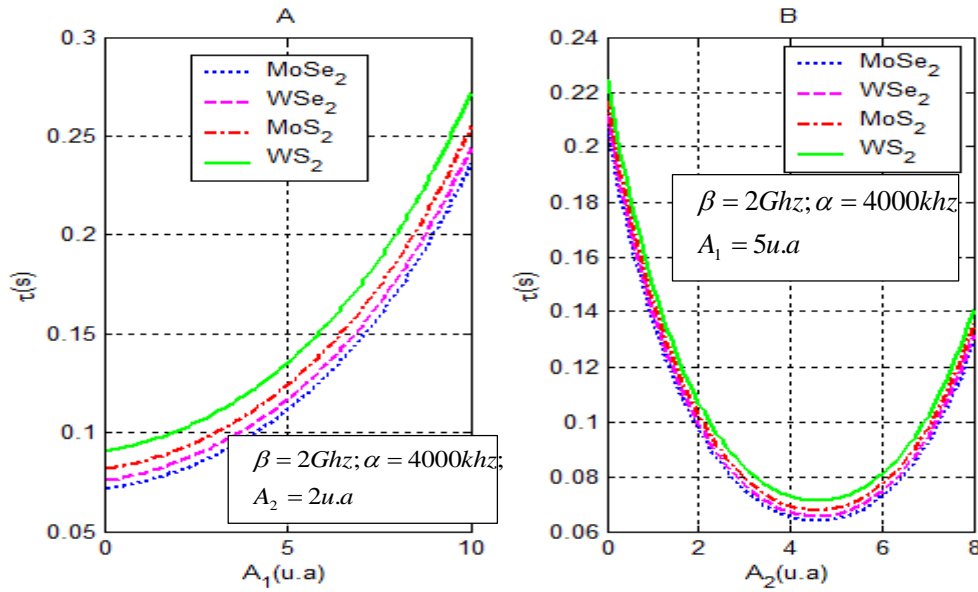


Figure 45 : Life time of polaron with SO phonon mode as function of amplitude of RW (Fig.45A) and amplitude of MW (Fig.45B) for different TMDs monolayer

3.2 STABILITY, OPTICAL ABSORPTION AND BANDGAP MODULATION

3.2.1 STABILITY OF BIPOLARON

- **The numerical result of the stability of bipolaron is obtained with Eq. (250).**

In Fig.46, the binding energy with magnetic field is presented for intermediate coupling regime. One can observe that the binding energy decrease with increasing of magnetic field. The increase of magnetic field enhances the average of coulomb repulsion between the electrons, this result is in accordance with the work of Brosens and Devreese [177]. Thus, despite the enhances of coulomb repulsion, the phonon mediated attractive electron-electron attraction still dominated. That is the reason that the binding energy remain positive and indicated that in all selected TMDs monolayer, the bipolaron is stable. From Fig.47, the binding energy decreases as η_0 increases, then the bipolaron is stable in the different monolayer TMDs as the binding energy remain positive. This result can be used to develop more efficient and durable batteries, or to create new electronic devices that are more energy efficient and can operate at high temperatures.

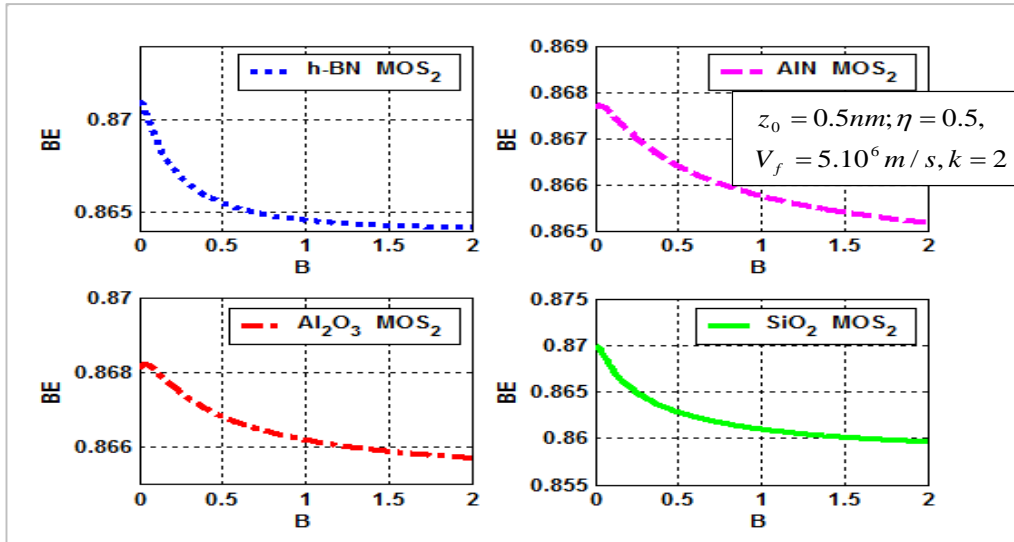


Figure 46 : Binding energy of the bipolaron versus magnetic field in MoS₂ for different polar substrate (intermediate coupling regime)

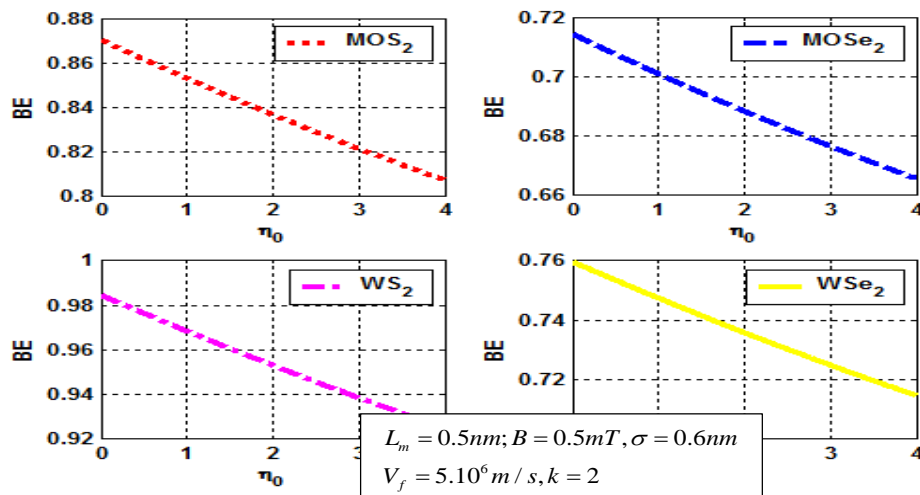


Figure 47 : Binding energy of the bipolaron with parameter η_0 in weak coupling regime for different TMDs monolayer

3.2.2 MAGNITUDE OF BANDGAP MODULATION

3.2.2.1 CASE OF POLARON

- The numerical result of the magnitude of the bandgap modulation of polaron are obtained with Eq. (172).

Fig.48 presents the variation of the magnitude of bandgap modulation as function of the frequency of the RW for SO phonon mode. On can observed that the MBM oscillate

periodically at same amplitude with the increasing of the RW frequency. Thus the MBM fluctuate with the increasing of the frequency of the RW, this result was predictable in Fig.18 as the energies fluctuate with the frequency of RW. So RW can be necessary to create fluctuation in the MBM of the MoS₂ monolayer.

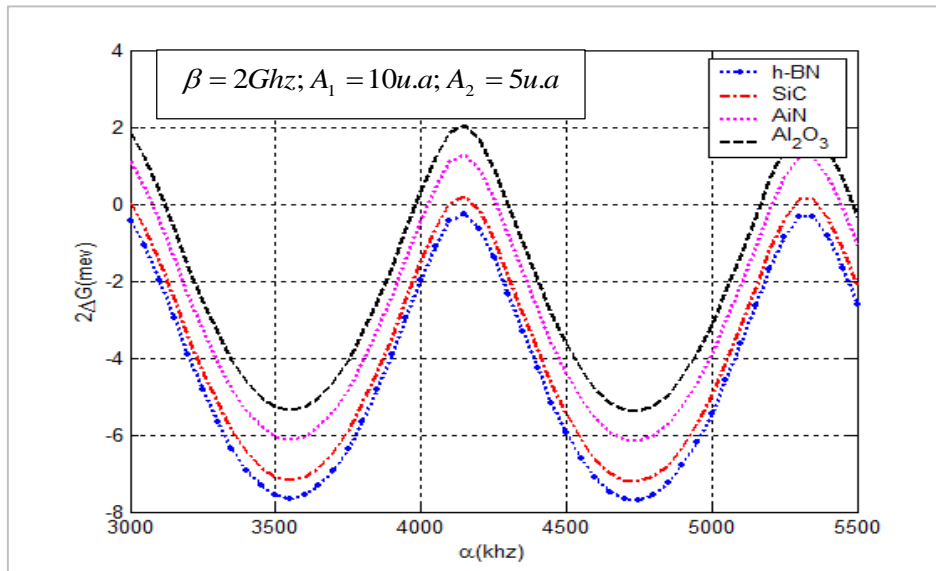


Figure 48 : The MBM of polaron with SO phonon mode as function of frequency of RW for different polar substrates

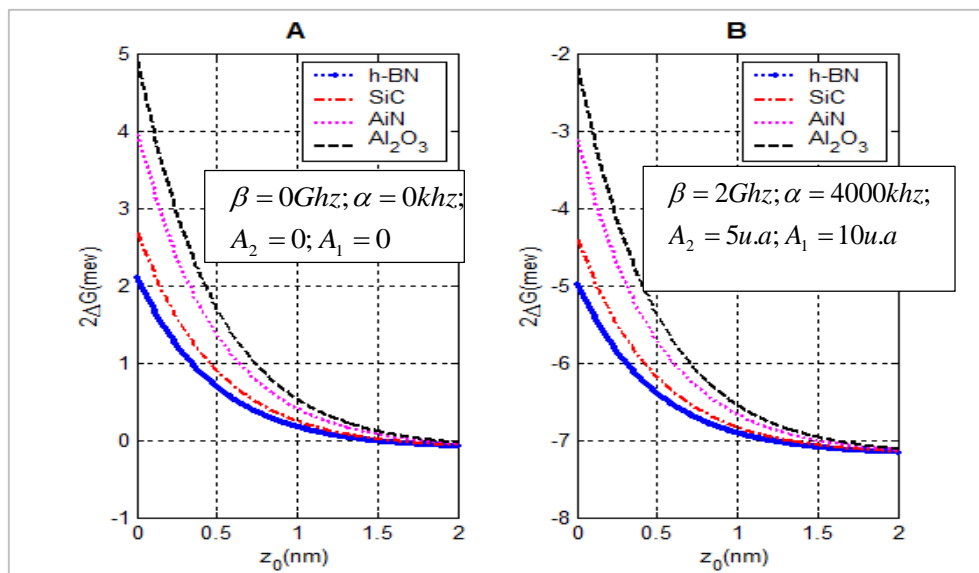


Figure 49 : The MBM of polaron with SO phonon mode as function of internal distance for different polar substrates. (Fig.48A) without RW and MW, (Fig.48B) with RW and MW

Fig.49 shows the variations of the MBM for SO phonon as function of internal distance between MoS₂ monolayer and different polar substrates in the case without radiofrequency and

microwave (Fig.49A) and in the case with both microwave and radiofrequency (Fig.49B). It can observe that the MBM decrease sharply with the increasing of the internal distance between polar substrate and MoS₂. This behavior is similar to that obtained in [51]. In Fig.49A the MBM is positive whereas in Fig.49B the MBM is negative showing that the RW and MW increase the modulated bandgap in MoS₂ monolayer. These figures also present the dependence of MBM as function of different polar substrates, it can be observed that the MBM increase with the increasing of the of the polarizability parameters, thus the highest MBM is obtained with Al₂O₃ polar substrate and the lowest with h-BN polar substrate, this is in accordance with [51].

Fig.50 presents the MBM of LO phonon mode as function of amplitude of the RW and MW for different TMDs monolayer. It can be observed that the MBM is a decreasing function of the amplitude of the RW and the MW. As in the Fig.49, the RW or the MW increase the ground state energy thus, increase the modulated bandgap of the monolayer. In this same plot is presented the variation of the MBM as function of different TMDs monolayer and one can remarked that the MBM decrease in all monolayer.

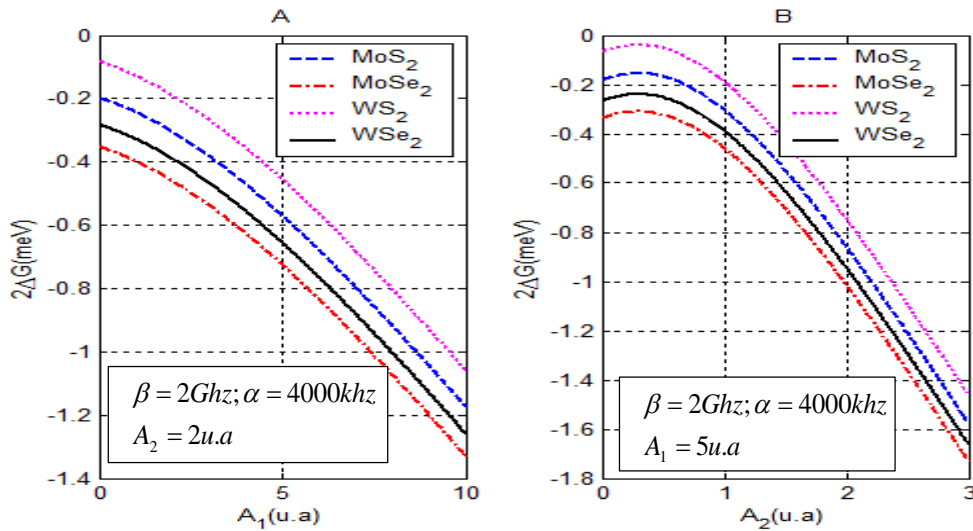


Figure 50 : The MBM of polaron with LO phonon mode as function of amplitude of RW (Fig.50A) and amplitude of MW (Fig.50B) for different TMDs monolayer

3.2.2.2 CASE OF BIPOLARON

- **The numerical results of the magnitude of the bandgap modulation of bipolaron are obtained with Eq. (172) with the energies given by Eqs. (246) and (247)**

In Fig.51 (a). we present the dependences of MBM on the magnetic field for bipolaron in different monolayer TMDs at intermediate coupling regime. It can be seen that the MBM

increases with magnetic field. For various TMDs, the MBM are also shown, one can observe that it varies with TMDs monolayer. The most important MBM is obtained with WS_2 and the less with $MoSe_2$, thus among the selected TMDs the latter strongly enhances the conductivity. A significant change of MBM relates to each TMDs highlights the impact of the magnetic field on the bandgap modulation in TMDs monolayer. Fig.51 (b). presents the dependence of MBM on the magnetic field in different monolayer at strong coupling regime. As in the intermediate regime we can see that MBM increases with magnetic field. We also observe that the MBM varies with TMDs monolayer, then the most important is obtained with MoS_2 and the less with WSe_2 which is not the case in intermediate coupling regime. Thus the electron phonon coupling affect the MBM for different TMDs monolayer in the presence of bipolaron. Fig.51 (c). presents the MBM versus η_0 for different monolayers in weak coupling regime. One can observed that MBM increases with increasing the coupling parameter η_0 . Same result was obtained by [51]. These results show that the bipolaron strongly affects the bandgap of TMDs. Since the coupling parameter characterizes the material, strong coupling favor the modulation of the bandgap. The WSe_2 presents the highest MBM. In the investigation of carriers LO phonon coupling in monolayer TMDs, defined a new parameter g_f defined by sohier [178] as the coupling strength, which is analogous to the parameter η_0 and pointed out that the 2D Fröhlich coupling is much stronger in TMDs. Moreover, we noticed that the values obtained for the bandgap modulation due to carrier-LO phonon coupling are very close to experimental results [179, 180]. Then, the LO phonons increase the modulated bandgap then consequently decrease conductivity in TMDs. Among the selected TMDs, the one with highest performance in conductivity is the MoS_2 .

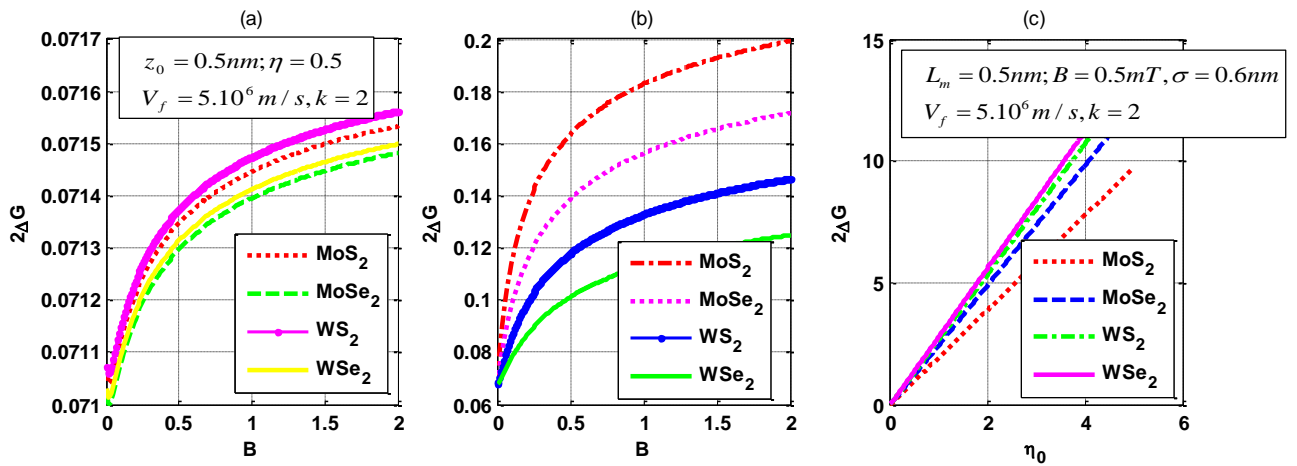


Figure 51 : Magnitude of bandgap modulation different TMDs as function of :

(a) Magnitude of bandgap modulation versus magnetic field in intermediate coupling regime for (b) Magnitude of bandgap modulation versus magnetic field in strong coupling regime (c) Magnitude of bandgap modulation Versus η_0 for different monolayer in weak coupling regime

3.2.3 OPTICAL ABSORPTION COEFFICIENT

3.2.3.1 CASE OF EXCITON-POLARON

- **The numerical results of optical absorption of exciton-polaron are obtained from Eqs. (240) and (241)**

Figs.52 and 53 illustrate the behavior of the optical absorption of the exciton-polaron coupling versus the incident photon energy for various TMDs monolayers with the LO phonon and in a weak and an intermediate coupling regime respectively. One can notice that no absorption can be observed for $\hbar\Omega < \hbar\omega_{LO}$, then a minimum value for the absorption is at $\hbar\Omega = \hbar\omega_{LO}$. For this value, the absorption coefficient increase until a maximum value and decrease slowly. Thus, optical absorption only occurs when the energy of the photon exceeds the energy of the optical phonon. In fact, this behavior of the absorption of an exciton-polaron is similar to those obtained in other quasi-particles in ionic crystal and polar semiconductor [160-162]. It could be observed that in all TMDs monolayer, the peak of the absorption is reached for the same value of the photon energy. The absorption peak corresponds to the emission of a quantum of energy, thus in all TMDs monolayer this emission occurs at the value of photon energy of around 1.6meV. The value of the absorption increases in the following order MoSe₂, MoS₂, WSe₂ and WS₂. This may be due to the fact that the absorption is inversely proportional to the mass of electron in different TMDs. This highlights that smallest the effective mass of carriers in monolayer is, highest the absorption of exciton-polaron is. Mentioned that the parameter η_0 in the formula of the absorption for LO phonon is assumed ($\eta_0 = 0.1$) for all monolayer then the magnitude of the optical absorption of exciton-polaron increases with the increasing of η_0 . This result is in accordance with that given in [162]. By comparing the two coupling regimes, the particle is more absorbent in the intermediate coupling regime than in the weak coupling regime, thus the electron-phonon coupling can be used to improve the absorption of exciton-polaron in TMDs monolayer.

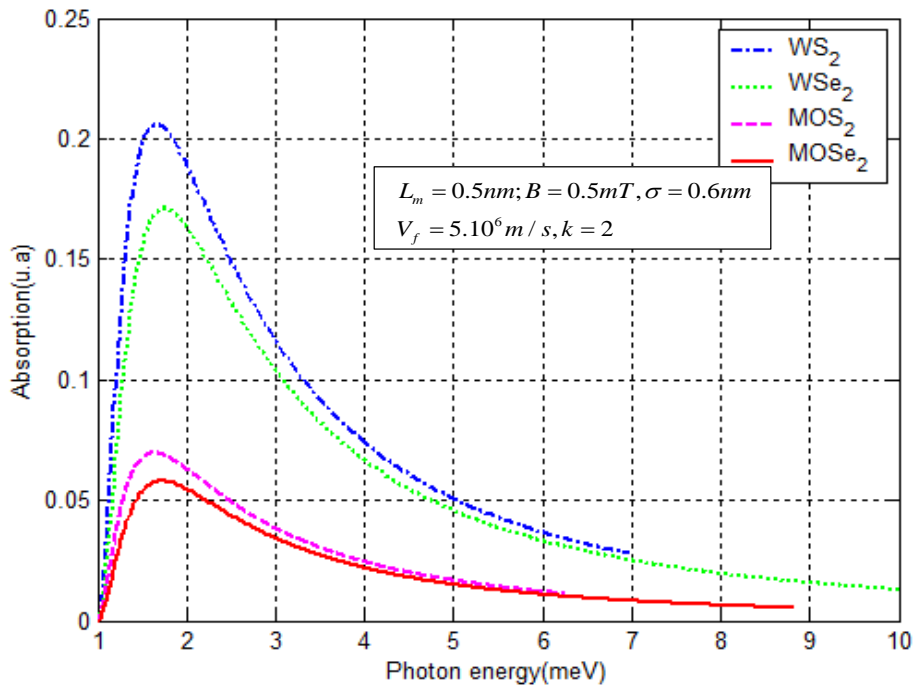


Figure 52 : Absorption of exciton-polaron as function of photon energy in weak coupling regime for LO phonon for different TMDs monolayer

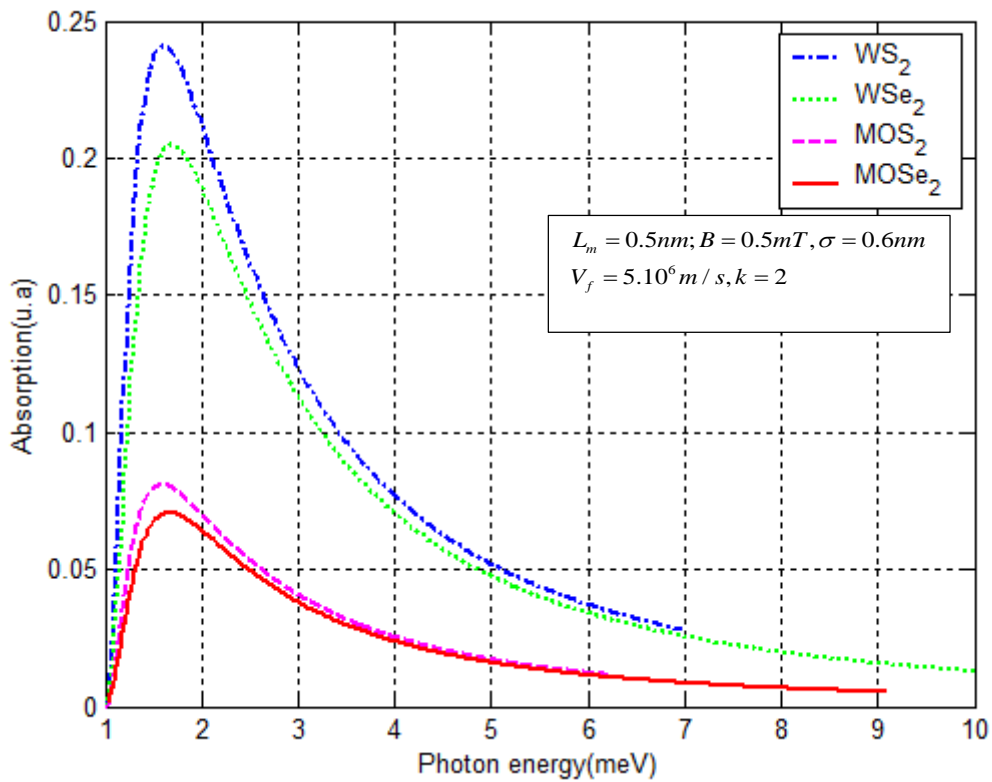


Figure 53 : Absorption of exciton-polaron as function of photon energy in intermediate coupling regime for LO phonon for different TMDs monolayer

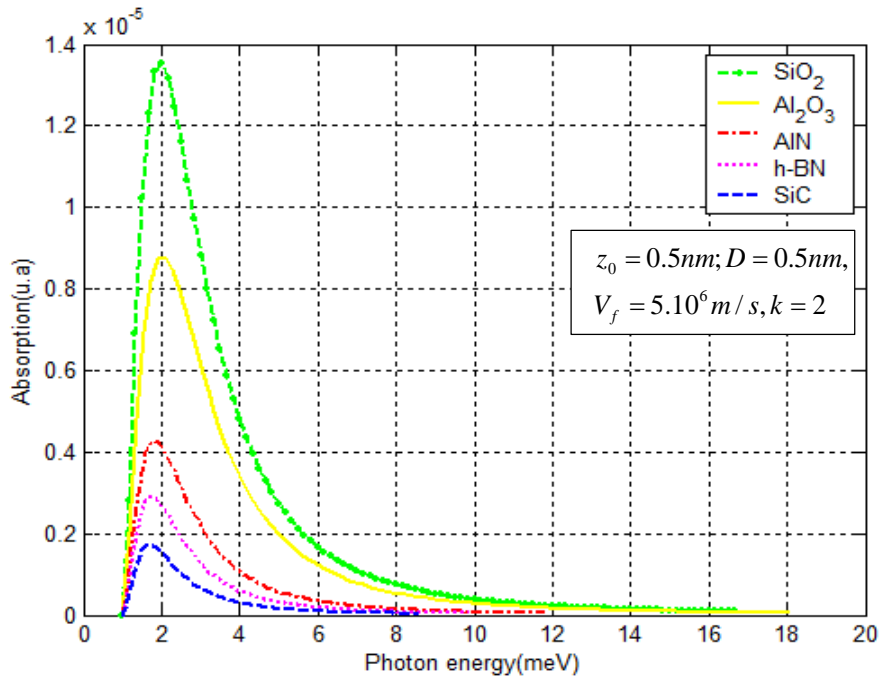


Figure 54 : Absorption of exciton-polaron versus photon energy in weak coupling regime coupling for different polar substrate

The plot of optical absorption of exciton-polaron coupling with SO phonon as function of the incident photon energy is presented in the case of the weak coupling regime (Fig.54) and the intermediate coupling regime (Fig.55) in WS₂ monolayer on different polar substrates. One can observe that the behavior of the absorption is similar to the case of LO phonon. Moreover, the intensity of the absorption is highest for certain polar substrates. The peak of the absorption is at the photon energy of around 2meV for all polar substrate. According to the formula of the optical absorption for SO phonon, the parameter η reflects the polarizability which is also the coupling strength between electron and SO phonon. In this figure, the contribution of the polarizability for different polar substrates is also presented. We can remark that the absorption of an exciton-polaron does not increase linearly with the polarizability. This is in good agreement with the result obtained in the case of polaron [162].

Fig.56 presents 3D plot of the optical absorption of the exciton-polaron coupling with SO phonon as function of the magnetic field and internal distance between TMDs and polar substrates for WS₂ monolayer in intermediate coupling regime. One can observe that the optical absorption increase sharply with increasing of magnetic field, this means that the strength of electron-SO phonon coupling is directly affected by magnetic field. Furthermore, the influence of the internal distance between monolayer TMDs and polar substrates in presented in this

figure. This result reveals that increasing the magnetic field may be useful in enhancing the absorption of the exciton-polaron in TMDs.

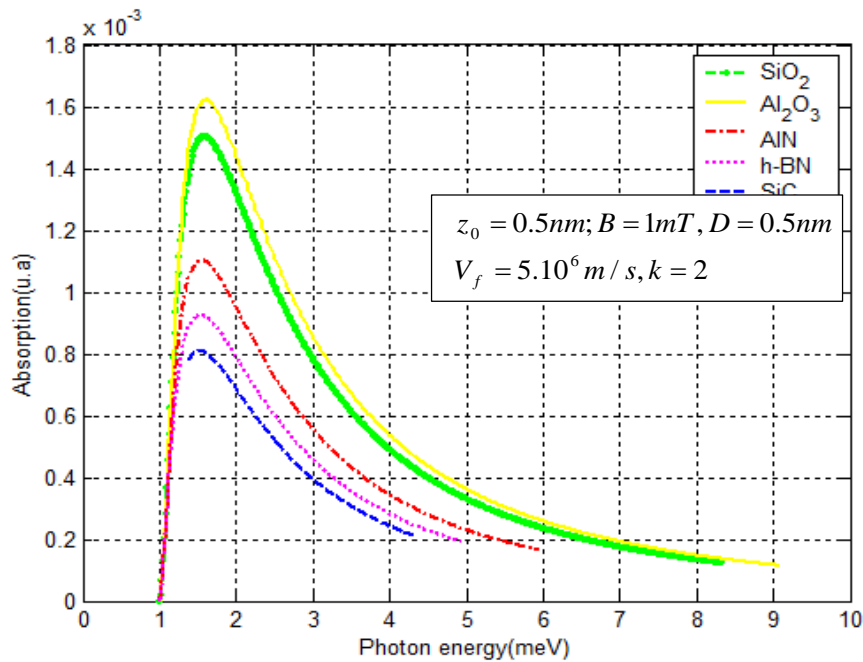


Figure 55 : Absorption of exciton-polaron versus photon energy for intermediate coupling regime coupling with SO phonon for different TMDs monolayer

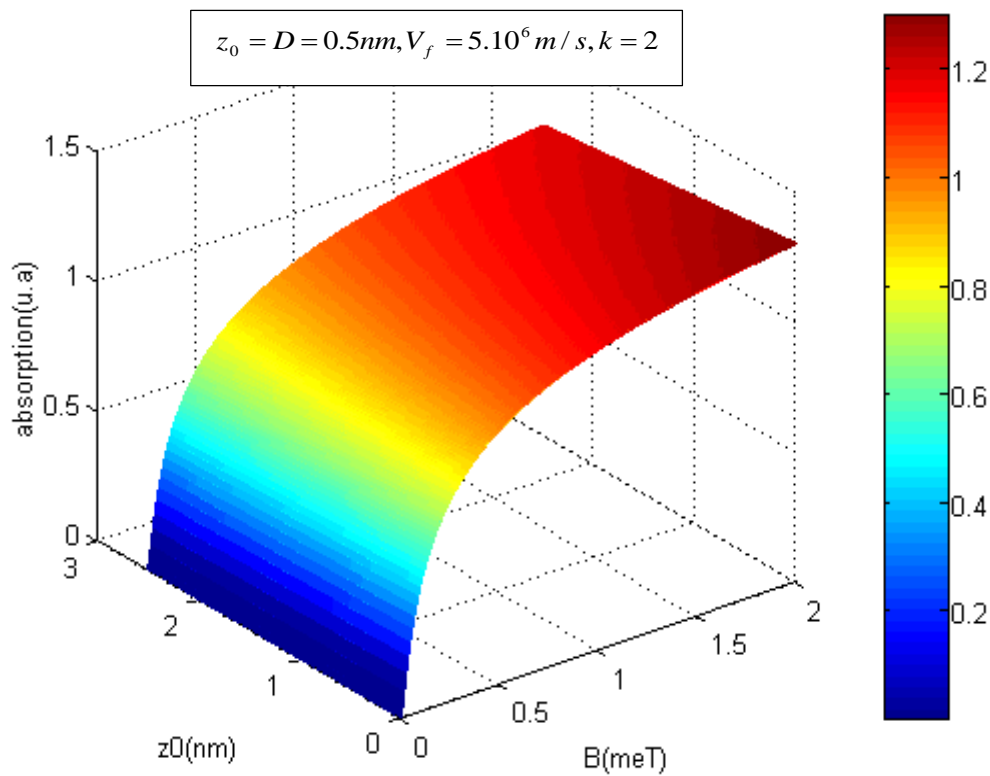


Figure 56 : Absorption of exciton-polaron as function magnetic field and the internal distance between TMDs and polar substrates in intermediate coupling regime

The optical absorption of exciton-polaron versus the photon energy is presented in the Fig.57 for LO phonon mode and for differentd TMDs monolayer. One can observe that the optical absorption is higher in the case of intermediate coupling regime ($a=0.5$) and lower in the weak coupling regime ($a=1$) for all the monolayers. This result confirm the comparison made between Figs. 52 and 53, thus the particle absorbs better in intermediate coupling regime than in weak coupling regime confirming that the electron-phonon coupling regime is necessary to increase optical absorption of exciton-polaron in TMDs monolayer.

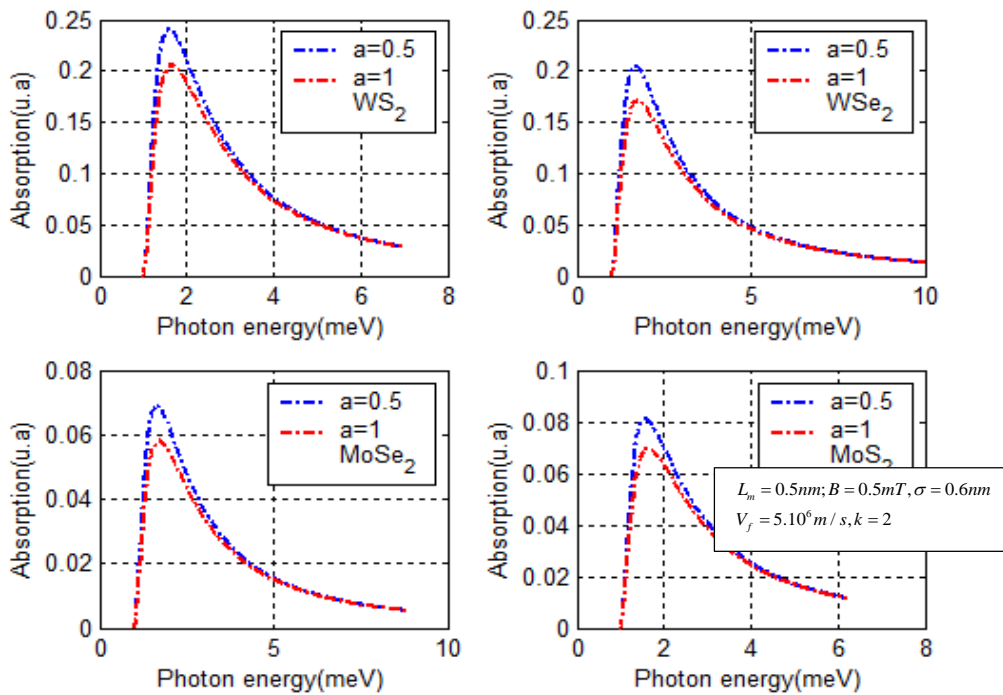


Figure 57 : Absorption of exciton-polaron as function of photon energy for LO phonon for different electron phonon coupling in differents TMDs Monolqyer

3.2.3.2 OPTICAL ABSORPTION OF BIPOLARON

- The numerical results of optical absorption of bipolaron are obtained from Eqs. (251) and (252)

Fig.58 illustrates the optical absorption of the bipolaron versus the incident photon energy for LO phonons in different layers of TMDs with a weak coupling regime. It can be noted that there is no absorption for $\hbar\Omega < \hbar\omega_{LO}$. The threshold value of absorption is at $\hbar\Omega = \hbar\omega_{LO}$. At this value the optical absorption increases and arrives at a maximum and decreases slowly with increasing of photon energy. In fact, these optical absorption behaviors

are consistent with previous work on monolayer TMDs and others [160, 162, 181]. Optical absorption is similar for different TMDs but the strength is not the same for each TMD. This behavior may be attributed to the fact that the optical absorption is proportional to the phononic energy of the bipolaron in the different TMDs. This suggests that the lower the phononic energy of the bipolaron in the TMDs, the lower the optical absorption of a bipolaron. A number of past works have been carried out to study the coupling force in such monolayers [178, 182] Then in MoS₂, bipolaron has enough energy to absorb photon than WSe₂, this can be due to the dominance of electron-phonon and photon-phonon interactions. Comparing the optical absorption in intermediate coupling regime (not shown) with the one in weak coupling regime we observe a similar behavior. This can explain why both couplings can be considered identically in some cases.

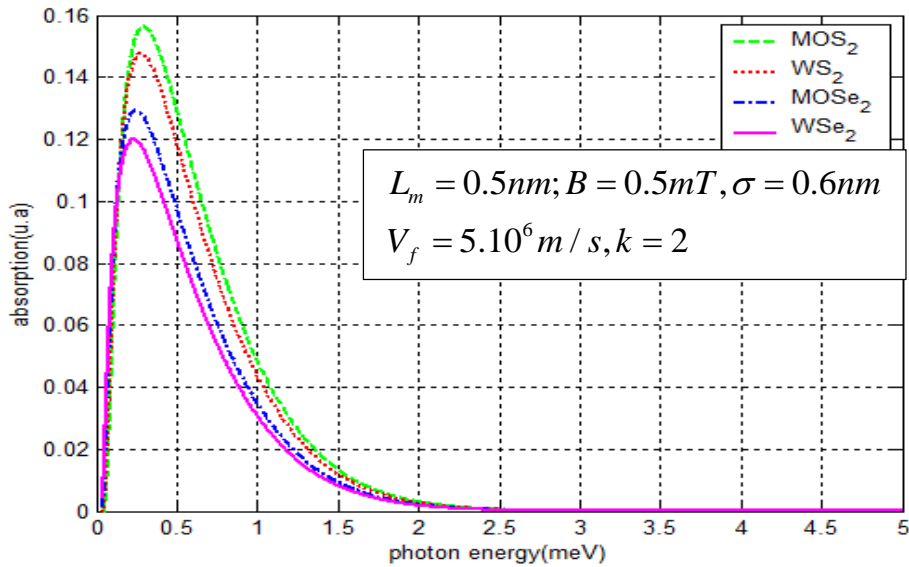


Figure 58 : Optical absorption coefficient of bipolaron versus photon energy in LO phonon in different monolayer TMDs materials for bipolaron in weak coupling regime

Fig.59 displays the dependences of optical absorption with magnetic field and internal distance between TMDs monolayer and polar substrates for the monolayer MoS₂ on SiO₂ substrate. One can observe that the optical absorption increase with the increasing of the magnetic field, increase slowly with the internal distance between TMDs monolayer and polar substrates. For high value of magnetic field, the optical absorption increase slowly. We also observe that optical absorption increase with internal distance separating the monolayer from polar substrates, proving that the strength of the electron-SO coupling directly depends on the internal distance between the TMDs and the polar substrates. This result is in agreement with that of Li

and Wang [162]. In fact, in some studies [183, 184], carrier phonon coupling between 2D materials and the polar substrate has also been recognized, where the trends are comparable for the coupling strength with the internal distance.

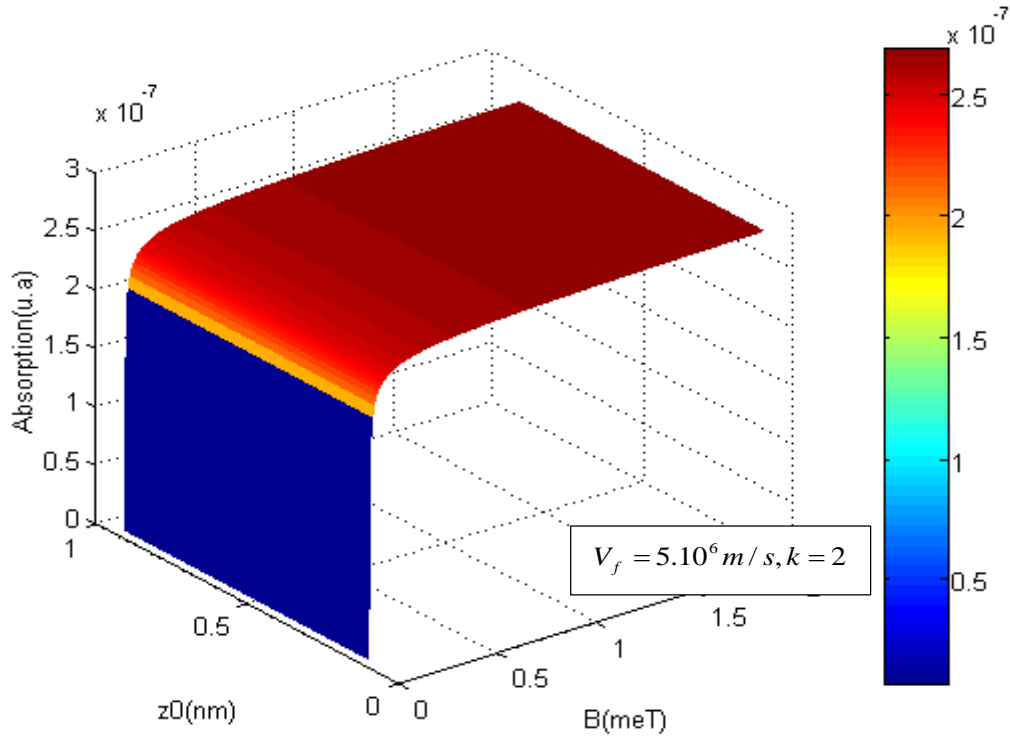


Figure 59 : Optical absorption coefficient of bipolaron (case of SO phonon) versus magnetic field and interal distance between TMDs and polar substrates in MoS₂ intermediate coupling regime

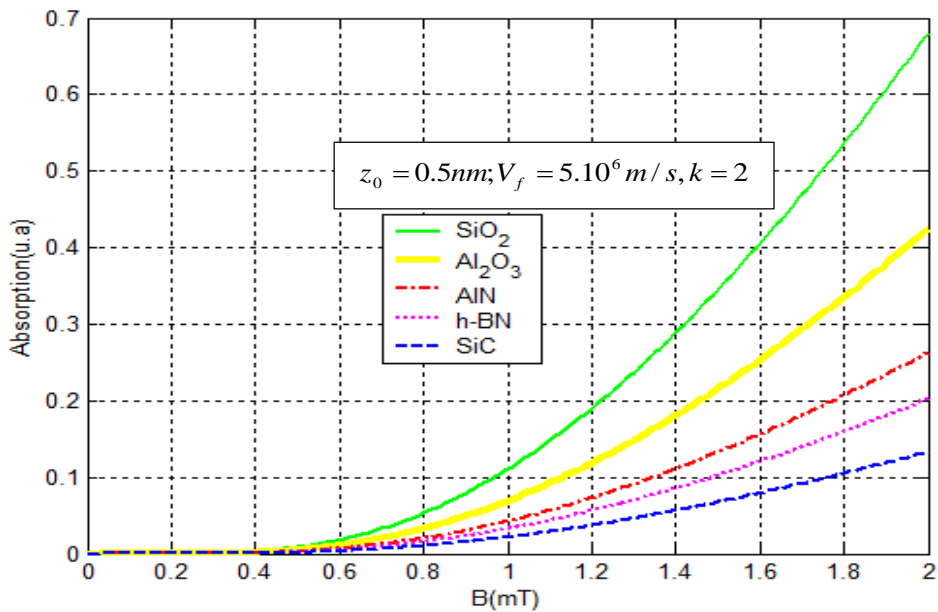


Figure 60 : Optical absorption coefficient of bipolaron (case of SO phonon) versus magnetic field B in MoS₂ intermediate coupling regime for different polar substrate

The optical absorption of SO bipolaron at intermediate coupling regime in monolayer MoS₂ for different polar substrates is shown in Fig.60 One can observe the variation of optical absorption with the polar substrates. For $B < 0.6mT$, no absorption is observed in MoS₂ then for $B = 0.6mT$ a significant change of absorption relates to each substrates highlights the impact of the magnetic field on the optical absorption in MoS₂ monolayer. The greatest optical absorption is observed in SiO₂ polar substrate this result is in agreement with those of Hein et al. [185] and lowest for SiC.

3.3 DECOHERENCE OF POLARON, EXCITON-POLARON AND BIPOLARON

3.3.1 TRANSITION FREQUENCY

3.3.1.1 TRANSITION FREQUENCY OF POLARON

- **Polaron under electric field: the results obtained is from Eq. (137) with energies given by Eqs. (147) and (148)**

Since the polaron states are shifted between the two states, it behaves as a qubit called polaron qubit. The 3D plot of the transition frequency of polaron qubit is presented in Fig.61 as function of effective confinement length and electric field. We observe that the transition frequency increases with increasing of the confinement length, thus transition frequency can be controlled by varying confinement length. In this qubit system formed by ground and first excited states, the polaron qubit is confined. The increasing of effective confinement length resulting from the large transition frequency destroys the superposition states. This result shows that decoherence process can be reduced in system of polaron qubits by decreasing the effective confinement length. In the same figure, one can remark that the transition frequency increases with the increasing of electric field strength. Thus in TMDs system decoherence can also be destroyed by increasing the strength of electric field.

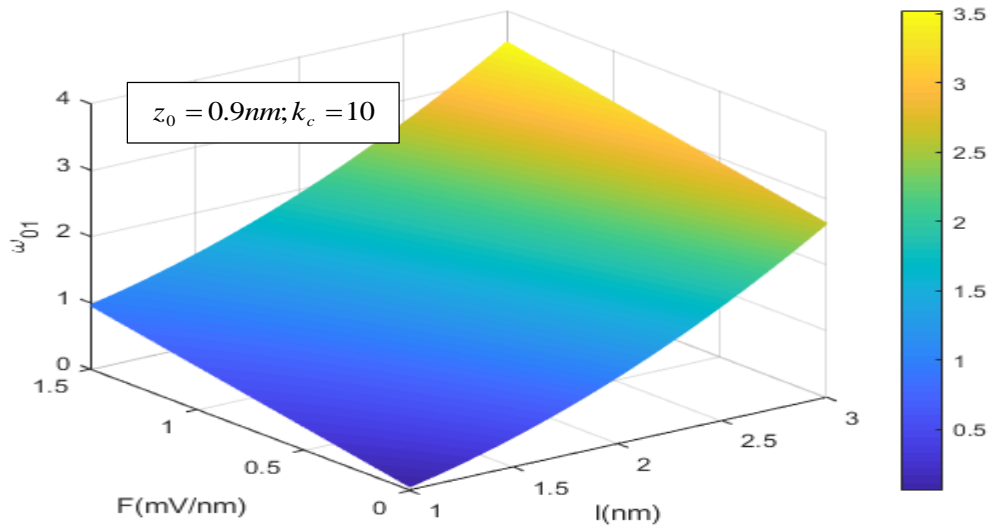


Figure 61 : Transition frequency of polaron qubit versus effective confinement length for different value of electric field

In Fig.62, transition frequency as function of electric field strength is presented for different TMDs monolayer. It is observed that the transition frequency increases linearly with the increasing of the electric field. This confirms the result obtained in Fig.60. The variation of transition frequency as function of different TMDs monolayer layer is also presented in Fig.62 and one can observed that greater the effective mass of electron in TMDs monolayer is greater the transition frequency is.

- **Polaron under microwave and radiowave: the results obtained is from Eq. (137) with energies given by Eqs. (163) and (165)**

Fig.63 presents the variation of the transition frequency for SO phonon on the MoS₂ monolayer as function amplitude of the MW for different polar substrates. From this figure it is observed that the transition frequency is a decreasing function of the amplitude of the microwave. Thus, the influence of the MW on the first excited state is weaker than on the fundamental state. In this same plot on can see that the transition frequency decrease with the increasing of the polarizability parameter. So the energy gap will increase with the increasing of the amplitude of the MW or increasing the polarizability parameter of the substrates and lead to reduction of transition frequency.

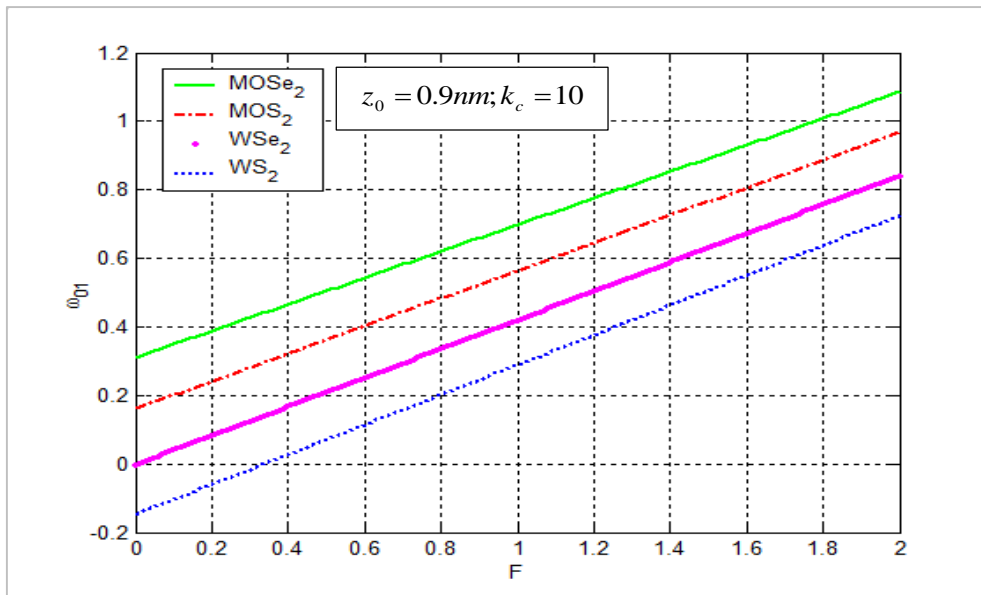


Figure 62 : Transition frequency of polaron versus electric field strength for different TMDs monolayer

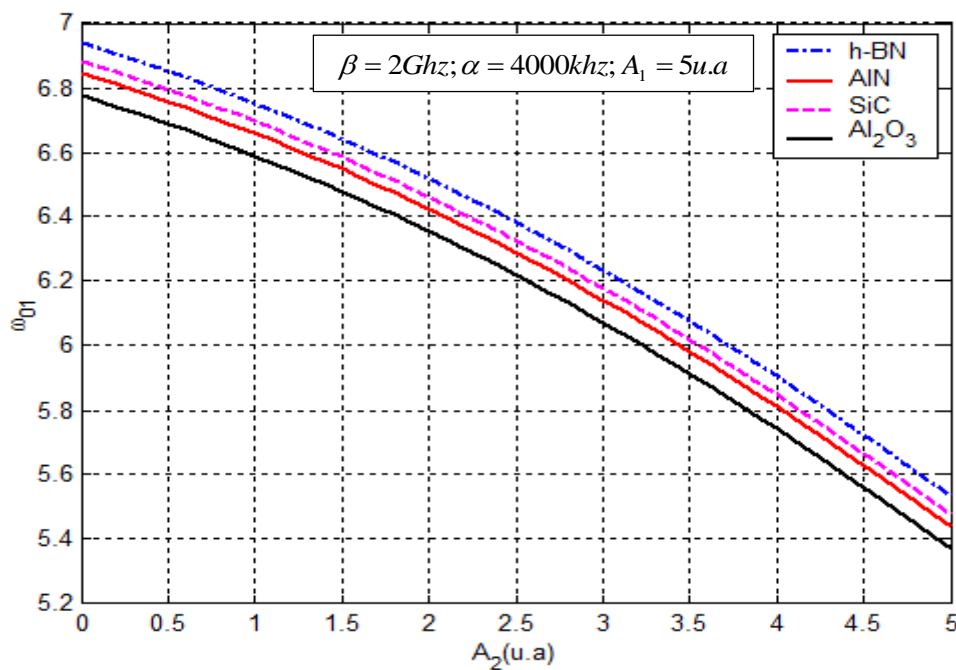


Figure 63 : Transition frequency of polaron with SO phonon mode as function of amplitude of MW for different polar substrates

Fig.64 displays the dependence of transition frequency for SO phonon mode as function of amplitude of the RW for different TMDs monolayer. From Fig.64, we can observe that the variation of the transition frequency with amplitude are different in various ranges: when the amplitude is small, the transition frequency increase sharply with increasing of the amplitude and reaches a maximum, when the amplitude continues to increase, the transition frequency

decrease from the maximum. This behavior of transition frequency is similar to that obtain in ref [186]. The transition frequency is more significant when the amplitude of the RW is small. In this same figure, one can observe that the transition frequency increases with the decrease of the intrinsic gap of the monolayers. Thus the energy gap decrease with decrease of the intrinsic gap of monolayers which leads to the increase of transition frequency.

In fig.65, the 3D plot of the transition frequency for SO phonon mode as function of the frequency of the RW and the amplitude of the MW is presented. one can see that the transition frequency oscillates periodically with the increasing of the frequency of the RW conserving the same amplitude and period of oscillation, also the transition frequency oscillates with the increasing of the amplitude of the MW. Both the frequency of RW and the amplitude of MW create fluctuation in the transition frequency.

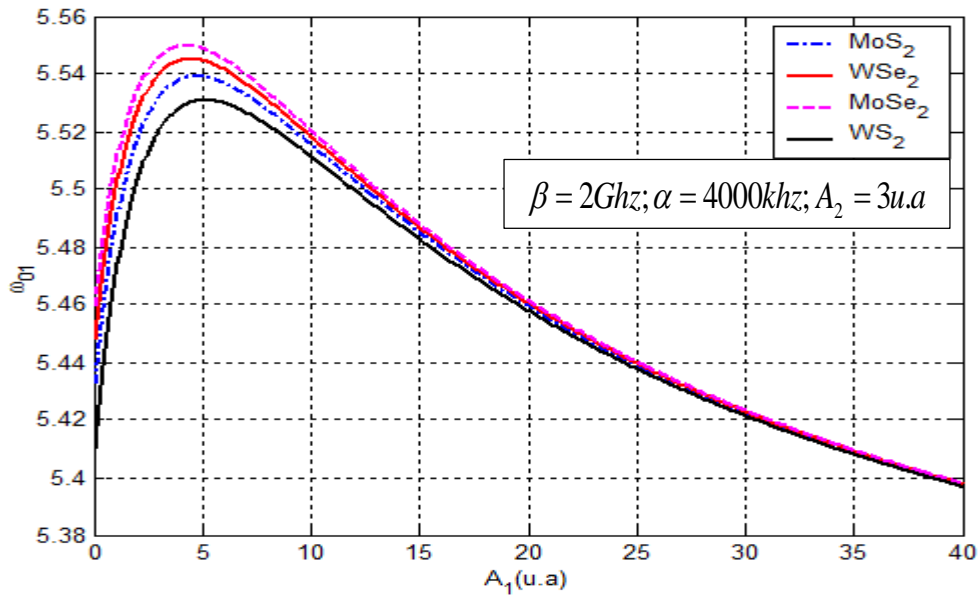


Figure 64 : variation of transition frequency of polaron for SO phonon mode as function of amplitude of the RW for different TMDs

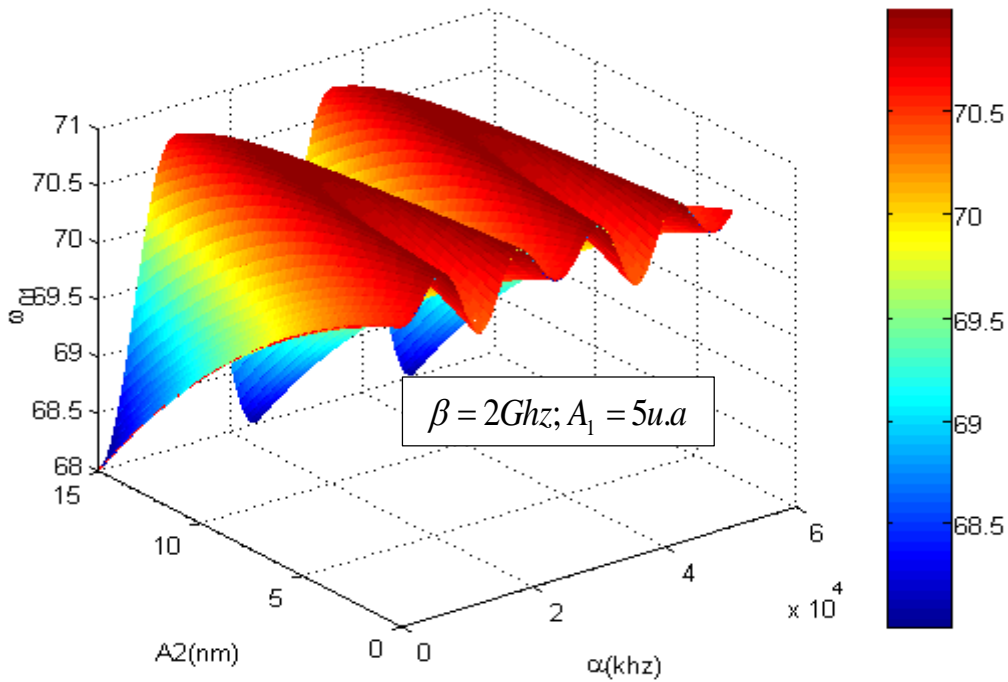


Figure 65 : Transition frequency of polaron for SO phonon mode as function of frequency of RW and amplitude of MW

3.3.1.2 TRANSITION FREQUENCY OF EXCITON-POLARON

- **Magnetic barrier effect on exciton-polaron: the results obtained is from Eq. (137) with energies given by Eqs. (211) and (213)**

In Fig.66, we present the feature of the transition frequency of exciton-polaron with respect to magnetic barrier length for different monolayer TMDs. It is observed that the transition frequency increases with high magnetic length values. This finding is in agreement with Refs. [187-189]. The increasing of magnetic length resulting from the large transition frequency destroys the superposition states as well as quantum entanglement. So, the quantum system tends to become classical system. This result shows that decoherence process can be reduced in system of exciton-polaron qubits by decreasing the magnetic barrier length.

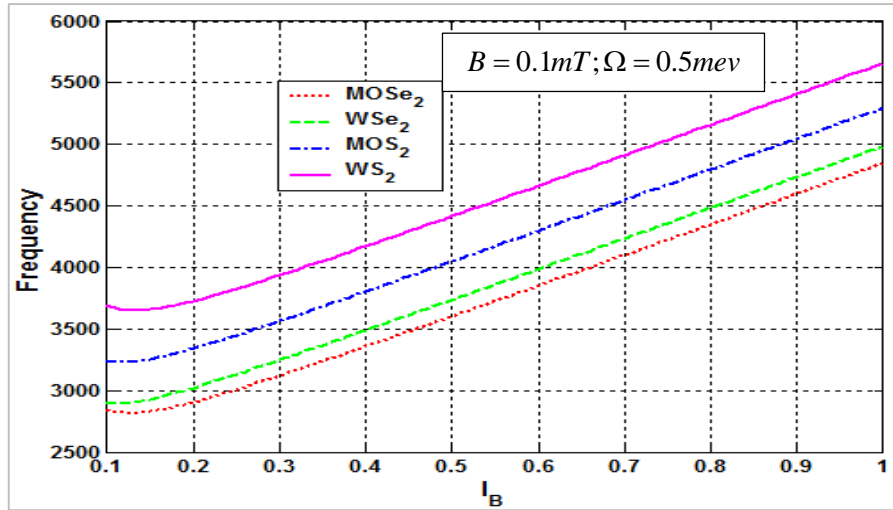


Figure 66 : Transition frequency of exciton-polaron as function of the length of magnetic barrier for different TMDs monolayer

Since the frequency is related to fundamental and first excited states, it permits us to show that transition between one state to another is possible. This figure also shows that in all chosen TMDs monolayer the transition is feasible and can be increased by varying the length of the magnetic barrier. The monolayer that presents the great ability for electron to translate from one state to another is WS₂ and that of the smaller ability is MoSe₂. As seen above on the energy results, it is easier to talk about electron population in the conduction band (first excited state) and electron depopulation in the valence band (ground state). This result gives extremely successful insight to the understanding of the optoelectrical properties of direct bandgap semiconductors.

3.3.1.3 TRANSITION FREQUENCY OF BIPOLARON

- **Bipolaron in quantum pseudodot:** the results obtained is from Eq. (137) with energies given by Eqs. (262) and (263)

As the bipolaron states are shifted between the two states, it behaves as a qubit called bipolaron qubit. The variation of transition frequency of bipolaron qubit is plotted in Fig.67 as function of the zero point of the pseudo-harmonic potential for different values of the chemical potential. We observe that the transition frequency decreases with increasing the zero point of the pseudo-harmonic potential, thus transition frequency can be controlled by varying the zero point of the pseudo-harmonic potential. In this qubit system formed by the two states, the

bipolaron qubit is confined. The decreasing of the zero point of the pseudo-harmonic potential resulting to the large transition frequency which destroys the superposition states.

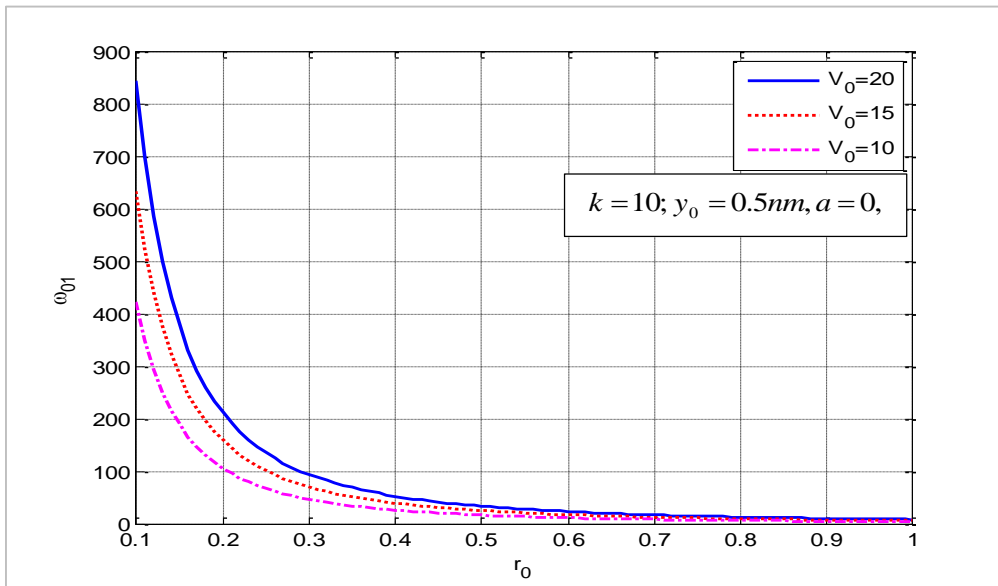


Figure 67 : Transition frequency of bipolaron versus zero point of the pseudo-harmonic potential for various the chemical potential of the two-dimensional electron gas

This result shows that the decoherence process can be reduced in system of bipolaron qubits by increasing the zero point of the pseudo-harmonic potential. In the same figure, the variation of transition frequency versus the chemical potential is also presented and one can observe that the transition frequency increases with the increasing of the chemical potential. Thus in TMDs monolayer system the decoherence can also be destroyed by increasing the chemical potential of the two-dimensional electron gas.

In Fig.68, transition frequency as function of the chemical potential of the two-dimensional electron gas is presented for different TMDs monolayer. It is observed that the transition frequency increases linearly with the increasing the chemical potential of the two-dimensional electron gas, this result is in agreement with [190] who obtained a linear variation of oscillating frequency in RbCl quantum pseudodot qubit under electric field. This increasing behaviors confirms the result obtained in Fig.67. The influence of the chemical potential of the two-dimensional electron gas on the ground state is smaller than that of the first excited state. The variation of transition frequency as function of different TMDs monolayer layer is also presented in Fig.68 and one can observed the behaviors of transition frequency is the same of all chosen TMDs, but greater the effective mass of electron in TMDs monolayer is greater the

transition frequency is. Here our results suggest that in TMDs pseudodot system the transition frequency can be controlled either by tuning the chemical potential of the two-dimensional electron gas or the zero point of the pseudo-harmonic potential.

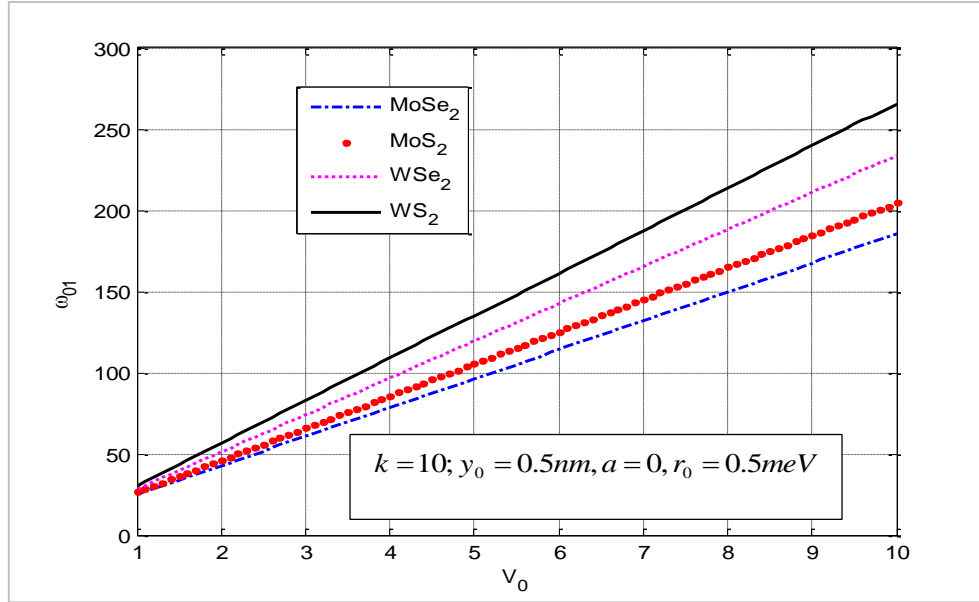


Figure 68 : Transition frequency bipolaron versus the chemical potential of the two-dimensional electron gas for different TMDs monolayer

3.3.2 DENSITY PROBABILITY

3.3.2.1 CASE POLARON

- **Polaron under electric field: the results obtained is from Eq. (136) with energies given by Eqs. (147) and (148)**

Figs.69 and 70 display the electron probability density as function of time. It is observed that the probability density oscillates periodically with time, this result is also obtained in [191]. Furthermore, in Fig.69, we observe that as the electric field strength increases period of oscillation and decreases the amplitude. In Fig.70, we observe that the period remains constant as we varying different TMDs monolayer. As the electron probability density is related to transition frequency, our system can be used to transfer information when electron is in superposition states. Thus our results exhibit an information transfer in the system and then as we increase the strength of electric field, we increase the frequency of information transfer in our system. For different TMDs monolayer we have the same frequency of information transfer. This result is also important for the construction of logic gates and is in agreement with [192].

It is also shown that the strength of electric field is useful to control the state of the quasi-particle and increase information transfer, which is in accordance with [191, 147].

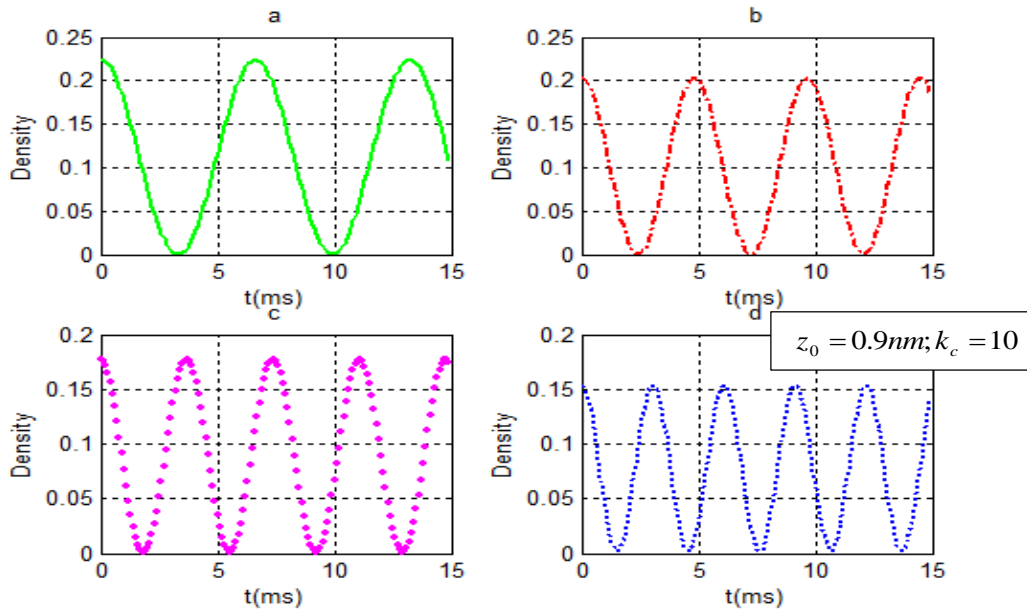


Figure 69 : Probability density of polaron versus time: (a) $F = 0.1mV / nm$, (b) $F = 0.5mV / nm$, (c) $F = 1mV / nm$, (d) $F = 1.5mV / nm$

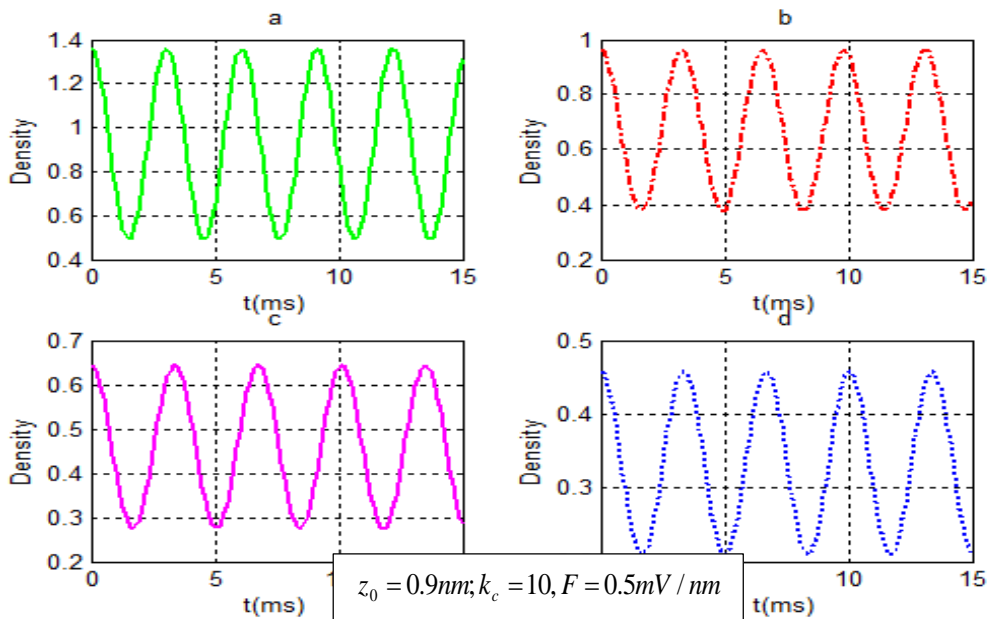


Figure 70 : Probability density of polaron versus time: (a) MoSe₂, (b) MoS₂, (c) WSe₂, (d) WS₂,

3.3.2.2 CASE OF EXCITON-POLARON

- **Magnetic field effect on exciton-polaron:** the result obtained is from Eq. (136) with energies given by Eqs. (211) and (213)

The electron probability density variation with respect to magnetic barrier length for different TMDs monolayer is presented in Fig.71. One can observe that probability density oscillates at same amplitude demonstrating an interstate transfer of information for all monolayers. Carrier doping with good transport properties enables us to adjust the band pattern of TMDs and control their features. By increasing the magnetic field impurities in monolayer TMDs, holders are allowed to fill the conduction (valence) band to points K/K' resulting in the Pauli blocking effect, as derived from the Pauli exclusions rule. This case is more feasible because we showed that the exciton-polaron is influenced by the surrounding. As the superposition state is the major cause of decoherence in a system, the magnetic barrier can be used to control it. Because of efficient Coulomb interactions, monolayer TMD represent systems that interact strongly, even with high carrier densities.

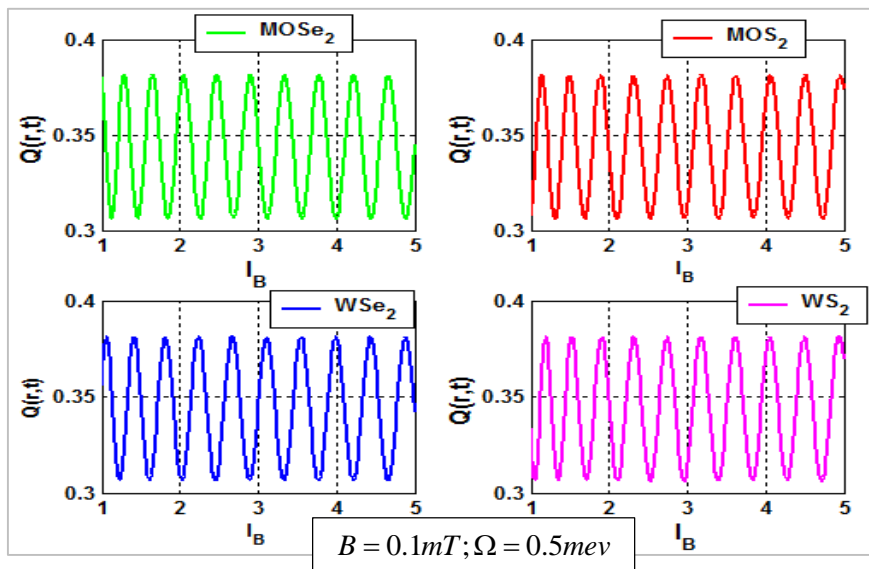


Figure 71 : variation of probability of excitonic-polaron density as function of the length of magnetic barrier for various TMDs monolayer

The probability density is linked to the transition frequency, then the electron is in superposition state, thus the entire system of exciton-polaron can be used to transfer information. Thus a localized state is observed. TMD monolayers modulated by magnetic barrier is an excellent structure for information transfer and can be important in the conception of some electronic component as logic gates [193].

3.3.2.3 CASE OF BIPOLARON

- **Bipolaron in quantum pseudodot:** the results obtained is from Eq. (136) with energies given by Eqs. (262) and (263)

Fig.72 presents the electron probability density as function of time. One can observe that the probability density oscillates periodically with time, this result is also obtained in [191]. Still in Fig.72 we see that as the chemical potential of the two-dimensional electron gas increases, the period of oscillation decreases and the amplitude remains constant. In Fig.73, the electron probability density versus the zero point of the pseudo-harmonic potential is presented, we see that the probability density oscillates with the zero point of the pseudo-harmonic potential. The period of oscillation increases with the increasing of the zero point of the pseudo-harmonic potential and the amplitude remains constant. The electron probability density is linked to transition frequency; thus our system can be used to transfer information in superposition states. The results unveil an information transfer between the ground and first excited states and then as we increase the value of the chemical potential of the two-dimensional electron gas, we increase the frequency of information transfer in our system.

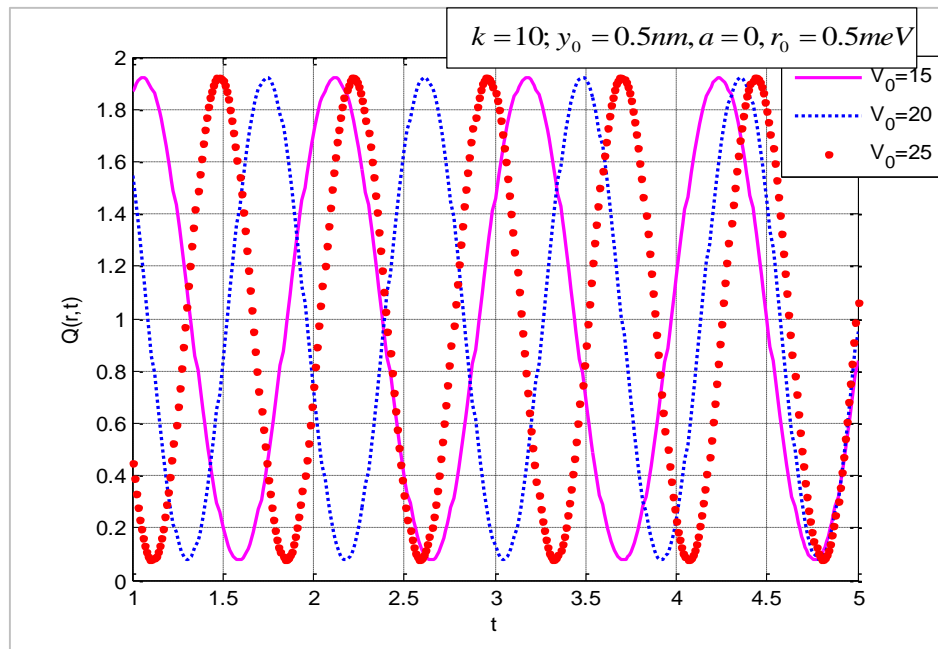


Figure 72 : Density probability of bipolaron as function of time for different values of the chemical potential of the two-dimensional electron gas for

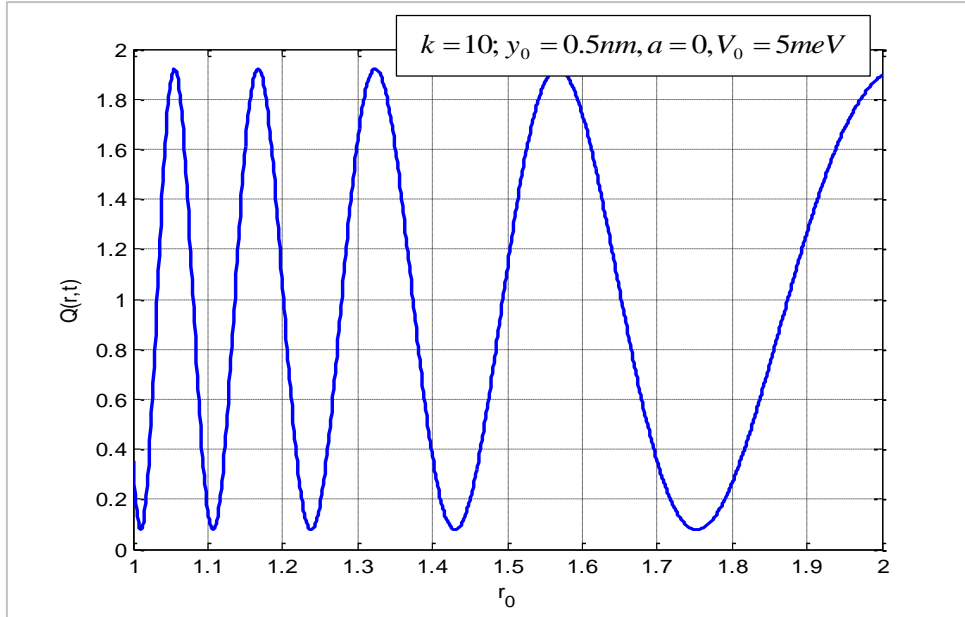


Figure 73 : density probability of bipolaron versus the zero point of the pseudo-harmonic potential

In the same way as we increase the zero point of the pseudo-harmonic potential, we decrease the frequency of information transfer in our system. This result is besides significant for the production of logic gates and is in agreement with [192]. As the chemical potential of the two-dimensional electron gas equals to add extra confinement to the electron, which will lead to an overlap of electron wave function, thus the electron probability density increase with increasing of the chemical potential of the two-dimensional electron gas, this result is similar to those obtained by Liang and Xiao with electric field [194]. Our result here suggests that the chemical potential of the two-dimensional electron gas and the zero point of the pseudo-harmonic potential is useful to control the state of the bipolaron in TMDs monolayer pseudodot and improves the information transfer.

3.3.3 SHANNON ENTROPY

3.3.3.1 SHANNON ENTROPY OF POLARON

- **Polaron under electric field: the results obtained is from Eq. (135) with energies given by Eqs. (147) and (148)**

In Fig.74, the Shannon entropy is plotted as function of time for different values of the electric field. One can observe that entropy changes with time conserving the same amplitude. The amplitude of entropy is different to zero for Figs.74a and 74b showing that the system totally losses it pure state this is in accordance with [190]. In Figs.74c and 74d, it is seen that the polaron qubits can conserve its pure states since the entropy vanishes for some values of

time and the electric field. This result shows that the control of the coherence of polaron qubits in TMDs monolayer can be done by modulating the electric field. Fig.75 presents the entropy of polaron as a function of electric field for different TMDs monolayer. It is observed that the entropy evolves with electric field

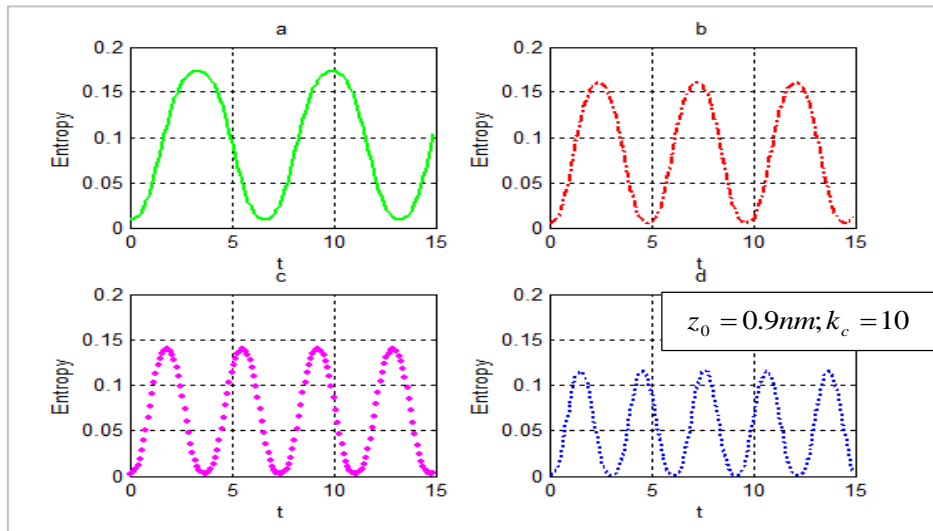


Figure 74 : Shannon entropy of polaron versus time: (a) $F = 0.1mV / nm$, (b) $F = 0.5mV / nm$, (c) $F = 1mV / nm$, (d) $F = 1.5mV / nm$

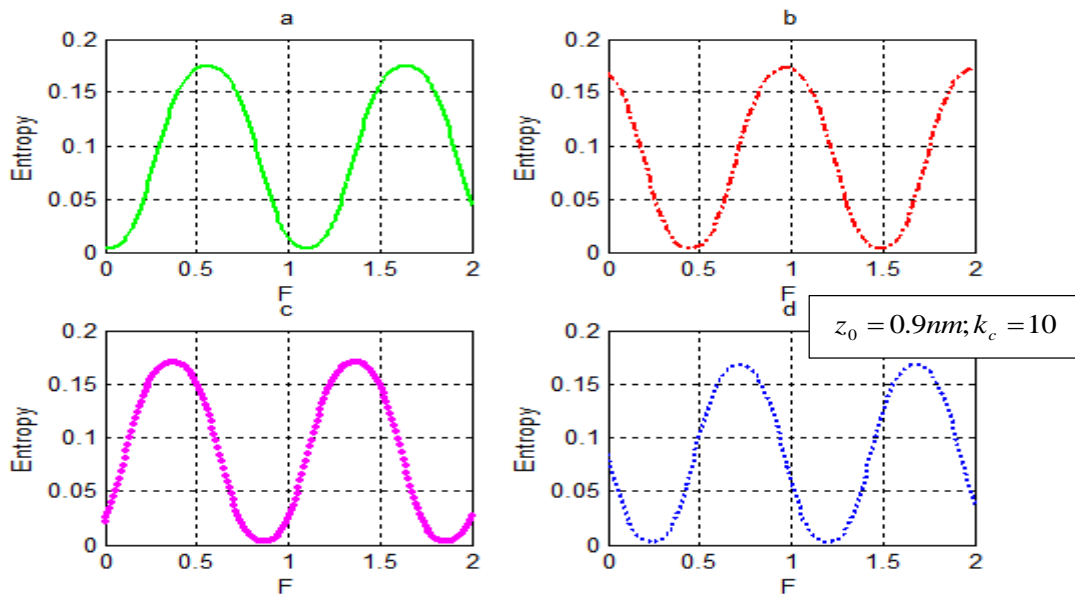


Figure 75 : Shannon entropy of polaron versus electric field : (a) MoSe₂, (b) MoS₂, (c) WSe₂, (d) WS₂, conserving the same amplitude and period. The TMDs monolayer with diselenide are in opposition of phase with those with disulfide. The entropy is not zero showing that the system entirely losses its pure state. Thus in TMDs monolayer under electric field, there is information transfer between electron-phonon interactions showing that decoherence process is a

consequence of this transfer of information. Therefore, electric field is a viable tool to control the coherence of a system in TMDs monolayer.

3.3.3.2 SHANNON ENTROPY OF EXCITON-POLARON

- **Magnetic barrier effect on exciton-polaron: the results obtained is from Eq. (135) with energies given by Eqs. (211) and (213)**

The variation of Shannon entropy with respect to time and the length of magnetic barrier are respectively displayed in Figs.76 and 77. In Fig.76, it is showed that entropy uniformly oscillates over time with same oscillation amplitudes in all monolayers and the entropy of the system is not zero. This implies that the exciton-polaron manages the decay of its pure states. Indeed, entropy is a concept in Information theory that studies the quantification, storage, and communication of information [191], thus amplitude of oscillations observed evolves with time showing that there is sometimes a death and revival of quantum states. As Shannon's entropy is a measure for examining quantum information theory, this behaviour may be the reason why quantum states are stored in TMDs systems to transmit information. we observed that entropy involves with time conserving their amplitude and period in all chosen TMDs monolayer. The entropy is not zero showing that in all TMDs monolayer the system entirely losses it pure states. Thus in all TMDs monolayer there is information transfer between electron-phonon interaction demonstrating that decoherence is a consequence of information transfer. The amplitude of the entropy is less different in all chosen TMDs monolayer proving that the deformation potential of these monolayer also affect the coherence of the system in those monolayer. We also observed in this figure that the monolayer with sulfur displays higher ground state energy than selenide. In Fig.77, we can see that the entropy enhances with the magnetic barrier keeping a constant amplitude for all monolayers. This shows that cohesive state overlay (i.e., quantum coherence) is a fundamental property of quantum mechanics which makes the difference with classical mechanics [195].

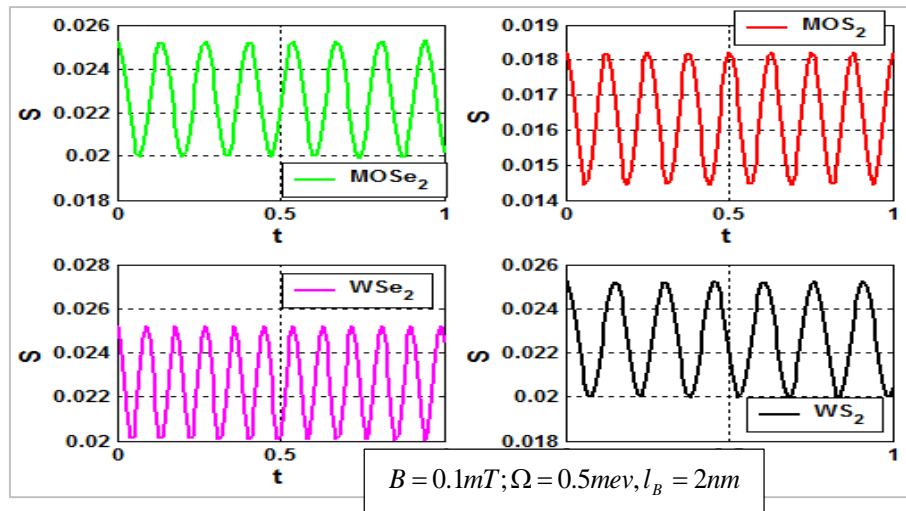


Figure 76 : variation of the entropy of exciton-polaron versus time for various TMD

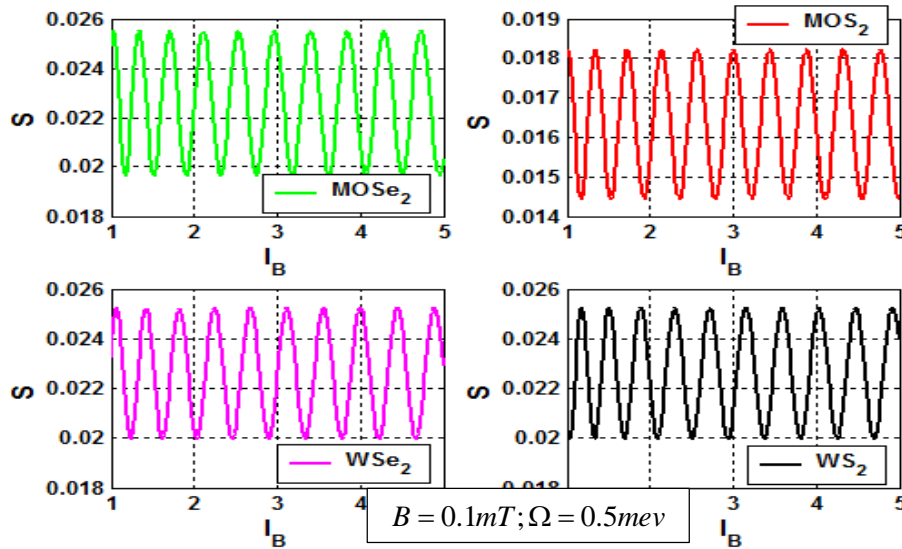


Figure 77 : variation of Shannon entropy of exciton-polaron with respect to the length of magnetic barrier for different TMDs monolayer

The process of decoherence may be regarded as a result of the transfer of information between electron and phonon, whereas in the TMD monolayer, more transfer of energy takes place between the electron (hole)-phonon interplay. Thus, the adjustment of the length of the magnetic barrier is relevant to the coherency of the system studied. We note high fluctuations in entropy in both situations, which is a sign of a damaging interference that induces a strong decoherence. Thus both the length of the magnetic barrier and the deformation potential of different TMD monolayer are important parameters useful to control the decoherence of a system.

3.3.3.3 SHANNON ENTROPY OF BIPOLARON

- **Bipolaron in quantum pseudodot: the results obtained is from Eq. (135) with energies given by Eqs. (262) and (263)**

Fig.78 illustrates Shannon’s entropy plot as a function the chemical potential of the two-electron gas. One can observe that entropy fluctuates with the chemical potential of the two-electron gas conserving the same oscillations amplitude and period. Fig.79 presents Shannon’s entropy as function of the zero point of the pseudo-harmonic potential. We observed that entropy oscillates with the zero point of the pseudo-harmonic potential conserving the same amplitude and period of oscillation increase with the increasing of zero point of the pseudo-harmonic potential. In both figures, the oscillations decrease and increase at certain periods, showing that at certain moment, quantum state is loosed and appear after.

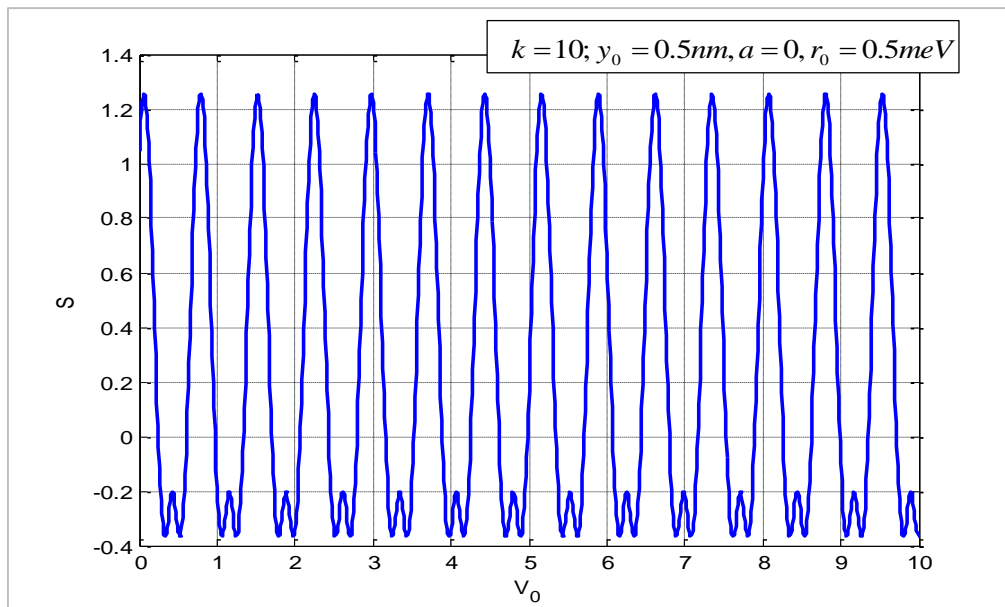


Figure 78 : Shannon entropy of bipolaron versus the chemical potential of the two-electron gas

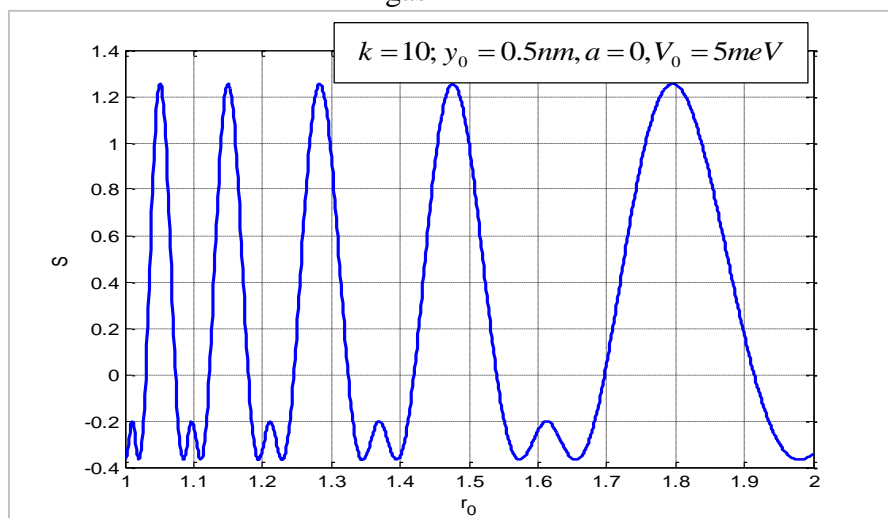


Figure 79 : Shannon entropy of bipolaron versus zero point of the pseudo-harmonic potential

As Shannon entropy is a parameter useful in quantum information theory, the gains and losses of entropy can explain the loses and gains of information's when the decoherence process is controlled. This result is in accordance with the one obtained by Kenfack et al. [191]. we can also observe that the entropy is zero for some value of the chemical potential of the two-electron gas or the zero point of the pseudo-harmonic potential, this means that the state is pure for this value. Notice that the chemical potential of the two-electron gas and the zero point of the pseudo-harmonic potential influences the Shannon entropy, our result also presented the negative values of Shannon entropy which physically means that the density probability is highly localized and the bipolaron is more stable in this region of the quantum system. A similar result is obtained by Edet and Ikot [196] when studying Shannon information entropy in presence of magnetic and AB fields. Studying the Shannon entropy proves that checking the coherence of the system can be done by varying the value of the chemical potential of the two-electron gas or the zero point of the pseudo-harmonic potential.

3.3.4 DECOHERENCE TIME

3.3.4.1 DECOHERENCE TIME OF EXCITON-POLARON

- **Magnetic barrier effect on excition-polaron: the result obtained is from Eq. (138e) with energies given by Eqs. (211) and (213)**

Fig.80 displays decoherence time versus magnetic barrier length. Decoherence time is firstly constant with small length of magnetic barrier and then increases sharply with increasing of the length of magnetic barrier. The magnetic barrier can be considered as an outer excitation source, explaining that when the excitation increases, the system quickly loses coherence. This behaviour for decoherence time is in accordance to that obtained by Fotue et al [187] in presence of magnetic field. Thus, in TMDs monolayer, the magnetic barrier both increases the confinement of the electron and the rate of decoherence in the system. In this plot one can also observe that decoherence time is similar in both selenide and sulphide monolayers. In single-layer TMDs, the high effective masses of the carriers, the large mobility and the robust quantum confinement induce intense exciton resonances with high energies also in all Monolayers the decoherence is in the order of milliseconds. Coherent exciton-polaron control for thin optoelectronic atomic structures requires an appreciation and quantification of exciton decoherence rates. In this study, we indicate how the magnetic barrier influences cohesive quantum dynamics of exciton-polaron in TMDs monolayers. As the decoherence time of

increase with magnetic barrier length, this result is applicable in the domain of quantum information and the quantum computer which requires a long decoherence time.

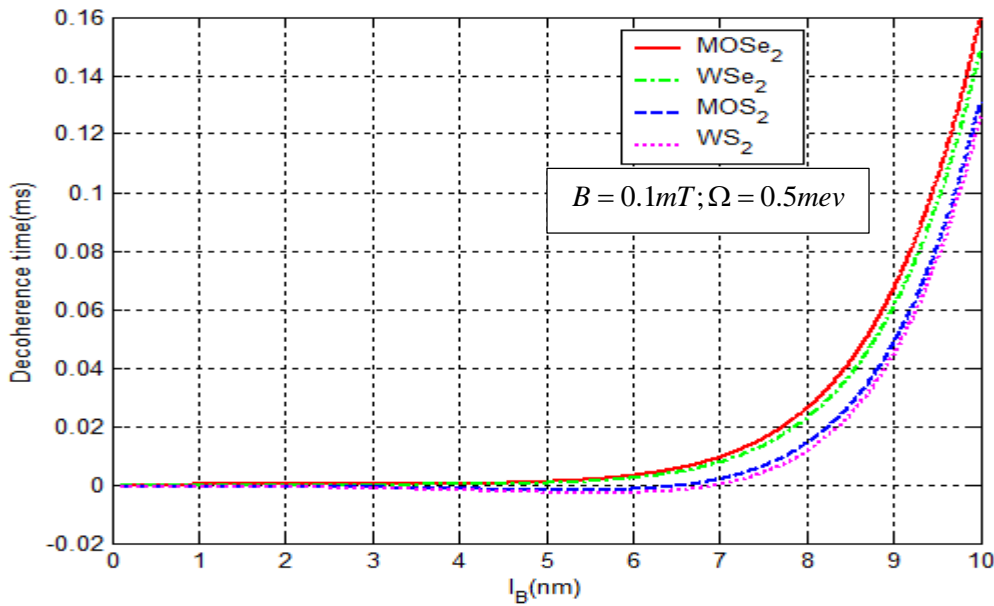


Figure 80 : Decoherence time of exciton-polaron versus the length of magnetic barrier for different TMDs monolayers.

3.3.4.2 DECOHERENCE TIME OF BIPOLARON

- **Bipolaron in quantum pseudodot: the results obtained is from Eq. (138e) with energies given by Eqs. (262) and (263)**

Figs.81 and 82 displays decoherence time versus dispersion coefficient respectively for different values of the chemical potential of the two-dimensional electron gas (Fig.81) and the zero point of the pseudo-harmonic potential (Fig.82). Decoherence time increase linearly with increasing of the dispersion coefficient. This result is similar to that obtained by Kenfack et al [191] in Shannon entropy and decoherence of polaron in asymmetric polar semiconductor quantum wire. Thus when the dispersion coefficient increases, the system quickly loses coherence. Also in Fig.81 are presented the variation of decoherence time as function of the chemical potential of the two-dimensional electron gas, on can remarked that decoherence time decrease with the increasing of the chemical potential of the two-dimensional electron gas. The duration of the bipolaron in the superposition state is longer with small value of chemical potential of the two-dimensional electron gas.

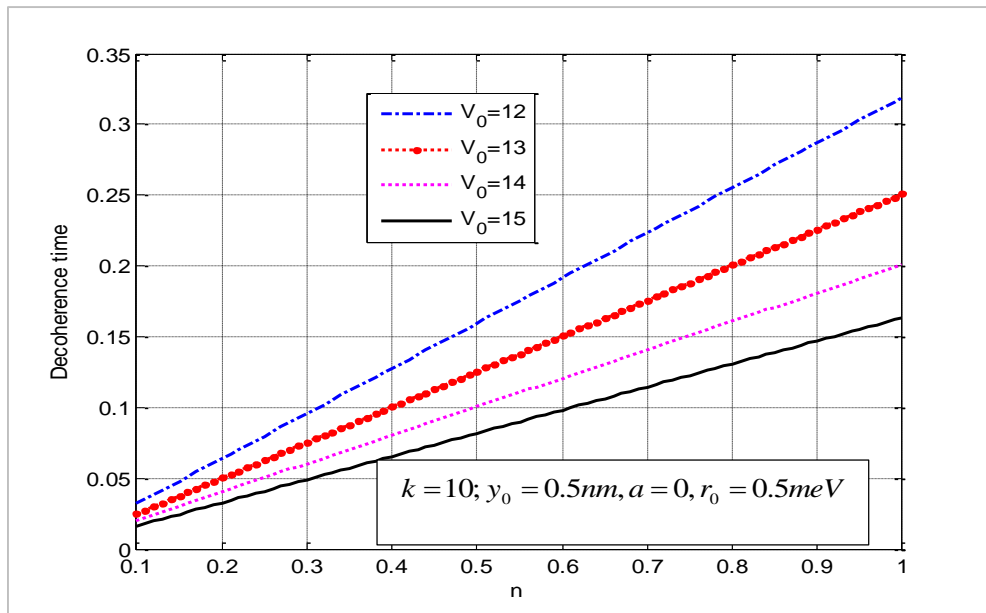


Figure 81 : Decoherence time of bipolaron versus dispersion coefficient for different value of the chemical potential of the two-dimensional electron gas

In Fig.82, on can also observed that the decoherence time increase with the increasing of the dispersion coefficient and increase very little with the increasing of zero point of the pseudo-harmonic potential. The duration of the bipolaron in the superposition state is longer with high value of the dispersion coefficient. Our result suggests that decoherence process of bipolaron in TMDs pseudodot can be controlled by the dispersion coefficient and the zero point of the pseudo-harmonic potential. Thus, as the pseudodot potential can be consider as an outer excitation source, it can affect the decoherence process of bipolaron in TMDs.

In Fig.83 is presented the variation of decoherence time as function of the chemical potential of the two-electron gas for different TMDs monolayers. It is observed that decoherence time decrease parabolically as the chemical potential of the two-dimensional of electron gas increase. This result is in accordance with Fig.82. Decoherence time significantly depends on value of the chemical potential of the two-dimensional electron gas. This result is exciting because it shows that increasing the chemical potential of the two-dimensional of electron gas shrinks the phenomenon of decoherence. Thus a system involving of a bipolaron in TMDs monolayers in pseudodot can be used for the fabrication of a qubit which requires a very small decoherence time. Furthermore, in this figure are also presented decoherence time in function of different TMDs monolayers, one can observe that decoherence time is similar in both selenide and sulphide monolayers. Our result can found it application in quantum cryptographie which require a short decoherence time.

We have therefore noticed that in TMDs under various configurations, the decoherence time is of the order of milliseconds, which is fairly short time. Which mean that the system remains coherent for a longer period of time, which is very favorable for quantum applications

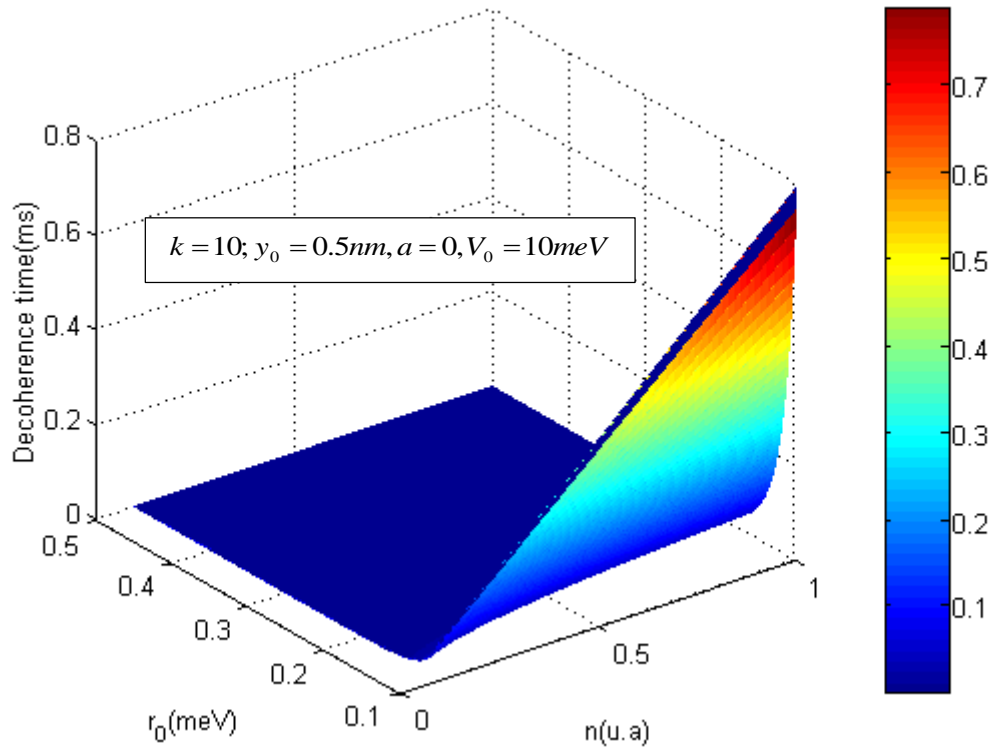


Figure 82 : Decoherence time of bipolaron versus dispersion coefficient and the zero point of the pseudo-harmonic potential

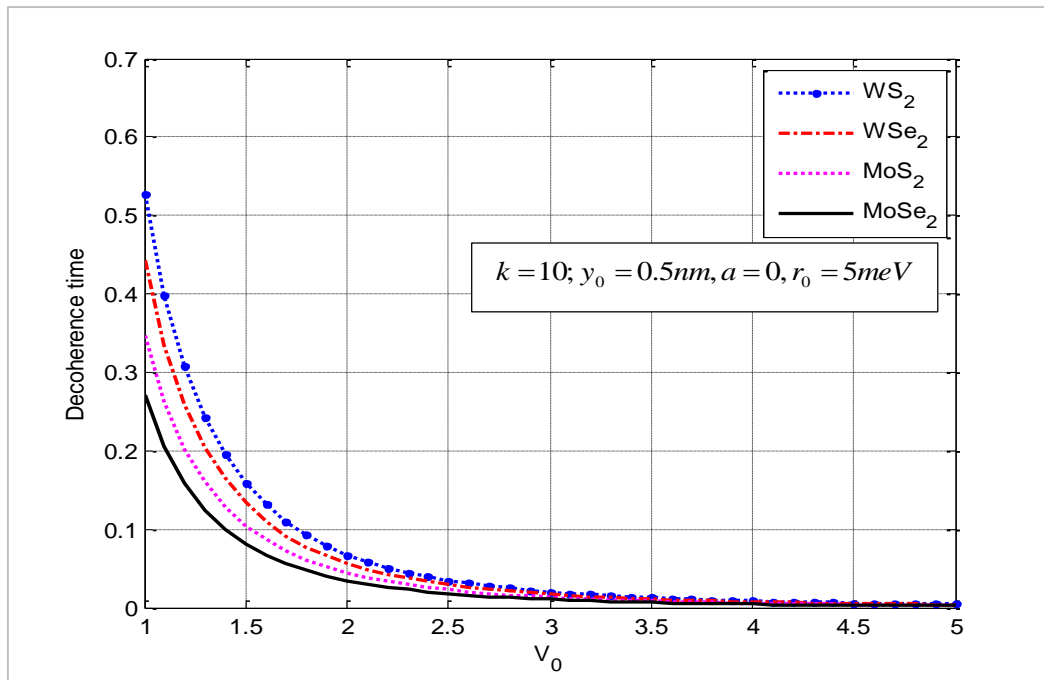


Figure 83 : Decoherence time of bipolaron as function of the chemical potential of the two-electron gas for different TMDs monolayer

CONCLUSION

In this chapter, we have displayed the numerical results obtained from the study of the properties of polaron, exciton-polaron and bipolaron in TMDs monolayer. Firstly, we display the dynamic properties of quasiparticles versus various external potential. Secondly, we present the optical properties such as optical absorption and conductivity of exciton-polaron and bipolaron in TMDs. Finally, we highlighted the decoherence parameters of quasiparticles in TMDs. Discussions made shown that the characteristics of these quasi-particle can be modified and improve to build nanodevices with good efficiency.

GENERAL CONCLUSION AND PERSPECTIVES

In this thesis, we have investigated the electric field, the pseudo harmonic potential, the magnetic barrier and both microwave and radiowave on polaron, exciton-polaron and bipolaron in Transition Metal Dichalcogenides (MoS₂, MoSe₂, WS₂, WSe₂) on one hand. These effects were isolated in the different systems proposed. On the other hand, the electron phonon coupling contribution on exciton-polaron and bipolaron in TMDs under magnetic field have also been investigated. We have calculated the ground state energy, the first excited state energy, the lifetime, the mobility, the MBM, the stability, the decoherence time, the transition frequency, the probability density and the Shannon entropy in the ground and the first excited states of those quasiparticles in TMDs by using various variational methods. We came out that a single qubit can be obtained as a kind of two level system in TMDs.

In the case of polaron in TMDs, it was found that the ground and first excited state energies are increasing function of the electric field, the effective confinement strength, polar substrates, the effective mass of electron in different monolayers and the internal distance between the monolayers and polar substrates. But these state energies are decreasing function of the wave vector. The ground state energy oscillates with the increasing of the frequency of microwaves and radiowave but is an increasing function of their amplitudes. The movement of polaron in TMDs is increase by the increasing of the electric field, the amplitude of the radiowave or microwaves, but this movement can be reducing by increasing the wave vector or the internal distance between TMDs and polar substrates. Thus the polaron move more freely in the WS₂ monolayer. The lifetime of polaron is reduce with the increasing of the electric field and increase with the increasing of the wave vector up to $k_c < 2$, then for $k_c > 2$ the lifetime becomes linear with the increasing of wave vector. Also, lifetime of polaron is an increasing function of the amplitude of the microwave and radiowave both with LO and SO phonons. The polaron lives long in the WS₂ monolayer. Then in TMDs monolayer the lifetime of polaron in the other of the milliseconds. According to the transition frequency, it was found that in presence of electric field the transition frequency is an increasing function of the electric field and effective confinement strength whereas in presence of both radiowave and microwave it decrease with their amplitude and fluctuate with their frequency. Furthermore, the presence of the polar substrates reduces the transition frequency to one state to another, also the effective mass of electron in different monolayer affected the transition frequency. It has been found that

the probability density oscillates periodically with time when the polaron is in the superposition state of the ground and the first-excited state. The probability density increases with a decrease of the electric field or the effective mass of electron in different monolayer. Thus, varying the strength of the electric field on a polaron, our system can increase the probability density. Besides, entropy evolves periodically with time and also with the electric field and is not zero proving that the system entirely loses its pure state. Thus in TMDs monolayer there is information transfer between electron and phonon through interaction showing that the decoherence process is a consequence of information transfer. The magnitude of the bandgap modulation was also investigated in presence of both the microwave and radiowave and it was found that the MBM is a decreasing function of the amplitude of the microwave or radiowave, it is also a decreasing function of the internal distance between TMDs monolayer and polar substrates, then it is an increasing function of the polarizability of the substrates and also of the effective mass of electron in monolayer.

For the case of exciton-polaron, since the binding energy of the exciton-polaron is very important, exciton-polaron are said to be stable quasiparticles in the presence of a magnetic field. This stability is increased by the presence of the magnetic barrier. Therefore, it is easier to speak of electron population in the conduction band and electron depopulation in the valence band. The dimensionality of the system has a key role to play in the development of the system. The advantages of quantum confinement, the reduction of the dimensionality of the system are revealed in the energy of the exciton-polaron. We showed that molybdenum has a higher ground state energy than tungsten. We have seen that the effective mass decreases as the length of the magnetic barrier becomes high. With large values of the length of the magnetic barrier, there is a greater change in the mass of the exciton-polaron. This is due to the interaction between the acoustic phonon and the exciton-polaron. This result proves that the transport properties of an exciton-polaron are robust. In WS_2 , the transport properties may be more interesting than those of MoSe_2 . Those parameters evaluated inform on the efficient transport characteristics of the studied system. We have also shown that mobility increases in all single-layer TMDs with increasing of the length of the magnetic barrier. To characterize the environments that conduct electric current, we need to introduce magnetism into an exciton-polaron system. It is desirable to understand the physics of multiple bodies in TMDs in order to use 2D appliances to develop optoelectronic systems. The results also reveal that the exciton-polaron is also interesting in quantum information theory due to the observed localized states. The outer magnetic barrier therefore affects the system coherence. Decoherence process is reduced enabling the transfer of

information in TMD monolayers. Finally, the modulation of the length of the magnetic barrier is primordial to control the exciton-polaron transport and coherence of the system.

Concerning the bipolaron in pseudodot quantum qubit, it was found that mobility and transition frequency of bipolaron are an increasing function of the chemical potential of the two-dimensional electron gas and also an increasing function of the effective mass of electron in TMDs, thus, bipolaron moves more freely in WS₂ monolayer; moreover, the mobility and transition frequency decreases with the increasing of the zero point of the pseudo-harmonic potential. Thus both the chemical potential of the two-dimensional electron gas and the zero point of the pseudo-harmonic potential can be used to control displacement and the transition of electron to one state to another in TMDs. The electron density probability oscillates with the zero point of the pseudo-harmonic potential and the period increase with the increasing of the zero point of the pseudo-harmonic potential. We also shown that the zero point of the pseudo-harmonic potential and the chemical potential of the two-dimensional electron gas destroys decoherence of bipolaron state in TMDs. The pseudodot effect on bipolaron will be a main issue which can help to improve the control of the decoherence of bipolaron in TMDs.

We theoretically study the energy, the effective mass and the optical absorption of the exciton-polaron and the optical absorption of the bipolaron and its effects on the bandgap modulation in TMDs monolayer under the applied magnetic field. It was found that the energies of Landau level of exciton-polaron are governed by the interaction between the intensity of the electron-phonon coupling and the optical phonon energy. The type of electron phonon coupling affects the zero energy of the Landau level. It was also shown that in the presence of the bipolaron, the MBM of TMDs are flexible, the magnetic field strongly affects the MBM in intermediate and strong coupling regime, thus enhances the conductivity of TMDs monolayer and that in weak coupling regime, the magnetic field cannot be used to tune the MBM. It was also found from the energy and optical absorption results that the LO phonon has always more impact on those parameters than the SO one. The result of the optical absorption shows that it increases in the following order MoSe₂, MoS₂, WSe₂, and WS₂ for exciton-polaron in TMDs whereas in the case of bipolaron MoS₂, has enough energy to absorb than WSe₂. The absorption can be increased by reducing the internal distance between monolayer and polar substrate or by increasing the magnetic field, the magnetic field and the internal distance separating the monolayer and polar substrates affects the optical absorption in the TMDs. By study the stability of bipolaron, it was shown that despite the fact that the coulomb repulsion is enhances, the phonon mediated attractive electron-electron attraction still dominated. Thus, the binding

energy remain positive and indicated that in all selected TMDs monolayer, the bipolaron is stable.

This thesis brings new ideas and offers a possible approach to develop new challenges to further optimize the efficiency of TMDs in technology. Also, our results are meaningful for the design and implementation of quantum computers both theoretically and experimentally and also for the control of decoherence in quantum systems. The results obtained are also very helpful in quantum optics, quantum cryptography, quantum information and electronic nanodevices.

Nevertheless, there are still some unanswered questions which we think can be the subject of future investigations:

- ❖ Deal with applications, in future works we will study dynamic and decoherence of polaron and bipolaron taking into account the influences of many parameters to bring out these results in a realistic experimental system and show their significant implication in quantum computation
- ❖ Study the relaxation of the particle that can be the cause of decoherence;
- ❖ Extends the studies to TMDs multilayers and metallic TMDs
- ❖ Study the properties of polaron and bipolaron and exciton-polaron in TMDs multilayers by taking into, the screening effect.
- ❖ Consider spins to investigate Zeeman effect when calculations are done in the ground state;
- ❖ Study the stability of exciton-polaron in TMDs monolayers

REFERENCES

- [1] C.K. Tillmann, 'Quantum transport in semiconductor nanostructures'. Technische Universität München Physik-Department Institut für Theoretische Physik (2009).
- [2] X. Duan, C. Wang, A. Pan, R. Yu and X. Duan, 'Two-dimensional transition metal dichalcogenides as atomically thin semiconductors: opportunities and challenges'. *Chem. Soc. Rev.*, **44** (2015) 8859.
- [3] B. Radisavljevic, A. Radenovic, J. Brivio, V. Giacometti and A. Kis, 'Single-layer MoS₂ transistors'. *Nat. Nanotechnol.*, **6** (2011) 147.
- [4] O. Lopez-Sanchez, D. Lembke, M. Kayci, A. Radenovic and A. Kis, 'Ultrasensitive photodetectors based on monolayer MoS₂'. *Nat. Nanotechnol.*, **8** (2013) 497.
- [5] T. Cao, G. Wang, W. Han, H. Ye, C. Zhu, J. Shi and J. Feng, 'Valley-selective circular dichroism of monolayer molybdenum disulphide'. *Nat. Commun.* **3** (2012) 887.
- [6] H. Zeng, J. Dai, W. Yao, D. Xiao and X. Cui, 'Valley polarization in MoS₂ monolayers by optical pumping'. *Nat. Nanotechnol.*, **7** (2012) 490.
- [7] "2-D materials enhance a 3-D world" (<https://phys.org/news/2017-01-d-materials-world.html>). *phys. org*. Retrieved Mar 9, 2017.
- [8] "This 'nanocavity' may improve ultrathin solar panels, video cameras and more" (<https://phys.org/news/2016-05-nanocavity-ultrathin-solar-panels-video.html#nRlv>). *phys. org*. Retrieved Mar 9, 2017.
- [9] K. S. Novoselov, V. I. Fal'ko, L. Colombo, P. R. Gellert, M. G. Schwab and K. Kim, 'A roadmap for graphene'. *Nature*, **490** (2012) 192.
- [10] J. Shah, 'Ultrafast spectroscopy of semiconductors and semiconductor nanostructures'. Springer Science and Business Media **115** (2013).
- [11] S. Rudin, T. Reinecke and B. Segall, 'Temperature-dependent excitation linewidths in semiconductors'. *Phys. Rev. B*, **42** (1990) 11218.
- [12] J.T. Devreese, 'Frohlich polaron from 0D to 3D: concepts and recent developments'. *J. phys.: Condens. Mat.*, **19** (2007) 255201.
- [13] N.N. Bogolubov and N.N. Bogolubov (2008), 'Aspects of Polaron Theory Equilibrium and Nonequilibrium Problems'. World Scientific Publishing Co. Pte. Ltd. Moscow State University and Russian Academy of Sciences, Russia, ISBN-13 978-981-283-398-3
- [14] S.I. Pekar, 'The method of effective masses of electrons in crystals'. *J. Exp. Theor. Phys.*, **16** (1946) 341.
- [15] D. Emin and T. Holstein, 'Adiabatic theory of an electron in a deformable continuum'. *Phys. Rev. Lett.*, **36** (1976) 323.
- [16] D. Emin, 'Formation, motion, and high-temperature superconductivity of large bipolaron'. *Phys. Rev. Lett.*, **62** (1989) 1544.

- [17] J.T. Devreese, 'Polarons'. *Phys. Today*, **67** (2014) 54
- [18] A. Mauger, 'Magnetic polaron: theory and experiment'. *Phys. Rev. B* **27** (1983) 2308.
- [19] H. Fröhlich, H. Pelzer, and S. Zienau, 'XX properties of slow electrons in polar materials'. *Phil. Mag.*, **41** (1950) 221.
- [20] R.P. Feynman, 'Slow electron in a polar crystal'. *Phys. Rev.*, **97** (1955) 660.
- [21] N.N. Bogolubov, 'About one New form of adiabatic perturbation theory in the problem of particle interacted with quantum field'. *Ukrainian Math. J.*, **2** (1950) 3.
- [22] N.N. Bogolubov and N.N. Bogolubov, 'Aspects of the polaron theory'. *JINR Communications*, P-17-81-85 Dubna (1981).
- [23] N.N. Bogolubov and N.N. Bogolubov, 'some aspects of polaron theory'. *World Scientific Publishing Company*, **4** (1988).
- [24] F. Wang, Y. Wu, M.S. Hybertsen and T.F. Heinz, 'Auger recombination of excitons in one-dimensional systems'. *Phys. Rev. B*, **73** (2006) 245424.
- [25] C. Trallero-Giner, D.G. Santiago-Pérez and V.M. Fomin, 'New magneto-polaron resonances in a monolayer of a transition metal dichalcogenides', *Scientific Reports*, **13** (2023) 292.
- [26] L.E. Calvet, R.G. Wheeler and M.A. Reed, 'Electron transport measurement of Schottky barrier inhomogeneities'. *Appl. Phys. Lett.*, **80** (2002) 1761.
- [27] L.E. Calvet, R.G. Wheeler and M.A. Reed, 'Observation of the linear stark effect in a single acceptor in Si'. *Appl. Phys. Lett.*, **98** (2007) 096805.
- [28] R. Saito, Y. Tatsumi, S. Huang, X. Ling and M.S. Dresselhaus, 'Raman spectroscopy of transition metal dichalcogenides'. *J. Phys.: Condens. Mat.*, **28** (2016) 353002.
- [29] S.E. Economou, J.I. Climente, A. Badolato, A.S. Bracker, D. Gammon and M.F. Doty, 'Scalable qubit architecture based on holes in quantum dot molecules'. *Phys. Rev.*, **86** (2012) 085319.
- [30] S. Manzeli, D. Ovchinnikov, D. Pasquier, O.V. Yazyev and A. Kis, '2D transition metal dichalcogenides'. *Nat. Rev. Mat.*, **28** (2017)1.
- [31] C.Y. Hsieh, A. Rene and P. Hawrylak, 'Herzberg circuit and berry's phase in chirality-based coded qubit in a triangular triple quantum dot'. *Phys. Rev. B*, **86** (2012) 115312.
- [32] M.M. Glazov, M.A. Semina, C. Robert, B. Urbaszek, T. Armand and X. Marie, 'Intervalley polaron in atomically thin transition metal dichalcogenides'. *Phys. Rev. B*, **100** (2019) 041301
- [33] Y. Sun, et Al., 'Effective velocities of polaron spin states in monolayer transition metal dichalcogenides'. *J. Phys. : Condens. Mat.*, **33** (2021) 235303.
- [34] X.Y. Dong, R.Z. Li, J.P. Deng and Z.W. Wang, 'Interlayer exciton-polaron effect in transition metal dichalcogenides Van der Waals heterostructures'. *J. Phys. Chem. Of Solids* **134** (2019) 1.

- [35] D. Fazzi, S. Fabiano, T-P. Ruoko, K. Meerholz and F. Negri, ‘polaron in pi-conjugated ladder-type polymers: broken symmetry density functional description’. *J. Mater. Chem. C*, **7** (2019) 12876.
- [36] F. Ceballos, Q. Cui, M.Z. Bellus and H. Zhao, ‘Exciton formation in monolayer transition metal dichalcogenides’. *Nanoscale*, **8** (2016) 11681.
- [37] Z. Cuilan, C. Chunyu and X. Jinglin, ‘Influence of an anisotropic parabolic potential on the quantum dot qubit’. *J. of Semicon.*, **34** (2013) 112002. DOI: 10.1088/1674-4926/34/11/112002
- [38] S. Chen and J.L Xiao, ‘The decoherence of the unsymmetrical parabolic confinement potential quantum dot qubit’. *Chinese J. of Electronics*, **18** (2009) 262.
- [39] J.P. Barnes and W.S. Warren, ‘Decoherence and programmable quantum computation’. *Phys. Rev. A*, **60** (1999) 4363.
- [40] D. Tolkunov and V. Privman, ‘Short decoherence for general system-environment interactions’. *Phys. Rev. A*, **69** (2004) 062309.
- [41] A. Grodecka and P. Machnikowski, ‘partly noiseless encoding of quantum information in quantum dot arrays against phonon-induced pure dephasing’. *Phys. Rev. B*, **73** (2006) 125306.
- [42] M. Lovric, H.G. Krojanski and D. Suter, ‘Decoherence in large quantum registers under variable interaction with the environment’. *Phys. Rev. A*, **75** (2007) 042305.
- [43] G.-Q. Hai, L. Cândido, G. A. Braulio-Brito and F.M. Peeters, ‘Electron pairing: from metastable electron pair to bipolaron’. *J. Phys. Commun.* **2** (2018) 035017.
- [44] M. Pasek and G. Orso, ‘Induced pairing of fermionic impurities in one-dimensional strongly correlated bose gas’. *Phys. Rev. B*, **100** (2019) 245419.
- [45] Z. Nie, Y. Shi, S. Qin, Y. Wang, H. Jiang, Q. Zheng and F. Wang, ‘Tailoring exciton dynamic of monolayer transition metal dichalcogenides by interfacial electron-phonon coupling’. *Commun. Phys.*, **2** (2019) 1.
- [46] D.H. Lee, S.J. Choi, H. Kim, Y.S. Kim and S. Jung, ‘Direct probing of phonon mode electron-phonon scatterings in two-dimensional semiconductor transition metal dichalcogenides’. *Nat. Commun.*, **12** (2021) 1.
- [47] I. Petsagkourakis, N. Kim, K. Tybrandt, I. Zozoulenko and X. Crispin, ‘Poly(3,4-ethylenedioxythiophene): chemical synthesis transport properties, and thermoelectric devices’. *Adv. Electron. Mater.* **5** (2019) 1800918.
- [48] S. Chen, et Al., ‘On the anomalous optical conductivity dispersion of electrically conducting polymers: ultra-wide spectral range ellipsometry combined with a drude-lorentz model’. *J. Mater. Chem. C*, **7** (2019) 4350.
- [49] C. Kenfack-Sadem, C. M. Ekengoue, J. E. Danga, M. F. C. Fobasso, J. V. Nguepnang, A. J. Fotue and L. C. Fai, ‘Laser control of magneto-polaron in transition metal dichalcogenides triangular quantum well’. *Phys. Lett. A*, **384** (2020) 126662.

- [50] A. Ramasubramaniam, D. Naveh and E. Towe, 'Tunable band gaps in bilayer transition-metal dichalcogenides'. *Phys. Rev. B*, **84** (2011) 295325.
- [51] C. Kenfack-Sadem, A.K. Tegoumfouet, A. Kenfack-Jiotsa and R.M. Tsiaze, 'Dynamics and decoherence of exciton-polaron in monolayer transition metal dichalcogenides'. *J. Electron. Mater.*, **50** (2021) 2921.
- [52] A. Thilagam, 'Excitonic polaron in low transition metal dichalcogenides'. *Physica B: Condens. Mater.* **464** (2015) 44.
- [53] Y. Xiao, Z.Q. Li and Z.W. Wang, 'Polaron effect on the bandgap modulation in monolayer transition metal dichalcogenides'. *J. Phys: Condens. Mater.* **29** (2017) 48500.
- [54] Y. Ge, First-principles study of charge density waves, electron-phonon coupling, and superconductivity in transition metal dichalcogenides, Doctoral dissertation, Georgetown university, (2013).
- [55] M. Van der Donck, M. Zareina and F.M. Peeters, 'Excitons, trions and biexcitons in transition-metal dichalcogenides: magnetic- field dependence'. *Phys. Rev. B*, **97** (2018) 195408.
- [56] T.V. Dikko, A.J. Fotue, S.C. Kenfack, R.K. Tsiaze, E. Baloitcha and M.N. Honkounou, 'Thermodynamic properties of a monolayer transition metal dichalcogenides (TMD) quantum dot in the presence of magnetic field'. *Phys. Lett. A*, **385** (2021) 126958.
- [57] B. Amin, N. Singh and U. Schwingenschlogl, 'Heterostructures of transition metal dichalcogenides'. *Phys. Rev. B*, **92** (2015) 075439.
- [58] S. Wang, et Al., 'Phase-dependent band gap engineering in alloys of metal-semiconductor transition metal dichalcogenides'. *Adv. Funct. Mater.*, **30** (2020) 2004912.
- [59] S.Z. Butler, et Al., 'Progress, challenge and opportunities in two-dimensional materials beyond graphene'. *ACS. Nano.*, **7** (2013) 2898.
- [60] U. Halim, C. R. Zheng, Y. Chen, Z. Lin, S. Jiang, R. Cheng, Y. Huang and X. Duan, 'A rational design of cosolvent exfoliation of layered materials by directly probing liquid- solid interaction'. *Nat. Commun.*, **4** (2013) 2213.
- [61] D. Jariwala, et Al., 'Emerging device applications for semiconducting two-dimensional transition metal dichalcogenides'. *ACS. Nano.* **8** (2014) 1102.
- [62] S. Mahatha, et Al., 'Electronic structure investigation of MoS₂ and MoSe₂ using angle-resolved photoemission spectroscopy and ab initio structure studies'. *J. Phys.: Condens. Mat.* **4** (2012) 475504.
- [63] A. Pakdel, et Al., 'Low-dimensional boron nitride nanomaterials'. *Mater. Today* **15** (2012) 256.
- [64] L. Song, et Al., 'Anomalous insulator-metal transition in boron nitride-graphene hybrid atomic layers'. *Phys. Rev. B*, **86** (2012) 075429.
- [65] R. Dutta, et Al., 'Optical enhancement of indirect bandgap 2D transition metal dichalcogenide for multi-functional optoelectronic sensors'. *Advanced Mater.* **35** (2023) 2303272

- [66] H. Zhang, 'Ultrathin two-dimensional materials'. ACS. Nano., **9** (2015) 9451.
- [67] S. Das, et al., 'Synthesis, properties, and applications of 2-D materials: A comprehensive review'. Crit. Rev. Solid State Mater. Sci., **39** (2014) 231.
- [68] M. Chhowalla, H. S. Shin, G. Eda, L. J. Li, K. P. Loh and H. Zhang, 'The chemistry of two-dimensional layered transition metal dichalcogenide nanosheets'. Nat. Chem., **5** (2013) 263.
- [69] R. A. Gordon, D. Yang, E.D. Crozier, D.T. Jiang and R.F. Frindt, 'Structures of exfoliated single layers of WS₂, MoS₂, and MoSe₂ in aqueous suspension'. Phys. Rev. B, **65** (2002) 125407.
- [70] W. Bao, et al., 'High mobility ambipolar MoS₂ field effect transistors: substrate and dielectric effects'. Appl. Phys. Lett. **102** (2013) 042104.
- [71] N. Choudhary, et al., 'Two-dimensional lateral heterojunction through bandgap engineering of MoS₂ via oxygen plasma'. J. Phys.: Condens. Mat., **28** (2016) 3640
- [72] M.R. Islam, et al., 'Tuning the electrical property via defect engineering of single layer MoS₂ by oxygen plasma'. Nanoscale **6** (2014) 10033.
- [73] K.F. Mak, et al., 'Atomically thin MoS₂: A new direct-gap semiconductor'. Phys. Rev. Lett. **105** (2010) 136805.
- [74] N. Choudhary, et al., 'Centimeter scale patterned growth of vertical stacked few layer only 2D MoS₂/ WS₂ van der Waals heterostructure'. Sci. Rep. **6** (2016) 1.
- [75] A.K. Geim and I.V. Grigorieva, 'Van der Waals heterostructures'. Nature **499** (2013) 419.
- [76] O.V. Yazyev and A. Kis, « MoS₂ and semiconductors in the flatland », Mater. Today, Ecole Polytechnique Fédérale De Lausanne, (2014).
- [77] K.K. Kam, 'Electrical properties of WSe₂, WS₂, MoSe₂, MoS₂, and their use as photoanodes in a semiconductor liquid junction solar cell', Thèse de Doctorat, Iowa State University, (1982).
- [78] D. Duphil, 'Synthèse et caractérisation de nanoparticules et de fullerènes de métaux de transition MX₂ (où M = W, Mo ; X = S, Se)', thèse de doctorat en science des matériaux, université Paris XII-Val De Marne (2003).
- [79] C. BALLIF, 'Propriétés électriques et optiques de couches minces de WS₂ et MoS₂ en vue d'applications photovoltaïques', thèse de doctorat en science, Ecole Polytechnique Fédérale De Lausanne (1998).
- [80] K.S. Novoselov, et al., 'Electric field effect in atomically thin carbon films'. Science, **306** (2004) 666
- [81] Z. Yin, et al., 'Single-layer MoS₂ phototransistors'. ACS Nano, **6** (2012) 74.
- [82] H. Li, et al., 'Fabrication of single and multilayer MoS₂ film-based field-effect transistors for sensing NO at room temperature'. Small, **8** (2012) 63.

- [83] G.F. Walker, 'Macroscopic swelling of vermiculite crystals in water'. *Nature*, **187** (1960) 312
- [84] J. Feng, et al., 'Metallic few-layered VS₂ ultrathin nanosheets: high two-dimensional conductivity for in-plane supercapacitors'. *J. Am. Chem. Soc.*, **133** (2011) 17832.
- [85] J. Feng, et al., 'Giant moisture responsiveness of VS₂ ultrathin nanosheets for novel touchless positioning interface'. *Adv. Mater.*, **24** (2012) 1969.
- [86] M.B. Dines, 'Intercalation in layered compounds'. *J. Chem. Educ.*, **51** (1974) 221.
- [87] D. Yang and R.F. Frindt, 'Li-intercalation and exfoliation of WS₂'. *J. Phys. Chem. Solids*, **57** (1996) 1113.
- [88] G. Eda, H. Yamaguchi, D. Voiry, T. Fujita, M.W. Chen and M. Chhowalla, 'Photoluminescence from chemically exfoliated MoS₂'. *Nano Lett.*, **11** (2011) 5111.
- [89] H. Henck, 'Hétérostructures de Van der Waals à base de Nitrure', Doctoral dissertation, Université Paris-Saclay (ComUE) (2017)
- [90] Y-C. Lin, et al., 'Wafer-scale MoS₂ thin prepared MoO₃ sulfurization'. *Nanoscale*, **4** (2012) 6637.
- [91] J-G. Song, et al., 'layered-controlled, wafer-scale, and conformal synthesis of tungsten disulfide nanosheets using atomic layer deposition'. *ACS Nano*, **7** (2013) 11333.
- [92] R. A Bromley, R.B. Murray and A.D. Yoffe, 'The band structures of some transition metal dichalcogenides. III. Group VIA: trigonal prism material'. *J. Phys. C: solid State Phys.*, **5** (1972) 759.
- [93] R. Roldan, J.A. Silva-Guillén, M.P Lopez-Sancho¹, F. Guinea, E. Cappelluti and P. Ordejon, 'Electronic properties of single-layer and multilayer transition metal dichalcogenides MX₂ (M = Mo, W and X = S, Se)', Wiley Online Library, *Annalen der Physik* (2014)
- [94] A. Kumar and P.K. Ahluwalia, 'Electronic structure of transition metal dichalcogenides monolayer 1H-MX₂ (M=Mo, W; X=S, Te, Se) from ab-initio theory: new direct band gap semiconductors'. *Eur. Phys. J. B*, **85** (2012) 1.
- [95] J. Kang, W. Cao, X. Xie, D. Sarkar, W. Liu and K. Banerjee, 'Graphene and beyond-graphene 2D crystals for next generation green electronics'. *Proc. SPIE* **9083** (2014) 908305.
- [96] G. Fiori, et Al., 'Electronics based on two- dimensional materials'. *Nat. Nanotechnol.* **9** (2014) 768.
- [97] E.G. da Silveira Firmiano, et Al. 'Supercapacitor electrodes obtained by directly bonding 2D MoS₂ on reduced graphene oxide'. *Adv. Energy Mater.*, **4** (2014) 1301380.
- [98] S. Ratha and C.S. Rout, 'Supercapacitor electrodes based on tungsten disulfide-reduced graphene oxide hybrids synthesized by facile hydrothermal method'. *ACS Appl. Mater. Interfaces*, **5** (2013) 11427.
- [99] L. Wang, Y Ma, M. Yang and Y. Qi, 'One-pot synthesis of 3D flower-like heterostructured SnS₂/ MoS₂ for enhanced supercapacitor behavior'. *RSC Adv.* **5** (2015) 89069.

- [100] Y. Yon, K. Ganapathi and S. Salahuddin, 'How good can monolayer MoS₂ transistors be?'. *Nano Lett.*, **11** (2011) 3768.
- [101] G. Du, Z. Guo, S. Wang, R. zeng, Z. Chen and H. Liu, 'Superior stability and hihh capacity of restacked molybdenum disulfide as anode material for lithium on batteries'. *Chem. Commun.*, **46** (2010) 1106.
- [102] J. Xiao, D. Choi, L. Cosimbescu, P. Koech, J. Liu and J.P. Lemmon, 'Exfoliated MoS₂ nanocomposite as an anode material for lithium ion batteries'. *Chem. Mater.*, **22** (2010) 4522.
- [103] K. Chang and W. Chen, 'L-cysteine-assisted synthesis of layered MoS₂/graphene composites with excellent electrochemical performances for lithium ion batteries *ACS Nano*, **5** (2011) 4720.
- [104] G.R. Bhimanapati, et Al., 'Recent advances in two-dimensional materials beyond graphene'. *ACS Nano*, **9** (2015) 11509.
- [105] A.C. Ferrari, et Al., 'Science and technology roadmap for graphene, related two-dimensional crystals, and hybrid systems'. *Nanoscale* **7** (2015) 4598.
- [106] C. Kittel, 'Introduction to Solid State Physics', (1986). (Wiley, 2nd ed)
- [107] X. Zhang, X.F. Qiao, W. Shi, J.B. Wu, D.S. Jiang and P.H. Tang, *Chem. Soc. Rev.*, **44** (2015) 2757.
- [108] C.T. Walker, and G.A. Slack, 'Who named the-one?'. *Am. J. Phys.*, **38** (1970) 1380.
- [109] L.D. Landau, 'on the momentum of a system of two photons' *Doklady Akad. Nauk SSSR*. **60** (1948).
- [110] A.S. Alexandrov, A.M. Bratkovsky and N.F. Mott, 'Hall effect and resistivity of High-T_c oxides in the bipolaron model'. *Phys. Rev. Lett.* **72** (1994) 1734.
- [111] L.D. Landau and S.I. Pekar, 'effective mass of a polaron'. *J. Exp. Theor. Phys.*, **18** (1948) 419.
- [112] J.T. Devreese, 'Polarons'. In Lerner, R.G.; Trigg, G.L. (eds.). *Encyclopedia of Physics*. 2 (Third ed.). Weinheim: Wiley-VCH. (2005). pp. 2004-2027
- [113] F.G. Bassani, et Al., 'Electron gas with polaronic effects: beyond the mean-field theory'. *Physica Status Solidi B*, **237** (2003) 173.
- [114] M. Hohenadler, G. Hager, G. Wellein and H. Fehske, 'Carrier-density effects in many-polaron systems'. *J. Phys.: Condens. Mat.*, **19** (2007) 255210.
- [115] N. Bondarenko, 'Theoretical studies of lattice- and spin-polarons'. Thesis at Uppsala University, ISBN 978-91-513-0235-5 (2018).
- [116] S. Mukhopadhyay and A. Chatterjee, 'formation and stability of a singlet optical bipolaron in a parabolic quantum dot'. *J. Phys.: Cond. Mat.*, **8** (1996) 4017.
- [117] S.G. Suprun and B.Y. Moizhes, 'Role of electron correlation in the creation of a pekar bipolaron'. *Fizika Tverdogo Tela*, **24** (1982) 1571.

- [118] J. Adamowski and S. Bednarek, 'Stability of large bipolarons'. *J. Phys.: Condens. Mat.*, **4** (1992) 2845.
- [119] S. Sil, A.K. Giri and A. Chatterjee, 'Stability of the Frohlich bipolaron in two and three dimensions'. *Phys. Rev. B*, **43** (1991) 12642.
- [120] G. Verbist, F.M. Peeters and J.T. Devreese, 'The stability region of bipolaron formation in two and three dimensions in relation to high-*t_c* superconductivity'. *Solid State Commun.*, **76** (1990) 1005.
- [121] G. Verbist, F.M. Peeters and J.T. Devreese, 'Large bipolaron in two and three dimensions'. *Phys. Rev. B*, **43** (1991) 2712.
- [122] H. Hiramoto and Y. Toyozawa, 'Inter-polaron interaction and bipolaron formation'. *J. Phys. Society of Japan*, **54** (1985) 245.
- [123] A.V.P. Abreu, L.A. Ribeiro Junior, G.G. Silva, M.L. Pereira Junior, B.G. Enders, A.L.A. Fonseca and G.M. eSilva, 'Stability conditions of armchair graphene nanoribbon bipolarons'. *J. Mol. Mod.*, **25** (2019) 1.
- [124] A. Nocera, J. Sous, A.E. Feiguin and M. Berciu, 'Bipolaron liquids at strong peierls electron-phonon coupling'. *Phys. Rev. B*, **104** (2021) L201109.
- [125] V. Lakhno, *Physica C: Superconducting and its applications*, **561** (2018) 1.
- [126] J. Pollmann and H. Buttner, 'Upper bounds for the ground-state energy of the exciton-phonon system'. *Solid State Commun.*, **17** (1975) 1171.
- [127] J. Pollmann and H. Buttner, 'Effective Hamiltonians and binding energies of Wannier excitons in polar semiconductors'. *Phys. Rev. B*, **16** (1977) 4480.
- [128] P. Petelenz and V.H. Smith Jr, 'Triplet exciton mobilities in weak donor acceptor complexes'. *Chem. Phys. Lett.* **82** (1981) 430.
- [129] D.M. Larsen, 'Perturbation theory for the two- dimensional polaron in a field'. *Phys. Rev B*, **33** (1986) 799.
- [130] S.A.E. Moskalenko, S.A. Moskalenko and D.W. Snoke, 'Bose-Einstein condensation of excitons and biexcitons: and coherent nonlinear optics with excitons', Cambridge University Press, (2000).
- [131] C. Kenfack-Sadem, A.K. Tegumfouet, A.B. Moubissi, N. Cortés, M.F.C. Fobasso, M. Masale and A. Kenfack-Jiotsa, 'Magnetic barrier and electric field effects on exciton-polaron relaxation and transport properties in transition metal dichalcogenides'. *Phys. Rev.B*, **107** (2023) 075134.
- [132] V. Preisler, et Al., 'Evidence for excitonic polarons in InAs/GaAs quantum dot'. *Phys. Rev. B* **73** (2006) 075320.
- [133] S. Hurtado Parra, D.B. Straus, B.T. Fichera, N. Lotov, C.R. Kagan and J.M. Kikkawa, 'Large exciton-polaron formation in 2D hybrid perovskites via time-resolved'. *ACS Nano*. **16** (2022) 21259.

- [134] W. Qui, Y.J. Chen, Y. Sun and J.L. Xiao, Iran. ‘The optical polaron effect on the coherent time of a qubit in the RbCl quantum dot with two-dimensional pseudo-harmonic potential’. *J. Sci. Tech. Trans. A: Science*, **44** (2020) 1237.
- [135] Y.C. Chen and J.L. Xiao, ‘The effect of Temperature and electric field on a quantum pseudodot qubit’. *Int. J. Theo. Phys.* **57** (2018) 533.
- [136] Y. Sun and J.L. Xiao, ‘The magnetic field effect on the coherence time of qubit in RbCl crystal quantum pseudodot’. *Opt. Quant. Electron.*, **51** (2019) 1.
- [137] S.H. Chen and J.L. Xiao, ‘Properties of unsymmetrical parabolic confinement potential quantum dot qubit’. *Commun. Theor. Phys.*, **50** (2008) 1287.
- [138] W. Xiao and J.L. Xiao, ‘Coulomb bound potential quantum rod qubit’. *Superlattices Microstructures*, **52** (2012) 851.
- [139] Z.X. Li and J.L. Xiaob, ‘Ground state lifetime of strong-coupled polaron in an asymmetric quantum dot’. *J. At. Mol. Sci.*, **2** (2011) 74.
- [140] C.H. Bennett and D.P. Divincenzo, ‘Quantum information and computation’. *Nature*, **404** (2000) 247.
- [141] I. D’Amico, ‘Quantum dot-based quantum buses for quantum computer hardware architecture’. *Microelectronics J.*, **37** (2006) 1440.
- [142] Y. Yi-Fu, J.L. Xiao, J.W. Yin and Z.W. Wang, ‘The ground-state lifetime of polaron in a parabolic quantum dot’. *Chin. Phys. B*, **17** (2008) 2236.
- [143] J. Shah, ‘Ultrafast Spectroscopy of semiconductor and Semiconductor Nanostructures’. Springer, Berlin (1996).
- [144] S. Coe, W.K. Woo, M. Bawendi and V. Bulovic, ‘Electroluminescence from single monolayers of nanocrystals in molecular organic dices’. *Nature*, **420** (2002) 800.
- [145] T.D. Lee, F. Low and D. Pines, ‘The motion of slow electrons in a polar crystal’. *Phys. Rev.*, **90** (1953) 297.
- [146] W.J. Huybrechts, ‘Internal excited state of optical polaron’. *J. Phys. C: Solid State Phys.*, **10** (1977) 3761.
- [147] A.J. Fotue et Al., ‘Decoherence of polaron in asymmetric quantum dot qubit under an electromagnetic field’. *Am. J. Mod. Phys.*, **4** (2015) 138.
- [148] L.F Lemmens, J. De Sitter and J.T. Devreese, ‘Ground-state theorem for free polarons’. *Phys. Rev. B*, **8** (1973) 2717.
- [149] C.Y. Cai, C.L. Zhao and J.L. Xiao, ‘Influence of temperature and magnetic field on the first excited state of a quantal pseudodot’. *J. Electron. Matter*, **46** (2017) 971.
- [150] A.J. Fotue, S.C. Kenfack, M. Tiotsop, N. Issofa, A.V. Wirngo, M.P. Djemmo, H. Fotsin and L.C. Fai, ‘Shannon entropy and decoherence of bound magnetopolaron in a modified cylindrical quantum dot’. *Phys. Lett. B*, **29** (2015) 1550241.

- [151] M.F.C. Fobasso, C. Kenfack-Sadem, E. Baloitcha, A.J. Fotué and L.C. Fai, ‘Lifetime and dynamics of polaron and bipolaron in graphene nanoribbon under lase’. *Eur. Phys. J. Plus* **135** (2020) 1.
- [152] A. Thilagam, ‘Exciton-phonon interaction in fractional dimensional space’. *Phys. Rev. B*, **56** (1997) 9798.
- [153] T. Takagahara, ‘Localization and homogeneous dephasing relaxation of quasi-two-dimensional excitons in quantum-well heterostructures *Phys. Rev. B*, **32** (1985) 7013.
- [154] T. Takagahara, ‘Localization and energy transfer of quasi-txo-dimensional excitons in GaAs-AlAs quantum-well heterostructures’. *Phys. Rev. B*, **32** (1985) 6552.
- [155] N. Myoung, G. Ihm and S.J. Lee, ‘Transport in armchair graphene nanoribbons modulated by magnetic barriers’. *Physica E: Low-dimensional. Syst. Nano.*, **42** (2010) 2808.
- [156] A.J. Fotue, J.R.D. Djomou, S.C. Kenfack, M.F.C. Fobasso and L.C. Fai, ‘Stability and decoherence of optical bipolaron in symmetric quantum dot’. *Eur. J. Phys. Plus* **135** (2020) 1.
- [157] F.E. Low and D. Pines, ‘Mobility of slow electrons in polar crystals’. *Phys. Rev. B*, **98** (1955) 414.
- [158] Y. Sun, Z.H. Ding and J.L. Xiao, ‘Temperature effect on first excited state energy and transition frequency of a strong- coupling polaron in a symmetry RbCl quantum dot’. *Phys. B*, **444** (2014) 103.
- [159] G-B. Liu, H. Pang, Y. Yao and W. Yao, ‘Intervalley coupling by quantum do confinement potentials in monolayer transition metal dichalcogenides’. *News J. Phys.*, **16** (2014) 05011.
- [160] J.T. Devreese, Fröhlich Polarons-Lecture Course Including Detailed Theoretical derivations (Universiteit Antwerpen, Belgium, 2016) e-print arXiv: 1012.4576v6.
- [161] J.T. Devreese, W. Huybrechts and L. Lemmeks, ‘On the optical absorption of free polaron at weak coupling’. *Physica Status Solidi (b)* **48** (1971) 77.
- [162] P.F. Li and Z.W. Wang, ‘Optical absorption of Frohlich polaron in monolayer transition metal dichalcogenides’. *J. Appl. Phys.*, **123** (2018) 204308.
- [163] Y-H. Ruan, and Q-H. Chen, ‘Ground and excited states of the two and three dimensional bipolaron in a quantum dot’. *Comm. Theor. Phys.*, **48** (2007) 169.
- [164] Z.W. Wang, L. Liu and Z.Q. Li, ‘Energy gap induced by surface optical polaron in graphene on polar substrates’. *Appl. Phys. Lett.*, **106** (2015) 101601.
- [165] Y. Ding, Y. Wang, J. Ni, L. Shi, S. Shi and W. Tang, ‘First principle study of structural, vibrational and electronic properties of graphene-like MX_2 ($\text{M}=\text{Mo}, \text{Nb}, \text{Ta}$; $\text{X}=\text{S}, \text{Se}, \text{Te}$) monolayers’. *Phys. B: Condens. Mat.*, **406** (2011) 2254.
- [166] I.T. Lin and J.M. Liu, ‘Surface polar optical phonon scattering of carriers in graphene on various substrates’. *Appl. Phys. Lett.*, **103** (2013) 081606.
- [167] A. Kuc, N. Zibouche, and T. Heine, ‘Influence of quantum confinement on electronic structure of the transition metal sulfide TS_2 ’. *Phys. Rev. B*, **83** (2011) 245213

- [168] A. Mogulkoc, Y. Mogulkoc, A.N. Rudenko and M.I. Katsnelson, ‘Polaronic effects in monolayer black phosphorus on polar substrates’. *Phys. Rev. B*, **93** (2016) 085417.
- [169] J.V. Nguenpang, A.K. Tegumfouet, C. Kenfack-Sadem and A. Kenfack-Jiotsa, ‘Polaron dynamic and decoherence in transition metal dichalcogenides under electric field’. *Indi. J. Phys.* **96** (2021) 2001
- [170] Y.F. Huangfu and Z.W. Yan, ‘Bound polaron in a spherical quantum dot under electric field’. *Physica E: Low-dimensional Sysys. and Nano.*, **40** (2008) 2982.
- [171] J.R. Djomou, S.C. Kenfack, A.J. Fotue, M.F.C. Fobasso and L.C. Fai, ‘Contribution of bulk and surface phonons to the properties in a Zn1-XCdXSe/ZnSe heterojunction confined in a triangular potential’. *Physica B: Condens. Mat.*, **548** (2018) 58.
- [172] Z.W. Wang, W.P. Li, Y. Xiao, R.Z. Li and Z.Q. Li, ‘Influence of exciton-phonons coupling on the exciton binding energy in monolayer transition metal dichalcogenides’. *Appl. Phys. Lett.*, **110** (2017) 231603.
- [173] Z. Yu et Al., ‘Analyzing the carrier mobility in transition metal dichalcogenides MoS₂ Field effect transistor’. *Adv. Functional Mater.*, **27** (2017) 1604093.
- [174] F.C.F. Mbognou, C. Kenfack-Sadem, A.J. Fotue, M.N. Hounkonnou, D. Akay and L.C. Fai, ‘Thermodynamics properties and optical conductivity of bipolaron in graphene nanoribbon under laser irradiation’. *J. Low Temp. Phys.*, **203** (2021) 204.
- [175] A.L. Vartanian, ‘Confined and interface polarons in cylindrical nanowires in an electric field’. *Phys, Eur. Phys. J. B*, **83** (2011) 481.
- [176] J. Singh, *Excitation Energy Transfer Processes in Condensed Matter* (Berlin: Springer) **1** 1994
- [177] F. Brosens and J.T. Devreese, ‘Stability of bipolarons in the presence of magnetic field’. *Phys. Rev. B* **54** (1996) 9792.
- [178] T. Sohler, M. Calandra, and F. Mauri, ‘Two-dimensional Frohlich interaction in transition metal dichalcogenides monolayers: theoretical modeling and first principles calculations’. *Phys. Rev. B* **94** (2016) 085415.
- [179] S. Tongay, J. Zhou, C. Ataca, K. Lo, T.S. Matthews, J. Li, J.C. Grossman, and J. Wu, ‘Thermally driven crossover from indirect toward direct bandgap 2D semiconductors MoSe₂ versus MoS₂’. *Nano. Lett.* **12** (2012) 5576.
- [180] A. Arora, K. Nogajewski, M. Molas, M. Koperski, and M. Potemski, ‘Exciton band structure in layered MoS₂ from a monolayer to the bulk limit’. *Nanoscale*, **7** (2015) 20769.
- [181] T. Sohler, M. Gibertini, M. Calandra, F. Mauri, and N. Marzari, ‘Breakdown of optical phonons splitting in two-dimensional materials’. *Nano. Lett.*, **17** (2017). 3758.
- [182] K.K. Kaasbjerg, K.S. Bhargavi, and S.S. Kubakaddi, ‘Hot-electron cooling by acoustic and optical phonons in monolayer of MoS₂ and others transition metal dichalcogenides’. *Phys. Rev. B*, **90** (2014) 165436).

- [183] J. Ryou, Y.S. Kim, S. Kc, and K. Cho, ‘Monolayer MoS₂ bandgap modulation by dielectric environments tunable bandgap transistors’. *Sci. Rep.*, **6** (2016) 1.
- [184] C. Chen et Al., Emergence of Frohlich polaron from interlayer electron-phonon coupling in van der Waals heterostructure. *ArXiv preprint arXiv :1707.00184* (2017).
- [185] N.D. Hien et Al., ‘Magneto-optical transport properties of monolayer transition metal dichalcogenides’. *Phys. Rev. B*, **101** (2020) 045424.
- [186] X.F. Bai, Y.W. Zhao, W. Xin and H.W. Yin, ‘Transition probability and frequency of an electron in an asymmetric gaussian confinement potential quantum dot with electromagnetic field’. *Iran. J. Sci. Techn. Trans. A: Sci.* **43** (2019) 2027.
- [187] A.J. Fotue, M. Tiotsop, N. Isofa, S.C. Kenfack, A.V. Wirngo, H. Fotsin and L.C. Fai, ‘Bound magnetopolaron in an asymmetric cylindrical quantum dot qubit in an electric field’. *Am. J. Mod. Phys.*, **4** (2015) 109.
- [188] B.S. Kandemir and A. Cetin, ‘Impurity magnetopolaron in a parabolic quantum dot the squeezed state variational approach’. *J. Phys. Condens. Mat.*, **17** (2005) 667.
- [189] Y. Lepine and G. Bruneau, ‘The effect of an anisotropic confinement on the ground state energy of a polaron in a parabolic quantum dot’. *J. Phys. Condens. Mat.*, **10** (1998) 1495.
- [190] Z.H. Liang and J.L. Xiao, ‘Effect of electric field on RbCl quantum pseudodot qubit’. *Ind. J.Phys.*, **92** (2018) 437.
- [191] S.C. Kenfack, A.J. Fotué, M.F.C Fobasso, G.N Bawe Jr and L.C Fai, ‘Shannon entropy and decoherence of polaron in asymmetric polar semiconductor quantum wire’. *Superlattices and Microstructures* **111** (2017) 32.
- [192] W.P. Li, J.W Yin, Y.F Yu, Z.W Wang and J.L Xiao, ‘The effect of magnetic on the properties of a parabolic quantum dot qubit’. *J. Low Temp. Phys.*, **160** (2010) 112.
- [193] L. Mandel and E. Wolf, *Optical Coherence and Quantum Optics* (Cambridge, England: Cambridge University Press) 1995.
- [194] P. Vogt et Al., ‘Silicene: compelling experimental evidence for graphenelike two-dimensional silicon’. *Phys. Rev. Lett.*, **108** (2012) 155501.
- [195] A. Streltsov, G. Adesso, and M.B. Plenio, ‘Colloquium: coherence as a resource’. *Rev. Mod. Phys.*, **89** (2017) 041003.
- [196] C.O. Edet and A.N. Ikot, ‘Shannon information entropy in the presence of magnetic and Aharanov-Bohm (AB) fields’. *Eur. Phys. J. Plus*, **136** (2021) 1.

LIST OF PUBLICATIONS

1. **J.V. Nguepnang**, A.K. Tegoumfouet, C. Kenfack-Sadem and A. Kenfack-Jiotsa, polaron dynamic and decoherence in transition metal dichalcogenides under electric field. *Indian J. Phys.* **96** (7) 2001-2010 (2022).
2. C. Kenfack-Sadem, **J.V. Nguepnang**, A. Kenfack-Jiotsa, F.F. Mbougou, T.V. Dikko and M.N. Hounkounou, Magnetic effect on dynamic and decoherence of exciton-polaron in transition metal dichalcogenides. *Physica Scripta* **96** (12) 125824 (2021).
3. **J.V. Nguepnang**, C. Kenfack-Sadem, A. Kenfack-Jiotsa, C. Guimapi, A.J. Fotue and A.E. Merad, Electron-phonon coupling contribution on the optical absorption and the dynamic of exciton-phonon in monolayer transition metal dichalcogenides. *Opt. Quant. Electron.* **53** (11) 1-21 (2021).
4. **J.V. Nguepnang**, C. Kenfack-Sadem, A. Kenfack-Jiotsa, M.F.C. Fobasso, and Y. Sun, Optical signature of bipolaron in monolayer transition metal dichalcogenides: all coupling approach. *Opt. Quant. Electron.* **53** (12) 1-17 (2021).